On the Random-Matrix Theory of Quantum Transport

P R O E F S C H R I F T

TER VERKRIJGING VAN DE GRAAD VAN DOCTOR
AAN DE RIJKSUNIVERSITEIT TE LEIDEN, OP GEZAG
VAN DE RECTOR MAGNIFICUS DR. W. A. WAGENAAR,
HOOGLERAAR IN DE FACULTEIT DER SOCIALE WETENSCHAPPEN,
VOLGENS BESLUIT VAN HET COLLEGE VAN DEKANEN
TE VERDEDIGEN OP WOENSDAG 11 JUNI 1997
TE KLOKKE 15.15 UUR

DOOR

Piet Wibertus Brouwer

GEBOREN TE CAPELLE A.D. IJSSEL IN 1971

Promotiecommissie:

Promotor:	Prof. dr. C. W. J. Beenakker
Referent:	Prof. dr. J. M. J. van Leeuwen
Overige leden:	Prof. dr. P. J. van Baal
	Prof. dr. M. Büttiker (Université de Genève)
	Prof. dr. L. J. de Jongh
	Prof. dr. ir. W. van Saarloos

Het onderzoek beschreven in dit proefschrift is onderdeel van het wetenschappelijk programma van de Stichting voor Fundamenteel Onderzoek der Materie (FOM) en de Nederlandse Organisatie voor Wetenschappelijk Onderzoek (NWO).

aan mijn ouders

Contents

1 Introduction

Electronic systems intermediate between the macroscopic and microscopic regimes are referred to as "mesoscopic". Mesoscopic systems are so small, that a complete quantum-mechanical treatment of the electrons is required if one wants to describe its transport properties. On the other hand, they are so large, that an exact microscopic description, starting from the precise location of impurities and sample boundaries, is not useful, since only the slightest change of the microscopic details will completely change the result. Instead, in mesoscopic physics, a statistical approach is taken: one considers an average over an ensemble of macroscopically equivalent, but microscopically different samples. An example of such an ensemble is a set of dirty wires with the same density of impurities, but with different impurity configurations.

This thesis is about the random matrix theory of quantum transport through mesoscopic systems. The adjective "quantum" indicates that the quantummechanical motion of the electrons is essential. Transport properties of a mesoscopic system can differ significantly from what one would expect on the basis of a classical description. Well-known examples are universal conductance fluctuations and weak localization in disordered wires. The signatures of phase-coherent transport exhibit a high degree of universality. They are independent of sample size or disorder strength and depend entirely on the dimension and the fundamental symmetries of the system (time-reversal symmetry, spin-rotation symmetry). Random matrix theory, originally introduced by Wigner and Dyson to describe the fluctuation properties of resonance spectra of heavy nuclei, provides a natural tool for the study of mesoscopic physics, the universality of quantum interference phenomena in mesoscopic systems being intimately connected to the universality of the statistical properties of the eigenvalues and eigenvectors of large random matrices. For a review of quantum transport in mesoscopic systems, the reader is referred to Refs. [1–3]. The random matrix theory of quantum transport of reviewed in Ref. [4, 5].

In this thesis we establish the relation between random matrix theory of quantum transport and a microscopic description, we discuss how to include deviations from the universal behavior due to the presence of tunnel barriers or dephasing into the random matrix theory, and we consider the dependence of transport properties on an external parameter (Fermi energy, magnetic field). Special attention is paid to normal-metal–superconductor junctions, where the interplay between the phase coherent motion in the normal metal and the superconductivity gives rise to a wide variety of unusual quantum interference phenomena. The present chapter contains background material and a brief introduction to these topics.

1.1 Scattering theory

The scattering matrix represents the solution of the Schrödinger equation for a sample that is connected to semi-infinite leads, in a way that is appropriate for a theory of quantum transport. Below we recall the definition of the scattering matrix and its relation to the conductance via the Landauer formula.

1.1.1 Definition of the scattering matrix

In Fig. 1-1 a mesoscopic sample connected to two ideal leads is shown. For simplicity we assume that the leads are two-dimensional with the same width W. We consider non-interacting spinless "electrons" that are described by a Schrödinger equation

$$\frac{1}{2m}\left[i\hbar\vec{\nabla}+\frac{e}{c}\vec{A}(\vec{r})\right]^2\psi(\vec{r})+V(\vec{r})\psi(\vec{r})=E\psi(\vec{r}), \tag{1.1.1}$$

where $V(\vec{r})$ is the impurity potential, $\vec{A}(\vec{r})$ the vector potential, and the boundary conditions are such that the wavefunction $\psi(\vec{r})$ vanishes outside the sample and the leads. Inside the ideal leads, the potential $V(\vec{r})$ and the magnetic field vanish. Hence the solution of the Schrödinger equation is a combination of plane waves moving to and from the sample,

$$\psi(\vec{r}) \;=\; (k_x W)^{-1/2}\cos(k_y y)\,e^{\pm ik_x x},\;\; k_x^2+k_y^2=k^2\equiv\frac{2mE}{\hbar^2}. \tag{1.1.2}$$

The coordinates x and y refer to the longitudinal and transversal directions, respectively (see Fig. 1-1), and the wavefunctions in Eq. (1.1.2) are normalized such that they carry unit flux. Because of the boundary condition $\psi(x,\pm W/2)=0$, the transversal momentum k_y is quantized. It can take $N=\mathrm{int}(kW/\pi)$ different values $k_y=n\pi/W$ with $n=1,2,\ldots,N$, and thus defines N propagating modes in the lead. Sometimes, these modes are referred to as "channels". We denote the modes in the left (right) lead by ψ_n^{iL} (ψ_n^{iR}) and ψ_n^{oL} (ψ_n^{oR}), where the superscript i (o) is for waves moving towards (from) the sample.

Inside the leads, every solution of the Schrödinger equation (1.1.1) can be written as a sum of ingoing and outgoing propagating waves and evanescent waves [solutions of the form (1.1.2) with imaginary k_x]. Far from the sample, the evanescent waves play no role, and only the propagating waves remain,

$$\psi(\vec{r}) \;=\; \sum_{n=1}^{N}\left[c_n^{iL}\psi_n^{iL}(\vec{r})+c_n^{oL}\psi_n^{oL}(\vec{r})\right]\;\text{if } x\to-\infty, \tag{1.1.3}$$

$$\psi(\vec{r}) \;=\; \sum_{n=1}^{N}\left[c_n^{iR}\psi_n^{iR}(\vec{r})+c_n^{oR}\psi_n^{oR}(\vec{r})\right]\;\text{if } x\to\infty. \tag{1.1.4}$$

The solution of the Schrödinger equation provides a linear relation between coefficients c^{iL}, c^{iR}, c^{oL}, and c^{oR}, which we write as

$$\begin{pmatrix}c^{oL}\\ c^{oR}\end{pmatrix}=S(E)\begin{pmatrix}c^{iL}\\ c^{iR}\end{pmatrix}. \tag{1.1.5}$$

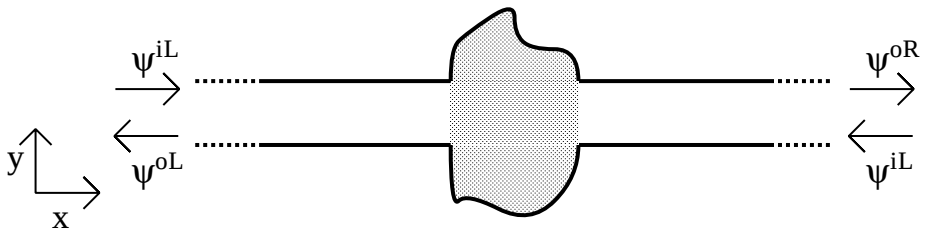

Figure 1-1. Mesoscopic sample (dotted) connected to two semi-infinite ideal leads. The leads have width W and the sample is located between $x = -L/2$ and $x = L/2$.

(Here c^{iL} is the column vector of the coefficients c_n^{iL} etc...) By definition, the $2N \times 2N$ matrix S is the scattering matrix. It is convenient to decompose S into $N \times N$ transmission and reflection matrices r, r', t, and t',

$$S = \begin{pmatrix} r & t' \\ t & r' \end{pmatrix}. \tag{1.1.6}$$

For a wave approaching the sample through the left lead, the reflection matrix r describes the reflected wave exiting through the left lead, and the transmission matrix t describes the transmitted wave in the right lead. Similarly, r' and t' describe reflection and transmission for waves coming from the right lead.

Flux conservation requires that the scattering matrix is unitary

$$SS^\dagger = \mathbb{1}. \tag{1.1.7}$$

If the Hamiltonian preserves time-reversal symmetry [i.e. if there is no vector potential $\vec{A}$ in Eq. (1.1.1)], we find that for every solution $\psi(\vec{r})$, the time-reversed wave function $\psi^*(\vec{r})$ is a solution of the Schrödinger equation as well. Under the operation of time-reversal, the coefficients c_n^i (c_m^o) map to the complex conjugates c_n^{o*} (c_m^{i*}). Hence we have

$$\begin{pmatrix} c^{iL} \\ c^{iR} \end{pmatrix}^* = S \begin{pmatrix} c^{oL} \\ c^{oR} \end{pmatrix}^*. \tag{1.1.8}$$

It follows that the scattering matrix S obeys $SS^* = \mathbb{1}$. In combination with flux conservation [Eq. (1.1.7)], we find that the scattering matrix S is symmetric, $S = S^{\mathrm{T}}$ (the superscript T indicates the transpose of a matrix).

For particles with spin $1/2$, the wave function $\psi(\vec{r})$ in Eq. (1.1.1) is a spinor,

$$\psi(\vec{r}) = \begin{pmatrix} \psi^\uparrow(\vec{r}) \\ \psi^\downarrow(\vec{r}) \end{pmatrix}. \tag{1.1.9}$$

Describing the scattering states in the leads by spinor coefficients c_m^i and c_n^o as well, we

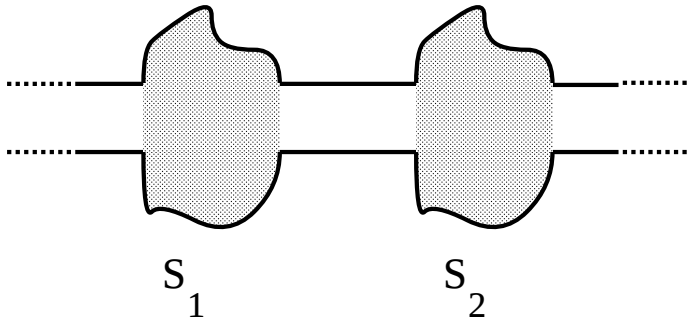

Figure 1-2. Two mesoscopic samples in series. The samples are connected by an ideal lead, so that a scattering approach is appropriate. The left sample has scattering matrix S_1, the right sample has scattering matrix S_2.

arrive at a scattering matrix S that consists of complex quaternions [1]. As in the case of spinless particles, flux conservation requires that that S is unitary, $SS^\dagger = \mathbb{1}$. Under the operation of time-reversal, the spinor coefficients c_n^i (c_m^o) map to $i\sigma_y c_n^{o*}$ ($i\sigma_y c_m^{i*}$), where σ_y is the second Pauli matrix. It follows that the scattering matrix S obeys $SS^* = \mathbb{1}$, where S^* is the quaternion complex conjugate.

Let us now consider the scattering matrix of two mesoscopic samples in series (see Fig. 1-2). We assume, that the two samples are connected by an ideal lead, so that their scattering matrices S_1 and S_2 are well defined. By elimination of the amplitudes of the propagating waves in the lead connecting the two samples, we find the scattering matrix S of the complete system. It has reflection and transmission matrices

$$\begin{aligned} r &= r_1 + t_1'(1 - r_1' r_2)^{-1} r_2 t_1, \\ t &= t_2(1 - r_1' r_2)^{-1} t_1, \\ t' &= t_1'(1 - r_2 r_1')^{-1} t_2, \\ r' &= r_2' + t_2(1 - r_2 r_1')^{-1} r_1' t_2'. \end{aligned} \tag{1.1.10}$$

A more convenient way to find the scattering properties of two samples in a series is the use of a transfer matrix M. The transfer matrix relates the amplitudes in the left and on the right of the sample,

$$\begin{pmatrix} c^{oR} \\ c^{iR} \end{pmatrix} = M \begin{pmatrix} c^{iL} \\ c^{oL} \end{pmatrix}. \tag{1.1.11}$$

Transfer matrices have a multiplicative composition law,

$$M = M_2 M_1. \tag{1.1.12}$$

[1] A quaternion q is a linear combination of the unit matrix and the three Pauli matrices, $q = q_0\mathbb{1} + i\sum_{j=1}^3 q_j\sigma_j$. A quaternion is called real (complex) if the components q_j ($j = 0, 1, 2, 3$) are real (complex) numbers. Quaternions have different rules for the complex conjugate, transposition, and the trace: The complex (hermitian) conjugate $q^* = q_0^* + i\sum_{j=1}^3 q_j^*\sigma_j$ ($q^\dagger = q_0^* - i\sum_{j=1}^3 q_j^*\sigma_j$). The trace of a quaternion is $\mathrm{tr}\, q = q_0$. The complex (hermitian) conjugate Q^* ($Q^\dagger$) of a quaternion matrix Q is the (transpose of the) matrix of complex (hermitian) conjugates. The dual $Q^{\mathrm{R}} = Q^{*\dagger}$. The trace of a quaternion matrix is $\sum_i \mathrm{tr}\, Q_{ii}$.

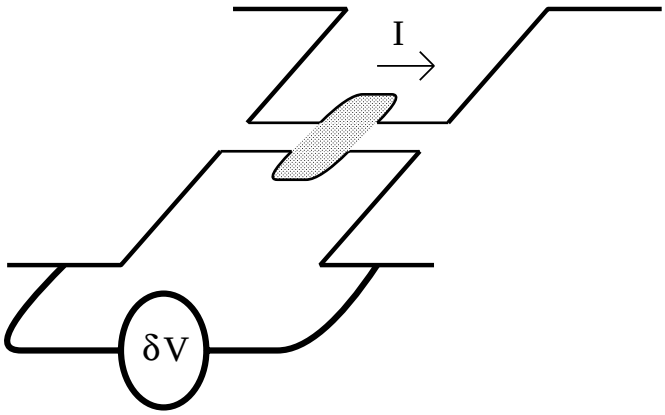

Figure 1-3. Mesoscopic sample (dotted) connected to two electron reservoirs by ideal leads. A voltage difference $\delta V = (1/e)\delta\mu$ between the reservoirs causes a current I through the sample.

Analogous to the decomposition of the scattering matrix in terms of reflection and transmission matrices, we can also decompose the transfer matrix in four blocks,

$$M = \begin{pmatrix} m_{11} & m_{12} \\ m_{21} & m_{22} \end{pmatrix}. \tag{1.1.13}$$

The four blocks of M are related to the reflection and transmission matrices r, r', t, and t' through

$$\begin{aligned} m_{11} &= t^{\dagger -1}, \;\; m_{12} = r' t'^{-1}, \;\; m_{21} = -t'^{-1} r, \;\; m_{22} = t'^{-1}, & (1.1.14) \\ \Longleftrightarrow \;\; r &= -m_{22}^{-1} m_{21}, \;\; r' = m_{12} m_{22}^{-1}, \;\; t = m_{11}^{\dagger -1}, \;\; t' = m_{22}^{-1}. & (1.1.15) \end{aligned}$$

The multiplicative composition law makes the transfer matrix appropriate for a description of quantum transport through a disordered wire.

1.1.2 Landauer formula

The viewpoint that conductance can be seen as a scattering problem goes back to Landauer [7], and has been developed by Imry [8], Büttiker [9], and others. (See Ref. [1] for a review with more applications.)

To derive the Landauer formula, we consider a mesoscopic sample at zero temperature which is connected to electron reservoirs 1 and 2 by means of two ideal leads (Fig. 1-3). The reservoirs are held at chemical potentials μ_1 and μ_2. States with ingoing wave boundary conditions for lead 1 are fed from reservoir 1, so they are occupied for energies $E \leq \mu_1$. Similarly, states coming from lead 2 are occupied for energies $E \leq \mu_2$. Per mode and per unit of energy, the current that is injected from a reservoir into the leads is $2e/h$. For current injected from reservoir 1 in mode n, a fraction $\sum_m |t_{mn}|^2$ is transmitted into lead 2, the rest is reflected back into lead 1. Similarly, for the current that is injected from

reservoir 2 in mode n, a fraction $\sum_m |t'_{mn}|^2$ is transmitted into lead 1, the remainder being reflected. It follows that the currents I is given by

$$\begin{aligned} I &= \frac{2e}{h} \sum_{m,n=1}^{N} \left[\int^{\mu_1} dE (\delta_{mn} - |r_{mn}(E)|^2) - \int^{\mu_2} dE |t'_{mn}(E)|^2 \right], \\ &= \frac{2e}{h} \sum_{m,n=1}^{N} \left[\int^{\mu_1} dE |t_{mn}(E)|^2 - \int^{\mu_2} dE (\delta_{mn} - |r'_{mn}(E)|^2) \right]. \end{aligned} \quad (1.1.16)$$

Here we defined $r_{nm}(E) = r'_{nm}(E) = \delta_{mn}$ and $t_{mn}(E) = t'_{mn}(E) = 0$ if the mode corresponding to n or m is not propagating at energy E. Unitarity of S ensures that $I = 0$ if $\mu_1 = \mu_2$. To first order in the difference $\delta\mu = \mu_1 - \mu_2$, we find

$$\delta I = \frac{2e}{h} \sum_{m,n=1}^{N} |t_{mn}(\mu)|^2 \delta\mu. \quad (1.1.17)$$

Hence the conductance $G = \delta I/\delta V = e\delta I/\delta\mu$ is given by the formula

$$G = \frac{2e^2}{h} \sum_{m,n=1}^{N} |t_{mn}|^2 = \frac{2e^2}{h} \mathrm{tr}\, t t^\dagger, \quad (1.1.18)$$

which is known as the Landauer formula.

1.2 Random matrix theory of a quantum dot

Since the 1950s, when Wigner and Dyson [10–12] first proposed random matrix theory as a tool for the statistical analysis of resonance spectra of heavy nuclei, random matrix theory has found applications in many other branches of physics, including atomic physics, mesoscopic physics, quantum chromo dynamics, and biophysics [13].

In mesoscopic physics, the Wigner-Dyson random matrix theory is appropriate for a statistical description of chaotic quantum dots. A quantum dot is a small metal island, usually confined by gates, and coupled to electron reservoirs by point contacts. The adjective chaotic is used for weakly disordered quantum dots (metal grains) as well as for ballistic dots where the classical motion of the electrons is chaotic. On time scales longer than the time $\tau_{\rm erg}$ needed for ergodic exploration of the phase space, disordered and ballistic quantum dots show the same universal behavior. For a disordered dot with size L, Fermi velocity v_F, and mean free path ℓ, the ergodic time is the time of diffusion through the quantum dot, $\tau_{\rm erg} = L^2/v_F\ell$ ($E_c = \hbar/\tau_{\rm erg}$ is the Thouless energy). For ballistic dots, $\tau_{\rm erg} \sim L/v_F$. In a chaotic quantum dot, the other relevant time scales (dwell time $\tau_{\rm dwell}$, dephasing time τ_ϕ) are much larger than the ergodic time. In this sense, a quantum dot is effectively zero-dimensional, which explains the origin of the name "dot".

Here some of the basic concepts of the Wigner-Dyson random matrix theory are reviewed, with an emphasis on the applications to chaotic quantum dots.

1.2.1 Closed system: random Hamiltonian

A closed quantum dot is characterized through its energy levels and wavefunctions. The precise value of the energy levels and the amplitude of the wavefunction is very sensitive to the impurity configuration or the sample boundaries. Therefore, one usually considers a statistical ensemble of chaotic quantum dots, which have slightly different shapes, Fermi energy, or impurity configuration. Statistical properties of the energy levels and wavefunctions for such an ensemble turn out to be universal. They are independent of the size or shape of the quantum dot, or the impurity concentration, and depend entirely on the basic symmetries of the system: time-reversal symmetry, spin-rotational symmetry, and spatial symmetries. The universality breaks down if energy differences exceed the inverse ergodic time $\hbar/\tau_{\rm erg}$, i.e. if the non-chaotic dynamics on time scales shorter than $\tau_{\rm erg}$ is probed.

The universal statistical properties of a chaotic quantum dot are the same as those of a big random Hermitian matrix H that has the same symmetries as the microscopic Hamiltonian of the quantum dot. For a disordered quantum dot, this correspondence was first conjectured by Gorkov and Eliashberg [14], and later proven by Efetov [15]; for ballistic dots, numerical evidence was first given by Bohigas, Giannoni, and Schmit [16], and an analytical justification was given only very recently by Andreev, Agam, Simons, and Altshuler [17]. The energy levels of the quantum dot correspond to the eigenvalues of the random matrix H, and the wavefunction to its eigenvectors. The precise distribution of the random matrix H is not relevant. This is the celebrated universality of random matrix theory. It is the same universality that governs the statistical properties of the energy levels and wavefunctions of a chaotic quantum and ensures that they do not depend on microscopic details.

Random matrix theory was developed by Wigner and Dyson for the study of nuclear resonance spectra. Wigner originally proposed an ensemble of Hermitian matrices H where all matrix elements are independent Gaussian distributed random numbers. This is the Gaussian ensemble of random-matrix theory. One distinguishes three fundamental symmetry classes, depending on whether the elements of H are real, complex, or real quaternion numbers. The three classes are labeled by the symmetry index β, which counts the degrees of freedom of the matrix elements of H: $\beta = 1$, 2, or 4 if the elements of H are real, complex, or real quaternion numbers, respectively. Real matrices are appropriate for systems with time-reversal symmetry, complex matrices describe a system in which time-reversal symmetry is broken by a magnetic field, while matrices of real or complex quaternions describe a system of spin $1/2$ particles, where spin-rotation symmetry is broken by a spin-orbit interaction. (Hermitian matrices of complex quaternions are not considered explicitly; they behave the same as complex matrices of the double size.) The four possibilities are summarized in Table 1-1.

Though mathematically convenient, the Gaussian distribution is not essential. It is more natural to consider an ensemble of Hermitian matrices with a distribution of the general form

$$P(H) \propto \exp\left[-\beta \mathrm{tr}\, V(H)\right], \tag{1.2.1}$$

where V is some function of H. The choice $V(H) \propto H^2$ corresponds to the Gaussian

TRS	SRS	elements of H	symmetry index
yes	yes	real numbers	$\beta = 1$
yes	no	real quaternions	$\beta = 4$
no	yes	complex numbers	$\beta = 2$
no	no	complex quaternions	$\beta = 2$

Table 1-1. Four symmetry classes, depending on the presence/absence of time-reversal symmetry and spin-rotational symmetry (SRS). The case $\beta = 2$ refers to both cases where time-reversal symmetry is broken.

ensemble. (The factor β in the exponent is added for convenience.) Let $E_1, \ldots, E_M$ be the eigenvalues of the $M \times M$ hermitian matrix H, and let U be the matrix of its eigenvectors. The matrix U is orthogonal (unitary, symplectic) for $\beta = 1$ (2, 4). (It is assumed that the distribution of H does not depend on the eigenvector matrix U.) To find the distribution of the eigenvalues E_j, we use the jacobian between the volume elements dH and the volume elements dU for the matrix U and $\prod_j dE_j$ for the eigenvalues E_j,

$$dH = dU\, J(\{E_j\}) \prod_{j=1}^{M} dE_j, \quad J(\{E_j\}) = \prod_{i<j}^{M} |E_i - E_j|^\beta. \tag{1.2.2}$$

The volume element dU corresponds to the invariant measure on the orthogonal (unitary, symplectic) group.[2] The distribution of the eigenvalues E_j thus reads

$$\begin{aligned} P(\{E_j\}) &\propto J(\{E_j\}) \prod_{j=1}^{N} e^{-\beta V(E_j)} \\ &= \exp\left(\beta \sum_{i<j} \ln|E_i - E_j| - \beta \sum_{j=1}^{N} V(E_j) \right). \end{aligned} \tag{1.2.3}$$

The jacobian $J(\{E_j\})$ causes a repulsion between the levels E_j and E_i ($i, j = 1, \ldots, M$), proportional to $|E_i - E_j|^\beta$.[3] The distribution (1.2.3) resembles a partition function for a gas of N particles in one dimension at positions E_j, subject to a potential $V(E)$, and with a logarithmic Coulomb interaction. The symmetry index β plays the role of the inverse temperature.

[2] The invariant or Haar measure dU on the orthogonal (unitary, symplectic) group is the unique measure dU that is invariant under the group transformations $U \to VUV'$, where V is an arbitrary orthogonal (unitary, symplectic) matrix. An explicit representation of the invariant measure can be found in Sec. 3.1 of this thesis.

[3] To see why the repulsion between levels E_i and E_j is proportional to $|E_i - E_j|^\beta$, notice that to first order in perturbation theory for nearly degenerate levels E_i and E_j, the difference $(E_i - E_j)^2 = (\langle i|H|i\rangle - \langle j|H|j\rangle)^2 + 4|\langle i|H|j\rangle|^2$. The total number of degrees of freedom on the r.h.s. is $\beta + 1$, hence $P(E_i - E_j) \propto |E_i - E_j|^\beta$.

The random matrix H serves as a model for a microscopic Hamiltonian only if we take the limit $M \to \infty$. Contact with a physical Hamiltonian is then made for the distributions of a *finite* number of levels and/or eigenfunction elements, but not for the joint distribution of all M eigenvalues E_j. While Eq. (1.2.3) contains the joint distribution of *all* levels, the main problem in random matrix theory is to extract the physically relevant statistical properties that concern only a *few* levels, such as the density of states, level correlators, or spacing distributions.

The distribution (1.2.3) of the eigenvalues E_j consists of two parts: the Jacobian factor $J(\{E_j\})$, accounting for the "interaction" between the energy levels, and the potential $V(E)$. Their roles are quite different. The potential $V(E)$ determines the average density of states $\langle\rho(E)\rangle$, where

$$\rho(E) = \sum_j \delta(E - E_j). \tag{1.2.4}$$

For the Gaussian ensemble with $V(H) = MH^2/4\lambda^2$ we find for large M and for all three symmetry classes $\beta = 1$, 2, and 4

$$\langle\rho(E)\rangle = \frac{M}{2\pi\lambda^2}\sqrt{4\lambda^2 - E^2}. \tag{1.2.5}$$

The parameter λ governs the mean level spacing $\Delta = \pi\lambda/M$ at the origin $E = 0$. The density of states for the Gaussian ensemble is known as Wigner's semi-circle law. The semi-circular density of states is a characteristic of the Gaussian ensemble, and has no physical relevance: different potentials V have different densities of states.

While the average density of states is determined by the potential V, the fluctuations around the average are determined by the level interactions originating from the jacobian $J(\{E_j\})$ rather than by the potential V, provided energy differences are measured in units of the mean level spacing Δ. The jacobian $J(\{E_j\})$ only depends on the symmetry index β. Hence, up to a scaling factor Δ, spectral fluctuations are universal, and do not depend on the details of the random matrix ensemble. An example is the two-level correlator [6],

$$T_2(E, E') = \langle\rho(E)\rho(E')\rangle - \langle\rho(E)\rangle\langle\rho(E')\rangle - \langle\rho(E)\rangle\delta(E - E'), \tag{1.2.6}$$

which takes the value

$$T_2(E, E') = -\frac{\sin^2[\pi(E - E')/\Delta]}{\pi^2(E - E')^2}, \tag{1.2.7}$$

if $M \to \infty$, irrespective of the confining potential V. Eq. (1.2.7) holds for the unitary ensemble ($\beta = 2$). The expressions for the orthogonal and symplectic ensembles ($\beta = 1$ and 4) are also universal, but more complicated.

For a random matrix ensemble, the universality of the spectral correlators breaks down at energy differences which are comparable to the energy scale E_c on which variations of the mean density of states $\langle\rho(E)\rangle$ occur. For the Gaussian ensemble, this is the scale λ, i.e. the width of the semi-circle. The universality of random matrix theory implies that the ratio $E_c/\Delta \to \infty$ as $M \to \infty$ for each potential V. In a real quantum dot, the role of the cutoff energy E_c is played by the inverse ergodic time $\hbar/\tau_{\rm erg}$: Spectral correlators are universal for energy differences below E_c only; they are sample-specific for distances above E_c.

The circular ensembles, introduced by Dyson [18], consist of unitary rather than Hermitian matrices. Dyson used the circular ensembles as a mathematically more elegant tool to study level statistics. In contrast to Hermitian matrices, the unitary matrices form a compact manifold. Hence there is no need to introduce a potential V to ensure normalization of the probability distribution in the circular ensemble. There are three circular ensembles, consisting of uniformly distributed unitary symmetric, unitary, and unitary self-dual matrices (a unitary self-dual matrix is a unitary matrix S consisting of complex quaternions that satisfies $SS^* = 1$), and labeled by $\beta = 1$, 2, and 4, respectively. They are called the circular orthogonal ensemble (COE), circular unitary ensemble (CUE), and circular symplectic ensemble (CSE).

An $N \times N$ matrix S from the circular ensemble has eigenvalues $e^{i\phi_j}$ with $0 \leq \phi_j < 2\pi$ and $j = 1, \ldots, N$, while the eigenvectors form an orthogonal (unitary, symplectic) matrix U for $\beta = 1$ (2, 4). The uniform distribution of S implies the distribution

$$P(\{\phi_j\}) \propto \prod_{i<j} |e^{i\phi_i} - e^{i\phi_j}|^\beta \tag{1.2.8}$$

for the eigenphases ϕ_j. In Dysons original picture, the eigenphases ϕ_j are viewed as energy levels. Their mean level spacing is $\Delta = 2\pi/N$. In the limit $N \to \infty$, the statistics of the eigenphases ϕ_j on the scale Δ turns out to be the same as those of the energy levels E_j from the Gaussian ensemble. This is another manifestation of the universality of random matrix theory.

1.2.2 Open system: Random scattering matrix

While a closed quantum dot is characterized by energy levels and eigenfunctions, an open dot which is connected to leads is described through its scattering matrix S. The aim of a random matrix theory of quantum transport is a random matrix theory of the statistical distribution of the scattering matrix.

The distribution of the scattering matrix of an open quantum dot is less universal than the distribution of the energy levels and wavefunctions of a closed quantum dot. The reason is quite trivial, because the scattering matrix depends on the size and transparency of the point contacts. If the point contacts are wide, the dimension N of the scattering matrix is large; if they are narrow, N is small. Similarly, if the contacts contain a tunnel barrier, most particles are reflected before they can even enter the dot, so that elements of transmission matrices t and t' are typically smaller than those of the reflection matrices r and r'. Apart from this trivial nonuniversality, the statistics of the scattering matrix of a chaotic quantum dot is universal in the sense that it does not depend on the size or shape of the quantum dot and on the impurity concentration. The only condition for universality is that the particles explore the complete phase space ergodically before they exit, i.e. that the dwell time $\tau_{\rm dwell}$ must be much larger than the ergodic time $\tau_{\rm erg}$. This condition is satisfied for a chaotic quantum dot with point contacts. Another difference between a random matrix theory of the scattering matrix and the random matrix theory of energy levels is that, unlike the Hamiltonian, the scattering matrix is by definition a finite-dimensional matrix. We

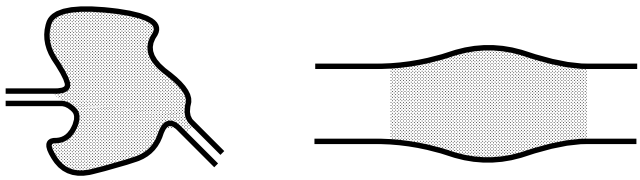

Figure 1-4. The Wigner-Dyson random matrix theory for the scattering matrix is appropriate if the dwell time $\tau_{\rm dwell} \gg \tau_{\rm erg}$, where $\tau_{\rm erg}$ is the time needed for ergodic exploration of the phase space of the sample. This condition is obeyed in chaotic quantum dots (left), but not in bulk metals with wide contacts (right).

can not take the limit $N \to \infty$ for an ensemble of scattering matrices; leads with one propagating mode at the Fermi level can be well realized in experiments, so that a 2×2 scattering matrix makes perfect sense. While the universality of random matrix theory for large random matrices ensures that the choice of the precise potential V in Eq. (1.2.1) is irrelevant for the level statistics, no such freedom exists for a random matrix theory of the scattering matrix.

Two approaches are used to obtain a random matrix theory of the scattering matrix of a chaotic quantum dot. The first approach is the "Hamiltonian approach". It uses random matrix theory for the $M \times M$ Hamiltonian H of the closed quantum dot without leads, and then constructs the $N \times N$ scattering matrix $S(E)$ from H using a standard method in scattering theory, known as R-matrix theory,

$$S(E) = \frac{1 - iK}{1 + iK}, \quad K = W \frac{1}{E - H} W^\dagger. \tag{1.2.9}$$

Here W is a non-random $N \times M$ matrix containing the matrix elements between the states of the sample without leads and the scattering states in the leads. All non-universalities that have to do with the contacts are contained in the matrix W. Since the limit $M \to \infty$ has been taken for the random matrix H, the statistics of the finite-dimensional $N \times N$ scattering matrix S does not depend on the precise distribution of H: it is universal. A review of the Hamiltonian approach can be found in Ref. [19]. Verbaarschot, Weidenmüller, and Zirnbauer [20] have mapped the Hamiltonian approach to the zero-dimensional supersymmetric non-linear σ model of Efetov [15], which in turn has been derived from microscopic models [15, 17].

The second approach is the "scattering matrix approach". It consists of a random matrix theory which applies directly to the scattering matrix S, without the intermediate use of a Hamiltonian. In contrast to the Hamiltonian approach, where the distribution of H is irrelevant, in the scattering matrix approach the details of the distribution of S are important. Blümel and Smilansky [21] have proposed that scattering from a chaotic quantum dot with ballistic point contacts is described by the circular ensemble,

$$P(S) = \text{constant}, \tag{1.2.10}$$

where S is only restricted by symmetry (S is symmetric for $\beta = 1$ and self-dual for $\beta = 4$).

Baranger and Mello [22], and Jalabert, Pichard, and Beenakker [23] have investigated the consequences of Eq. (1.2.10) for quantum transport. For this purpose, the polar decomposition of the scattering matrix is used,

$$S = \begin{pmatrix} u & 0 \\ 0 & v' \end{pmatrix} \begin{pmatrix} \sqrt{1-\mathcal{T}} & i\sqrt{\mathcal{T}} \\ i\sqrt{\mathcal{T}} & \sqrt{1-\mathcal{T}} \end{pmatrix} \begin{pmatrix} u' & 0 \\ 0 & v \end{pmatrix}, \tag{1.2.11}$$

where u, u', v, and v' are $N \times N$ unitary matrices and $\mathcal{T}$ is a diagonal matrix. In the presence of time-reversal symmetry, we have $u^* u' = 1$, $v^* v' = 1$. The (diagonal) elements T_j ($j = 1, \ldots, N$) of $\mathcal{T}$ are the eigenvalues of $tt^\dagger$. They are called transmission eigenvalues. In terms of the transmission eigenvalues, the Landauer formula for the conductance reads

$$G = \frac{2e^2}{h} \sum_{j=1}^{N} T_j. \tag{1.2.12}$$

The distribution of the transmission eigenvalues T_j is found from the jacobian between the volume elements dS on the one hand and du, dv, du', dv', and $\prod_{j=1}^{N} dT_j$ on the other hand,

$$dS = du\, dv\, du'\, dv' \prod_{i<j} |T_i - T_j|^\beta \prod_{j=1}^{N} T_j^{-1+\beta/2} dT_j. \tag{1.2.13}$$

(For $\beta = 1$ and 4 the volume elements du' and dv' are absent due to the symmetry restriction $u^* u' = 1$, $v^* v' = 1$.) Hence we may write

$$\begin{aligned} P(T_1, \ldots, T_N) &= \prod_{i<j} |T_i - T_j|^\beta \prod_{j=1}^{N} T_j^{-1+\beta/2} \\ &= \exp\left(\beta \sum_{i<j} \ln|T_i - T_j| - \beta \sum_{j=1}^{N} V(T_j) \right), \end{aligned} \tag{1.2.14}$$

where the potential $V(T)$ reads

$$V(T) = \begin{cases} \frac{2-\beta}{2\beta} \ln T & \text{if } 0 \le T \le 1, \\ \infty & \text{otherwise.} \end{cases}$$

The formal analogy between distribution (1.2.14) of transmission eigenvalues for a chaotic quantum dot and the distribution of the eigenvalues E_j (1.2.3) of a random hermitian matrix allows one to apply the machinery developed for the study of energy levels of random Hermitian matrices to the problem of transmission eigenvalues. The essential difference between Eqs. (1.2.3) and (1.2.14) is that the former makes sense for large matrices only, while the latter is appropriate for any finite number N of transmission eigenvalues, including $N = 1$.

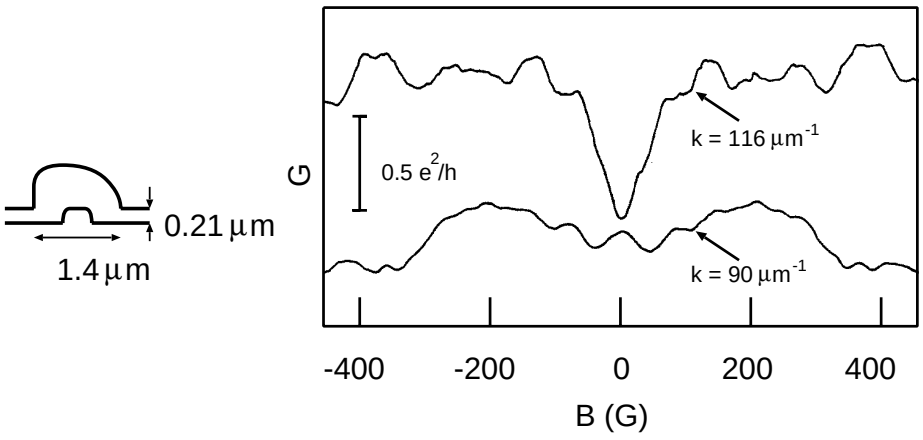

Figure 1-5. Magnetoconductance for a quantum dot shaped like a "stomach" (left) for two different values of the Fermi wavevector k. The width of the point contacts is $0.21\,\mu$m, corresponding to $N = 7$ propagating modes in the point contacts for the upper curve and $N = 6$ for the lower one. The conductance shows universal fluctuations as a function of the magnetic field B and the Fermi wavevector k. Due to weak localization, the ensemble averaged conductance shows a minimum at $B = 0$. For the lower curve, the minimum at $B = 0$ is obscured by the conductance fluctuations, which have the same magnitude. [Figure taken from M. W. Keller et al., Phys. Rev. B **53**, 1693 (1996).]

For single-mode leads, there is only one transmission eigenvalue $T = (h/2e^2)G$ with distribution

$$P(T) = (\beta/2)T^{-1+\beta/2} \tag{1.2.15}$$

The conductance distribution is highly non-Gaussian. For many-mode leads, an approach similar to that for the analysis of spectral correlations of large Hermitian random matrices is taken. One thus finds that the conductance distribution is a Gaussian, with mean and variance given by

$$\langle G\rangle \;=\; \frac{2e^2}{h}\left[\frac{N}{2}+\frac{\beta-2}{4\beta}+\mathcal{O}(N^{-1})\right],\;\; \mathrm{var}\,G = \frac{e^4}{2\beta h^2}. \tag{1.2.16}$$

The leading $\mathcal{O}(N)$ term of $\langle G\rangle$ is the "classical" conductance: classically, only half of the electrons entering the chaotic quantum dot is transmitted, which accounts for an average transmission $1/2$ per mode. The $\mathcal{O}(N^0)$ corrections to the average conductance and the conductance fluctuations are signatures of quantum transport. The $\mathcal{O}(N^0)$ correction to $\langle G\rangle$ is known as the weak localization correction. It is a quantum interference contribution due to the constructive interference of time-reversed paths which slightly enhances the reflection probability. A magnetic field destroys the interference, and thus destroys the weak localization correction to the conductance.

1.3 Random matrix theory of a disordered wire

The Wigner-Dyson random matrix theory does not apply to a disordered wire, because the particles do not have the time to explore the complete phase space of the wire ergodically before they exit. However, in a wire that is much longer than wide, electron motion is still ergodic in the transverse direction. The transverse ergodicity allows for a random matrix theory of transport through a disordered wire.

As in the case of the chaotic quantum dot, two approaches can be taken: A Hamiltonian approach and a scattering matrix approach. The Hamiltonian approach is mapped onto the one-dimensional supersymmetric nonlinear σ model of Efetov and Larkin [24], the scattering matrix approach takes the form of a one-dimensional scaling theory for the transmission eigenvalues of the scattering matrix, derived by Dorokhov [25] and Mello, Pereyra, and Kumar [26]. (For later derivations, see Refs. [27–30].) In both approaches, we may think of the the wire as being built from many weakly disordered slices. If many of these building blocks are put together to form a wire, a central limit theorem ensures universality of the transport properties of the wire, irrespective of the precise microscopic properties of the building block.

1.3.1 Scaling equation for the transmission eigenvalues

The idea behind the scaling equation for the transmission eigenvalues $T_1, \ldots, T_N$ of a disordered wire is that they execute a "Brownian motion" as the length of the wire is increased. The Fokker-Planck equation for this Brownian motion process is known as the Dorokhov-Mello-Pereyra-Kumar (DMPK) equation.

For the derivation of the DMPK equation, the disordered wire is built from many weakly disordered slices and connect them by ideal leads. Weak disorder means $\lambda_F \ll \ell$, where ℓ is the mean free path and λ_F the Fermi wavelength. The slices are so thick that they can be regarded as macroscopic (thickness $\delta L \gg \lambda_F$), and so thin that they are only weakly scattering ($\delta L \ll \ell$). The wire has N propagating modes at the Fermi level. The ideal leads between the slices are necessary for a description in terms of scattering matrices. We now add one extra slice to such a disordered wire (Fig. 1-6) and consider the corresponding change of the transmission eigenvalues.

Let S_1 be the scattering matrix of a disordered wire before the slice is added and let S_2 be the scattering matrix of the slice (see Fig. 1-6). The corresponding transmission and reflection matrices are labeled by a subscript 1 or 2.

We denote the scattering matrix of the total system by S. To find the transmission eigenvalues of S, it is sufficient to consider its reflection matrix r. [The transmission eigenvalues T_n ($n = 1, \ldots, N$) are the eigenvalues of $1 - rr^\dagger$.]

For an ensemble of disordered wires, the scattering matrices S_1 and S_2 are statistically independent. In Refs. [29], an ansatz for the statistical distribution of the reflection matrix r_2 of the slice is proposed,

$$\langle (r_2)_{mn} \rangle \;=\; \mathcal{O}(\delta L)^2,$$

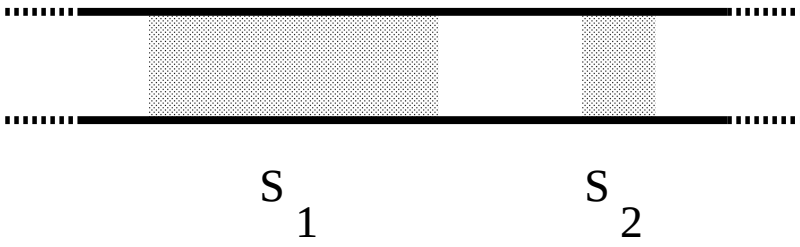

Figure 1-6. A thin slice (with scattering matrix S_2) is added to a disordered wire (with scattering matrix S_1).

$$\langle (r_2)_{kl} (r_2)^*_{mn} \rangle = \frac{\beta \delta L}{(\beta N + 2 - \beta)\ell} \left(\delta_{km}\delta_{ln} + \frac{2-\beta}{\beta} \delta_{kn}\delta_{lm} \right) + \mathcal{O}(\delta L)^2. \quad (1.3.1)$$

(For $\beta = 4$, the complex conjugate should be replaced by the hermitian conjugate of a quaternion.) This ansatz is known as the Equivalent channel model. It also follows from a microscopic model for a disordered wire, which is explained in Sec. 1.3.3. In order to find the transmission eigenvalues $T_1, \ldots, T_N$ of S, we use the polar decomposition (1.2.11) for S_1, and the composition rule (1.1.10). We then find

$$u_1^\dagger r r^\dagger u_1 = w w^\dagger, \;\; w = \sqrt{1-\mathcal{T}_1} - \sqrt{\mathcal{T}_1} \left(1 - \tilde{r}_2 \sqrt{1-\mathcal{T}_1} \right)^{-1} \tilde{r}_2 \sqrt{\mathcal{T}_1}, \quad (1.3.2)$$

where $\tilde{r}_2 = v_1 r_2 v_1'$ and $\mathcal{T}_1$ is the diagonal matrix of transmission eigenvalues corresponding to S_1. The distribution of $\tilde{r}_2$ is the same as that of r_2, because the distribution of r_2 is invariant under transformations $r_2 \to w r_2 w'$ with unitary w and w' ($w'w^* = 1$ for $\beta = 1, 4$). We expand Eq. (1.3.2) in powers of $\tilde{r}_2$ and apply second order perturbation theory to find the increment δT_n of the transmission eigenvalues. The average over r_2 yields

$$\begin{aligned} \ell \left\langle \frac{\delta T_n}{\delta L} \right\rangle &= -T_n + \frac{2T_n}{\beta N + 2 - \beta} \left(1 - T_n + \frac{\beta}{2} \sum_{m \neq n} \frac{T_n + T_m - 2T_n T_m}{T_n - T_m} \right), \\ \ell \left\langle \frac{\delta T_n \delta T_m}{\delta L} \right\rangle &= \delta_{mn} \frac{4T_n^2 (1 - T_n)}{\beta N + 2 - \beta}. \end{aligned} \quad (1.3.3)$$

It then follows from the general theory of Brownian motion [32] that the probability distribution $P(\{T_j\})$ of the transmission eigenvalues $T_1, \ldots, T_n$ of the disordered wire obeys the Fokker-Planck equation

$$\begin{aligned} \frac{\partial P(\{T_j\})}{\partial L} &= \sum_{n=1}^N \frac{\partial}{\partial T_n} \left(-\left\langle \frac{\delta T_n}{\delta L} \right\rangle P + \frac{1}{2} \sum_{m=1}^N \frac{\partial}{\partial T_m} \left\langle \frac{\delta T_n \delta T_m}{\delta L} \right\rangle P \right) \\ &= \frac{2}{\ell(\beta N + 2 - \beta)} \sum_{n=1}^N T_n^2 \frac{\partial}{\partial T_n} (1 - T_n) J(\{T_j\}) \frac{\partial}{\partial T_n} \frac{P(\{T_j\})}{J(\{T_j\})}, \quad (1.3.4) \\ J(\{T_j\}) &= \prod_{k<l} |T_k - T_l|^\beta. \quad (1.3.5) \end{aligned}$$

This is the DMPK equation. Usually, it is written down in terms of parameters $\lambda_j = 1/T_j - 1$. (The parameters λ_j are natural in a transfer-matrix approach.)

The study of the DMPK equation has developed into a field of its own. For a comprehensive review, the reader is referred to Ref. [5]. For a thick wire ($N \gg 1$), there are three characteristic regimes: the ballistic regime $L \lesssim \ell$, the diffusive regime $\ell \lesssim L \lesssim \xi$, and the localized regime $L \gtrsim \xi$ ($\xi = \beta N \ell$ is the localization length).

- The ballistic regime is not very interesting. All transmission eigenvalues are close to 1, and the conductance $G \simeq 2e^2 N/h$. The conductance fluctuations are small [var G is of relative order $(\ell/L)^2$].

- In the diffusive regime $\ell \lesssim L \lesssim \xi$ the density of transmission eigenvalues of bimodal,

$$\langle \rho(T) \rangle \simeq \frac{N\ell}{LT(1-T)^{1/2}}. \tag{1.3.6}$$

  Approximately a fraction ℓ/L of the transmission eigenvalues is close to 1, the remainder being close to 0. Statistical properties of the conductance are commonly expressed in terms of a large-N expansion. The conductance distribution is Gaussian, with mean and variance given by

$$\langle G \rangle = \frac{2e^2}{h}\left(\frac{N\ell}{L} + \frac{\beta-2}{3\beta} + \mathcal{O}(N^{-1})\right), \quad \text{var}\, G = \left(\frac{2e^2}{h}\right)^2 \frac{2}{15\beta} + \mathcal{O}(N^{-1}). \tag{1.3.7}$$

  The $\mathcal{O}(1)$ contribution to the average conductance is the weak localization correction [33, 34]. It is called "weak" because it is small compared to the leading $\mathcal{O}(N)$ term, and "localization" because it is a negative correction to the conductance (for $\beta = 1$; for $\beta = 4$ the name "weak anti-localization" is more appropriate). Both the weak localization correction and the variance of the conductance [35, 36] are universal, since they depend on the symmetry index β, and on the fundamental constants e and h only, and not on the sample-specific parameters N, ℓ, and L. Weak localization and universal conductance fluctuations are signatures of quantum transport. Weak localization is due to constructive interference of time-reversed paths, and is destroyed if time-reversal symmetry is broken by a magnetic field. Conductance fluctuations are also caused by interference of Feynman paths, but no intuitive picture exists. (Similar universal quantum interference effects are found for a chaotic quantum dot in with many-mode point contacts, see Sec. 1.2.)

- In the localized regime, all transmission eigenvalues are exponentially small. The conductance G is determined by the largest transmission eigenvalue T_1. It is found that $\log T_1$ has a Gaussian distribution with mean $-2L/\xi$ and variance $4L/\xi$. Hence the distribution of the conductance is log-normal,

$$-\langle \ln(hG/2e^2) \rangle = (1/2)\text{var}\,[\ln(hG/2e^2)] = 2L/\xi. \tag{1.3.8}$$

For the distribution of the conductance in the diffusive regime, the DMPK equation merely confirms results that were already known from diagrammatic perturbation theory [33–36]. The advantage of the DMPK equation is that it gives access to the complete distribution of transmission eigenvalues. This is important for other transport properties, like the shot noise power [37] or the conductance of a normal sample with one superconducting contact (see next section). The DMPK equation is the natural theoretical tool for the description of the log-normal conductance distribution in the localized regime.

1.3.2 Distribution of the unitary matrices in the polar decomposition

The DMPK equation describes the distribution of the transmission eigenvalues $T_1, \ldots, T_N$ of a disordered wire. For some applications, it is not sufficient to know the distribution the transmission eigenvalues; we also need the unitary matrices u, u', v, and v' that appear in the polar decomposition of the scattering matrix. Little is known about their distribution. Here we investigate the consequences of the equivalent-channel assumption (1.3.1) for their distribution.

Consider the polar decomposition of the scattering matrix S_2 of the thin slice,

$$S_2 = \begin{pmatrix} u_2 & 0 \\ 0 & v_2' \end{pmatrix} \begin{pmatrix} \sqrt{1-\mathcal{T}} & i\sqrt{\mathcal{T}} \\ i\sqrt{\mathcal{T}} & \sqrt{1-\mathcal{T}} \end{pmatrix} \begin{pmatrix} u_2' & 0 \\ 0 & v_2 \end{pmatrix}, \tag{1.3.9}$$

For $\beta = 1, 4$ we have $u_2^* u_2' = v_2^* v_2' = 1$. The distribution (1.3.1) implies that for a thin slice — after integration over v_2 and v_2' — the unitary matrices u_2 and u_2' are uniformly distributed in the unitary group, independent of the transmission eigenvalues. This turns out to be true for wires of arbitrary length. To see, we use induction. We assume that the uniform distribution of u and u' is true for the scattering matrices S_1 and S_2 of the wire and the slice separately, and then show that it holds for the scattering matrix S of the total system. If we add the slice on the right side, we find

$$r = r_2 + t_2'(1 - r_1 r_2')^{-1} r_1 t_2. \tag{1.3.10}$$

In terms of the polar decompositions of S_1 and S_2, we have

$$r = u_2\sqrt{1-\mathcal{T}_2}v_2 - u_2\sqrt{\mathcal{T}_2}\left(1 - w_1\sqrt{1-\mathcal{T}_1}w_1'\sqrt{1-\mathcal{T}_2}\right)^{-1} w_1\sqrt{1-\mathcal{T}_1}w_1'\sqrt{\mathcal{T}_2}v_2, \tag{1.3.11}$$

where $w_1 = v_2 u_1$ and $w_1' = u_1' v_2'$. Since u_1 and u_1' are uniformly distributed, w_1 and w_1' are so too. As the scattering matrices S_1 and S_2 are independently distributed, the distribution of r is invariant under transformations $r \to u r u'$, which proves the uniform distribution of the matrices u and u' for the polar decomposition of S.

In their original paper, Mello, Pereyra, and Kumar [26] assumed that all four unitary matrices u_2, u_2', v_2, and v_2' from the polar decomposition of the scattering matrix of the thin slice are uniformly distributed in the unitary group (only restricted by symmetry). This much stronger assumption is known as the isotropy assumption. For the results presented in this thesis, the isotropy assumption is not necessary; it is sufficient to use the equivalent channel assumption (1.3.1) of Mello and Tomsovic [29].

1.3.3 Microscopic model

Dorokhov [31] has formulated a microscopic model for which the statistical distribution of the reflection matrix of a thin slice is given by Eq. (1.3.1). In this model, the wire is modeled by N parallel one-dimensional chains. The disorder is modeled by a Gaussian white noise potential that admits inter-chain hopping. The wavefunction is represented by a vector $\psi_n(x)$, and the Hamiltonian reads

$$\mathcal{H}\psi_n(x) = \frac{-\hbar^2}{2m}\vec{\nabla}^2\psi_n(x) + \frac{k\hbar^2}{2m}\sum_m u_{nm}(x)\psi_m(x) = E\psi_n(x). \tag{1.3.12}$$

Here the wavenumber $k = 2\pi/\lambda_F$ is defined through $E = \hbar^2k^2/2m$ and $u_{nm}(x)$ is a random disorder potential with a Gaussian distribution with zero mean and with variance

$$\langle u_{kl}(x)u_{mn}(x')\rangle = \frac{4}{\ell N}\delta(x-x')\left[\delta_{kn}\delta_{lm} + \frac{2-\beta}{\beta}\delta_{km}\delta_{ln}\right], \tag{1.3.13}$$

where ℓ is the mean free path. The matrix $u(x)$ consists of real (complex, quaternion) numbers for $\beta = 1$ (2, 4). We now consider a thin disordered slice which lies between $x = 0$ and $x = \delta L$, where $\lambda_F \ll \delta L \ll \ell$. Up to second order Born approximation we find for the reflection matrix r of this thin slice

$$r_{mn} = i\int_0^{\delta L} dx u_{mn}(x)e^{2ikx} - \sum_{l=1}^{N}\int_0^{\delta L} dx \int_0^{\delta L} dx' e^{ikx'}u_{ml}(x)u_{ln}(x')e^{ikx}e^{ik|x'-x|}.$$

The first two moments of r are computed using the Gaussian white noise distribution of u. After integration over rapidly oscillating terms, we find

$$\begin{aligned}
\langle r_{mn}\rangle &= 0, \\
\langle r_{kl}r_{mn}\rangle &= 0, \\
\langle r_{kl}r^*_{mn}\rangle &= \frac{\beta\delta L}{\ell(\beta N + 2 - \beta)}\left(\delta_{km}\delta_{ln} + \frac{2-\beta}{\beta}\delta_{kn}\delta_{lm}\right),
\end{aligned}$$

This is precisely the distribution of Eq. (1.3.1).

1.4 Normal-metal–superconductor junctions

Being the result of interference between (quantummechanical) waves, signatures of quantum transport are strongly dependent on boundary conditions. Any agent that modifies the boundary conditions, also modifies the phases of the electrons and thus rearranges the interference pattern. An example is the Aharonov-Bohm effect, where the conductance of a mesoscopic ring depends sensitively on the amount of flux through the ring, while the magnetic field in the metal itself is zero. The flux through the ring modifies the phase of the electrons, but does not change their classical motion.

A more fundamental change of boundary conditions is caused by the presence of a superconducting contact. At the normal-metal–superconductor (NS) interface, the dissipative electrical current in the normal metal is converted to a dissipationless supercurrent by the mechanism of Andreev reflection [38]. Andreev reflection is special, because in addition to a modification of phases, it also couples the motion of electrons (occupied states at an energy ε above the Fermi level) and holes (vacancies at energy ε below the Fermi level). The interplay between Andreev reflection at the normal-metal–superconductor interface and the quantum interference inside the normal metal results in new and unexpected signatures of quantum transport [39].

In this section, we briefly discuss the scattering theory of Andreev reflection. The advantage of the scattering theory is that it allows us to relate transport properties of hybrid normal-metal–superconductor structures to the scattering matrix of the normal metal only. In this way we can directly apply our results for the statistical distribution of the scattering matrix of a normal metal chaotic quantum dot or a disordered wires to mesoscopic samples with a superconducting contact.

1.4.1 Andreev reflection

The microscopic equation for a system with both normal metals and superconductors is the Bogoliubov-De Gennes equation [40]. It has the form of two coupled Schrödinger equations for the electron and hole wavefunctions $u(\vec{r})$ and $v(\vec{r})$,

$$\begin{pmatrix} \mathcal{H}_0 & \Delta(\vec{r}) \\ \Delta^*(\vec{r}) & -\mathcal{H}_0^* \end{pmatrix} \begin{pmatrix} u(\vec{r}) \\ v(\vec{r}) \end{pmatrix} = \varepsilon \begin{pmatrix} u(\vec{r}) \\ v(\vec{r}) \end{pmatrix}. \tag{1.4.1}$$

Electrons are occupied states at an energy ε above the Fermi level E_F, holes are empty states at an energy ε below E_F. The operator $\mathcal{H}_0$ is the single-electron Hamiltonian and $\Delta(\vec{r})$ is the pair potential, which is determined by the self-consistency equation

$$\Delta(\vec{r}) = g(\vec{r}) \sum_{\varepsilon>0} v^*(\vec{r}) u(\vec{r}) [1 - 2 f(\varepsilon)] \tag{1.4.2}$$

where g is the BCS interaction constant and $f(\varepsilon)$ is the Fermi function. In the normal metal, $g = 0$ and hence $\Delta = 0$. At the superconducting side of the interface, $\Delta(\vec{r})$ approaches its bulk value $\Delta_0 e^{i\phi}$ only at a finite distance from the interface. Here, we neglect the suppression of Δ near the interface, and use a step-function model for $\Delta(\vec{r})$. This is allowed for junctions between a normal metal and a superconductor that consists of a point contact or a tunnel barrier [41]. In this approximation, the Bogoliubov-De Gennes equation reduces to a simple scattering problem for the electrons and holes in the normal metal.

For a scattering theory of Andreev reflection, we consider a normal-metal–superconductor (NS) interface as shown in Fig. 1-7. The normal metal on the left is an ideal lead with N propagating modes at the Fermi level. The pair potential vanishes in the normal metal, so that the solution of the Bogoliubov-de Gennes equation consists of separate plane waves

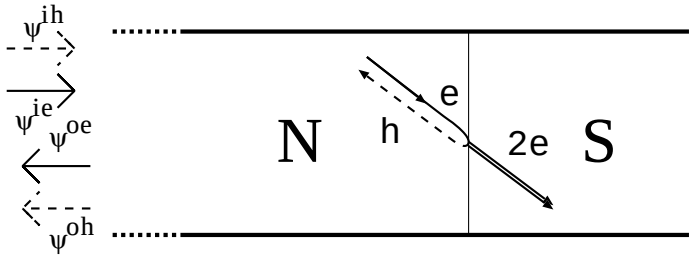

Figure 1-7. Schematic drawing of an NS interface. At the interface, an electron coming from N (solid arrow) is retroreflected as a hole (dashed). At the same time, a Cooper pair is added to the superconducting condensate. The normal metal side of the interface is connected to an ideal lead, where the wavefunctions for the electrons and the holes are given by incoming and outgoing plane waves.

for the electrons and the holes. Proceeding as in Sec. 1.1, where we discussed the scattering theory for normal metals, we denote the amplitudes of the incoming and outgoing electron and hole waves with c_n^{ie}, c_n^{oe}, c_n^{ih}, and c_n^{oh} ($n = 1, \ldots, N$). At the superconducting side of the interface, no propagating solutions of the Bogoliubov-de Gennes equation exist for excitation energies $\varepsilon < \Delta_0$.

In the limit $\varepsilon \ll \Delta, E_F$, the appropriate solution of the Bogoliubov-de Gennes equation leads to the $2N \times 2N$ scattering matrix $\boldsymbol{S}_{\mathrm{A}}$ for Andreev reflection [42]

$$\begin{pmatrix} c^{oe} \\ c^{oh} \end{pmatrix} = \boldsymbol{S}_{\mathrm{A}}(\varepsilon) \begin{pmatrix} c^{ie} \\ c^{ih} \end{pmatrix}, \quad \boldsymbol{S}_{\mathrm{A}}(\varepsilon) = -i \begin{pmatrix} 0 & e^{i\phi} \\ e^{-i\phi} & 0 \end{pmatrix}. \tag{1.4.3}$$

An electron coming from the normal metal is reflected as a hole and vice versa. The total charge in the process of Andreev reflection is conserved by the addition of a Cooper pair to the superconducting condensate. If the NS interface is non-ideal (e.g. if it contains a tunnel barrier), the scattering matrix $\boldsymbol{S}_{\mathrm{A}}$ also contains diagonal blocks.

The scattering matrix $\boldsymbol{S}^{\mathrm{A}}$ has an electron-hole (*e*-*h*) grading. If we want to consider the scattering properties of a system that contains both a normal metal (e.g. a chaotic quantum dot or a disordered wire) and a superconductor, it is necessary to extend the notation with *e*-*h* graded scattering matrices $\boldsymbol{S}$ to the normal metal. Since electrons and holes do not interact in a normal metal, the scattering matrix $\boldsymbol{S}_{\mathrm{N}}(\varepsilon)$ for normal scattering of electrons and holes is block diagonal,

$$\boldsymbol{S}_{\mathrm{N}}(\varepsilon) = \begin{pmatrix} S(\varepsilon) & 0 \\ 0 & S(-\varepsilon)^* \end{pmatrix}. \tag{1.4.4}$$

The matrix $S(\varepsilon)$ is the well-known scattering matrix for a normal metal sample with two normal contacts. Holes, being the time-reversed particles of electrons, are described by the complex conjugate scattering matrix $S(-\varepsilon)^*$. The off-diagonal blocks of $\boldsymbol{S}_{\mathrm{N}}$ are zero.

1.4.2 Conductance of an NS junction

What is the conductance of a normal metal with one normal and one superconducting contact? At the normal-metal–superconductor interface, electron are reflected as holes, so that charge is transported in units of $2e$. Hence, if the transmission of the normal metal is perfect, the replacement of one normal contact by a superconductor doubles the conductance. (The conductance is $4e^2/h$ per propagating mode, compared to $2e^2/h$ for normal contacts.) The problem is more complicated if the normal metal is resistive. The complication arises, because in order to contribute to the conductance, both the electron and the Andreev-reflected hole must pass through the resistive metal. A simple estimate for the conductance $G_{\rm NS}$ of an NS junction is that the effective length of the resistive normal metal is multiplied by a factor two,

$$G_{\rm NS}(L) = 2G_{\rm N}(2L). \tag{1.4.5}$$

For a disordered junction ($G_{\rm N}(L) \propto 1/L$), the increase of the effective length essentially compensates the extra factor two due to the doubling of the charge quantum.

The simple estimate (1.4.5) does not take quantum interference into account. Lambert [43] and Takane and Ebisawa [44] have derived a generalization of the Landauer formula for the differential conductance $G_{\rm NS} = dI/dV$ of a normal-metal–superconductor junction, that admits a complete phase-coherent treatment of the transport problem. Their conductance formula relates $G_{\rm NS}$ to an off-diagonal block of the *e-h* graded scattering matrix $\boldsymbol{S}$ of the NS junction

$$G_{\rm NS}(V) = \frac{4e^2}{h} \mathrm{tr}\, S^{eh}(eV) S^{eh\dagger}(eV). \tag{1.4.6}$$

It remains to compute the scattering matrix $\boldsymbol{S}$ from the individual scattering matrices $\boldsymbol{S}_{\rm N}$ and $\boldsymbol{S}_{\rm A}$ for the normal metal and the NS interface. This was done by Beenakker [42] for the general setup shown in Fig. 1-8. The system consists of a normal metal sample, with scattering matrix $S(\varepsilon)$. The normal sample is connected two ideal leads with N propagating modes each. The left lead is coupled to a normal reservoir, the right one is coupled to a superconductor. The $2N \times 2N$ reflection and transmission matrices of the normal metal also have an electron-hole grading,

$$\boldsymbol{r}(\varepsilon) = \begin{pmatrix} r(\varepsilon) & 0 \\ 0 & r(-\varepsilon)^* \end{pmatrix}, \quad \boldsymbol{t}(\varepsilon) = \begin{pmatrix} t(\varepsilon) & 0 \\ 0 & t(-\varepsilon)^* \end{pmatrix} \text{ etc.} \tag{1.4.7}$$

Then the $2N \times 2N$ scattering matrix $\boldsymbol{S}$ of the complete system follows from a composition rule similar to Eq. (1.1.10),

$$\boldsymbol{S}(\varepsilon) = \boldsymbol{r}(\varepsilon) + \boldsymbol{t}'(\varepsilon) \left[1 - \boldsymbol{S}_{\rm A}(\varepsilon)\boldsymbol{r}'(\varepsilon)\right]^{-1} \boldsymbol{S}_{\rm A}(\varepsilon)\boldsymbol{t}(\varepsilon). \tag{1.4.8}$$

Substitution of Eq. (1.4.8) into the general conductance formula (1.4.6) yields

$$G_{\rm NS}(V) = \frac{4e^2}{h} \,\mathrm{tr}\, mm^\dagger, \quad m = t(-eV)^* \left(1 + r(eV)r(-eV)^*\right)^{-1} t'(eV). \tag{1.4.9}$$

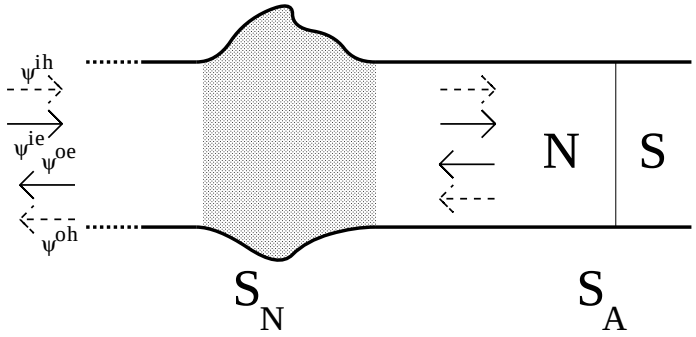

Figure 1-8. Normal metal sample (dotted) connected to two ideal leads. One lead is coupled to a superconductor. The system is described by two scattering matrices, $\boldsymbol{S}_{\rm N}$ and $\boldsymbol{S}_{\rm A}$, for scattering from the normal metal sample and from the normal-metal–superconductor interface, respectively.

If the applied bias eV is much less than the inverse dwell time in the normal metal, we may neglect the difference between $S(eV)$ and $S(-eV)$. If in addition, there is no magnetic field, one finds that Eq. (1.4.9) simplifies considerably [42],

$$G_{\rm NS} = \frac{4e^2}{h} \sum_{n=1}^{N} \frac{T_n^2}{(2-T_n)^2}. \tag{1.4.10}$$

The conductance depends on the transmission eigenvalues T_n of the normal metal only. For nonzero excitation energy or in the presence of a magnetic field no such simplification occurs; the conductance of the NS junction depends on the entire scattering matrix of the normal metal.

Remarkably, for a disordered NS junction, the conductance formula (1.4.9) turns out to agree precisely with the simple estimate (1.4.5) up to small corrections of order e^2/h. This phenomenon is commonly referred to as "reentrant superconductivity", because the equality of $G_{\rm N}$ and $G_{\rm NS}$ that is implied by Eq. (1.4.5) is true for high temperatures $kT \gg \hbar v_F \ell/L^2$ and $T = 0$, but not for intermediate temperatures $0 \lesssim kT \lesssim \hbar v_F \ell/L^2$. Eq. (1.4.5) is not valid for quantum interference effects (weak-localization, conductance fluctuations), which can be found from a complete quantummechanical treatment only.

The advantage of the formulation in terms of the scattering matrices $\boldsymbol{S}_{\rm N}$ and $\boldsymbol{S}_{\rm A}$ is that it allows us to separate the contributions from the normal metal and the superconductor. We can use the same scattering matrix $S(\varepsilon)$ for applications to transport through a normal metals with or without superconducting contacts. In this way, transport properties of NS junctions can be obtained without much extra work, once the problem is solved for the normal metal without the superconducting contact.

1.5 This thesis

In this thesis, we consider the microscopic justification of the random matrix theory of quantum transport as well as applications to chaotic quantum dots, disordered wires, and

normal-metal–superconductor junctions.

The Chapters 2–4 are about the random matrix theory of chaotic quantum dots. The equivalence between the scattering matrix approach and the Hamiltonian approach for quantum transport through chaotic quantum dots is established. In view of the equivalence of the Hamiltonian approach and the microscopic theory, this provides a microscopic justification of the random scattering matrix approach to chaotic scattering. In Ch. 2, we address the distribution of the scattering matrix, a model for dephasing is discussed in Ch. 3, and Ch. 4 deals with the dependence on external parameters, such as the Fermi energy or the magnetic field. The random matrix theory of a disordered wire is studied in Chapter 5. We prove that the one-dimensional nonlinear σ-model and the Dorokhov-Mello-Pereyra-Kumar equation are equivalent. This completes the microscopic justification of the random matrix theory of quantum transport. In chapter 6, a diagrammatic technique for integration over the unitary group is developed. The diagrammatic technique is an important tool for the computation of transport properties in the scattering matrix approach. Finally, Chapter 7 contains applications to hybrid normal-metal–superconductor structures. We use the diagrammatic technique of Ch. 6 to compute the weak-localization correction to the conductance and the conductance fluctuations. Below a brief introduction to each of the chapters is given.

Chapter 2: Chaotic quantum dots with non-ideal leads.

In Sec. 1.2 we discussed the two approaches for the random matrix theory of quantum transport through chaotic quantum dots. In the Hamiltonian approach, the scattering matrix is computed from the random Hamiltonian H of the closed quantum dot and a non-random matrix W that describes the overlap between the states inside the quantum dot and the scattering states in the leads. In the scattering matrix approach, the scattering matrix S itself is a random matrix, drawn from the circular ensemble of random matrix theory. The validity of the Hamiltonian approach has been established through a mapping onto the zero-dimensional nonlinear σ-model [20], which in turn has been derived from microscopic theory [15, 17]. We establish the validity of the circular ensemble by deriving it from the Hamiltonian approach, building on earlier work by Lewenkopf and Weidenmüller [45].

The advantage of the circular ensemble is that is conceptually simpler than the Hamiltonian approach, which requires a σ-model formulation for actual calculations [20]. Its limitation, however, is that the circular ensemble is appropriate for chaotic quantum dots with ideal ballistic point contacts (ideal leads) only. The Hamiltonian approach, on the other hand, can also describe tunneling point contacts (non-ideal leads).

In Sec. 2.1 we consider the special case of a quantum dot with two single-mode point contacts. The point contacts contain tunnel barriers. We describe the system consisting of the chaotic quantum dot and the tunnel barriers by three separate scattering matrices. The scattering matrix S_d of the chaotic cavity is taken from the circular ensemble,

$$P(S_d) = \text{constant}, \tag{1.5.1}$$

while the scattering matrices S_b of the tunnel barriers are fixed. To obtain the scattering properties of the total system we change to a transfer matrix formulation. We multiply the

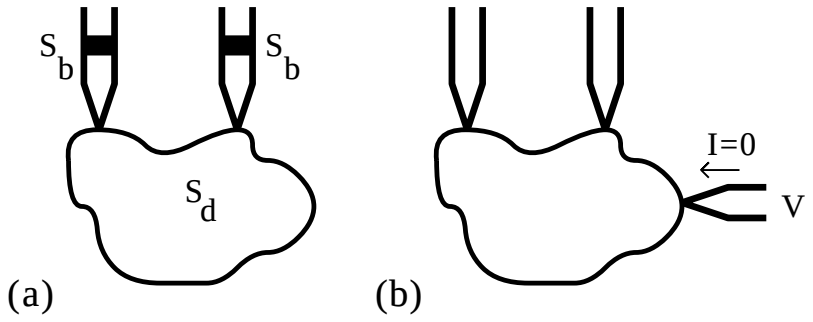

Figure 1-9. (a) A chaotic quantum dot with ballistic point contacts and leads containing tunneling point contacts. The scattering matrix S_d of the quantum dot is taken from the circular ensemble, the scattering matrices S_b of the tunnel barriers are fixed. (b) A quantum dot with a voltage probe. The voltage probe is an extra lead that is coupled to a reservoir, of which the potential V is adjusted in such a way, that the current I through the voltage probe is zero.

transfer matrices M_d and M_b of the dot and the barriers, respectively, and find the transfer matrix M of the total system.

$$M = M_b M_d M_b. \tag{1.5.2}$$

The resulting distribution of the conductance G agrees completely with previous work of Prigodin, Efetov, and Iida [48], who used the σ-model formulation of the Hamiltonian approach.

For the general case of a $N \times N$ scattering matrix, we take a slightly different approach. Starting point is that the direct scattering from the tunnel barriers results in a nonzero value of the ensemble averaged scattering matrix $\bar{S}$. It is convenient to adopt $\bar{S}$ as a measure for the non-ideality of the leads [46]. Mello, Pereyra, and Seligman [47] derived an extension of the circular ensembles with a nonzero value of $\bar{S}$. Requiring analycity of the scattering matrix in the upper half of the complex plane, ergodicity (energy average equals ensemble average), and maximum information entropy of the distribution, they arrived at a distribution known as the Poisson kernel [49],

$$P_{\bar{S}}(S) \propto \left|\det(1 - \bar{S}^\dagger S)\right|^{-(\beta N + 2 - \beta)}. \tag{1.5.3}$$

The use of the maximum entropy principle is necessary, because the Poisson kernel is not the only ensemble with nonzero $\bar{S}$ that obeys the analycity and ergodicity requirement.

In Sec. 2.2, we derive the Poisson kernel from the Hamiltonian approach, thus providing a microscopic justification of the Poisson kernel for scattering from a chaotic quantum dot. For technical reasons, we replace the Gaussian distribution for the $M \times M$ random Hamiltonian H of the quantum dot by a Lorentzian one,

$$P(H) \propto \det\left(\lambda^2 + (H - \varepsilon)^2\right)^{-(\beta M + 2 - \beta)/2}. \tag{1.5.4}$$

(The parameter λ governs the mean level spacing at $E = 0$.) The replacement of the Gaussian distribution by the Lorentzian distribution is allowed, because in the limit $M \rightarrow$

∞ the scattering matrix distribution does not depend on the precise distribution of H. We finally show that the Poisson kernel also agrees with the approach of Sec. 2.1, where separate scattering matrices for the tunnel barriers are combined with a uniform distribution of scattering matrices for the quantum dot.

Chapter 3: Dephasing in quantum dots.

The quantummechanical phase of the electrons is only conserved for some finite time τ_ϕ, the dephasing time. Dephasing may be caused by electron-electron interactions, or by interactions with external sources (radiation, fluctuations of gate voltages, etc.) For a comparison between theory and experiment, it is necessary to know how dephasing affects the signatures of quantum transport. The dephasing time τ_ϕ can be measured from the weak localization correction δG, since δG is unaffected by thermal smearing (see Fig. 1-10).

A controlled way to introduce dephasing is to attach a voltage probe to the sample [50]. A voltage probe is an extra lead, coupled to an electron reservoir of which the potential is chosen such that no current is drawn (see Fig. 1-9b). Although a voltage probe draws no current, it destroys phase coherence, because it allows electrons to temporarily exit the sample, and loose their phase memory in the reservoir.

In Sec. 3.1, we consider the effect of such a voltage probe on the phase-coherent conductance of a chaotic quantum dot with two single-mode leads. We start from a situation where a voltage probe with one propagating mode is coupled to the quantum dot by means of a high tunnel barrier. In this limit, phase coherence is not affected. The conductance distribution is highly non-Gaussian [cf. Eq. (1.2.15)]. We slowly increase the amount of dephasing by first decreasing the reflection of the tunnel barrier, and then increasing the number of modes N in the voltage probe. If the voltage probe contains many modes, phase coherence is completely destroyed, and the conductance distribution becomes a delta function around the classical value e^2/h.

Can we use a voltage probe as a model for real dephasing in a quantum dot? For a voltage probe with only a few modes, the answer is clearly no, because (1) it allows for integer dephasing rates only and (2) dephasing occurs uniformly in space, while the dephasing caused by the voltage probe is restricted to a very small space. The introduction of a tunnel barrier (with transparency Γ) in the voltage probe cures the first problem, but causes a new one: we now have two model parameters (Γ and N) to describe dephasing, while dephasing is characterized by a single dephasing time τ_ϕ only.

A different way to treat dephasing is used in the Hamiltonian approach [51, 52]. Here, a spatially uniform absorbing potential, which removes particles from the phase coherent motion in the quantum dot, is added to the Hamiltonian. The drawback of this "imaginary-potential model" is that an absorbing potential does not conserve the particle number.

In Sec. 3.2 both approaches are reconciled. A new version of the voltage probe model is presented that does not suffer from the problems sketched above. It consists of a voltage probe with many propagating channels ($N \gg 1$), and with a high tunnel barrier ($\Gamma \ll 1$), such that the product $\gamma = N\Gamma$ is finite. The parameter γ is related to the dephasing rate and the mean level spacing Δ, $\gamma = h/\tau_\phi\Delta$. We show that the new version of the voltage probe model is consistent with the Hamiltonian approach: For a chaotic quantum dot, the escape

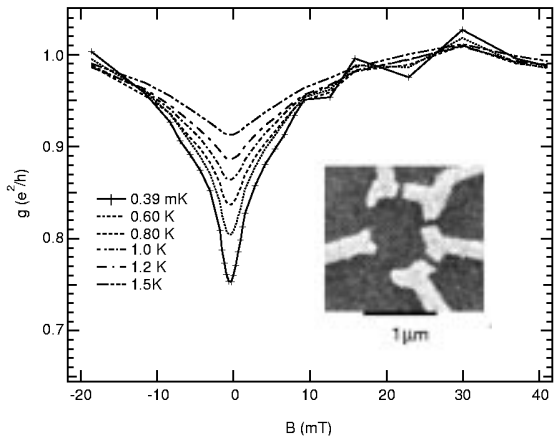

Figure 1-10. Ensemble-averaged magnetoconductance $\langle G(B)\rangle$ for a quantum dot with two single-mode point contacts (inset). The reduction of $\langle G(B)\rangle$ near $B = 0$ is due to weak localization. The reduction is destroyed if time-reversal symmetry is broken by a weak magnetic field. The size of the weak-localization correction is affected by dephasing, but not by thermal smearing. Therefore, weak localization can be used to measure the dephasing time τ_ϕ. [Figure taken from C. M. Marcus et al., Chaos, Solitons & Fractals, to be published.]

of particles through a tunneling point contact with $N \to \infty$ and $\Gamma \to 0$ is rigorously equivalent to the absorption by a spatially uniform imaginary potential.

Chapter 4: Time delay in chaotic scattering.

This chapter deals with the dependence of the scattering matrix on the energy E and on another external parameter X, like the shape of the quantum dot or the magnetic field.

In the random Hamiltonian approach to chaotic scattering, the energy dependence of the scattering matrix follows manifestly from Eq. (1.2.9), while the dependence on the external parameter X is modeled through the random Hamiltonian [53]

$$H(X) = H_0 + XH_1, \tag{1.5.5}$$

where H_0 and H_1 are both taken from the Gaussian ensemble. The scale for the external parameter X is not universal. Equivalently, the X-dependence of the energy levels and eigenvectors of can be described through a Brownian motion model for the random Hamiltonian $H(X)$ [54, 55]. The drawback of the Hamiltonian approach is that calculations — which as before require a mapping to the zero-dimensional nonlinear σ-model — are even more complicated than for the parameter-independent statistics of the scattering matrix. On the other hand, in the random scattering matrix approach, no successful model for the energy and magnetic field dependence of S is known. A Brownian motion model for the parameter-dependence of unitary matrices proved unsuccessful [56–58].

In Sec. 4.1, we propose a new model for the energy-dependence of S in the random scattering matrix approach. (The X-dependence of S is considered in Sec. 7.3.) In this

model, a fictitious stub (a closed lead) with N_s propagating modes is attached to the quantum dot. Scattering from the complete system, consisting of the cavity and the stub, is still chaotic. We describe reflection at the closed end of the stub by an E- and X-dependent reflection matrix $r_s(E, X)$. The scattering matrix U of the quantum dot with the stub replaced by a regular open lead has dimension $N + N_s$, where N is the number of modes in the real point contacts. In our model, we take $N_s \gg N$ and neglect the E and X dependence of U. Neglecting the E and X dependence of U is allowed if $N_s \gg N$ and if the particles spend most of the time inside the stub. Scattering from the dot is chaotic, so that U is distributed according to the circular ensemble. Hence, we find that the $N \times N$ scattering matrix $S(E, X)$ reads

$$S(E, X) \;=\; U_{ll} + U_{ls}\,[1 - r_s(E, X)U_{ss}]^{-1}\, r_s(E, X)U_{sl}, \tag{1.5.6}$$

the matrices U_{ij} being the four blocks of U for transmission and reflection from and to the stub (s) or the two leads (l). An important consequence of the model (1.5.6) is that the probability distribution of the parameter dependent ensemble of scattering matrices $S(E, X)$ is invariant under transformations

$$S(E, X) \to V S(E, X) V', \tag{1.5.7}$$

where V and V' are arbitrary unitary matrices that do not depend on E and X ($V = V^{\mathrm{T}}$ for $\beta = 1$ and $V = V^{\mathrm{R}}$ for $\beta = 4$). A justification of Eq. (1.5.6) starting from the Hamiltonian approach is given in appendix A of this chapter.

Eisenbud [59], Wigner [60] and Smith [61] have shown that the derivative $\partial S/\partial E$ is closely related to the time a particle spends inside the quantum dot after it is injected through one of the point contacts, the so-called delay time. For the description of delay times in a multichannel scattering problem, Smith introduced the hermitian time-delay matrix $Q = -i\hbar S^\dagger \partial S/\partial E$ and showed that the time-delay for a particle entering in a given mode j in the lead is given by the diagonal element Q_{jj}. In Sec. 4.2 we compute the entire distribution of time-delay matrix Q. We also compute the distribution of a the matrix $-iS^\dagger \partial S/\partial X$ parameterizing the derivative $\partial S/\partial X$. Our derivation builds on work by Wigner [62] and Gopar, Mello, and Büttiker [63], and makes essential use of the invariance property (1.5.7).

As applications, we consider the a.c. conductance $G(\omega)$ of a chaotic quantum dot (Sec. 4.1) and the distribution of the parametric derivatives $\partial G/\partial E$ and $\partial G/\partial X$ of the conductance (Sec. 4.3).

Chapter 5: Localization in disordered wires.

There exist two approaches for the theory of localization in disordered wires: the one-dimensional nonlinear σ-model of Efetov and Larkin [24], and the scaling equation for the transmission eigenvalues of Dorokhov [25] and Mello, Pereyra, and Kumar [26]. The one-dimensional nonlinear σ-model has been derived in three different ways: From a microscopic model with a Gaussian white noise potential [24], the block-random matrix model of Iida, Weidenmüller, and Zuk [64], and from a band-random matrix approach [65].

In this chapter, we construct a mapping between the two approaches, thus showing that they are equivalent. This brings together two lines of research which have developed independently for more than a decade.

Chapter 6: Diagrammatic technique for integration over the unitary group.

Now that we have established the validity of the scattering matrix approach to quantum transport through chaotic quantum dots and disordered wires, we need the tools to compute physical observables. A technical problem that arises both for quantum dots and for disordered wires is the need to integrate rational functions of a unitary matrix. For chaotic quantum dots, the unitary matrix is the scattering matrix S itself, while for the disordered wire, the unitary matrix is the matrix u of the polar decomposition (1.2.11).

For a quantum dot with single-mode point contacts, or for a wire with only a few propagating modes, the sizes of the unitary matrices are small. Then it is possible to use an explicit parameterization of the unitary matrix (e.g. in terms of Euler angles), and find the distribution of the conductance through a straightforward (but often tedious) integration. This method is used in e.g. in Secs. 2.1 and 3.1.

However, if the size N of the unitary matrix is large, explicit parameterization is not feasible. On the other hand, for applications in the regime of weak-localization and universal conductance fluctuations, an expansion in $1/N$ is sufficient. Examples of such $1/N$ expansions are Eq. (1.2.16) and (1.3.7) for the average and variance of the conductance of a quantum dot and a disordered wire, respectively. In this chapter we develop a diagrammatic technique for integration over the unitary group, that allows for a systematic expansion in powers of $1/N$.

As applications of the diagrammatic technique, we compute the average and variance of the conductance of a quantum dot with non-ideal leads, using the Poisson kernel (see Ch. 2). We also compute the average and variance of the conductance of a normal-metal–superconductor junction. This application has some overlap with the next chapter.

Chapter 7: Normal-metal–superconductor junctions.

Numerical simulations by Marmorkos, Jalabert, and Beenakker [66] have revealed that the variance of the conductance of a disordered normal-metal–superconductor (NS) junction is independent of a magnetic field, up to the 10% accuracy of the numerical simulations (see Fig. 1-11). This is remarkable, because in normal metals, var G is reduced by a factor 2 if time-reversal symmetry is broken by a magnetic field. The factor 2 reduction follows from quite general principles of random matrix theory (the Dyson-Mehta theorem [67]), or from symmetry considerations within diagrammatic perturbation theory (equal contributions from diffusons and cooperons [35, 36]). No symmetry argument could be found why the factor 2 should be a factor 1 in the presence of a superconductor.

An analytical theory for the conductance fluctuations in NS junction exists only for the case that time-reversal symmetry is present (no magnetic field; symmetry index $\beta = 1, 4$) [68]. In this case, the conductance $G_{\rm NS}$ depends entirely on the transmission eigenvalues

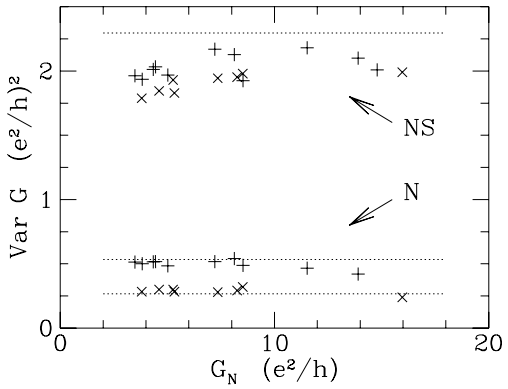

Figure 1-11. Numerical simulation of the variance of the conductance of a disordered wire with one normal and one superconducting contact (NS) or with two normal contacts (N). The variance is computed at different values of the average conductance $G_{\rm N}$ of the normal metal, and of the magnetic field ($+$ for zero field, $\times$ for a flux of $10h/e$ through the disordered region). The dotted lines are the analytical predictions from Eq. (1.3.7) and Eq. (1.4.10). No analytical prediction for the case of a NS junction with a nonzero magnetic field is shown. The figure is taken from Ref. [66].

of the disordered wire [cf. Eq. (1.4.10)],

$$G_{\rm NS} = \frac{4e^2}{h} \sum_{n=1}^{N} \frac{T_n^2}{(2-T_n)^2}.$$

The case of broken time-reversal symmetry is more difficult, because then $G_{\rm NS}$ also depends on the unitary matrices u, u', v, and v' from the polar decomposition of the scattering matrix.

In this chapter, we present analytical calculations for the case of broken time-reversal symmetry. Starting point is the general conductance formula (1.4.9). In addition to an average over the transmission eigenvalues T_j, we need to average over the unitary matrices u and u' from the polar decomposition of S. The diagrammatic technique of Ch. 6 was developed to tackle this problem. For the variance of the conductance (Sec. 7.1), we find that the effect of a magnetic field is about 7%. This is small enough to explain why the difference was not observed in the numerical simulations of Ref. [66], and large enough to tell that there is no need to look for a symmetry argument. Nevertheless, we found an approximate symmetry argument which relates the conductance fluctuations in an NS junction to those in a normal metal system with a spatial symmetry.

In Sec. 7.2, we consider weak localization in NS junctions. Here, weak localization is defined as the $\mathcal{O}(1)$ term δG in the large-N expansion of the conductance,

$$G = G_0 + \delta G + \mathcal{O}(N^{-1}). \tag{1.5.8}$$

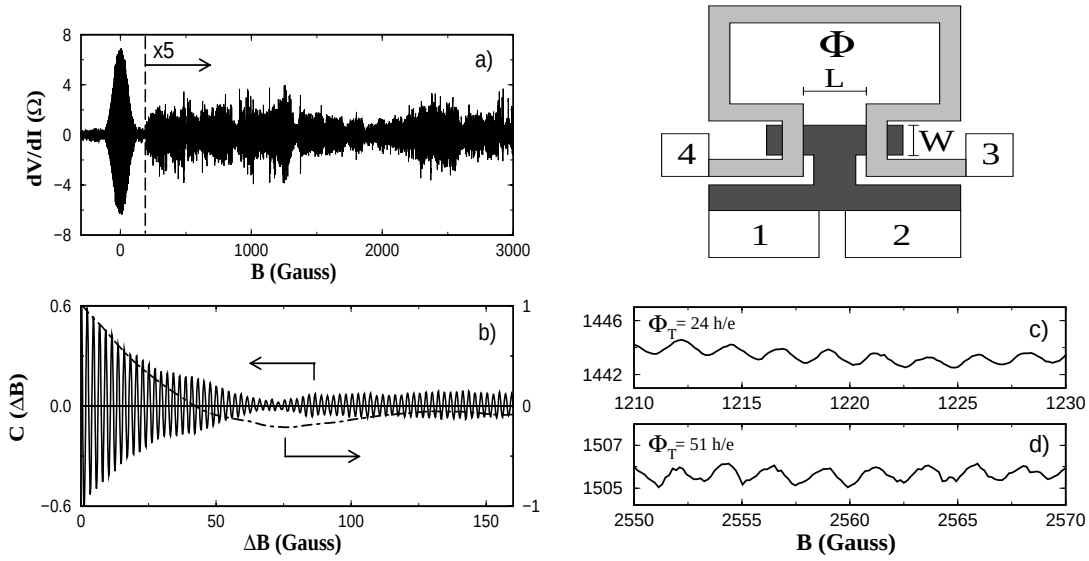

Figure 1-12. Top right: Experimental setup for a measurement of sample specific phase dependent conductance fluctuations of Den Hartog et al. [70]. A T-shaped microstructure is connected to two ends of a superconducting ring. The flux Φ through the ring determines the phase difference $\phi = 2e\Phi/\hbar$ between the two superconducting contacts. Top left: Magnetoresistance after subtraction of a ϕ-independent background. The background resistance and the envelope of the oscillations fluctuate as a random function of B. The large oscillations near $B = 0$ are not sample-specific. They are due to the proximity effect (induced superconductivity in the normal metal), see e.g. Ref. [69]. Bottom right: sample specific magnetoconductance oscillations data at $T = 50\,\mathrm{mK}$. The flux Φ_T indicates the flux through the T-shaped sample itself. Bottom left: Autocorrelation function $c(\Delta B) = \langle R(B)R(B+\Delta B)\rangle / \langle R(B)\rangle^2$ for the phase dependent conductance oscillations of the resistance trace shown in the upper left panel (solid line) and the correlation function for the background resistance (dashed line). (Figure taken from Ref. [70])

For normal metals, $\delta G = 0$ in the presence of a magnetic field. For a disordered NS junction, we find that $\delta G \neq 0$ even in the presence of a magnetic field. This anomalous weak localization correction is caused by destructive interference of paths that differ an even number of Andreev reflections. The weak localization correction is destroyed if both a magnetic field and a finite bias are applied, to break both time-reversal symmetry and electron-hole degeneracy.

In Sec. 7.3, we consider a chaotic quantum dot which is attached to two superconductors. The order parameters of the superconductors have a phase difference ϕ. We calculate the magnetic-field and phase-difference dependent conductance autocorrelator

$$C(\delta B, \delta\phi) \;=\; \langle G(B,\phi)G(B+\delta B,\phi+\delta\phi)\rangle - \langle G\rangle^2 \tag{1.5.9}$$

using the diagrammatic technique of Ch. 6 and the stub-method of Ch. 4. These calculations are motivated by recent experiments of Den Hartog et al. [70], who measured the ϕ- and B-dependence of the conductance in a T-shaped microstructure (see Fig. 1-12). The horizonal arm of the T is connected to a superconducting ring, and the vertical arm is connected to a normal electrode. The phase difference between the two superconducting contacts is varied by changing the flux through the superconducting ring. Although our calculations are performed for a different model (the T-shaped samples of Ref. [70] are not chaotic), we find qualitative agreement with the experimental observations of Den Hartog et al.

References

[1] C. W. J. Beenakker and H. van Houten, Solid State Phys. **44**, 1 (1991).

[2] B. L. Altshuler, P. A. Lee, and R. A. Webb, eds., *Mesoscopic Phenomena in Solids* (North Holland, Amsterdam, 1991).

[3] E. Akkermans, G. Montambaux, J.-L. Pichard, and J. Zinn-Justin, eds., *Mesoscopic Quantum Physics* (North-Holland, Amsterdam, 1995).

[4] A. D. Stone, P. A. Mello, K. A. Muttalib, and J.-L. Pichard in Ref. [2].

[5] C. W. J. Beenakker, Rev. Mod. Phys. (July 1997, cond-mat/9612179).

[6] M. L. Mehta, *Random Matrices* (Academic, New York, 1991).

[7] R. Landauer, IBM J. Res. Dev. **1**, 223 (1957).

[8] Y. Imry, in *Directions in Condensed Matter Physics*, G. Grinstein, G. Mazenko, eds., World Scientific, Singapore (1986).

[9] M. Büttiker, Phys. Rev. Lett. **57**, 1761 (1986); IBM J. Res. Develop. **32**, 317 (1988).

[10] E. P. Wigner, in *Proc. Canadian Mathematical Congress* (Univ. of Toronto Press, Toronto, 1957); reprinted in Ref. [12].

[11] F. J. Dyson, J. Math. Phys. **3**, 140 (1962).

[12] Many of the original papers are reprinted in C. E. Porter, *Statistical Theories of Spectra: Fluctuations* (Academic, New York, 1965).

[13] T. Guhr, A. Müller-Groeling, and H. A. Weidenmüller, submitted to Phys. Rep.

[14] L. P. Gor'kov and G. M. Eliashberg, Zh. Eksp. Teor. Fiz. **48**, 1407 (1965) [Sov. Phys. JETP **21**, 940].

[15] K. B. Efetov, Adv. Phys. **32**, 53 (1983).

[16] O. Bohigas, M. J. Giannoni, and C. Schmit, Phys. Rev. Lett. **52**, 1 (1984); O. Bohigas in *Chaos and Quantum Physics*, edited by M.-J. Giannoni, A. Voros, and J. Zinn-Justin (North-Holland, Amsterdam, 1991).

[17] A. V. Andreev, O. Agam, B. D. Simons, and B. L. Altshuler, Phys. Rev. Lett. **76**, 3947.

[18] F. J. Dyson, J. Math. Phys. **3**, 140 (1962); **3**, 157 (1962).

[19] H. A. Weidenmüller, Physica A **167**, 28 (1990).

[20] J. J. M. Verbaarschot, H. A. Weidenmüller, and M. R. Zirnbauer, Phys. Rep. **129**, 367 (1985).

[21] R. Blümel and U. Smilansky, Phys. Rev. Lett. **60**, 477 (1988); **64**, 241 (1990); U. Smilansky, in *Chaos and Quantum Physics*, edited by M.-J. Giannoni, A. Voros, and J. Zinn-Justin (North-Holland, Amsterdam, 1991).

[22] H. U. Baranger and P. A. Mello, Phys. Rev. Lett. **73**, 142 (1994).

[23] R. A. Jalabert, J.-L. Pichard, and C. W. J. Beenakker, Europhys. Lett. **27**, 255 (1994).

[24] K. B. Efetov and A. I. Larkin, Zh. Eksp. Theor. Fiz. **85**, 764 (1983) [Sov. Phys. JETP **58**, 444 (1983)].

[25] O. N. Dorokhov, Pis'ma Zh. Eksp. Teor. Fiz. **36**, 259 (1982) [JETP Lett. **36** (1992)].

[26] P. A Mello, P. Pereyra, and N. Kumar, Ann. Phys. **181**, 290 (1988).

[27] P. A. Mello and B. Shapiro, Phys. Rev. B **37**, 5860 (1988).

[28] P. A. Mello and A. D. Stone, Phys. Rev. B **44**, 3559 (1991).

[29] P. A. Mello and S. Tomsovic, Phys. Rev. Lett. **67**, 342 (1991).

[30] A. M. S. Macêdo and J. T. Chalker, Phys. Rev. B **46**, 14985 (1992).

[31] O. N. Dorokhov, Phys. Rev. B **37**, 10526 (1988).

[32] N. G. Van Kampen, *Stochastic Processes in Physics and Chemistry* (North-Holland, Amsterdam, 1981).

[33] P. W. Anderson, E. Abrahams, and T. V. Ramakrishnan, Phys. Rev. Lett. **43**, 718 (1979).

[34] L. P. Gor'kov, A. I. Larkin, and D. E. Khmel'nitskiĭ, Pis'ma Zh. Eksp. Teor. Fiz. **30**, 248 (1979) [JETP Lett. **30**, 228 (1979)].

[35] B. L. Al'tshuler, Pis'ma Zh. Eksp. Teor. Fiz. **41**, 530 (1985) [JETP Lett. **41**, 648 (1985)].

[36] P. A. Lee and A. D. Stone, Phys. Rev. Lett. **55**, 1622 (1985).

[37] C. W. J. Beenakker and M. Büttiker, Phys. Rev. B **46**, 1889 (1992).

[38] A. F. Andreev, Zh. Eksp. Teor. Fiz. **46**, 1823 (1964) [Sov. Phys. JETP **19**, 1228 (1964)].

[39] C. W. J. Beenakker, in *Mesoscopic Quantum Physics*, edited by E. Akkermans, G. Montambaux, J.-L. Pichard, and J. Zinn-Justin (North-Holland, Amsterdam, 1995).

[40] P. G. de Gennes, *Superconductivity of Metals and Alloys* (Benjamin, New York, 1966).

[41] K. K. Likharev, Rev. Mod. Phys. **51**, 101.

[42] C. W. J. Beenakker, Phys. Rev. Lett. **67**, 3836 (1991); **68**, 1442 (E) (1992).

[43] C. J. Lambert, J. Phys. Condens. Matter **3**, 6579 (1991).

[44] Y. Takane and H. Ebisawa, J. Phys. Soc. Japan **60**, 3130 (1991).

[45] C. H. Lewenkopf and H. A. Weidenmüller, Ann. Phys. **212**, 53 (1991).

[46] P. A. Mello in Ref. [3]

[47] P. A. Mello, P. Pereyra, and T. H. Seligman, Ann. Phys. (N.Y.) **161**, 254 (1985).

[48] V. N. Prigodin, K. B. Efetov and S. Iida, Phys. Rev. Lett. **71**, 1230 (1993).

[49] L. K. Hua, *Harmonic Analysis of Functions of Several Complex Variables in the Classical Domains* (Amer. Math. Soc., Providence, 1963).

[50] M. Büttiker, Phys. Rev. B **33**, 3020 (1986); IBM J. Res. Dev. **32**, 63 (1988).

[51] K. B. Efetov, Phys. Rev. Lett. **74**, 2299 (1995).

[52] E. McCann and I. V. Lerner, J. Phys. Condens. Matter **8**, 6719 (1996).

[53] A. Pandey and M. L. Mehta, Commun. Math. Phys. **87**, 449 (1983).

[54] F. J. Dyson, J. Math. Phys. **3**, 1191 (1962); J. Math. Phys. **13**, 90 (1972).

[55] G. Lenz and F. Haake, Phys. Rev. Lett. **65**, 2325 (1990); F. Haake, *Quantum Signatures of Chaos* (Springer, Berlin, 1992).

[56] K. Frahm and J.-L. Pichard, J. Phys. I France **5**, 877 (1995).

[57] J. Rau, Phys. Rev. B **51**, 7734 (1995).

[58] A. M. S. Macêdo, Phys. Rev. B **53**, 8411 (1996).

[59] L. Eisenbud, Dissertation (Princeton Univ., 1948).

[60] E. P. Wigner, Phys. Rev. **98**, 145 (1955)

[61] F. T. Smith, Phys. Rev. **118**, 349 (1960).

[62] E. P. Wigner, Ann. Math. **53**, 36 (1951); Proc. Cambridge Phil. Soc. **47**, 790 (1951); Ann. Math. **55**, 7 (1952).

[63] V. A. Gopar, P. A. Mello, and M. Büttiker, Phys. Rev. Lett. **77**, 3005 (1996).

[64] S. Iida, H. A. Weidenmüller, and J. Zuk, Phys. Rev. Lett. **64**, 583 (1990); Ann. Phys. **200**, 219 (1990).

[65] Y. V. Fyodorov and A. D. Mirlin, Phys. Rev. Lett. **67**, 2405 (1991).

[66] I. K. Marmorkos, C. W. J. Beenakker, and R. A. Jalabert, Phys. Rev. B **48**, 2811 (1993).

[67] F. J. Dyson and M. L. Mehta, J. Math. Phys. **4**, 701 (1963).

[68] C. W. J. Beenakker and B. Rejaei, Phys. Rev. Lett. **71**, 3689 (1993); J. T. Chalker and A. M. S. Macêdo, Phys. Rev. Lett. **71**, 3693 (1993).

[69] Yu. V. Nazarov, in *Quantum Dynamics of Submicron Structures*, edited by H. A. Cerdeira, B. Kramer, and G. Schön, NATO ASI Series E291 (Kluwer, Dordrecht, 1995).

[70] S. G. den Hartog, C. M. A. Kapteyn, B. J. van Wees, T. M. Klapwijk, W. van der Graaf, and G. Borghs, Phys. Rev. Lett. **76**, 4592 (1996).

2 Chaotic quantum dots with nonideal leads

2.1 Conductance distribution of a quantum dot with nonideal single-channel leads

An ensemble of mesoscopic systems has large sample-to-sample fluctuations in its transport properties, so that the average is not sufficient to characterize a single sample. To determine the complete distribution of the conductance is therefore a fundamental problem in this field. Early work focused on an ensemble of disordered wires. (See Ref. 1 for a review). The distribution of the conductance in that case is either normal or log-normal, depending on whether the wires are in the metallic or insulating regime. Recently, it was found that a "quantum dot" has a qualitatively different conductance distribution [2–4]. A quantum dot is a small confined region, having a large level spacing compared to the thermal energy, which is weakly coupled by point contacts to two electron reservoirs. The classical motion within the dot is assumed to be ballistic and chaotic. An ensemble consists of dots with small variations in shape or in Fermi energy. The capacitance of a dot is assumed to be sufficiently large that the Coulomb blockade can be ignored, i.e. the electrons are assumed to be non-interacting. Two altogether different approaches have been taken to this problem.

Baranger and Mello [3], and Jalabert, Pichard, and Beenakker [4] started from random-matrix theory [5]. The scattering matrix S of the quantum dot was assumed to be a member of the circular ensemble of $N \times N$ unitary matrices, as is appropriate for a chaotic billiard [6, 7]. In the single-channel case ($N = 1$), the distribution $P(T)$ of the transmission probability T [and hence of the conductance $G = (2e^2/h)T$] was found to be

$$P(T) = \tfrac{1}{2}\beta T^{-1+\beta/2}, \tag{2.1.1}$$

where $\beta \in \{1, 2, 4\}$ is the symmetry index of the ensemble ($\beta = 1$ or 2 in the absence or presence of a time-reversal-symmetry breaking magnetic field; $\beta = 4$ in zero magnetic field with strong spin-orbit interaction). Eq. (2.1.1) was found to be in good agreement with numerical simulations of transmission through a chaotic billiard connected to ideal leads having a single propagating mode [3]. (The case $\beta = 4$ was not considered in Ref. 3.)

Previously, Prigodin, Efetov, and Iida [2] had applied the method of supersymmetry to the same problem, but with a different model for the point contacts. They considered the case of broken time-reversal symmetry ($\beta = 2$), for which Eq. (2.1.1) would predict a uniform conductance distribution. Instead, the distribution of Ref. 2 is strongly peaked near zero conductance. The tail of the distribution (towards unit transmission) is governed by resonant tunneling, and is consistent with earlier work by Jalabert, Stone, and Alhassid [8] on resonant tunneling in the Coulomb-blockade regime.

It is the purpose of the present section to bridge the gap between these two theories, by considering a more general model for the coupling of the quantum dot to the reservoirs. Instead of assuming ideal leads, as in Refs. 3 and 4, we allow for an arbitrary transmission probability Γ of the propagating mode in the lead, as a model for coupling via a quantum point contact with conductance below $2e^2/h$. Eq. (2.1.1) corresponds to $\Gamma = 1$ (ballistic point contact). In the limit $\Gamma \ll 1$ (tunneling point contact) we recover, for $\beta = 2$, the result of Ref. 2. We consider also $\beta = 1$ and 4 and show that — in contrast to Eq. (2.1.1) — the limit $\Gamma \ll 1$ depends only weakly on the symmetry index β. In the crossover region from ballistic to tunneling conduction we find a remarkable Γ-dependence of the conductance fluctuations: The variance is monotonically decreasing for $\beta = 1$ and 2, but it has a *maximum* for $\beta = 4$ at $\Gamma = 0.74$.

The system under consideration is illustrated in the inset of Fig. 2-2b. It consists of a quantum dot with two single-channel leads containing a tunnel barrier (transmission probability Γ). We assume identical leads for simplicity. The transmission properties of this system are studied in a transfer matrix formulation. The transfer matrix M_d of the quantum dot can be parameterized as [9, 10]

$$M_d = \begin{pmatrix} u_1 & 0 \\ 0 & v_1 \end{pmatrix} \begin{pmatrix} \sqrt{1+\lambda_d} & \sqrt{\lambda_d} \\ \sqrt{\lambda_d} & \sqrt{1+\lambda_d} \end{pmatrix} \begin{pmatrix} u_2 & 0 \\ 0 & v_2 \end{pmatrix}, \tag{2.1.2}$$

where the parameter λ_d is related to the transmission probability T_d of the dot by

$$T_d = (1+\lambda_d)^{-1}. \tag{2.1.3}$$

The numbers u_j and v_j satisfy constraints that depend on the symmetry of the Hamiltonian of the quantum dot:

$$u_j = e^{i\phi_j} a_j, \qquad v_j = e^{-i\phi_j} a_j, \tag{2.1.4}$$

with a_j a real ($\beta = 1$), complex ($\beta = 2$), or real quaternion ($\beta = 4$) number of modulus one. In general the choice for u_j and v_j and their parametrisation (2.1.4) is not unique. Uniqueness can be achieved by requiring that

$$a_1 = 1, \qquad 0 \le \phi_j < \pi \quad (j = 1, 2). \tag{2.1.5}$$

As in Refs. 3 and 4, we assume that the scattering matrix S_d of the quantum dot is a member of the circular ensemble, which means that S_d is uniformly distributed in the unitary group (or the subgroup required by time reversal and/or spin rotation symmetry). The corresponding probability distribution of the transfer matrix M_d is

$$P_d(M_d)\, dM_d = \tfrac{1}{2}\beta(1+\lambda_d)^{-1-\beta/2} d\lambda_d d\phi_1 d\phi_2 da_2. \tag{2.1.6}$$

The transfer matrix M_b of the tunnel barrier in the lead is given by

$$M_b = \begin{pmatrix} \sqrt{1+\mu} & \sqrt{\mu} \\ \sqrt{\mu} & \sqrt{1+\mu} \end{pmatrix}, \tag{2.1.7}$$

with $\Gamma = (1+\mu)^{-1}$. The transfer matrix M of the total system follows from the matrix product

$$M = M_b M_d M_b. \tag{2.1.8}$$

From Eqs. (2.1.2)–(2.1.8) we straightforwardly compute the transmission probability T of the total system and its probability distribution $P(T)$. The result for T is

$$\begin{aligned} T &= \Big(1+\lambda_d + m\lambda_d \cos^2\psi_- + m(\lambda_d+1)\cos^2\psi_+ + \\ &\qquad 2\sqrt{\lambda_d(\lambda_d+1)m(m+1)}\cos\psi_-\cos\psi_+\Big)^{-1}, \end{aligned} \tag{2.1.9}$$

where we have abbreviated

$$m = 4(1-\Gamma)\Gamma^{-2}, \quad \psi_\pm = \phi_1 \pm \phi_2. \tag{2.1.10}$$

The variables a_j, and with them all β-dependence, drop out of this expression. Eq. (2.1.9) can be inverted[1] to yield λ_d in terms of ϕ_1 and ϕ_2 for given T and Γ. The probability distribution $P(T)$ then follows from

$$P(T) = \frac{\beta}{2\pi^2}\int_0^\pi d\phi_1 \int_0^\pi d\phi_2\, (1+\lambda_d)^{-1-\beta/2}\left|\frac{\partial\lambda_d}{\partial T}\right|, \tag{2.1.11}$$

where the integration is over all $\phi_i \in (0,\pi)$ for which λ_d is real and positive.

For $\Gamma = 1$ the function $P(T)$ is given by Eq. (2.1.1), as found in Refs. 3 and 4. In Fig. 2-2 the crossover from a ballistic to a tunneling point contact is shown. For $\Gamma \ll 1$ and $T \ll 1$, $\Gamma^2 P(T)$ becomes a Γ-independent function of T/Γ^2, which is shown in the inset of Fig. 2-2c. Several asymptotic expressions for $P(T)$ can be obtained from Eq. (2.1.11) for $\Gamma \ll 1$,

$$\beta = 1: \; P(T) = \begin{cases} \dfrac{8}{\pi^2\Gamma}T^{-1/2} & (T \ll \Gamma^2), \\ \dfrac{\Gamma}{\pi^2}T^{-3/2} & (\Gamma^2 \ll T \ll 1), \end{cases} \tag{2.1.12}$$

$$\beta = 2: \; P(T) = 4\Gamma\frac{\Gamma^2+T}{(\Gamma^2+4T)^{5/2}} \qquad (T \ll 1), \tag{2.1.13}$$

$$\beta = 4: \; P(T) = 24T\Gamma\frac{3\Gamma^4+4T\Gamma^2+3T^2}{(\Gamma^2+4T)^{9/2}} \qquad (T \ll 1). \tag{2.1.14}$$

The $\beta = 2$ expression (2.1.13) for $P(T)$ in the tunneling regime agrees precisely with the supersymmetry calculation of Prigodin, Efetov, and Iida [2].[2] Eq. (2.1) does not cover the

[1] Inversion of Eq. (2.1.9) requires some care. Since a shift $\psi_+ \to \psi_+ + \pi$ changes the sign of the term containing the square root in Eq. (2.1.9), solving for λ_d with ψ_1 and $\psi_1 + \pi$ yields exactly two (complex) solutions in total. This allows one to construct a single-valued function $\lambda_d(\psi_+, \psi_-)$ such that these two solutions are given by $\lambda_d(\psi_+, \psi_-)$ and $\lambda_d(\psi_+ + \pi, \psi_-)$. This function λ_d is understood as the inverse of Eq. (2.1.9).

[2] To compare with Ref. 2 we identify $\alpha_1 = \alpha_2 = \frac{1}{2}\Gamma \ll 1$ and take the limit $\alpha \to 0$ of Eq. (7) in that paper. This yields our Eq. (2.1.13). Here α_1, α_2, and α are, respectively, the level broadening (divided by the level spacing) due to coupling to lead 1 and 2, and due to inelastic scattering processes (which we have not included in our formulation, whence $\alpha \to 0$).

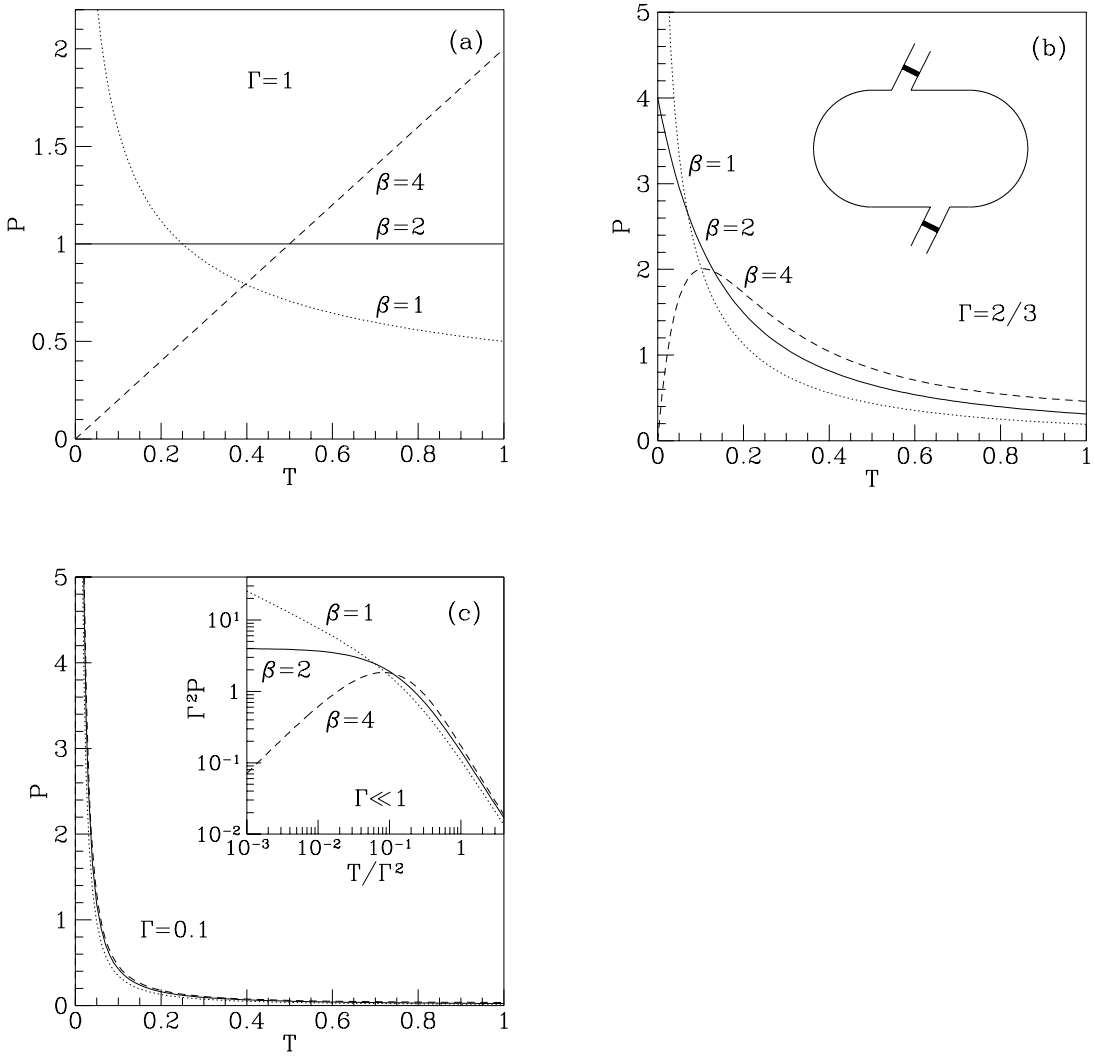

Figure 2-2. Distribution of the transmission probability T through a quantum dot with non-ideal leads, for three values of the transmission probability Γ of the leads. The curves are computed from Eq. (2.1.11) for each symmetry class ($\beta = 1, 2, 4$). The inset of (b) shows the quantum dot, the inset of (c) shows the asymptotic behavior of $P(T)$ for $\Gamma \ll 1$ on a log-log scale.

range near unit transmission. As $T \to 1$ (and $\Gamma \ll 1$), $P(T) \to c_\beta \Gamma$, with $c_1 = \frac{1}{2\pi}$, $c_2 = \frac{1}{4}$, and $c_4 = \frac{3}{8}$.

A quite remarkable feature of the quantum dot with ideal leads is the strong β-dependence of $P(T)$ (cf. Fig. 2-2a). For $\Gamma \ll 1$, the β-dependence is much less pronounced. For $T \gg \Gamma^2$ the leads dominate the transmission properties of the total system, thereby suppressing the β-dependence of $P(T)$ (although not completely). For very small transmission coefficients ($T \ll \Gamma^2$) the non-ideality of the leads is of less importance, and the characteristic β-dependence of Eq. (2.1.1) is recovered (see inset of Fig. 2-2c).

Moments of $P(T)$ can be computed in closed form for all Γ directly from Eq. (2.1.9). The first two moments are (recall that $m = 4(1-\Gamma)\Gamma^{-2}$):

$$\langle T \rangle = \begin{cases} \frac{1}{2} m^{-1} \left[\sqrt{1+m} - \frac{1}{\sqrt{m}} \ln(\sqrt{1+m} + \sqrt{m}) \right] & (\beta = 1), \\ \frac{2}{3} m^{-2} \left[(m-2)\sqrt{1+m} + 2 \right] & (\beta = 2), \\ \frac{4}{15} m^{-3} \left[(3m^2 - 4m + 8)\sqrt{1+m} - 32 \right] & (\beta = 4), \end{cases}$$

$$\langle T^2 \rangle = \begin{cases} \frac{3}{64} m^{-2} \left[(4m-18)\sqrt{1+m} + \left(\frac{18}{\sqrt{m}} + 8\sqrt{m} \right) \ln(\sqrt{1+m} + \sqrt{m}) \right] & (\beta = 1), \\ \frac{4}{15} m^{-3} \left[\left(m^2 + 2m + 16 \right) \sqrt{1+m} - 10m - 16 \right] & (\beta = 2), \\ \frac{4}{35} m^{-4} \left[\left(3m^3 + 2m^2 - 40m - 144 \right) \sqrt{1+m} + 112m + 144 \right] & (\beta = 4). \end{cases}$$

For $\Gamma \ll 1$ one has asymptotically

$$\langle T^n \rangle = \frac{\beta \Gamma}{2(\beta+1)} \prod_{j=1}^{n-1} \frac{(\beta+2j)(2j-1)}{2j(\beta+2j+1)}. \tag{2.1.15}$$

The Γ-dependence of the variance $\mathrm{Var}\, T = \langle T^2 \rangle - \langle T \rangle^2$ of the transmission probability is shown in Fig. 2-3. In the crossover regime between a ballistic point contact ($\Gamma = 1$) and a tunneling point contact ($\Gamma \ll 1$), the three symmetry classes show striking differences. For $\beta = 1$ and 2 the conductance fluctuations decrease monotonically upon decreasing Γ, whereas they show non-monotonic behavior for $\beta = 4$. Notice also that the transition $\beta = 1 \to \beta = 2$, by application of a magnetic field, reduces fluctuations for $\Gamma > \Gamma_c$ but increases fluctuations for $\Gamma < \Gamma_c$, where $\Gamma_c = 0.92$.

In summary, we have computed the transmission probability of a ballistic and chaotic cavity for all possible values of the symmetry index β and for arbitrary values of the transparancy Γ of the single-channel leads. Our results describe the conductance of a quantum dot in the crossover regime from a coupling to the reservoirs by ballistic to tunneling point contacts. The theory unifies and extends known results [2–4]. The characteristic β-dependence of the distribution function that was found for ideal leads [Eq. (2.1.1)] is strongly suppressed for transmission probabilities T larger than Γ^2. A closely related phenomenon is the non-trivial Γ-dependence of the conductance fluctuations for the three symmetry classes. The theory is relevant for experiments on chaotic scattering in quantum dots with adjustable point contacts, which are of great current interest [11–13].

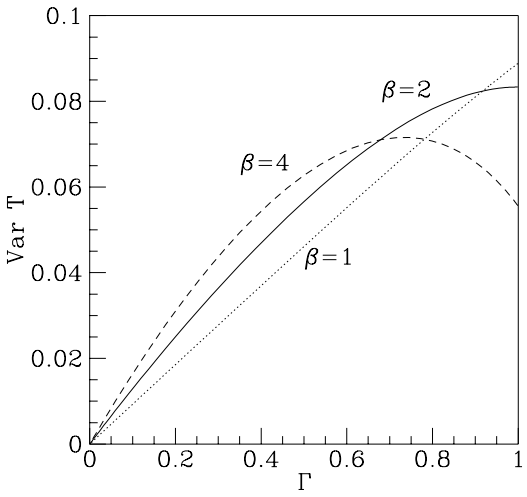

Figure 2-3. Variance of the transmission probability T as a function of the transmission probability of the leads Γ.

2.2 Generalized circular ensemble of scattering matrices for a chaotic cavity with non-ideal leads

Theoretical work [2–4, 8, 14–17] on phase-coherent conduction through cavities in which the classical electron motion can be regarded as chaotic has stimulated recent experiments [11–13, 18] on conductance fluctuations and weak-localization effects in quantum dots. If the capacitance of the quantum dot is large enough, a description in terms of non-interacting electrons is appropriate (otherwise the Coulomb blockade becomes important [2, 8]).

For an isolated chaotic cavity, it has been conjectured and confirmed by many examples that the statistics of the Hamiltonian H agrees with that of the Gaussian ensemble of random-matrix theory [19, 20]. If the chaotic behavior is caused by impurity scattering, the agreement has been established by microscopic theory: Both the Gaussian ensemble and the ensemble of Hamiltonians with randomly placed impurities are equivalent to a certain non-linear σ-model [21, 22]. Transport properties can be computed by coupling M eigenstates of H to N scattering channels [22–25]. Since $N \ll M$ this construction introduces a great number of coupling parameters, whereas only a few independent parameters determine the statistics of the scattering matrix S of the system [22].

For transport properties at zero temperature and infinitesimal applied voltage, one only needs to know S at the Fermi energy E_F, and an approach which starts directly from the ensemble of scattering matrices at a given energy is favorable. Following up on earlier work on chaotic scattering in billiards [6, 7], two recent papers [3, 4] have studied the transport properties of a quantum dot under the assumption that S is distributed according to Dyson's circular ensemble [5, 26]. In Refs. 3 and 4 the coupling of the quantum dot to

the external reservoirs was assumed to occur via ballistic point contacts (or "ideal leads"). The extension to coupling via tunnel barriers (non-ideal leads) was considered in Sec. 2.1. In all cases complete agreement was obtained with results which were obtained from the Hamiltonian approach [2, 23, 24]. This agreement calls for a general demonstration of the equivalence of the scattering matrix and the Hamiltonian approach, for arbitrary coupling of the quantum dot to the external reservoirs. It is the purpose of this section to provide such a demonstration. A proof of the equivalence of the Gaussian and circular ensembles has been published by Lewenkopf and Weidenmüller [25], for the special case of ideal leads. The present proof applies to non-ideal leads as well, and repairs a weak spot in the proof of Ref. 25 for the ideal case.

The circular ensemble of scattering matrices is characterized by a probability distribution $P(S)$ which is constant, that is to say, each unitary matrix S is equally probable. As a consequence, the ensemble average $\bar{S}$ is zero. This is appropriate for ideal leads. A generalization of the circular ensemble which allows for non-zero $\bar{S}$ (and can therefore be applied to non-ideal leads) has been derived by Mello, Pereyra, and Seligman [27, 28], using a maximum entropy principle. The distribution function in this generalized circular ensemble is known in the mathematical literature [29] as the Poisson kernel,

$$P(S) \propto \left|\det(1 - \bar{S}^\dagger S)\right|^{-(\beta N + 2 - \beta)} . \tag{2.2.1}$$

Here $\beta \in \{1, 2, 4\}$ is the symmetry index of the ensemble of scattering matrices: $\beta = 1$ or 2 in the absence or presence of a time-reversal-symmetry breaking magnetic field; $\beta = 4$ in zero magnetic field with strong spin-orbit scattering. (In Refs. [27] and [28] only the case $\beta = 1$ was considered.) One verifies that $P(S) =$ constant for $\bar{S} = 0$. Eq. (2.2.1) was first recognized as a possible generalization of the circular ensemble by Krieger [30], for the special case that $\bar{S}$ is proportional to the unit matrix.

In this section we present a microscopic justification of the Poisson kernel, by deriving it from an ensemble of random Hamiltonians which is equivalent to an ensemble of disordered metal grains. For the Hamiltonian ensemble we can use the Gaussian ensemble, or any other ensemble to which it is equivalent in the limit $M \to \infty$ [31]. (The microscopic justification of the Gaussian ensemble only holds for $M \to \infty$.) For technical reasons, we use a Lorentzian distribution for the Hamiltonian ensemble, which in the limit $M \to \infty$ can be shown to be equivalent to the usual Gaussian distribution. The technical advantage of the Lorentzian ensemble over the Gaussian ensemble is that the equivalence to the Poisson kernel holds for arbitrary $M \geq N$, and does not require taking the limit $M \to \infty$.

The outline of this section is as follows: In Sec. 2.2.1 the usual Hamiltonian approach is summarized, following Ref. 22. In Sec. 2.2.2, the Lorentzian ensemble is introduced. The eigenvalue and eigenvector statistics of the Lorentzian ensemble are shown to agree with the Gaussian ensemble in the limit $M \to \infty$. In Sec. 2.2.3 we then compute the entire distribution function $P(S)$ of the scattering matrix from the Lorentzian ensemble of Hamiltonians, and show that it agrees with the Poisson kernel (2.2.1) for arbitrary $M \geq N$. In Sec. 2.2.4 the Poisson kernel is shown to describe a quantum dot which is coupled to the reservoirs by means of tunnel barriers. We conclude in Sec. 2.2.5.

2.2.1 Hamiltonian approach

The Hamiltonian approach [22, 25, 32] starts with a formal division of the system into two parts, the leads and the cavity (see Fig. 2-4a). The Hamiltonian of the total system is represented in the following way: Let the set $\{|a\rangle\}$ represent a basis of scattering states in the lead at the Fermi energy E_F ($a = 1, \ldots, N$), with N the number of propagating modes at E_F. The set of bound states in the cavity is denoted by $\{|\mu\rangle\}$ ($\mu = 1, \ldots, M$). We assume $M \geq N$. The Hamiltonian $\mathcal{H}$ is then given by [22]

$$\mathcal{H} = \sum_a |a\rangle E_F \langle a| + \sum_{\mu,\nu} |\mu\rangle H_{\mu\nu} \langle \nu| + \sum_{\mu,a} \left(|\mu\rangle W_{\mu a} \langle a| + |a\rangle W^*_{\mu a} \langle \mu| \right). \tag{2.2.2}$$

The matrix elements $H_{\mu\nu}$ form a hermitian $M \times M$ matrix H, with real ($\beta = 1$), complex ($\beta = 2$), or real quaternion ($\beta = 4$) elements. The coupling constants $W_{\mu a}$ form a real (complex, real quaternion) $M \times N$ matrix W. The $N \times N$ scattering matrix $S(E_F)$ associated with this Hamiltonian is given by

$$S(E_F) = 1 - 2\pi i W^\dagger (E_F - H + i\pi W W^\dagger)^{-1} W. \tag{2.2.3}$$

For $\beta = 1, 2, 4$ the matrix S is respectively unitary symmetric, unitary, and unitary self-dual.

Usually one assumes that H is distributed according to the Gaussian ensemble,

$$P(H) = \frac{1}{V} \exp\left(-\tfrac{1}{4} \beta M \lambda^{-2} \mathrm{tr}\, H^2 \right), \tag{2.2.4}$$

with V a normalization constant and λ an arbitrary coefficient which determines the density of states at E_F. The coupling matrix W is fixed. Notice that $P(H)$ is invariant under transformations $H \to UHU^\dagger$ where U is orthogonal ($\beta = 1$), unitary ($\beta = 2$), or symplectic ($\beta = 4$). This implies that $P(S)$ is invariant under transformations $W \to UW$, so that it can only depend on the invariant $W^\dagger W$. The ensemble-averaged scattering matrix $\bar{S}$ can be calculated analytically in the limit $M \to \infty$, at fixed N, E_F, and fixed mean level spacing Δ. The result is [22]

$$\bar{S} = \frac{1 - \pi W^\dagger W/\lambda}{1 + \pi W^\dagger W/\lambda}. \tag{2.2.5}$$

It is possible to extend the Hamiltonian (2.2.2) to include a "background" scattering matrix S_0 which does not couple to the cavity [33]. The matrix S_0 is symmetric for $\beta = 1$ and can be decomposed as $S_0 = O e^{2i\Phi} O^T$, where the matrix O is orthogonal and Φ is real and diagonal. In the limit $M \to \infty$, the average scattering matrix $\bar{S}$ is now given by [33]

$$\bar{S} = O e^{i\Phi} \frac{1 - \pi W^\dagger W/\lambda}{1 + \pi W^\dagger W/\lambda} e^{i\Phi} O^T. \tag{2.2.6}$$

Lewenkopf and Weidenmüller [25] used this extended version of the theory to relate the Gaussian and circular ensembles, for $\beta = 1$ and $\bar{S} = 0$. Their argument is based on the assumption that Eq. (2.2.6) can be inverted, to yield $W^\dagger W$ and S_0 as a function of $\bar{S}$. Then

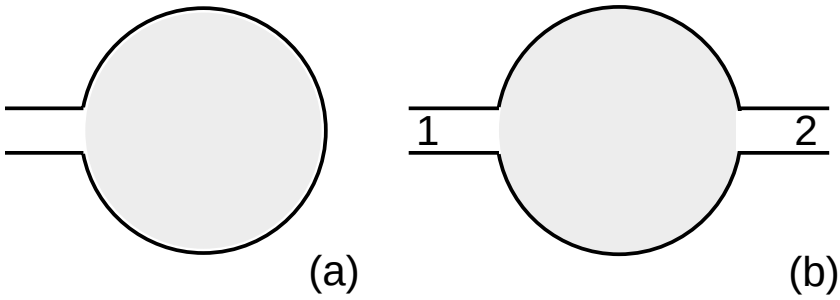

Figure 2-4. Schematic drawing of a disordered cavity (grey) attached to a lead. There are N scattering channels in the lead, which are coupled to M bound levels in the cavity. In (a) only one lead is drawn. A system with more leads (b) is described by combining them formally into one lead.

$P(S) = P_{\bar{S}}(S)$ is fully determined by $\bar{S}$ (and does not require separate knowledge of $W^\dagger W$ and S_0). Under the transformation $S \to USU^T$ (with U an arbitrary unitary matrix), $\bar{S}$ is mapped to $U\bar{S}U^T$, which implies

$$P_{\bar{S}}(S) = P_{U\bar{S}U^T}(USU^T). \tag{2.2.7}$$

For $\bar{S} = 0$ one finds that $P(S)$ is invariant under transformations $S \to USU^T$, so that $P(S)$ must be constant (circular ensemble). There is, however, a weak spot in this argument: Equation (2.2.6) can *not* be inverted for the crucial case $\bar{S} = 0$. It is only possible to determine $W^\dagger W$, not S_0. This is a serious objection, since S_0 is not invariant under the transformation $S \to USU^T$, and one can not conclude that $P(S) =$ constant for $\bar{S} = 0$. We have not succeeded in repairing the proof of Ref. 25 for $\bar{S} = 0$, and instead present in the following subsections a different proof (which moreover can be extended to non-zero $\bar{S}$).

A situation in which the cavity is coupled to n reservoirs by n leads, having N_j scattering channels ($j = 1, \ldots, n$) each, can be described in the framework presented above by combining the n leads formally into a single lead with $N = \sum_{j=1}^{n} N_j$ scattering channels. Scattering matrix elements between channels in the same lead correspond to reflection from the cavity, elements between channels in different leads correspond to transmission. In this notation, the Landauer formula for the conductance G of a cavity with two leads (Fig. 2-4b) takes the form

$$G = \frac{2e^2}{h} \sum_{i=1}^{N_1} \sum_{j=N_1+1}^{N_1+N_2} |S_{ij}|^2. \tag{2.2.8}$$

2.2.2 Lorentzian ensemble

For technical reasons we wish to replace the Gaussian distribution (2.2.4) of the Hamiltonians by a Lorentzian distribution,

$$P(H) = \frac{1}{V} \lambda^{M(\beta M+2-\beta)/2} \det\left(\lambda^2 + (H-\varepsilon)^2\right)^{-(\beta M+2-\beta)/2}, \tag{2.2.9}$$

where λ and ε are parameters describing the width and center of the distribution, and V is a normalization constant independent of λ and ε. The symmetry parameter $\beta \in \{1, 2, 4\}$ indicates whether the matrix elements of H are real [$\beta = 1$, Lorentzian Orthogonal Ensemble (ΛOE)], complex [$\beta = 2$, Lorentzian Unitary Ensemble (ΛUE)], or real quaternion [$\beta = 4$, Lorentzian Symplectic Ensemble (ΛSE)]. (We abbreviate "Lorentzian" by a capital lambda, because the letter L is commonly used to denote the Laguerre ensemble.)

The replacement of (2.2.4) by (2.2.9) is allowed because the eigenvector and eigenvalue distributions of the Gaussian and the Lorentzian ensemble are equal on a fixed energy scale, in the limit $M \to \infty$ at a fixed mean level spacing Δ. The equivalence of the eigenvector distributions is obvious: The distribution of H depends solely on the eigenvalues for both the Lorentzian and the Gaussian ensemble, so that the eigenvector distribution is uniform for both ensembles. In order to prove the equivalence of the distribution of the eigenvalues $E_1, E_2, \ldots, E_M$ (energy levels), we compare the n-level cluster functions $T_n(E_1, E_2, \ldots, E_n)$ for both ensembles. The general definition of the T_n's is given in Ref. [5]. The first two T_n's are defined by

$$\begin{aligned} T_1(E) &= \langle \sum_{i=1}^{M} \delta(E - E_i) \rangle \qquad (2.2.10) \\ T_2(E_1, E_2) &= \langle \sum_{i=1}^{M} \delta(E_1 - E_i) \rangle \langle \sum_{j=1}^{M} \delta(E_2 - E_j) \rangle - \langle \sum_{i \neq j} \delta(E_1 - E_i) \delta(E_2 - E_j) \rangle . \end{aligned}$$

The brackets $\langle \ldots \rangle$ denote an average over the ensemble. The cluster functions in the Gaussian ensemble are known for arbitrary n [5], for the Lorentzian ensemble we compute them below.

From Eq. (2.2.9) one obtains the joint probability distribution function of the eigenvalues,

$$P(\{E_j\}) = \frac{1}{V} \lambda^{M(\beta M + 2 - \beta)/2} \prod_{i<j} |E_i - E_j|^{\beta} \prod_i \left(\lambda^2 + (E_i - \varepsilon)^2 \right)^{-(\beta M + 2 - \beta)/2} . \quad (2.2.11)$$

We first consider the case $\lambda = 1$, $\varepsilon = 0$. We make the transformation

$$S = \frac{1 + iH}{1 - iH} . \qquad (2.2.12)$$

The eigenvalues $e^{i\phi_j}$ of the unitary matrix S are related to the energy levels E_j by

$$e^{i\phi_j} = \frac{1 + iE_j}{1 - iE_j} \iff \phi_j = 2 \arctan E_j . \qquad (2.2.13)$$

The probability distribution of the eigenphases follows from Eqs. (2.2.11) and (2.2.13),

$$P(\{\phi_j\}) = \frac{1}{V} 2^{-M(\beta M + 2 - \beta)/2} \prod_{i<j} |e^{i\phi_i} - e^{i\phi_j}|^{\beta} . \qquad (2.2.14)$$

This is precisely the distribution of the eigenphases in the circular ensemble. The cluster functions in the circular ensemble are known [5, 26]. The n-level cluster functions T_n^Λ in the Lorentzian ensemble are thus related to the n-level cluster functions T_n^C in the circular ensemble by

$$T_n^\Lambda(E_1,\ldots,E_n) = T_n^C(2\arctan E_1,\ldots,2\arctan E_n)\prod_{j=1}^{n}\frac{2}{1+E_j^2}. \tag{2.2.15}$$

For $n=1$ one finds the level density

$$\rho(E) = \frac{M}{\pi(1+E^2)}, \tag{2.2.16}$$

independent of β. For $n=2$ one finds the pair-correlation function

$$T_2^\Lambda(E_1,E_2) = \frac{4\,\sin^2(M\arctan E_1 - M\arctan E_2)}{(1+E_1^2)(1+E_2^2)\,\sin^2(\arctan E_1 - \arctan E_2)}. \tag{2.2.17}$$

Eq. (2.2.17) holds for $\beta=2$. The expressions for $\beta=1,4$ are more complicated.

The n-level cluster functions for arbitrary λ and ε can be found after a proper rescaling of the energies. Eq. (2.2.15) generalizes to

$$\begin{aligned} &T_n^\Lambda(E_1,\ldots,E_n) = \\ &T_n^C\left(2\arctan\frac{E_1-\varepsilon}{\lambda},\ldots,2\arctan\frac{E_n-\varepsilon}{\lambda}\right)\prod_{j=1}^{n}\frac{2\lambda}{\lambda^2+(E_j-\varepsilon)^2}. \end{aligned} \tag{2.2.18}$$

The large-M limit of the T_n's is defined as

$$Y_n(\xi_1,\ldots,\xi_n) = \lim_{M\to\infty}\Delta^n T_n(\xi_1\Delta,\ldots,\xi_n\Delta). \tag{2.2.19}$$

For both the Gaussian and the Lorentzian ensembles, the mean level spacing Δ at the center of the spectrum in the limit $M\to\infty$ is given by $\Delta=\lambda\pi/M$. Therefore, the relevant limit $M\to\infty$ at fixed level spacing is given by $M\to\infty$, $\lambda\to\infty$, $\Delta=\lambda\pi/M$ fixed for both ensembles. Equation (2.2.18) allows us to relate the Y_n's in the Lorentzian and circular ensembles,

$$\begin{aligned} Y_n^\Lambda(\xi_1,\ldots,\xi_n) &= \lim_{M\to\infty}(2\pi/M)^n\,T_n^C(2\arctan(\pi\xi_1/M),\ldots,2\arctan(\pi\xi_n/M)) \\ &= \lim_{M\to\infty}(2\pi/M)^n\,T_n^C(2\pi\xi_1/M,\ldots,2\pi\xi_n/M) \\ &= Y_n^C(\xi_1,\ldots,\xi_n). \end{aligned} \tag{2.2.20}$$

It is known that the cluster functions Y_n^C in the circular ensemble are equal to the cluster functions Y_n^G in the Gaussian ensemble [5]. Equation (2.2.20) therefore shows that the Lorentzian and the Gaussian ensembles have the same cluster functions in the large-M limit.

The technical reason for working with the Lorentzian ensemble instead of with the Gaussian ensemble is that the Lorentzian ensemble has two properties which make it particularly easy to compute the distribution of the scattering matrix. The two properties are:

Property 1: If H is distributed according to a Lorentzian ensemble with width λ and center ε, then H^{-1} is again distributed according to a Lorentzian ensemble, with width $\tilde{\lambda} = \lambda/(\lambda^2 + \varepsilon^2)$ and center $\tilde{\varepsilon} = \varepsilon/(\lambda^2 + \varepsilon^2)$.

Property 2: If the $M \times M$ matrix H is distributed according to a Lorentzian ensemble, then every $N \times N$ submatrix of H obtained by omitting $M - N$ rows and the corresponding columns is again distributed according to a Lorentzian ensemble, with the same width and center.

The proofs of both properties are essentially contained in Ref. 29. In order to make this chapter self-contained, we briefly give the proofs in the appendix.

2.2.3 Scattering matrix distribution for the Lorentzian ensemble

The general relation between the Hamiltonian H and the scattering matrix S is given by Eq. (2.2.3). After some matrix manipulations, it can be written as

$$S = \left(1 + i\pi W^\dagger (H - E_F)^{-1} W\right) \left(1 - i\pi W^\dagger (H - E_F)^{-1} W\right)^{-1}. \tag{2.2.21}$$

We can write the coupling matrix W as

$$W = U Q \tilde{W}, \tag{2.2.22}$$

where U is an $M \times M$ orthogonal ($\beta = 1$), unitary ($\beta = 2$), or symplectic ($\beta = 4$) matrix, $\tilde{W}$ is an $N \times N$ matrix, and Q is an $M \times N$ matrix with all elements zero except $Q_{nn} = 1$, $1 \leq n \leq N$. Substitution into Eq. (2.2.3) gives

$$S = \left(1 + i\pi \tilde{W}^\dagger \tilde{H} \tilde{W}\right) \left(1 - i\pi \tilde{W}^\dagger \tilde{H} \tilde{W}\right)^{-1}, \tag{2.2.23}$$

where we have defined $\tilde{H} \equiv Q^T U^\dagger (H - E_F)^{-1} U Q$.

We assume that H is a member of the Lorentzian ensemble, with width λ and center 0. Then the matrix $H - E_F$ is also a member of the Lorentzian ensemble, with width λ and center E_F. Property 1 implies that $(H - E_F)^{-1}$ is distributed according to a Lorentzian ensemble with width $\tilde{\lambda} = \lambda/(\lambda^2 + E_F^2)$ and center $\tilde{\varepsilon} = E_F/(\lambda^2 + E_F^2)$. Orthogonal (unitary, symplectic) invariance of the Lorentzian ensemble implies that $U^\dagger (H - E_F)^{-1} U$ has the same distribution as $(H - E_F)^{-1}$. Using property 2 we then find that $\tilde{H}$ [being an $N \times N$ submatrix of $U^\dagger (H - E_F)^{-1} U$] is distributed according to the same Lorentzian ensemble (width $\tilde{\lambda}$ and center $\tilde{\varepsilon}$).

We now compute the distribution of the scattering matrix, first for a special coupling, then for the general case.

Special coupling matrix

First we will consider the special case that

$$\tilde{W} = \pi^{-1/2}\delta_{nm} \tag{2.2.24}$$

is proportional to the unit matrix. The relation (2.2.23) between the S and $\tilde{H}$ is then

$$S = \frac{1 + i\tilde{H}}{1 - i\tilde{H}}. \tag{2.2.25}$$

Thus the eigenvalues $\tilde{E}_j$ of $\tilde{H}$ and $e^{i\phi_j}$ of S are related via

$$e^{i\phi_j} = \frac{1 + i\tilde{E}_j}{1 - i\tilde{E}_j} \iff \phi_j = 2\arctan\tilde{E}_j. \tag{2.2.26}$$

Since transformations $\tilde{H} \to U\tilde{H}U^\dagger$ (with arbitrary orthogonal, unitary, or symplectic $N \times N$ matrix U) leave $P(\tilde{H})$ invariant, $P(S)$ is also invariant under $S \to USU^\dagger$. So $P(S)$ can only depend on the eigenvalues $e^{i\phi_j}$ of S. The distribution of the $\tilde{E}$'s is [cf. Eq. (2.2.11)]

$$P(\{\tilde{E}_j\}) = \frac{1}{V}\lambda^{N(\beta N+2-\beta)/2}\prod_{j<k}|\tilde{E}_j - \tilde{E}_k|^\beta \prod_j \left(\tilde{\lambda}^2 + (\tilde{E}_j - \tilde{\varepsilon})^2\right)^{-(\beta N+2-\beta)/2}. \tag{2.2.27}$$

From Eqs. (2.2.26) and (2.2.27) we obtain the probability distribution of the ϕ's,

$$\begin{aligned} P(\{\phi_j\}) &= \frac{1}{V}\left(\frac{1-\sigma\sigma^*}{2}\right)^{N(\beta N+2-\beta)/2} \\ &\quad \times \prod_{j<k}|e^{i\phi_j} - e^{i\phi_k}|^\beta \prod_j \left|1 - \sigma^* e^{i\phi_j}\right|^{-(\beta N+2-\beta)}, \qquad (2.2.28) \\ \sigma &= \frac{1-\tilde{\lambda}-i\tilde{\varepsilon}}{1+\tilde{\lambda}+i\tilde{\varepsilon}} = \frac{\lambda^2 + E_F^2 - \lambda - iE_F}{\lambda^2 + E_F^2 + \lambda + iE_F}. \qquad (2.2.29) \end{aligned}$$

Eq. (2.2.3) implies that $P(S)$ has the form of a Poisson kernel,

$$P(S) = \frac{\det(1 - \bar{S}\bar{S}^\dagger)^{(\beta N+2-\beta)/2}}{2^{N(\beta N+2-\beta)/2}V}\left|\det(1 - \bar{S}^\dagger S)\right|^{-(\beta N+2-\beta)}, \tag{2.2.30}$$

the average scattering matrix $\bar{S}$ being given by

$$\bar{S}_{nm} = \sigma\delta_{nm}. \tag{2.2.31}$$

Arbitrary coupling matrix

Now we turn to the case of arbitrary coupling matrix $\tilde{W}$. We denote the scattering matrix at coupling $\tilde{W}$ by S, and denote the scattering matrix at the special coupling (2.2.24) by S_0. The relation between S and S_0 is

$$S = r + t' S_0 (1 - r' S_0)^{-1} t \Longleftrightarrow S_0 = (t')^{-1}(S - r)(1 - r^\dagger S)^{-1} t^\dagger, \tag{2.2.32}$$

where we abbreviated

$$\begin{aligned} r &= (1 - \pi \tilde{W}^\dagger \tilde{W})(1 + \pi \tilde{W}^\dagger \tilde{W})^{-1}, \\ r' &= -\tilde{W}(1 - \pi \tilde{W}^\dagger \tilde{W})(1 + \pi \tilde{W}^\dagger \tilde{W})^{-1} \tilde{W}^{-1}, \\ t &= 2\pi^{1/2} \tilde{W}(1 + \pi \tilde{W}^\dagger \tilde{W})^{-1}, \\ t' &= 2\pi^{1/2}(1 + \pi \tilde{W}^\dagger \tilde{W})^{-1} \tilde{W}^\dagger. \end{aligned}$$

The symmetry of the coupling matrix $\tilde{W}$ is reflected in the symmetry of the $2N \times 2N$ matrix

$$S_1 = \begin{pmatrix} r & t' \\ t & r' \end{pmatrix}, \tag{2.2.33}$$

which is unitary symmetric ($\beta = 1$), unitary ($\beta = 2$) or unitary self-dual ($\beta = 4$).

The probability distribution P_0 of S_0 is given by Eq. (2.2.30). The distribution P of S follows from

$$P(S) = P_0(S_0) \frac{dS_0}{dS}, \tag{2.2.34}$$

where the Jacobian dS_0/dS is the ratio of infinitesimal volume elements around S_0 and S. This Jacobian is known [29, 34],

$$\frac{dS_0}{dS} = \left(\frac{\det(1 - r^\dagger r)}{|\det(1 - r^\dagger S)|^2} \right)^{(\beta N + 2 - \beta)/2}. \tag{2.2.35}$$

After expressing S_0 in terms of S by means of Eq. (2.2.32), we find that $P(S)$ is given by the same Poisson kernel as Eq. (2.2.30), but with a different $\bar{S}$,

$$\bar{S} = \frac{1 - \pi(\tilde{\lambda} + i\tilde{\varepsilon}) W^\dagger W}{1 + \pi(\tilde{\lambda} + i\tilde{\varepsilon}) W^\dagger W}. \tag{2.2.36}$$

In the limit $M \to \infty$ at fixed level spacing $\Delta = \lambda\pi/M$, Eq. (2.2.36) simplifies to

$$\bar{S} = \frac{\Delta M - \pi^2 W^\dagger W}{\Delta M + \pi^2 W^\dagger W}. \tag{2.2.37}$$

The extended version of the Hamiltonian approach which includes a background scattering matrix S_0 can be mapped to the case without background scattering matrix by a transformation $S \to S' = USU^T$ ($\beta = 1$), $S \to S' = USV$ ($\beta = 2$), or $S \to S' = USU^R$ ($\beta = 4$), where U and V are unitary matrices [33]. (U^T is the transposed of U, U^R is the

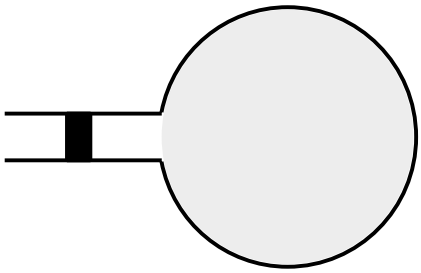

Figure 2-5. Schematic drawing of the chaotic cavity and the non-ideal lead containing a tunnel barrier.

dual of U.) The Poisson kernel is covariant under such transformations [27], i.e. it maps to a Poisson kernel with $\bar{S}' = U\bar{S}U^T$ ($\beta = 1$), $\bar{S}' = U\bar{S}V$ ($\beta = 2$), or $\bar{S}' = U\bar{S}U^R$ ($\beta = 4$). As a consequence, the distribution of S is given by the Poisson kernel for arbitrary coupling matrix W and background scattering matrix S_0. This proves the general equivalence of the Poisson kernel and the Lorentzian ensemble of Hamiltonians.

2.2.4 Ideal versus non-ideal leads

The circular ensemble of scattering matrices is appropriate for a chaotic cavity which is coupled to the leads by means of ballistic point contacts ("ideal" leads). In this section we will demonstrate that the generalized circular ensemble described by the Poisson kernel is the appropriate ensemble for a chaotic cavity which is coupled to the leads by means of tunnel barriers ("non-ideal" leads).

The system considered is shown schematically in Fig. 2-5. We assume that the segment of the lead between the tunnel barrier and the cavity is long enough, so that both the $N \times N$ scattering matrix S_0 of the cavity and the $2N \times 2N$ scattering matrix S_1 of the tunnel barrier are well-defined. The scattering matrix S_0 has probability distribution $P_0 =$ constant of the circular ensemble, whereas the scattering matrix S_1 is kept fixed.

We decompose S_1 in terms of $N \times N$ reflection and transmission matrices,

$$S_1 = \begin{pmatrix} r_1 & t_1' \\ t_1 & r_1' \end{pmatrix}. \tag{2.2.38}$$

The $N \times N$ scattering matrix S of the total system is related to S_0 and S_1 by

$$S = r_1 + t_1'(1 - S_0 r_1')^{-1} S_0 t_1. \tag{2.2.39}$$

This relation has the same form as equation (2.2.32). We can therefore directly apply equation (2.2.34), which yields

$$P(S) \propto |\det(1 - r_1^\dagger S)|^{-(\beta N + 2 - \beta)}. \tag{2.2.40}$$

Hence S is distributed according to a Poisson kernel, with $\bar{S} = r_1$.

2.2.5 Conclusion

In conclusion we have established by explicit computation the equivalence for $M \geq N$ of a generalized circular ensemble of scattering matrices (described by a Poisson kernel) and an ensemble of $M \times M$ Hamiltonians with a Lorentzian distribution. The Lorentzian and Gaussian distributions are equivalent in the large-M limit. Moreover, the Gaussian Hamiltonian ensemble and the microscopic theory of a metal particle with randomly placed impurities give rise to the same non-linear σ-model [21, 22]. Altogether, this provides a microscopic justification of the Poisson kernel in the case that the chaotic motion in the cavity is caused by impurity scattering. For the case of a ballistic chaotic cavity, a microscopic justification is still lacking.

The equivalence of the Poisson kernel and an arbitrary Hamiltonian ensemble can be reformulated in terms of a central limit theorem: The distribution of a submatrix of H^{-1} of fixed size N tends to a Lorentzian distribution when $M \to \infty$, independent of the details of the distribution of H. A central limit theorem of this kind for $N = 1$ has previously been formulated and proved by Mello [28].

Appendix A: Proof of properties 1 and 2 of Sec. 2.2.2

The two proofs given below are adapted from Ref. 29. The matrix H and its inverse H^{-1} have the same eigenvectors, but reciprocal eigenvalues. Therefore, property 1 of the Lorentzian ensemble is proved by showing that the distribution of the eigenvalues of H^{-1} is given by Eq. (2.2.11), with the substitutions $\lambda \to \tilde{\lambda}$ and $\varepsilon \to \tilde{\varepsilon}$. This is easily done,

$$
\begin{aligned}
&P(\{E_j^{-1}\}) = \\
&= \frac{1}{V}\lambda^{M(\beta M+2-\beta)/2} \prod_{i<j} |E_i - E_j|^\beta \prod_i \left[\left(\lambda^2 + (E_i-\varepsilon)^2\right)^{-(\beta M+2-\beta)/2} \left| \frac{dE_i}{d(E_i^{-1})} \right| \right] \\
&= \frac{1}{V}\lambda^{M(\beta M+2-\beta)/2} \prod_{i<j} \left| E_i E_j (E_i^{-1} - E_j^{-1}) \right|^\beta \prod_i \left[\left(\lambda^2 + (E_i-\varepsilon)^2\right)^{-(\beta M+2-\beta)/2} E_i^2 \right] \\
&= \frac{1}{V}\lambda^{M(\beta M+2-\beta)/2} \prod_{i<j} \left| E_i^{-1} - E_j^{-1} \right|^\beta \prod_i \left(\lambda^2 E_i^{-2} + (1-\varepsilon E_i^{-1})^2 \right)^{-(\beta M+2-\beta)/2} \\
&= \frac{1}{V}\tilde{\lambda}^{M(\beta M+2-\beta)/2} \prod_{i<j} \left| E_i^{-1} - E_j^{-1} \right|^\beta \prod_i \left(\tilde{\lambda}^2 + (E_i^{-1} - \tilde{\varepsilon})^2 \right)^{-(\beta M+2-\beta)/2} . \qquad \text{(A.1)}
\end{aligned}
$$

In order to prove property 2, we may assume that after rescaling of H we have $\lambda = 1$, $\varepsilon = 0$. First consider $N = M - 1$. In this case, one can write

$$
H = \begin{pmatrix} G & Y \\ Y^\dagger & Z \end{pmatrix}, \qquad \text{(A.2)}
$$

where G is the $N \times N$ submatrix of H whose distribution we want to compute, Y is a vector, with real ($\beta = 1$), complex ($\beta = 2$), or real quaternion elements ($\beta = 4$), and Z is

a real number. For the successive integrations over Z and Y we need two auxiliary results. First, for real numbers a, b, c such that $a > 0$ and $4ac > b^2$, and for real $m > 2$ we have

$$\int_{-\infty}^{\infty} dx\, (ax^2 + bx + c)^{-m} = \left(ac - \tfrac{1}{4}b^2\right)^{-m+1/2} a^{m-1}\pi^{1/2}\Gamma(m - 1/2)/\,\Gamma(m). \quad \text{(A.3)}$$

Second, if x is a d-dimensional vector with real components, and if $m > (d+1)/2$, then

$$\int_{-\infty}^{\infty} dx_1 \ldots \int_{-\infty}^{\infty} dx_d\, (1 + x^2)^{-m} = \pi^{d/2}\Gamma(m - d/2)/\,\Gamma(m). \quad \text{(A.4)}$$

Since $\det(1+H)^2$ is a quadratic function of Z, the integral over Z can now be carried out using Eq. (A.3). The result is:

$$\begin{aligned}\int dZ\, P(H) \;\; = \;\; & \frac{\pi^{1/2}\Gamma\left(\frac{1}{2}(\beta M + 1 - \beta)\right)}{V\Gamma\left(\frac{1}{2}(\beta M + 2 - \beta)\right)} \det(1+G^2)^{(-\beta M - 2 + \beta)/2} \times \\ & \left(1 + Y^\dagger (1+G^2)^{-1} Y\right)^{-\beta M - 1 + \beta}. \end{aligned} \quad \text{(A.5)}$$

Next, we integrate over Y. We may choose the basis for the Y-vectors so that $1+G^2$ is diagonal, with diagonal elements $1+G_i^2$. After rescaling of the Y-vectors to $Y_i' = Y_i(1+G_i^2)^{1/2}$ one obtains an integral similar to Eq. (A.4), with $d = \beta(M-1)$. The final result is

$$P(G) = \frac{\pi^{(\beta M - \beta + 1)/2}\,\Gamma\left(\frac{1}{2}(\beta M + 1 - \beta)\right)}{V\Gamma\left(\beta M + 1 - \beta\right)} \det(1+G^2)^{(-\beta(M-1) - 2 + \beta)/2}. \quad \text{(A.6)}$$

Property 2 now follows by induction. Notice that Eq. (A.6) allows us to determine the normalization constant V,

$$V = \pi^{(\beta M - \beta + 2)M/4} \prod_{j=1}^{M} \frac{\Gamma\left(\frac{1}{2}(\beta j + 1 - \beta)\right)}{\Gamma\left(\beta j + 1 - \beta\right)}. \quad \text{(A.7)}$$

References

[1] B. L. Altshuler, P. A. Lee, and R. A. Webb, eds., *Mesoscopic Phenomena in Solids* (North Holland, Amsterdam, 1991).

[2] V. N. Prigodin, K. B. Efetov and S. Iida, Phys. Rev. Lett. **71**, 1230 (1993).

[3] H. U. Baranger and P. A. Mello, Phys. Rev. Lett. **73**, 142 (1994).

[4] R. A. Jalabert, J.-L. Pichard, and C. W. J. Beenakker, Europhys. Lett. **27**, 255 (1994).

[5] M. L. Mehta, *Random Matrices* (Academic, New York, 1991).

[6] R. Blümel and U. Smilansky, Phys. Rev. Lett. **60**, 477 (1988); *ibid*. **64**, 241 (1990).

[7] U. Smilansky, in *Chaos and Quantum Physics*, edited by M.-J. Giannoni, A. Voros, and J. Zinn-Justin (North-Holland, Amsterdam, 1991).

[8] R. A. Jalabert, A. D. Stone, and Y. Alhassid, Phys. Rev. Lett. **68**, 3468 (1992).

[9] P. A. Mello and J.-L. Pichard, J. Phys. I (Paris) **1** (1991) 493.

[10] A. D. Stone, P. A. Mello, K. A. Muttalib, and J.-L. Pichard in Ref. 1.

[11] C. M. Marcus, A. J. Rimberg, R. M. Westervelt, P. F. Hopkins, and A. C. Gossard, Phys. Rev. Lett. **69**, 506 (1992); C. M. Marcus, R. M. Westervelt, P. F. Hopkins, and A. C. Gossard, Phys. Rev. B **48**, 2460 (1993); Chaos **3**, 643 (1993).

[12] M. W. Keller, O. Millo, A. Mittal, D. E. Prober, and R. N. Sacks, Surf. Sci. **305**, 501 (1994).

[13] A. M. Chang, H. U. Baranger, L. N. Pfeiffer, and K. W. West, Phys. Rev. Lett. **73**, 2111 (1994).

[14] R. A. Jalabert, H. U. Baranger, and A. D. Stone, Phys. Rev. Lett. **65**, 2442 (1990).

[15] H. U. Baranger, R. A. Jalabert, and A. D. Stone, Phys. Rev. Lett. **70**, 3876 (1993); Chaos **3**, 665 (1993).

[16] Z. Pluhăr, H. A. Weidenmüller, J. A. Zuk, and C. H. Lewenkopf, Phys. Rev. Lett. **73**, 2115 (1994).

[17] E. R. Mucciolo, V. N. Prigodin, and B. L. Altshuler, Phys. Rev. B **51**, 1714 (1995).

[18] J. P. Bird, K. Ishibashi, Y. Aoyagi, T. Sugano, and Y. Ochiai, Phys. Rev. **50**, 18678 (1994).

[19] O. Bohigas, M. J. Giannoni, and C. Schmit, Phys. Rev. Lett. **52**, 1 (1984); O. Bohigas in *Chaos and Quantum Physics*, edited by M.-J. Giannoni, A. Voros, and J. Zinn-Justin (North-Holland, Amsterdam, 1991).

[20] M. V. Berry, Proc. R. Soc. London A **400**, 229 (1985).

[21] K. B. Efetov, Adv. Phys. **32**, 53 (1983).

[22] J. J. M. Verbaarschot, H. A. Weidenmüller, and M. R. Zirnbauer, Phys. Rep. **129**, 367 (1985).

[23] S. Iida, H. A. Weidenmüller, and J. Zuk, Phys. Rev. Lett. **64**, 583 (1990); Ann. Phys. **200**, 219 (1990).

[24] A. Altland, Z. Phys. B. **82**, 105 (1991).

[25] C. H. Lewenkopf and H. A. Weidenmüller, Ann. Phys. **212**, 53 (1991).

[26] F. J. Dyson, J. Math. Phys. **3**, 140 (1962).

[27] P. A. Mello, P. Pereyra, and T. H. Seligman, Ann. Phys. (N.Y.) **161**, 254 (1985).

[28] P. A. Mello, in *Mesoscopic Quantum Physics*, edited by E. Akkermans, G. Montambaux, J.-L. Pichard, and J. Zinn-Justin (North-Holland, Amsterdam, 1995).

[29] L. K. Hua, *Harmonic Analysis of Functions of Several Complex Variables in the Classical Domains* (Amer. Math. Soc., Providence, 1963).

[30] T. J. Krieger, Ann. Phys. **42** (1967), 375.

[31] G. Hackenbroich and H. A. Weidenmüller, Phys. Rev. Lett. **74**, 4118 (1995).

[32] C. Mahaux and H. A. Weidenmüller, *Shell-model Approach to Nuclear Reactions* (North-Holland, Amsterdam, 1969).

[33] H. Nishioka and H. A. Weidenmüller, Phys. Lett. B **157**, 101 (1985).

[34] W. A. Friedman and P. A. Mello, Ann. Phys. **161**, 276 (1985).

3 Dephasing in quantum dots

3.1 Effect of a voltage probe on the phase-coherent conductance of a ballistic chaotic cavity

A basic notion in mesoscopic physics is that the measurement of a voltage at some point in the sample is an invasive act, which may destroy the phase coherence throughout the whole sample. Büttiker introduced a simple but realistic model for a voltage probe [1], and used it to investigate the transition from coherent to sequential tunneling through a double-barrier junction, induced by the coupling to a voltage lead of the region between the barriers. The mechanism by which the measurement of a voltage destroys phase coherence is that electrons which enter the voltage lead are reinjected into the system without any phase relationship. Büttiker's model has been applied successfully to a variety of physical situations [2–9], including diffusive transport in a disordered wire, ballistic transport through quantum point contacts, and edge-channel transport in the quantum Hall effect. In order to analyze their experimental data, Marcus et al. [10] proposed to use Büttiker's model to describe inelastic processes in ballistic and chaotic cavities ("quantum dots"). Here we present a detailed analysis of the effect of a voltage probe on the entire conductance distribution of such a system.

Several recent theoretical papers dealt with the phase-coherent conduction through a ballistic chaotic cavity, either by means of a semiclassical approach [11], or by means of the supersymmetry method [12–14], or by random-matrix theory [15, 16] (see also Ch. 2). Quantum interference has a striking effect on the conductance G of the quantum dot if it is coupled to source and drain reservoirs by means of two ballistic point contacts with a quantized conductance of $2e^2/h$. Classically, one would expect a conductance distribution $P(G)$ which is peaked at $G = e^2/h$, since half of the electrons injected by the source are transmitted on average to the drain. Instead, $P(G)$ was found to be [15, 16]

$$P(G) \propto G^{-1+\beta/2}, \quad 0 \leq G \leq 2e^2/h, \tag{3.1.1}$$

where $\beta \in \{1, 2, 4\}$ is the symmetry index of the ensemble of scattering matrices ($\beta = 1$ or 2 in the absence or presence of a time-reversal-symmetry breaking magnetic field; $\beta = 4$ in zero magnetic field with strong spin-orbit scattering). Depending on β, the conductance distribution is either uniform, peaked at zero or peaked at $2e^2/h$. As we will show, strong coupling of the quantum dot to a voltage lead causes a crossover from Eq. (3.1.1) to a Gaussian, peaked at e^2/h. A small displacement of the peak of the Gaussian for $\beta = 1$, and a β-dependent width of the peak are the remnants of the weak localization and mesoscopic fluctuation effects which are so pronounced in the case of complete phase coherence [15, 16].

A strong coupling of the voltage probe is achieved by means of a wide ballistic lead with many scattering channels (Sec. 3.1.3). If the voltage lead contains a single channel,

we may reduce the coupling to zero by means of a tunnel barrier in this lead (Sec. 3.1.2). Together, these two sections cover the full range of coupling strengths. In the next section we first formulate the problem in some more detail, and discuss the random-matrix method used to compute the conductance distribution.

3.1.1 Formulation of the problem

We consider a ballistic and chaotic cavity (quantum dot) coupled by two leads to source and drain reservoirs at voltages V_1 and V_2. A current $I = I_1 = -I_2$ is passed from source to drain via leads 1 and 2. A third lead is attached to the quantum dot and connected to a third reservoir at voltage V_3. This third lead is a voltage probe, which means that V_3 is adjusted in such a way, that no current is drawn ($I_3 = 0$). The coupling strength of the voltage probe is determined by the number N of scattering channels (propagating transverse modes at the Fermi-level) in lead 3 and by the transparency of a tunnel barrier in this lead. We assume that each of the N modes has the same transmission probability Γ through the tunnel barrier. We restrict ourselves to the case that the current-carrying leads 1 and 2 are ideal (no tunnel barrier) and single-channel (a single propagating transverse mode). This case maximizes the quantum-interference effects on the conductance. We assume that the capacitance of the quantum dot is sufficiently large that we may neglect the Coulomb blockade, and we will regard the electrons to be non-interacting.

The scattering-matrix S of the system has dimension $M = N + 2$ and can be written as

$$S = \begin{pmatrix} r_{11} & t_{12} & t_{13} \\ t_{21} & r_{22} & t_{23} \\ t_{31} & t_{32} & r_{33} \end{pmatrix} \tag{3.1.2}$$

in terms of reflection and transmission matrices r_{ii} and t_{ij}. The currents and voltages satisfy Büttiker's relations [17]

$$\frac{h}{2e^2} I_k = (N_k - R_{kk})\, V_k - \sum_{l \neq k} T_{kl} V_l, \;\; k = 1, 2, 3, \tag{3.1.3}$$

where $R_{kk} = \mathrm{tr}\, r_{kk} r_{kk}^\dagger$, $T_{kl} = \mathrm{tr}\, t_{kl} t_{kl}^\dagger$, and N_k is the number of modes in lead k. The two-terminal conductance $G = I/(V_1 - V_2)$ follows from Eq. (3.1.3) with $I_1 = -I_2 = I$, $I_3 = 0$:

$$G = \frac{2e^2}{h} \left(T_{12} + \frac{T_{13} T_{32}}{T_{31} + T_{32}} \right). \tag{3.1.4}$$

From now on, we will measure G in units of $2e^2/h$.

An ensemble of quantum dots is constructed by considering small variations in shape or Fermi energy. To compute the probability distribution $P(G)$ of the conductance in this ensemble we need to know the distribution of the elements of the scattering matrix. Our basic assumption, following Refs. [15] and [16], is that for ideal leads the scattering matrix is uniformly distributed in the space of unitary $M \times M$ matrices. This is the circular

ensemble of random-matrix theory [18, 19]. The distribution $P_0(S)$ for the case $\Gamma = 1$ is therefore simply

$$P_0(S) = \frac{1}{V}, \tag{3.1.5}$$

where $V = \int d\mu$ is the volume of the matrix space with respect to the invariant measure $d\mu$. Both V and $d\mu$ depend on the symmetry index $\beta \in \{1, 2, 4\}$, which specifies whether S is unitary ($\beta = 2$), unitary symmetric ($\beta = 1$), or unitary self-dual ($\beta = 4$).

A characteristic feature of the circular ensemble is that the average $\bar{S}$ of the scattering matrix vanishes. For non-ideal leads this is no longer the case, and Eq. (3.1.5) therefore has to be modified if $\Gamma \neq 1$. In Ch. 2 we showed, for a quantum dot with two non-ideal leads, how the probability distribution $P(S)$ of the scattering matrix can be computed by expressing the elements of the full scattering matrix S (quantum dot plus tunnel barriers) in terms of the scattering matrix S_0 of the quantum dot alone (with ideal leads). For an arbitrary number of leads the distribution takes the form of a Poisson kernel [20, 21],

$$P(S) = c\,|\det(1 - \bar{S}^\dagger S)|^{-\beta M - 2 + \beta}, \tag{3.1.6}$$

with normalization constant

$$c = \frac{1}{V}[\det(1 - \bar{S}^\dagger \bar{S})]^{\frac{1}{2}\beta M + 1 - \frac{1}{2}\beta}. \tag{3.1.7}$$

In the present case of two single-channel ideal leads and one non-ideal lead the average $\bar{S} = \int d\mu\, S P(S)$ of the scattering matrix is given by

$$\bar{S}_{nm} = \begin{cases} \sqrt{1-\Gamma} & \text{if } 3 \leq n = m \leq M, \\ 0 & \text{otherwise.} \end{cases} \tag{3.1.8}$$

One verifies that for $\Gamma = 1$, $P(S)$ reduces to the distribution (3.1.5) of the circular ensemble.

Eq. (3.1.1) holds for any $\beta \in \{1, 2, 4\}$. In what follows, however, we will only consider the cases $\beta = 1, 2$ of unitary or unitary symmetric matrices, appropriate for systems without spin-orbit scattering. The case $\beta = 4$ of unitary self-dual matrices is computationally much more involved, and also less relevant from a physical point of view.

As indicated by Büttiker [1], the cases $N = 1$ and $N > 1$ of a single- and multi-channel voltage lead are essentially different. Current conservation (i.e. unitarity of S) poses two restrictions on T_{31} and T_{32}: (i) $T_{31} \leq 1$, $T_{32} \leq 1$; and (ii) $T_{31} + T_{32} \leq N$. The second restriction is effective for $N = 1$ only. So for $N = 1$, current conservation imposes a restriction on the coupling strength of the voltage lead to the quantum dot which is not present for $N > 1$. We treat the cases $N = 1$ and $N > 1$ separately, in Secs. 3.1.2 and 3.1.3. For $N = 1$ we treat the case of arbitrary Γ, but for $N > 1$ we restrict ourselves for simplicity to $\Gamma = 1$.

3.1.2 Single-channel voltage lead

In the case $N = 1$, Eq. (3.1.1) reduces to

$$P(S) = \frac{1}{V}\Gamma^{\beta+1}\left(1 + (1-\Gamma)|S_{33}|^2 - 2(1-\Gamma)^{1/2}\,\mathrm{Re}\,S_{33}\right)^{-\beta-1}. \tag{3.1.9}$$

In order to calculate $P(G)$, we need to know the invariant measure $d\mu$ in terms of a parameterization of S which contains the transmission coefficients explicitly. The matrix elements of S, in the case $N = 1$, are related to R_{kk} and T_{kl} by $S_{kk} = \sqrt{R_{kk}}e^{i\phi_{kk}}$, $S_{kl} = \sqrt{T_{kl}}e^{i\phi_{kl}}$, where ϕ_{kl} are real phase shifts. When time-reversal symmetry is broken ($\beta = 2$), we choose R_{11}, R_{22}, T_{12}, T_{21}, ϕ_{13}, ϕ_{23}, ϕ_{33}, ϕ_{32}, and ϕ_{31} as independent variables, and the other variables then follow from unitarity of S. In the presence of time-reversal symmetry ($\beta = 1$), the symmetry $S_{kl} = S_{lk}$ reduces the set of independent variables to R_{11}, R_{22}, T_{12}, ϕ_{13}, ϕ_{23}, and ϕ_{33}.

We compute the invariant measure $d\mu$ in the same way as in Ref. [15]. Denoting the independent variables in the parameterization of S by x_i, we consider the change dS in S associated with an infinitesimal change dx_i in the independent variables. The invariant arclength $\mathrm{tr}\,dS^\dagger dS$ defines the metric tensor g_{ij} according to

$$\mathrm{tr}\,dS^\dagger dS = \sum_{i,j} g_{ij}\,dx_i\,dx_j. \tag{3.1.10}$$

The determinant $\det g$ then yields the invariant measure

$$d\mu = |\det g|^{1/2}\prod_i dx_i. \tag{3.1.11}$$

The result turns out to be independent of the phases ϕ_{kl} and to have the same form for $\beta = 1$ and 2,

$$d\mu = (\beta J)^{-1/2}\Theta(J)\prod_i dx_i. \tag{3.1.12}$$

The quantity J is defined by

$$J = \begin{cases} 0 \text{ if } R_{11} + T_{12} > 1 \text{ or } R_{22} + T_{21} > 1, \\ 4R_{22}T_{12}T_{13}T_{23} - (R_{22}T_{12} + T_{13}T_{23} - R_{11}T_{21})^2 \text{ otherwise,} \end{cases} \tag{3.1.13}$$

and $\Theta(J) = 1$ if $J > 0$ and $\Theta(J) = 0$ if $J \le 0$. The independent variables x_i are different, however, for $\beta = 1$ and $\beta = 2$ — as indicated above.

We have calculated the probability distribution of the conductance from Eqs. (3.1.4), (3.1.9), and (3.1.12). The results are shown in Fig. 3-1, for several values of Γ. For $\Gamma = 0$ (uncoupled voltage lead), $P(G)$ is given by [15, 16]

$$P(G) = \begin{cases} \frac{1}{2}G^{-1/2} & \text{if } \beta = 1, \\ 1 & \text{if } \beta = 2. \end{cases} \tag{3.1.14}$$

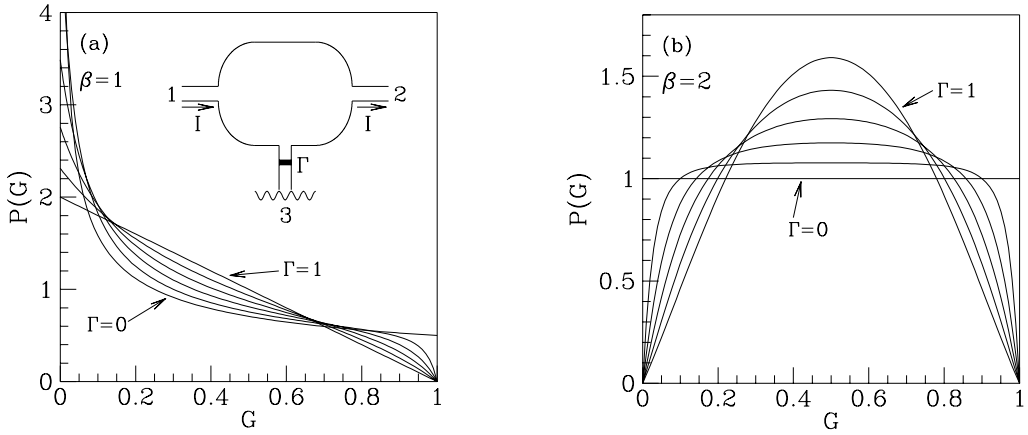

Figure 3-1. Distribution of the conductance G (in units of $2e^2/h$) for a single-channel voltage lead ($N = 1$). The voltage lead contains a tunnel barrier with transmission probability Γ, which varies from 0 to 1 with increments of 0.2. (a): time-reversal symmetry ($\beta = 1$); (b): broken time-reversal symmetry ($\beta = 2$). The quantum dot is shown schematically in the inset.

For $\Gamma = 1$ (maximally coupled single-channel voltage lead), we find

$$P(G)=\begin{cases} 2-2G & \text{if } \beta = 1, \\ \frac{4}{3}\left[2G-2G^2-(3G^2-2G^3)\ln G-(1-3G^2+2G^3)\ln(1-G)\right] & \text{if } \beta = 2. \end{cases} \tag{3.1.15}$$

The average $\langle G\rangle$ and variance $\operatorname{var} G$ of the conductance can be calculated in closed form for all Γ. We find that $\langle G\rangle$ is independent of Γ,

$$\langle G\rangle = \begin{cases} \frac{1}{3} & \text{if } \beta = 1, \\ \frac{1}{2} & \text{if } \beta = 2. \end{cases} \tag{3.1.16}$$

The variance does depend on Γ,

$$\operatorname{var} G = \begin{cases} \frac{1}{45}(1-\Gamma)^{-2}\left(4-11\Gamma+7\Gamma^2-3\Gamma^2\ln\Gamma\right) & \text{if } \beta = 1, \\ \frac{1}{36}(1-\Gamma)^{-3}\left(3-11\,\Gamma+17\,\Gamma^2-9\,\Gamma^3+4\,\Gamma^3\,\ln\Gamma\right) & \text{if } \beta = 2. \end{cases} \tag{3.1.17}$$

The breaking of phase coherence caused by the presence of a single-channel voltage lead is not strong enough to have any effect on the average conductance, which for $\beta = 1$ remains below the classical value of $1/2$. The variance of the conductance is reduced somewhat when Γ is increased from 0 to 1, but remains finite. (For $\beta = 1$ the reduction is with a factor $5/8$, for $\beta = 2$ with a factor $5/9$.) We will see in the next section, that the complete suppression of quantum interference effects requires a voltage lead with $N \gg 1$. Then $\langle G\rangle \to 1/2$ and $\operatorname{var} G \to 0$.

3.1.3 Multi-channel voltage lead

Now we turn to the case of a multi-channel ideal voltage lead ($N > 1$, $\Gamma = 1$). Current conservation yields:

$$\begin{aligned} T_{13} &= 1 - R_{11} - T_{12} = 1 - |S_{11}|^2 - |S_{12}|^2, \\ T_{31} &= 1 - R_{11} - T_{21} = 1 - |S_{11}|^2 - |S_{21}|^2, \\ T_{32} &= 1 - R_{22} - T_{12} = 1 - |S_{12}|^2 - |S_{22}|^2. \end{aligned} \tag{3.1.18}$$

To determine $P(G)$ it is thus sufficient to know the distribution $\tilde{P}(S_{11}, S_{12}, S_{21}, S_{22})$ of the matrix elements S_{kl} with $k, l \leq 2$. This marginal probability distribution has been calculated by Mello and coworkers [22] for arbitrary dimension $M \geq 4$ of S. As in Sec. 3.1.2 we parameterize $S_{kl} = \sqrt{T_{kl}} e^{i\phi_{kl}}$ if $k \neq l$ and $S_{kk} = \sqrt{R_{kk}} e^{i\phi_{kk}}$ ($k, l \leq 2$). We abbreviate $\prod_i dy_i \equiv dR_{11} dR_{22} dT_{12} dT_{22} \prod_{k,l=1}^{2} d\phi_{kl}$. For the cases $\beta = 1, 2$ one then has [22]

$$d\tilde{P} = \begin{cases} c_1 \delta(T_{12} - T_{21}) \delta(\phi_{12} - \phi_{21}) F^{(M-5)/2} \Theta(F) \prod_i dy_i & \text{if } \beta = 1, \\ c_2 F^{M-4} \Theta(F) \prod_i dy_i & \text{if } \beta = 2, \end{cases} \tag{3.1.19}$$

where F is defined by

$$F = \begin{cases} 0 \text{ if } R_{11} + T_{12} > 1 \text{ or } R_{22} + T_{21} > 1, \\ (1 - R_{11})(1 - R_{22}) + (1 - T_{12})(1 - T_{21}) - 1 \\ \qquad - 2(R_{11} R_{22} T_{12} T_{21})^{1/2} \cos(\phi_{11} + \phi_{22} - \phi_{12} - \phi_{21}) \text{ otherwise.} \end{cases} \tag{3.1.20}$$

The coefficients c_1 and c_2 are normalization constants. Calculation of the probability distribution of the conductance is now a matter of quadrature.

Results are shown in Fig. 3-2, for N up to 10. As N increases, $P(G)$ becomes more and more sharply peaked around $G = \frac{1}{2}$. In the limit $N \to \infty$, $P(G)$ approaches a delta function. Mean and variance are given by

$$\langle G \rangle = \begin{cases} \frac{1}{2} - \frac{1}{2} N^{-1} + \mathcal{O}(N^{-2}) & \text{if } \beta = 1, \\ \frac{1}{2} & \text{if } \beta = 2, \end{cases} \tag{3.1.21}$$

$$\operatorname{var} G = \begin{cases} \frac{3}{4} N^{-2} + \mathcal{O}(N^{-3}) & \text{if } \beta = 1, \\ \frac{1}{4} N^{-2} + \mathcal{O}(N^{-3}) & \text{if } \beta = 2. \end{cases} \tag{3.1.22}$$

The variance of G is reduced by a factor 3 when time-reversal symmetry is broken in the limit $N \to \infty$. The offset of $\langle G \rangle$ from $\frac{1}{2}$ when $\beta = 1$ is a remnant of the weak localization effect.

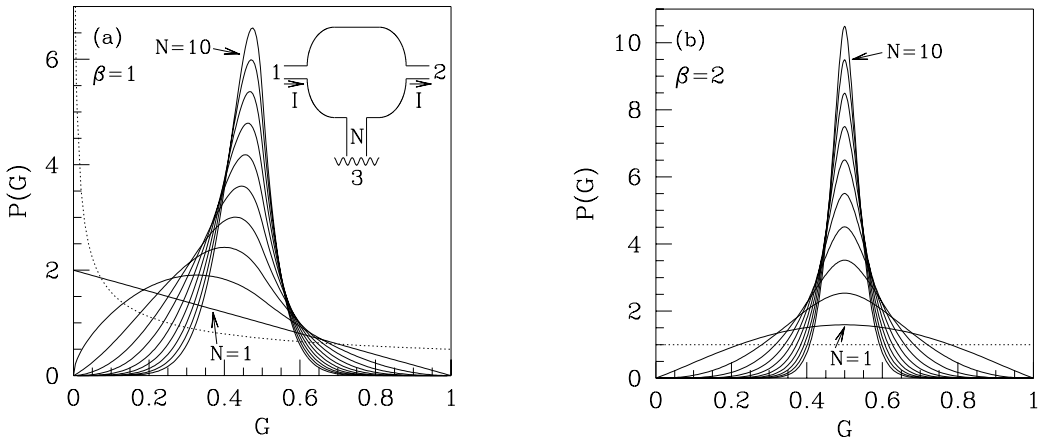

Figure 3-2. Conductance distribution for a multi-channel ideal voltage lead ($\Gamma = 1$). The number N of transverse modes in the lead varies from 1 to 10 with increments of 1 (solid curves). The dotted curve is the distribution in the absence of a voltage lead. The cases $\beta = 1$ and 2 are shown in (a) and (b) respectively.

3.1.4 Conclusion

We have calculated the entire probability distribution of the conductance of a quantum dot in the presence of a voltage probe, for single-channel point contacts to source and drain, in the presence and absence of time-reversal symmetry (no spin-orbit scattering). The average conductance is not changed if a single-channel voltage lead containing a tunnel barrier is attached, but the shape of the distribution changes considerably. A strikingly simple result is obtained for a single-channel ballistic voltage lead in zero magnetic field ($N = 1$, $\Gamma = 1$, $\beta = 1$), when $P(G) = 2 - 2G$, to be compared with $P(G) = \frac{1}{2}G^{-1/2}$ without the voltage probe [15, 16]. (In both cases $G \in [0, 1]$ is measured in units of $2e^2/h$.) When the number N of channels in the voltage lead is increased, the probability distribution becomes sharply peaked around $G = \frac{1}{2}$. Both the width of the peak and the deviation of its center from $\frac{1}{2}$ scale as $1/N$ for $N \gg 1$. The width is reduced by a factor $\sqrt{3}$ upon breaking the time-reversal symmetry.

The loss of phase coherence induced by a voltage probe can be investigated experimentally by fabricating a cavity with three leads attached to it. Furthermore, as emphasized by Marcus et al. [10], the inelastic scattering which occurs at finite temperatures in a quantum dot might well be modeled effectively by an imaginary voltage lead.

3.2 Voltage-probe and imaginary potential models for dephasing in a chaotic quantum dot

Extensive theoretical work has provided a detailed description of the universal features of phase-coherent transport in classically chaotic systems, such as universal conductance fluctuations, weak localization, and a non-Gaussian conductance distribution [12,15,16,23–29] (see also Ch. 2). The advances of submicron technology in the past decade have made these manifestations of quantum chaos in electronic transport accessible to experiment [30–37]. Although experiments on semiconductor quantum dots confirm the qualitative predictions of the phase-coherent theory, a quantitative comparison requires that loss of phase coherence be included into the theory. Two methods have been used for this purpose.

The first method, originating from Büttiker [1], is to include a fictitious voltage probe into the scattering matrix. The voltage probe breaks phase coherence by removing electrons from the phase-coherent motion in the quantum dot, and subsequently reinjecting them without any phase relationship. The conductance G_ϕ of the voltage probe (in units of $2e^2/h$) is set by the mean level spacing Δ in the quantum dot and the dephasing time τ_ϕ, according to $G_\phi = 2\pi\hbar/\tau_\phi\Delta$. This method was used in Refs. [25], [30], and [37] and in Sec. 3.1. The second method is to include a (spatially uniform) imaginary potential in the Hamiltonian, equal to $-i\hbar/2\tau_\phi$. This method was used in Refs. [26] and [28].

The two methods have given very different results for the distribution of the conductance G, in particular in the case that the current through the quantum dot flows through single-mode point contacts. While the distribution $P(G)$ becomes a delta peak at the classical conductance for very strong dephasing ($\tau_\phi \to 0$) in the voltage-probe model, $P(G)$ peaks at zero conductance in the imaginary potential model. It is the purpose of the present section to reconcile the two methods, and to compute the conductance distribution in the limit that the two methods are equivalent.

The origin of the differences lies with certain shortcomings of each model. On the one hand, the imaginary potential model does not conserve the number of electrons. We will show how to correct for this, thereby resolving an ambiguity in the formulation of the model noted by McCann and Lerner [28]. On the other hand, the voltage-probe model describes spatially localized instead of spatially uniform dephasing. This is perfectly reasonable for dephasing by a real voltage probe, but it is not satisfactory if one wants a fictitious voltage probe to serve as a model for dephasing by inelastic processes occurring uniformly in space. A second deficiency of the voltage-probe model is that inelastic scattering requires a continuous tuning parameter τ_ϕ, while the number of modes N_ϕ in the voltage probe can take on integer values only. Although the introduction of a tunnel barrier (transparency Γ_ϕ) in the voltage probe allows the conductance $G_\phi = N_\phi\Gamma_\phi$ to interpolate between integer values, the presence of *two* model parameters creates an ambiguity: The conductance distribution depends on N_ϕ and Γ_ϕ separately, and not just on the product $N_\phi\Gamma_\phi$ set by the dephasing time.

In this section we present a version of the voltage-probe model that does not suffer from this ambiguity and that can be applied to dephasing processes occurring uniformly in space. This version is equivalent to a particle-conserving imaginary potential model.

We show that the absorbing term in the Hamiltonian can be replaced by an absorbing lead (the voltage probe) in the limit $N_\phi \to \infty$, $\Gamma_\phi \to 0$ at fixed $G_\phi = N_\phi \Gamma_\phi$. This is the "locally weak absorption limit" of Zirnbauer [24]. Both shortcomings of the voltage-probe model are cured: The limit $N_\phi \to \infty$ together with ergodicity ensures spatial uniformity of the dephasing, while the conductance G_ϕ is the only variable left to parameterize the dephasing rate.

The outline of the section is as follows. In Sec. 3.2.1 we recall the voltage-probe model and derive the limit $N_\phi \to \infty$, $\Gamma_\phi \to 0$ at fixed $N_\phi \Gamma_\phi$ from the particle-conserving imaginary potential model. We then calculate the effect of dephasing on the conductance distribution in the case of single-mode point contacts (Sec. 3.2.2). The distribution narrows around the classical series conductance of the two point contacts when the dimensionless dephasing rate $\gamma = 2\pi\hbar/\tau_\phi \Delta$ becomes $\gg 1$, but not precisely in the way which was computed in Ref. [25] and Sec. 3.1. In Sec. 3.2.3 we briefly consider the case of multi-mode point contacts (number of modes $\gg 1$), which is less interesting. We conclude in Sec. 3.2.4.

3.2.1 Two models for dephasing

The system under consideration is shown in Fig. 3-3. It consists of a chaotic cavity, coupled by two point contacts (with N_1 and N_2 propagating modes at the Fermi energy E_F) to source and drain reservoirs at voltages V_1 and V_2. A current $I = I_1 = -I_2$ flows from source to drain. In the voltage-probe model [1], a fictitious third lead (N_ϕ modes) connects the cavity to a reservoir at voltage V_ϕ. Particle conservation is enforced by adjusting V_ϕ in such a way that no current is drawn ($I_\phi = 0$). The third lead contains a tunnel barrier, with a transmission probability Γ_ϕ which we assume to be the same for each mode. The scattering matrix S has dimension $M = N_1 + N_2 + N_\phi$ and can be written as

$$S = \begin{pmatrix} s_{11} & s_{12} & s_{1\phi} \\ s_{21} & s_{22} & s_{2\phi} \\ s_{\phi 1} & s_{\phi 2} & s_{\phi\phi} \end{pmatrix}, \tag{3.2.1}$$

in terms of $N_i \times N_j$ reflection and transmission matrices s_{ij}. Application of the relations [17]

$$I_k = \frac{2e^2}{h} \sum_l G_{kl} V_l, \quad k = 1, 2, \phi, \tag{3.2.2}$$

$$G_{kl} = \delta_{kl} N_k - \mathrm{tr}\, s_{kl} s_{kl}^\dagger, \tag{3.2.3}$$

yields the (dimensionless) conductance $G = (h/2e^2) I/(V_1 - V_2)$,

$$G = -G_{12} - \frac{G_{1\phi} G_{\phi 2}}{G_{\phi 1} + G_{\phi 2}}. \tag{3.2.4}$$

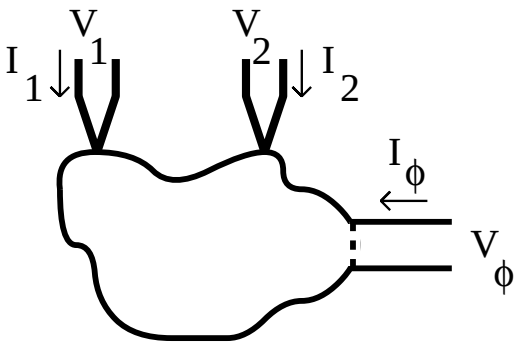

Figure 3-3. Chaotic cavity, connected to current source and drain reservoirs (1 and 2), and to a voltage probe (ϕ). The voltage probe contains a tunnel barrier (dotted line). The voltage V_ϕ is adjusted such that $I_\phi = 0$.

Using unitarity of S we may eliminate the conductance coefficients G_{kl} which involve the voltage probe,

$$G = -G_{12} + \frac{(G_{11}+G_{12})(G_{22}+G_{12})}{G_{11}+G_{12}+G_{21}+G_{22}}. \tag{3.2.5}$$

The remaining conductance coefficients are constructed from the matrix

$$\tilde{S} = \begin{pmatrix} s_{11} & s_{12} \\ s_{21} & s_{22} \end{pmatrix}, \tag{3.2.6}$$

which formally represents the scattering matrix of an absorbing system. The first term in Eq. (3.2.5) would be the conductance if the voltage probe would truly absorb the electrons which enter it. The second term accounts for the electrons that are reinjected from the phase-breaking reservoir, thereby ensuring particle conservation in the voltage-probe model.

The imaginary potential model relates $\tilde{S}$ to a Hamiltonian $\tilde{H}$ with a spatially uniform, negative imaginary potential $-i\gamma\Delta/4\pi$. As used in Refs. [26] and [28], it retains only the first term in Eq. (3.2.5), and therefore does not conserve particles. We correct this by including the second term. We will now show that this particle-conserving imaginary potential model is equivalent to the voltage-probe model in the limit $N_\phi \to \infty$, $\Gamma_\phi \to 0$, $N_\phi\Gamma_\phi \equiv \gamma$.

Our equivalence proof is based on the general relationship [38, 39]

$$\tilde{S} = 1 - 2\pi i \tilde{W}^\dagger (E_F - \tilde{H} + i\pi \tilde{W}\tilde{W}^\dagger)^{-1}\tilde{W} \tag{3.2.7}$$

between the $N \times N$ scattering matrix $\tilde{S}$ ($N = N_1 + N_2$) and the $N' \times N'$ Hamiltonian $\tilde{H}$ (the limit $N' \to \infty$ is taken later on). The Hamiltonian contains an imaginary potential, $\tilde{H}_{\mu\nu} = H_{\mu\nu} - i\delta_{\mu\nu}\gamma\Delta/4\pi$, with H a Hermitian matrix. For a chaotic cavity, H is taken

from the Gaussian ensemble of random matrix theory [19]. The $N' \times N$ matrix $\tilde{W}$ has elements (cf. Sec. 2.2)

$$\pi \tilde{W}_{\mu n}^2 \;=\; \pi^{-1}\delta_{\mu n} N' \Delta \left(2\Gamma_n^{-1} - 1 - 2\Gamma_n^{-1}\sqrt{1-\Gamma_n}\right). \tag{3.2.8}$$

Here Γ_n is the transmission probability of mode n in the leads and the energy Δ is the mean level spacing of H. We embed $\tilde{W}$ into an $N' \times N'$ matrix by the definition $\tilde{W}_{\mu n} = 0$ for $N < n \leq N'$, and define

$$\pi W_{\mu n}^2 = \pi \tilde{W}_{\mu n}^2 + \delta_{\mu n}\gamma\Delta/4\pi. \tag{3.2.9}$$

Substitution into Eq. (3.2.7) shows that $\tilde{S}$ is an $N \times N$ submatrix of an $N' \times N'$ unitary matrix

$$S = 1 - 2\pi i W^\dagger (E_F - H + i\pi W W^\dagger)^{-1} W. \tag{3.2.10}$$

We have neglected the difference between $\tilde{W}_{\mu\mu}$ and $W_{\mu\mu}$ for $1 \leq \mu \leq N$, which is allowed in the limit $N' \to \infty$. The matrix S is the scattering matrix of a cavity with three leads: Two real leads with N_1, N_2 modes, plus a fictitious lead with $N' - N$ modes. The transmission probability Γ_n of a mode in the fictitious lead follows from Eqs. (3.2.8) and (3.2.9),

$$\Gamma_n = \frac{4\pi^2 W_{nn}^2 N'\Delta}{(N'\Delta + \pi^2 W_{nn}^2)^2} \to \frac{\gamma}{N'} \text{ if } N' \to \infty, \tag{3.2.11}$$

where we have used that $\pi W_{nn}^2 = \gamma\Delta/4\pi$ for $N < n \leq N'$.

We conclude that the particle-conserving imaginary potential model and the voltage-probe model are equivalent in the limit $N_\phi = N' - N \to \infty$, $\Gamma_\phi = \gamma/N' \to 0$, $N_\phi\Gamma_\phi = \gamma(1 - N/N') \to \gamma$.

3.2.2 Single-mode point contacts

The effect of quantum-interference on the conductance is maximal if the point contacts which couple the chaotic cavity to the source and drain reservoirs have only a single propagating mode at the Fermi level. Then the sample-to-sample fluctuations of the conductance are of the same size as the average conductance itself. One thus needs the entire conductance distribution to characterize an ensemble of quantum dots. (An ensemble may be generated by small variations in shape or in Fermi energy.)

In the absence of dephasing, the conductance distribution $P(G)$ is highly non-Gaussian [12, 15, 16] (see Sec. 2.1). For ideal point contacts (transmission probabilities $\Gamma_1 = \Gamma_2 = 1$), one finds [15, 16]

$$P(G) = \tfrac{1}{2}\beta G^{(\beta-2)/2}. \tag{3.2.12}$$

The symmetry parameter $\beta = 2$ (1) in the presence (absence) of a time-reversal-symmetry breaking magnetic field. For high tunnel barriers ($\Gamma_1, \Gamma_2 \ll 1$), $P(G)$ is maximal for $G = 0$, and drops off $\propto G^{-3/2}$ for $G \gg \Gamma_1\Gamma_2$, see Ref. [12] and Sec. 2.1. In this section, we compute the conductance distribution in the presence of dephasing, using the voltage-probe model in the limit $N_\phi \to \infty$, $\Gamma_\phi \to 0$ at fixed $N_\phi\Gamma_\phi$, in which it is equivalent

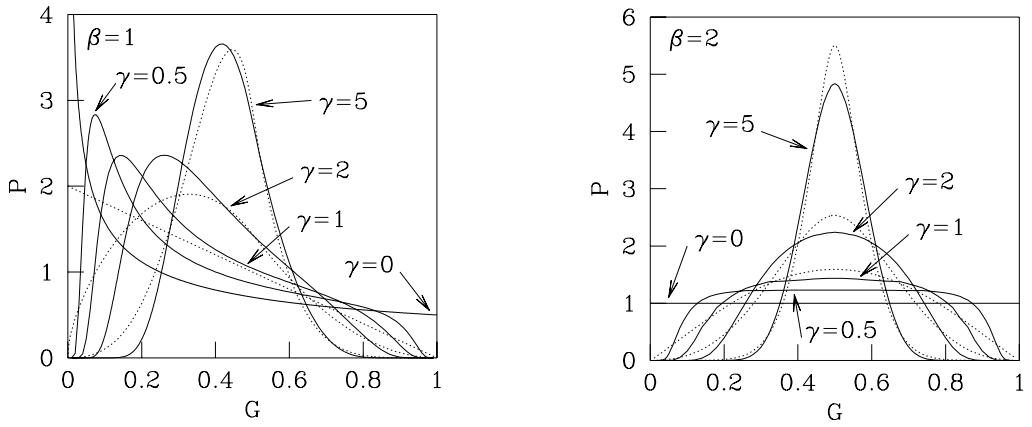

Figure 3-4. Solid curves: Conductance distributions of a quantum dot with two ideal single-mode point contacts, computed from Eqs. (3.2.19) and (3.2.21) for dephasing rates $\gamma = 0$, 0.5, 1, 2, and 5. The top panel is for zero magnetic field ($\beta = 1$), the bottom panel for broken time-reversal symmetry ($\beta = 2$). The dotted curves are the results of Refs. [25] and Sec. 3.1 for the model of an ideal voltage probe (without a tunnel barrier), in which dephasing is not fully uniform in phase space. For $\gamma = 0$ the two models coincide. The value $\gamma = 0.5$ is not accessible in the model of an ideal voltage probe (because $\gamma = N_\phi \Gamma_\phi$ can take on only integer values if $\Gamma_\phi = 1$).

to the current-conserving imaginary potential model. We focus on the case of ideal point contacts, and discuss the effect of tunnel barriers briefly at the end of the section.

In Sec. 2.2, it has been shown that the scattering matrix S is distributed according to the Poisson kernel [20, 21, 40],

$$P(S) = \frac{1}{V} \frac{\det(1 - \bar{S}\bar{S}^\dagger)^{(\beta M + 2 - \beta)/2}}{|\det(1 - \bar{S}S^\dagger)|^{\beta M + 2 - \beta}}, \tag{3.2.13}$$

where V is a normalization constant, $M = N_1 + N_2 + N_\phi$ is the dimension of S, and $\bar{S}$ is a diagonal matrix with diagonal elements $\bar{S}_{nn} = \sqrt{1 - \Gamma_n}$. Here Γ_n is the transmission probability of mode n ($\Gamma_n \equiv \Gamma_\phi$ for $N_1 + N_2 < n \leq M$). The measure dS is the invariant measure on the manifold of unitary (unitary symmetric) matrices for $\beta = 2$ (1).

We now specialize to the case of ideal single-mode point contacts, $N_1 = N_2 = 1$ and $\Gamma_1 = \Gamma_2 = 1$. We seek the distribution of the 2×2 submatrix $\tilde{S}$ defined in Eq. (3.2.6). We start with the polar decomposition of S,

$$S = \begin{pmatrix} u & 0 \\ 0 & v \end{pmatrix} \begin{pmatrix} \sqrt{1 - t^\dagger t} & it^\dagger \\ it & \sqrt{1 - tt^\dagger} \end{pmatrix} \begin{pmatrix} u' & 0 \\ 0 & v' \end{pmatrix}, \tag{3.2.14}$$

where u and u' (v and v') are 2×2 ($N_\phi \times N_\phi$) unitary matrices, and t is a $N_\phi \times 2$ matrix with all elements equal to zero except $t_{nn} = \sqrt{T_n}$, $n = 1, 2$. In the presence of time-reversal

symmetry, $u' = u^{\mathrm{T}}$ and $v' = v^{\mathrm{T}}$. In terms of the polar decomposition (3.2.14) we have

$$\tilde{S} = u \begin{pmatrix} \sqrt{1-T_1} & 0 \\ 0 & \sqrt{1-T_2} \end{pmatrix} u'. \tag{3.2.15}$$

The two parameters T_1 and T_2 govern the strength of the absorption by the voltage probe. For $T_1, T_2 \to 0$ the matrix $\tilde{S}$ is unitary and there is no absorption, whereas for $T_1, T_2 \to 1$ the matrix $\tilde{S}$ vanishes and the absorption is complete. Substitution of the invariant measure [29]

$$\begin{aligned} dS &= |T_1 - T_2|^{\beta} (T_1 T_2)^{(\beta N_\phi - 2 - \beta)/2} \\ &\quad \times du\, du'\, dv\, dv'\, dT_1\, dT_2 \end{aligned} \tag{3.2.16}$$

and the polar decomposition (3.2.14) into the Poisson kernel (3.2.13), yields the distribution of $\tilde{S}$ in the form

$$\begin{aligned} P(T_1, T_2, u, u') &= \Gamma_\phi^{N_\phi(\beta N_\phi + 2 + \beta)/2} |T_1 - T_2|^{\beta} \\ &\quad \times \frac{1}{V} \int dv \int dv' \, \frac{(T_1 T_2)^{(\beta N_\phi - 2 - \beta)/2}}{|\det(1 - v' v\, \tau)|^{\beta N_\phi + 2 + \beta}}, \end{aligned} \tag{3.2.17}$$

$$\tau = \sqrt{(1 - \Gamma_\phi)(1 - t t^{\dagger})}. \tag{3.2.18}$$

Since Eq. (3.2.17) is independent of u and u', the matrices u and u' are uniformly distributed in the unitary group, and the distribution of $\tilde{S}$ is completely determined by the joint distribution $P(T_1, T_2)$ of the absorption probabilities T_1 and T_2.

It remains to perform the integral over v and v' in Eq. (3.2.17). This is a non-trivial calculation, which we describe in the appendix. The final result in the limit $N_\phi \to \infty$, $\Gamma_\phi \to 0$ at fixed $\gamma = N_\phi \Gamma_\phi$ is

$$\begin{aligned} P(T_1, T_2) &= \tfrac{1}{8} T_1^{-4} T_2^{-4} \exp\left[-\tfrac{1}{2}\gamma(T_1^{-1} + T_2^{-1})\right] |T_1 - T_2| \Big[\gamma^2(2 - 2e^{\gamma} + \gamma + \gamma e^{\gamma}) \\ &\quad - \gamma(T_1 + T_2)(6 - 6e^{\gamma} + 4\gamma + 2\gamma e^{\gamma} + \gamma^2) \\ &\quad + T_1 T_2 (24 - 24e^{\gamma} + 18\gamma + 6\gamma e^{\gamma} + 6\gamma^2 + \gamma^3)\Big] \end{aligned} \tag{3.2.19}$$

for $\beta = 1$ (presence of time-reversal symmetry), and

$$\begin{aligned} P(T_1, T_2) &= \tfrac{1}{2} T_1^{-6} T_2^{-6} \exp\left[-\gamma(T_1^{-1} + T_2^{-1})\right] (T_1 - T_2)^2 \\ &\quad \times \Big[\gamma^4(1 - 2e^{\gamma} + e^{2\gamma} - \gamma^2 e^{\gamma}) - \gamma^3(T_1 + T_2)(4 - 8e^{\gamma} + 4e^{2\gamma} + 2\gamma \\ &\quad - 2\gamma e^{\gamma} - 2\gamma^2 e^{\gamma} - \gamma^3 e^{\gamma}) + \gamma^2(T_1^2 + T_2^2)(2 - 4e^{\gamma} + 2e^{2\gamma} + 4\gamma \\ &\quad - 4\gamma e^{\gamma} + \gamma^2 + \gamma^2 e^{\gamma} - \gamma^3 e^{\gamma}) + \gamma^2 T_1 T_2 (20 - 40e^{\gamma} + 20e^{2\gamma} + 16\gamma \\ &\quad - 16\gamma e^{\gamma} + 4\gamma^2 - 8\gamma^2 e^{\gamma} - 4\gamma^3 e^{\gamma} - \gamma^4 e^{\gamma}) - \gamma T_1 T_2 (T_1 + T_2)(12 \\ &\quad - 24e^{\gamma} + 12e^{2\gamma} + 24\gamma - 24\gamma e^{\gamma} + 12\gamma^2 + 2\gamma^3 - 2\gamma^3 e^{\gamma} - \gamma^4 e^{\gamma}) \\ &\quad + T_1^2 T_2^2 (12 - 24e^{\gamma} + 12e^{2\gamma} + 24\gamma - 24\gamma e^{\gamma} + 24\gamma^2 - 12\gamma^2 e^{\gamma} + 8\gamma^3 \\ &\quad + 4\gamma^3 e^{\gamma} + \gamma^4 - 2\gamma^4 e^{\gamma})\Big] \end{aligned} \tag{3.2.20}$$

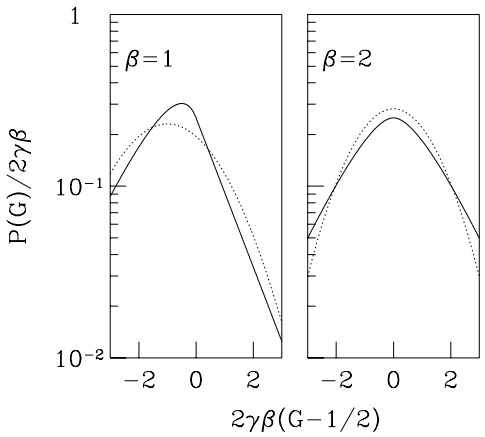

Figure 3-5. The limiting conductance distribution (3.2.22) for $\gamma \gg 1$ (solid curves). A Gaussian distribution with the same mean and variance is shown for comparison (dotted curves).

for $\beta = 2$ (absence of time-reversal symmetry).

To relate the conductance G to T_1, T_2, u, and u', we substitute the polar decomposition of S into Eq. (3.2.5), with the result

$$G = \sum_{i,j=1}^{2} u_{1i} u'_{i2} u^*_{1j} u'^*_{j2} \sqrt{(1-T_i)(1-T_j)} + (T_1+T_2)^{-1} \sum_{i,j=1}^{2} |u_{1i}|^2 |u'_{j2}|^2 T_i T_j . \tag{3.2.21}$$

Eqs. (3.2.19) and (3.2.21), together with the uniform distribution of the 2×2 matrices u, u' over the unitary group, fully determine the distribution $P(G)$ of the conductance of a chaotic cavity with two ideal single-mode point contacts. We parameterize u, u' in Euler angles and obtain $P(G)$ as a four-dimensional integral, which we evaluate numerically. The distribution is plotted in Fig. 3-4 (solid curves) for several values of the dimensionless dephasing rate $\gamma = 2\pi\hbar/\tau_\phi\Delta$. For $\gamma \gg 1$, the conductance distribution becomes peaked around the classical conductance $G = 1/2$,

$$P(G) \to \frac{\gamma\beta}{2}\left(1 + |x| - \delta_{\beta 1} x\right) e^{-|x|} \quad \text{if } \gamma \gg 1, \tag{3.2.22}$$

where $x = 2\gamma\beta(G - 1/2)$.[1] Notice that the distribution remains non-Gaussian for all values of γ. The limiting distribution (3.2.22) is plotted in Fig. 3-5, for $\beta = 1$ and 2. The

[1]The condition $\gamma \gg 1$ for very strong dephasing is understood as the regime $\tau_{\rm dwell} \gg \tau_\phi \gg \tau_{\rm erg}$, where $\tau_{\rm dwell}$ is the dwell time of the electrons in the quantum dot and $\tau_{\rm erg}$ the time scale for ergodic exploration of the complete phase space. The regime $\tau_\phi < \tau_{\rm erg}$ is considered in Ref. [28].

average and variance of the conductance are

$$\langle G\rangle = \tfrac{1}{2} - \tfrac{1}{2}\delta_{\beta 1}\gamma^{-1} + \mathcal{O}(\gamma^{-2}), \tag{3.2.23}$$

$$\operatorname{var} G = \tfrac{1}{4}(1+2\delta_{\beta 1})\gamma^{-2} + \mathcal{O}(\gamma^{-3}). \tag{3.2.24}$$

The effect of dephasing was previously studied in Ref. [25] and Sec. 3.1 for the case $\Gamma_\phi = 1$ of an ideal voltage probe (without a tunnel barrier). The corresponding results are also shown in Fig. 3-4 (dotted curves). We see that the limit $N_\phi \to \infty$, $\Gamma_\phi \to 0$ results in narrower distributions at the same value of $\gamma = N_\phi\Gamma_\phi$. In particular, the tails $G \to 0$ and $G \to 1$ are strongly suppressed even for the smallest γ, in contrast with the case of the ideal voltage probe. The physical reason for the difference is that keeping N_ϕ small and setting Γ_ϕ equal to 1 corresponds to dephasing which is not fully uniform in phase space, and therefore not as effective as the limit $N_\phi \to \infty$, $\Gamma_\phi \to 0$. For large γ, the difference vanishes, and the distribution (3.2.22) is recovered for an ideal voltage probe as well. (The fact that the conductance fluctuations around $G = 1/2$ are non-Gaussian was overlooked in Ref. [25] and Sec. 3.1.)

We have shown in the previous section that the voltage-probe model in the limit $N_\phi \to \infty$, $\Gamma_\phi \to 0$ is equivalent to the particle-conserving imaginary potential model. The requirement of particle conservation is essential. This is illustrated in Fig. 3-6a, where we compare our results with those obtained from the imaginary potential model without enforcing conservation of particles. [This model corresponds to setting $G = -G_{12}$ in Eq. (3.2.5) and was first solved in Ref. [12].] For $\gamma \gg 1$, the imaginary potential without particle conservation yields a distribution which is maximal at $G = 0$, instead of a strongly peaked distribution around $G = 1/2$ [cf. Eq. (3.2.22)].

The first two moments of the conductance can be computed analytically from equations (3.2.19) and (3.2.21). The resulting expressions (which are too lengthy to report here) are plotted in Fig. 3-6b. The markers at integer values of γ are the results of the ideal voltage-probe model of Refs. [25] and Sec. 3.1, where $\Gamma_\phi = 1$ and $\gamma = N_\phi = 0, 1, 2, \ldots$. The remarkable result of Sec. 3.1 that $\langle G\rangle$ is the same for $\gamma = 0$ and $\gamma = 1$ is special for dephasing by a single-mode voltage probe: The present model with spatially uniform dephasing has a strictly monotonic increase of $\langle G\rangle$ with γ for $\beta = 1$.

Sofar we have considered ideal point contacts. Non-ideal point contacts (i.e. point contacts with tunnel barriers) correspond to $\Gamma_1, \Gamma_2 < 1$ in the distribution (3.2.13) of S. Using the results of Sec. 2.2, this case can be mapped onto that of ideal point contacts by the parameterization [20, 21]

$$S = R + T(1 - S'R)^{-1}S'T, \tag{3.2.25}$$

where R and $T = i\sqrt{1-R^2}$ are diagonal matrices. The only nonzero elements of R are $R_{11} = \sqrt{1-\Gamma_1}$ and $R_{22} = \sqrt{1-\Gamma_2}$. The distribution of S' is given by the Poisson kernel (3.2.13) with $\Gamma_1 = \Gamma_2 = 1$. Physically, S' is the scattering matrix of the quantum dot without the tunnel barriers in the point contacts, while R (T) is the reflection (transmission) matrix of the tunnel barriers in the absence of the quantum dot, see Sec. 2.2. We may restrict the parameterization (3.2.25) to the 2×2 submatrix $\tilde{S}$,

$$\tilde{S} = \tilde{R} + \tilde{T}(1 - \tilde{S}'\tilde{R})^{-1}\tilde{S}'\tilde{T}, \tag{3.2.26}$$

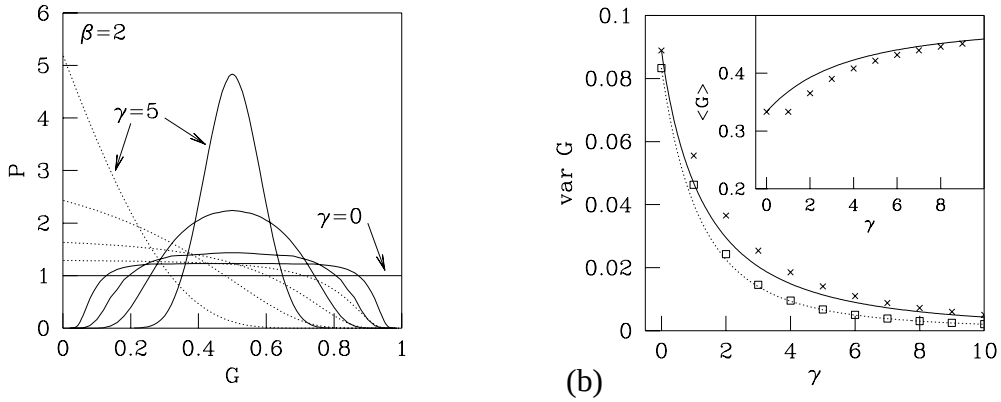

Figure 3-6. (a) Solid curves: Same as in Fig. 3-4, bottom panel. Dotted curves: Results of the imaginary potential model without particle conservation. (b) Variance of the conductance as a function of the dephasing rate γ, for $\beta = 1$ (solid curve) and $\beta = 2$ (dotted curve), computed from Eqs. (3.2.19) and (3.2.21). The crosses ($\beta = 1$) and squares ($\beta = 2$) at integer γ result from the model of Refs. [25] and Sec. 3.1 with the ideal voltage probe. The inset shows the average conductance for $\beta = 1$. (For $\beta = 2$ the average is trivially equal to $1/2$ for all γ in both models.)

where the matrices $\tilde{S}'$, $\tilde{R}$, and $\tilde{T}$ are the upper-left 2×2 submatrices of S', R, and T, respectively. The matrix $\tilde{S}'$ has the distribution given by Eqs. (3.2.17) and (3.2.19). The matrices $\tilde{R}$ and $\tilde{T}$ are fixed, so the distribution of $\tilde{S}$ follows directly from Eq. (3.2.26).

For strong dephasing ($\gamma \gg \Gamma_1, \Gamma_2$) we find that the conductance distribution becomes a Gaussian with mean and variance given by

$$\langle G \rangle = \frac{\Gamma_1 \Gamma_2}{\Gamma_1 + \Gamma_2} - \frac{2\Gamma_1^2 \Gamma_2^2 (4/\beta - \Gamma_1 - \Gamma_2)}{\gamma (\Gamma_1 + \Gamma_2)^3}, \tag{3.2.27}$$

$$\operatorname{var} G = \frac{4\Gamma_1^2 \Gamma_2^2 (\Gamma_1^2 + \Gamma_2^2 - \Gamma_1 \Gamma_2^2 - \Gamma_1^2 \Gamma_2)}{\beta \gamma (\Gamma_1 + \Gamma_2)^3}. \tag{3.2.28}$$

The average conductance $\langle G \rangle$ is the classical series conductance of the two point-contact conductances Γ_1 and Γ_2. Fluctuations around the classical conductance are of order $\gamma^{-1/2}$. For ideal point contacts ($\Gamma_1, \Gamma_2 \to 1$) the variance (3.2.28) vanishes. The higher-order fluctuations are non-Gaussian, described by Eq. (3.2.22).

Again our result is entirely different from that of the imaginary potential model without particle conservation [12, 28], where $P(G)$ becomes sharply peaked at $G = 0$ when $\gamma \gg \Gamma_1, \Gamma_2$. We have verified that we recover the results of Ref. [12] from our Eqs. (3.2.19) and (3.2.21) if we retain only the first term in Eq. (3.2.5), i.e. if we set $G = -G_{12}$. The results of Ref. [28] are recovered if we symmetrize this term, i.e. if we set $G = -(G_{12} + G_{21})/2$. (This is different from $-G_{12}$ if $\beta = 2$ and $\gamma \neq 0$.) Once particle conservation is enforced, the imaginary potential model leads unambiguously to Eq. (3.2.27).

3.2.3 Multi-mode point contacts

In this section we consider the case $N_1, N_2 \gg 1$ of a large number of modes in the two point contacts. The conductance distribution is then a Gaussian, hence it suffices to compute the first two moments of G. We first consider ideal point contacts ($\Gamma_1 = \Gamma_2 = 1$), and discuss the effect of tunnel barriers at the end.

For $N_1, N_2 \gg 1$ the integration over the scattering matrix S with the probability distribution (3.2.13) can be done using the diagrammatic technique of Ch. 6. The result for the average of the conductance coefficients G_{ij} is

$$\langle G_{ij}\rangle = N_i\delta_{ij} - \frac{N_iN_j}{N+N_\phi\Gamma_\phi} + \delta_{\beta,1}A_{ij}, \tag{3.2.29}$$

$$A_{ij} = \frac{N_iN_j(N+2N_\phi\Gamma_\phi - N_\phi\Gamma_\phi^2)}{(N+N_\phi\Gamma_\phi)^3} - \frac{\delta_{ij}N_i}{N+N_\phi\Gamma_\phi}, \tag{3.2.30}$$

up to terms of order N^{-1}. (Here we recall that $N = N_1 + N_2$.) For the covariances $\mathrm{cov}\,(G_{ij}, G_{kl}) \equiv \langle G_{ij}G_{kl}\rangle - \langle G_{ij}\rangle\langle G_{kl}\rangle$ we find

$$\begin{aligned}\mathrm{cov}\,(G_{ij}, G_{kl}) &= A_{ik}A_{jl} + \delta_{\beta,1}A_{il}A_{jk} \\ &\quad + \frac{2N_iN_jN_kN_lN_\phi(N_\phi+N)\Gamma_\phi^2(1-\Gamma_\phi)}{\beta(N+N_\phi\Gamma_\phi)^6}.\end{aligned} \tag{3.2.31}$$

In order to find the average and variance of the conductance in the presence of dephasing, we substitute Eqs. (3.2.30) and (3.2.31) into Eq. (3.2.5). The result is

$$\langle G\rangle = \frac{N_1N_2}{N}\left(1 - \frac{\delta_{\beta1}}{N+\gamma}\right), \tag{3.2.32}$$

$$\mathrm{var}\,G = \frac{2N_1^2N_2^2}{\beta N^2(N+\gamma)^2}, \tag{3.2.33}$$

with $\gamma = N_\phi\Gamma_\phi$.

Eq. (3.2.32) was previously obtained by Aleiner and Larkin [27]. Eq. (3.2.33) for var G agrees with the interpolation formula of Baranger and Mello [25]. The derivation presented here shows that this interpolation formula is in fact a rigorous result of perturbation theory. [However, the interpolation formula of Ref. [25] for $\langle G\rangle$ differs from Eq. (3.2.32).] In the final expression for $\langle G\rangle$ and var G only the product $N_\phi\Gamma_\phi$ appears, although the moments of the conductance coefficients G_{ij} depend on N_ϕ and Γ_ϕ separately. Apparently, in large-N perturbation theory the precise choice of N_ϕ and Γ_ϕ in the voltage-probe model is irrelevant, the conductance distribution being determined by the product $N_\phi\Gamma_\phi$ only. For small dephasing rates $\gamma \ll N$, Eq. (3.2.32) agrees with Efetov's result [26], who used the imaginary potential model without enforcing particle conservation. However, for $\gamma \gtrsim N$, our result differs from that of Ref. [26], indicating the importance of particle conservation once the dephasing rate γ and the dimensionless escape rate N through the point contacts become comparable.

We have carried out the same calculation for the case of non-ideal point contacts. The transmission probability of mode n is denoted by Γ_n ($n = 1, \ldots, N_1$ corresponding to the first point contact, $n = N_1 + 1, \ldots, N_1 + N_2$ to the second point contact). The result is

$$\langle G\rangle = \frac{g_1 g_1'}{g} - \delta_{\beta 1}\frac{g_2 g_1'^2 + g_1^2 g_2'}{g^2(g+\gamma)}, \tag{3.2.34}$$

$$\begin{aligned}\operatorname{var} G &= \frac{2g_1^2 g_1'^2}{\beta g^2(g+\gamma)^2} + \frac{4(g_1^4 g_2' - g_1^4 g_3' + g_2 g_1'^4 - g_3 g_1'^4)}{\beta g^4(g+\gamma)} \\ &\quad + \frac{3(g_1^4 g_2'^2 + g_2^2 g_1'^4)}{\beta g^4(g+\gamma)^2} - \frac{4g_1^2 g_1'^2(g_2+g_2')}{\beta g^3(g+\gamma)^2},\end{aligned} \tag{3.2.35}$$

$$g_p = \sum_{n=1}^{N_1}\Gamma_n^p, \quad g_p' = \sum_{n=1+N_1}^{N_1+N_2}\Gamma_n^p, \quad g = g_1 + g_1'. \tag{3.2.36}$$

One can check that Eq. (3.2.34) reduces to Eq. (3.2.32) for ideal point contacts (when $g_p = N_1$, $g_p' = N_2$). As in the case of single-mode point contacts, $\operatorname{var} G \propto \gamma^{-2}$ for $\gamma \gg 1$ without tunnel barriers, while $\operatorname{var} G \propto \gamma^{-1}$ otherwise.

3.2.4 Conclusion

In summary, we have demonstrated the equivalence of two models for dephasing, the voltage-probe model and the imaginary potential model. In doing so we have corrected a number of shortcomings of each model, notably the non-uniformity of the dephasing in the voltage-probe model of Ref. [25] and Sec. 3.1 and the lack of particle conservation in the imaginary potential model of Refs. [26] and [28]. We have calculated the distribution of the conductance and shown that it peaks at the classical conductance for strong dephasing once particle conservation is enforced, thereby reconciling the contradictory results of Ref. [25] and Sec. 3.1, on the one hand, and Refs. [26] and [28], on the other hand. We find that for ideal single-mode point contacts (no tunnel barriers), conductance fluctuations are non-Gaussian and $\propto \tau_\phi$ for strong dephasing ($\tau_\phi \to 0$). In the case of non-ideal point contacts (with tunnel barriers), fluctuations are larger ($\propto \sqrt{\tau_\phi}$) and Gaussian for $\tau_\phi \to 0$.

The effect of dephasing becomes appreciable when the dimensionless dephasing rate $\gamma = 2\pi\hbar/\tau_\phi\Delta$ is of the same order as the dimensionless escape rate $g = \sum_n \Gamma_n$ through the two point contacts. For $\gamma \gg g$, the weak-localization correction $\delta G = \langle G\rangle(\beta = 2) - \langle G\rangle(\beta = 1)$ and the conductance fluctuations are given by

$$\delta G = a_1 g/\gamma + \mathcal{O}(g/\gamma)^2, \tag{3.2.37}$$

$$\operatorname{var} G = b_1 g/\gamma + b_2(g/\gamma)^2 + \mathcal{O}(g/\gamma)^3, \tag{3.2.38}$$

where a_1, b_1, and b_2 are numerical coefficients determined by equations (3.2.23), (3.2.27), (3.2.32), and (3.2.34). For the special case of two single-mode point contacts, we have

$$a_1 = \frac{4\Gamma_1^2\Gamma_2^2}{(\Gamma_1+\Gamma_2)^4}, \tag{3.2.39}$$

$$b_1 = \frac{4\Gamma_1^2\Gamma_2^2(\Gamma_1^2+\Gamma_2^2-\Gamma_1\Gamma_2^2-\Gamma_1^2\Gamma_2)}{\beta(\Gamma_1+\Gamma_2)^4}. \tag{3.2.40}$$

The coefficient b_2 is only relevant if $\Gamma_1, \Gamma_2 \approx 1$, when $b_1 \approx (2-\Gamma_1-\Gamma_2)/4\beta \ll 1$ and $b_2 \approx (1+2\delta_{\beta 1})/16$. At finite temperatures, in addition to dephasing, the effect of thermal smearing becomes important [26]. Since thermal smearing has no effect on the average conductance, the weak-localization correction δG provides an unambiguous way to find the dephasing rate γ.

The fact that dephasing was not entirely uniform in phase space in the model of Ref. [25] and Sec. 3.1 leads to small but noticeable differences with the completely uniform description used here, in particular for the case of single-mode point contacts. The differences may result in a discrepancy $\Delta\gamma \approx 1$ in the estimated value of the dimensionless dephasing rate γ, if the ideal voltage-probe model of Ref. [25] and Sec. 3.1 is used instead of the model presented here. A difference $\Delta\gamma \approx 1$ is relevant, as experiments on semiconductor quantum dots can have dephasing rates as low as $\gamma \approx 2$ [41].

Both the voltage-probe model and the imaginary potential model only provide an effective description of dephasing. They cannot compete with a microscopic theory of inelastic scattering in quantum dots (see e.g. Refs. [42] and [43]). At this time, a microscopic theory for the effect of inelastic scattering on the conductance distribution does not yet exist. For the time being, the model presented here may well be the most realistic description available.

Appendix A: Calculation of $P(T_1, T_2)$

We start the calculation of $P(T_1, T_2)$ from the integral expression (3.2.17), in which we may replace the double integral of v and v' by a single integral of the matrix $v'v$ over the unitary group (for $\beta = 2$) or over the manifold of unitary symmetric matrices (for $\beta = 1$). We make a substitution of variables $v'v \to w$ via

$$v'v = \tau - \sqrt{1-\tau^2}\, w(1-\tau w)^{-1}\sqrt{1-\tau^2}. \tag{A.1}$$

The matrix τ was defined in Eq. (3.2.18). One verifies that the matrix w is unitary (unitary symmetric for $\beta = 1$). By Sec. 2.2, the Jacobian of this transformation is [20, 21]

$$\det\left(\frac{dv'v}{dw}\right) = \frac{V}{V'}\frac{|\det(1-v'v\tau)|^{\beta N_\phi+2-\beta}}{\det(1-\tau^2)^{(\beta N_\phi+2-\beta)/2}}, \tag{A.2}$$

where V and V' are normalization constants. This change of variables is a key step in the calculation, since the Jacobian (A.2) cancels the denominator of the integrand of Eq. (3.2.17) almost completely,

$$\begin{aligned} P(T_1,T_2) &= \frac{1}{V'}\int dw\, \Gamma_\phi^{\beta(6-\beta)}|T_1-T_2|^\beta \\ &\quad \times \prod_{j=1,2}(1+\Gamma_\phi T_j^{-1}-\Gamma_\phi)^{-(\beta N_\phi+6-\beta)/2} \end{aligned}$$

$$\times \prod_{j=1,2} T_j^{-2\beta-2} \, |\det(1-\tau w)|^{2\beta}. \tag{A.3}$$

We now consider separately the integral

$$\begin{aligned} I_\beta &= \int dw \, |\det(1-\tau w)|^{2\beta} \\ &= \int dw \, \det(1-\sqrt{\tau} w \sqrt{\tau})^\beta \det(1-\sqrt{\tau} w^{-1} \sqrt{\tau}). \end{aligned} \tag{A.4}$$

Here we have used that the matrix τ is a positive diagonal matrix. We now change variables $\sqrt{\tau} w^{-1} \sqrt{\tau} \to \tilde{w}^{-1}$. If the matrix τ were unitary, we could write

$$I_\beta = \int d\tilde{w} \, \det(1-\tau \tilde{w} \tau)^\beta \det(1-\tilde{w}^{-1})^\beta, \tag{A.5}$$

in view of the invariance of the measure $dw = d\tilde{w}$. However, τ is not unitary. A theorem due to Weyl allows us to continue Eq. (A.5) analytically to arbitrary τ [44].

To evaluate I_β, we decompose $\tilde{w}$ in eigenvectors and eigenphases, $\tilde{w} = U e^{i\Theta} U^\dagger$, where U is an orthogonal (unitary) matrix for $\beta = 1$ (2), and $\Theta_{ij} = \delta_{ij}\theta_j$, $0 \le \theta_j < 2\pi$. The invariant measure $d\tilde{w}$ reads [19]

$$d\tilde{w} = dU \prod_{i<j} |e^{i\theta_i} - e^{i\theta_j}|^\beta \prod_i d\theta_i. \tag{A.6}$$

After some algebraic manipulations, we arrive at

$$\begin{aligned} I_\beta &= \int d\theta_1 \ldots \int d\theta_{N_\phi} \prod_{i<j} |e^{i\theta_i} - e^{i\theta_j}|^\beta \prod_{j=1}^{N_\phi} \left(1 - e^{-i\theta_i}\right)^\beta \\ &\quad \times \prod_{j=1}^{N_\phi} \left[1 - (1-\Gamma_\phi) e^{i\theta_j}\right]^\beta \int dU \det A^\beta, \end{aligned} \tag{A.7}$$

where the 2×2 matrix A is given by

$$A_{ij} = \delta_{ij} - (1-\Gamma_\phi) \sum_{l=1}^{N_\phi} \frac{U_{il} U_{jl}^* e^{i\theta_l} \sqrt{T_i T_j}}{1 - (1-\Gamma_\phi) e^{i\theta_l}}. \tag{A.8}$$

The determinant of A is computed by a direct expansion. Since $N_\phi \gg 1$, we may consider the matrix elements U_{kl} as independent real (complex) Gaussian distributed variables with zero mean and variance $1/N_\phi$ for $\beta = 1$ (2). We write the result of the Gaussian integrations in terms of derivatives of a generating function F_β,

$$\prod_{j=1}^{N_\phi} \left[1 - (1-\Gamma_\phi) e^{i\theta_j}\right]^\beta \int dU \det A^\beta = D_\beta F_\beta. \tag{A.9}$$

The generating function F_β depends on the variables x_k, y_k, and z_k, where $k = 1$ for $\beta = 1$ and $k = 1, 2$ for $\beta = 2$,

$$F_\beta = \prod_{j=1}^{N_\phi} \prod_{k=1}^{\beta} (1 + x_k + y_k)[1 + f(x_k, y_k, z_k) e^{i\theta_j}], \tag{A.10}$$

$$f(x, y, z) = (1 + x + y)^{-1}(1 - \Gamma_\phi) \times \left[1 + x(1 - 2T_1) + y(1 - 2T_2) + z\sqrt{T_1 T_2}\right]. \tag{A.11}$$

The differential operator D_β reads

$$D_1 = \tfrac{1}{2} N_\phi^{-1}(\partial_{x_1} + \partial_{y_1}) + N_\phi^{-2} \partial_{z_1} \partial_{z_1}, \tag{A.12}$$

$$\begin{aligned} D_2 = {} & N_\phi^{-2}\left[\tfrac{1}{2}(\partial_{x_1}\partial_{x_2} + \partial_{y_1}\partial_{y_2}) - \tfrac{1}{4}(\partial_{x_1} - \partial_{y_2})^2\right] \\ & + N_\phi^{-3}(\tfrac{3}{2}\partial_{z_2}\partial_{z_2} - \tfrac{1}{2}\partial_{z_1}\partial_{z_1})(\partial_{x_1} + \partial_{y_1}) \\ & + N_\phi^{-4}\partial_{z_1}\partial_{z_2}\partial_{z_2}(3\partial_{z_2} - 2\partial_{z_1}). \end{aligned} \tag{A.13}$$

The derivatives in Eq. (A.9) should be evaluated at $x_k = y_k = z_k = 0$ ($k = 1, 2$).

We are left with an integral over the phases θ_j which is of the type

$$I'_\beta = \int d\theta_1 \ldots \int d\theta_n \prod_{i<j} |e^{i\theta_i} - e^{i\theta_j}|^\beta \times \prod_{j=1}^{n} (1 - e^{-i\theta_j})^\beta \prod_{k=1}^{\beta} \left(a_k - e^{i\theta_j}\right). \tag{A.14}$$

The integrand is a product of secular determinants $\det(\lambda - U)$ of a unitary matrix U. Integrals of this form were considered by Haake et al [45]. For $\beta = 1$ we can directly apply the results in their paper, for $\beta = 2$ we need to extend their method to include a product of four secular determinants. We find

$$I'_1 = \frac{(1 + n)(a_1^{n+3} - 1) - (3 + n)a_1(a_1^{n+1} - 1)}{(a_1 - 1)^3 (n - 1)}, \tag{A.15}$$

$$I'_2 = \frac{(a_1^{n+2} - 1)(a_2^{n+2} - 1)}{(a_1 - 1)^2 (a_2 - 1)^2} - \frac{(a_1^{n+2} - a_2^{n+2})(n + 2)}{(a_1 - 1)(a_2 - 2)(a_1 - a_2)}. \tag{A.16}$$

The desired integral I_β is obtained from I'_β by substitution of Eq. (A.15) with $n = N_\phi$, $a_k = f(x_k, y_k, z_k)$ into Eqs. (A.7)–(A.12). Substitution of I_β into Eq. (A.3) then leads to the final result (3.2.19).

References

[1] M. Büttiker, Phys. Rev. B **33**, 3020 (1986); IBM J. Res. Dev. **32**, 63 (1988).

[2] M. Büttiker, Phys. Rev. B **32**, 1846 (1985).

[3] H. U. Baranger, A. D. Stone, and D. P. DiVicenzo, Phys. Rev. B **37**, 6521 (1988).

[4] C. L. Kane, P. A. Lee, and D. P. DiVicenzo, Phys. Rev. B **38**, 2995 (1988).

[5] D. Kowal, U. Sivan, O. Entin-Wohlman, and Y. Imry, Phys. Rev. B **42**, 9009 (1990).

[6] S. Hershfield, Phys. Rev. B **43**, 11586 (1991).

[7] P. A. Mello, Phys. Rev. B **47**, 16358 (1993).

[8] S. Godoy and P. A. Mello, Europhys. Lett. **17**, 243 (1992); Phys. Rev. B **46**, 2346 (1992); V. A. Gopar, M. Martinez, and P. A. Mello, Phys. Rev. B **50**, 2502 (1994).

[9] For a review, see C. W. J. Beenakker and H. van Houten, Solid State Phys. **44**, 1 (1991).

[10] C. M. Marcus, R. M. Westervelt, P. F. Hopkins, and A. C. Gossard, Phys. Rev. B **48**, 2460 (1993); Chaos **3**, 643 (1993); C. M. Marcus, R. M. Clarke, I. H. Chan, C. I. Duruöz, and J. S. Harris, Semicond. Sci. Technol. **9**, 1897 (1994).

[11] H. U. Baranger, R. A. Jalabert, and A. D. Stone, Phys. Rev. Lett. **70**, 3876 (1993).

[12] V. N. Prigodin, K. B. Efetov, and S. Iida, Phys. Rev. Lett. **71**, 1230 (1993); Phys. Rev. B **51**, 17223 (1995).

[13] Z. Pluhăr, H. A. Weidenmüller, J. A. Zuk, and C. H. Lewenkopf, Phys. Rev. Lett. **73**, 2115 (1994).

[14] E. R. Mucciolo, V. N. Prigodin, and B. L. Altshuler, Phys. Ref. B **51**, 1714 (1995).

[15] H. U. Baranger and P. A. Mello, Phys. Rev. Lett. **73**, 142 (1994).

[16] R. A. Jalabert, J.-L. Pichard, and C. W. J. Beenakker, Europhys. Lett. **27**, 255 (1994).

[17] M. Büttiker, Phys. Rev. Lett. **57**, 1761 (1986); IBM J. Res. Dev. **32**, 317 (1988).

[18] F. J. Dyson, J. Math. Phys. **3**, 140 (1962).

[19] M. L. Mehta, *Random Matrices* (Academic, New York, 1991).

[20] L. K. Hua, *Harmonic Analysis of Functions of Several Complex Variables in the Classical Domains* (Amer. Math. Soc., Providence, 1963).

[21] P. A. Mello, P. Pereyra, and T. H. Seligman, Ann. Phys. (N.Y.) **161**, 254 (1985).

[22] P. Pereyra and P. A. Mello, J. Phys. A **16**, 237 (1983); W. A. Friedman and P. A. Mello, J. Phys. A **18**, 425 (1985).

[23] R. A. Jalabert, H. U. Baranger, and A. D. Stone, Phys. Rev. Lett. **65**, 2442 (1990).

[24] M. R. Zirnbauer, Nucl. Phys. A **560**, 95 (1993).

[25] H. U. Baranger and P. A. Mello, Phys. Rev. B **51**, 4703 (1995).

[26] K. B. Efetov, Phys. Rev. Lett. **74**, 2299 (1995).

[27] I. L. Aleiner and A. I. Larkin, Phys. Rev. B **54**, 14423 (1996).

[28] E. McCann and I. V. Lerner, J. Phys. Condens. Matter **8**, 6719 (1996).

[29] For a review, see: C. W. J. Beenakker, Rev. Mod. Phys. (July 1997, cond-mat/9612179).

[30] C. M. Marcus, A. J. Rimberg, R. M. Westervelt, P. F. Hopkins, and A. C. Gossard, Phys. Rev. Lett. **69**, 506 (1992).

[31] C. M. Marcus, R. M. Westervelt, P. F. Hopkins, and A. C. Gossard, Phys. Rev. B **48**, 2460 (1993).

[32] M. W. Keller, O. Millo, A. Mittal, D. E. Prober, and R. N. Sacks, Surf. Sci. **305**, 501 (1994).

[33] A. M. Chang, H. U. Baranger, L. N. Pfeiffer, and K. W. West, Phys. Rev. Lett. **73**, 2111 (1994).

[34] J. P. Bird, K. Ishibashi, Y. Aoyagi, T. Sugano, and Y. Ochiai, Phys. Rev. B **50**, 18678 (1994).

[35] J. P. Bird, K. Ishibashi, D. K. Ferry, Y. Ochiai, Y. Aoyagi, and T. Sugano, Phys. Rev. B **51**, 18037 (1995).

[36] I. H. Chan, R. M. Clarke, C. M. Marcus, K. Campman, and A. C. Gossard, Phys. Rev. Lett. **74**, 3876 (1995).

[37] R. M. Clarke, I. H. Chan, C. M. Marcus, C. I. Duruöz, J. S. Harris, K. Campman, and A. C. Gossard, Phys. Rev. B **52**, 2656 (1995).

[38] J. J. M. Verbaarschot, H. A. Weidenmüller, and M. R. Zirnbauer, Phys. Rep. **129**, 367 (1985).

[39] S. Iida, H. A. Weidenmüller, and J. A. Zuk, Phys. Rev. Lett. **64**, 583 (1990); Ann. Phys. (N.Y.) **200**, 219 (1990).

[40] H. U. Baranger and P. A. Mello, Europhys. Lett. **33**, 465 (1996).

[41] C. M. Marcus, S. R. Patel, A. G Huibers, S. M. Cronenwett, M. Switkes, I. H. Chan, R. M. Clarke, J. A. Folk, S. F. Godijn, K. Campman, and A. C. Gossard, *Chaos, solitons* & *Fractals* **8**, July 1997.

[42] U. Sivan, Y. Imry, and A. G. Aronov, Europhys. Lett. **28**, 115 (1994).

[43] B. L. Altshuler, Y. Gefen, A. Kamenev, and L. S. Levitov, Phys. Rev. Lett. **78**, 2803 (1997).

[44] H. Weyl, *The Classical Groups* (Princeton University Press, Princeton, 1946).

[45] F. Haake, M. Kuś, H.-J. Sommers, H. Schomerus, and K. Życzkowski, J. Phys. A: Math. Gen. **29**, 3641 (1996).

4 Time delay in chaotic scattering

4.1 Charge-Relaxation and dwell time in the fluctuating admittance of a chaotic cavity

A quantum dot is a small conducting island, formed with the help of gates, with a ballistic and chaotic classical dynamics, and coupled to electron reservoirs by ballistic point contacts. The search for signatures of phase-coherent transport through chaotic quantum dots focused on the d.c. conductance [1–4]. However, the a.c. response is also of interest [3,5,6], since it probes the charge distribution and its dynamics. While the d.c. conductance is entirely determined by the scattering properties of the quantum dot, a.c. transport requires that nearby conductors (gates) are taken into account as well [7–9]: charges may temporarily pile up in the quantum dot, thus interacting with the gates through long-range Coulomb forces.

Except for highly transmissive samples [9], the low-frequency dynamics of a mesoscopic conductor is governed by a charge-relaxation mode or an RC-relaxation time τ. However, as soon as weak localization [10] and universal conductance fluctuations [11] play a role, this is no longer a complete picture. In this section, we demonstrate that the weak localization effects and the a.c. conductance (admittance) fluctuations are primarily governed by a second time-scale, a dwell time τ_d, characteristic of the non-interacting system. The large disparity of these two time-scales ($\tau_d \gg \tau$ for a macroscopic quantum dot) dramatically affects the admittance and provides a signature that should be readily observed.

In a recent paper, Gopar, Mello, and Büttiker studied the capacitance fluctuations of a chaotic quantum dot, coupled to the outside world through one point contact with a single conducting channel only [5]. For the low-frequency fluctuations, weak localization effects are absent and the double-time scale behavior discussed here does not occur. In this section, we calculate the average and variance of the admittance for the case of a two-probe quantum dot with multichannel point contacts. Multichannel contacts are necessary to be in the regime of weak localization and universal conductance fluctuations. Moreover, the presence of two point contacts instead of one turns out to be essential for the existence of quantum interference effects to leading order in the frequency ω.

The system under consideration is depicted in Fig. 4-1a. Two electron reservoirs at voltages $U_1(\omega)$ and $U_2(\omega)$ are coupled to the quantum dot by two point contacts with $N_1, N_2 \gg 1$ modes, through which currents $I_1(\omega)$ and $I_2(\omega)$ are passed. The dot is coupled capacitively to a gate, connected to a reservoir at voltage $U_3(\omega)$, from which a current $I_3(\omega)$ flows. A geometrical capacitance C accounts for the capacitive coupling with the gate [5, 7]. We assume that the gate is macroscopic, i.e. that its density of states $dn_3/d\varepsilon \gg C/e^2$. The a.c. transport properties of the system are characterized by the dimensionless admittance $G_{\mu\nu}(\omega) = (h/2e^2)\delta I_\mu(\omega)/\delta U_\nu(\omega)$. We restrict ourselves to the

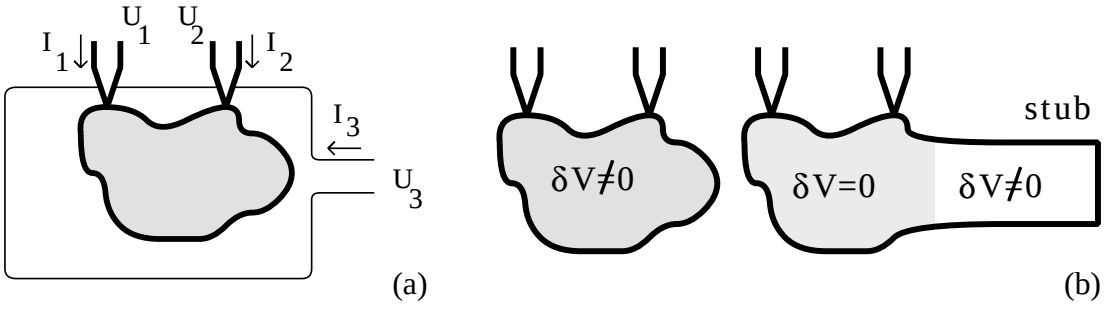

Figure 4-1. (a) Chaotic cavity (grey), coupled to source and drain reservoir (1 and 2) by point contacts. The cavity is coupled capacitively to the gate (3). (b) Construction of the energy dependent ensemble of scattering matrices. A change $\delta\varepsilon$ of the energy is replaced by a spatially uniform change $\delta V = -\delta\varepsilon/e$ of the potential in the cavity (left), which in turn is statistically equivalent to a chaotic cavity with $\delta V = 0$ (right), coupled to a closed lead (a stub) with an energy-dependent reflection matrix.

coefficients $G_{\mu\nu}(\omega)$ with $\mu, \nu = 1, 2$, the remaining coefficients being determined by current conservation and gauge invariance [7–9], $\sum_{\mu=1}^{3} G_{\mu\nu}(\omega) = \sum_{\nu=1}^{3} G_{\mu\nu}(\omega) = 0$. The emittance $E_{\mu\nu}$ is the first order term in a small-ω expansion of the admittance,

$$G_{\mu\nu}(\omega) = G_{\mu\nu} - i\omega E_{\mu\nu} + \mathcal{O}(\omega^2). \tag{4.1.1}$$

Here $G_{\mu\nu} \equiv G_{\mu\nu}(0)$ is the d.c. conductance. The emittance coefficients are the analogues of the capacitance coefficients for a purely capacitive system [8, 9].

A calculation of the admittance proceeds in two steps [7]. First, we calculate the unscreened admittance $G^u_{\mu\nu}(\omega)$, the direct response to the change in the external potentials (at fixed internal potential)

$$G^u_{\mu\nu}(\omega) = \int d\varepsilon\, \frac{f(\varepsilon - \frac{1}{2}\hbar\omega) - f(\varepsilon + \frac{1}{2}\hbar\omega)}{\hbar\omega} \mathrm{tr}\left[\delta_{\mu\nu}\mathbb{1}_\mu - S^\dagger_{\mu\nu}(\varepsilon - \tfrac{1}{2}\hbar\omega) S_{\mu\nu}(\varepsilon + \tfrac{1}{2}\hbar\omega)\right]. \tag{4.1.2}$$

Here $f(\varepsilon)$ is the Fermi function, $S_{\mu\nu}$ is the $N_\mu \times N_\nu$ scattering matrix for scattering from ν to μ, and $\mathbb{1}_\mu$ is the $N_\mu \times N_\mu$ unit matrix. Second, we take the screening due to the long-range Coulomb interactions into account, which was ignored in Eq. (4.1.2). For a single self-consistent potential within the cavity, the result is [7]

$$G_{\mu\nu}(\omega) \;=\; G^u_{\mu\nu}(\omega) + \frac{\sum_{\rho=1}^{2} G^u_{\mu\rho}(\omega) \sum_{\sigma=1}^{2} G^u_{\sigma\nu}(\omega)}{i\hbar\omega C/2e^2 - \sum_{\rho=1}^{2}\sum_{\sigma=1}^{2} G^u_{\rho\sigma}(\omega)}. \tag{4.1.3}$$

The average over the ensemble of quantum dots is performed using random-matrix theory [12]. We use an extension of the circular ensemble of uniformly distributed scattering matrices. This extension provides a statistical description of the energy-dependence of the

scattering matrix.[1] To construct the extended circular ensemble we first replace an energy shift $\delta\varepsilon$ by a uniform decrease $\delta V = -\delta\varepsilon/e$ of the potential V in the quantum dot. The key point of our method is to localize δV in a closed lead (a stub), see Fig. 4-1b. The stub contains $N_s \gg N_1 + N_2$ modes to ensure that it models a spatially homogeneous potential drop δV. The system consisting of the dot and the stub is described by the $N_s \times N_s$, ε-dependent reflection matrix $r_s(\varepsilon)$ of the stub and the $(N_1 + N_2 + N_s)$-dimensional scattering matrix U of the cavity at reference energy ε_0, with the stub replaced by a regular open lead. We choose the scattering basis in the stub and the cavity such that $r_s(\varepsilon_0) = 1$. For ε different from ε_0 we take

$$r_s(\varepsilon) = e^{i(\varepsilon-\varepsilon_0)\Phi}, \quad \phi = \mathrm{tr}\,\Phi \tag{4.1.4}$$

where the matrix Φ is Hermitian and positive definite. For $N_s \gg N_1 + N_2$, the precise choice of Φ becomes irrelevant, all information being contained in the single parameter ϕ. For the matrix U we assume a uniform distribution. In the presence of time-reversal symmetry, both U and Φ are symmetric. We finally express the scattering matrix $S(\varepsilon)$ in terms of U and $r_s(\varepsilon)$,

$$S(\varepsilon) \;=\; U_{ll} + U_{ls}\,[1 - r_s(\varepsilon)U_{ss}]^{-1}\,r_s(\varepsilon)U_{sl}. \tag{4.1.5}$$

The matrices U_{ij} in Eq. (4.1.5) are the four blocks of U, describing transmission and reflection from and to the stub (s) or the two leads (l). The parameter ϕ is related to the mean level density $\langle dn/d\varepsilon\rangle$ via $\phi = 2\pi\langle dn/d\varepsilon\rangle$.

We are now ready to calculate the average and fluctuations of the admittance. We first compute the average of the unscreened admittance $G^u_{\mu\nu}(\omega)$ with the help of the diagrammatic technique of Ch. 6,

$$\begin{aligned}\langle G^u_{\mu\nu}(\omega)\rangle \;&=\; \delta_{\mu\nu}N_\mu - \frac{N_\mu N_\nu}{N(1-i\omega\tau_d)} + \frac{(2-\beta)N_\mu}{\beta N(1-i\omega\tau_d)}\left(\frac{N_\nu(1-2i\omega\tau_d)}{N(1-i\omega\tau_d)^2} - \delta_{\mu\nu}\right)\\ &\quad + \mathcal{O}(N^{-1}),\end{aligned} \tag{4.1.6}$$

where $N = N_1 + N_2$ and $\tau_d = (h/N)\langle dn/d\varepsilon\rangle$ is the dwell time. The symmetry index $\beta = 1$ (2) in the absence (presence) of a time-reversal- symmetry breaking magnetic field; $\beta = 4$ in zero magnetic field with strong spin-orbit scattering. Since fluctuations in $G^u_{\mu\nu}(\omega)$ are of relative order N^{-2}, we may directly substitute the result (4.1.6) into Eq. (4.1.3), to obtain the first two terms in the large-N expansion of the screened admittance $\langle G_{\mu\nu}(\omega)\rangle$,

$$\begin{aligned}\langle G_{\mu\nu}(\omega)\rangle \;&=\; \delta_{\mu\nu}N_\mu - \frac{N_\mu N_\nu}{N(1-i\omega\tau)} + \frac{(2-\beta)N_\mu}{\beta N(1-i\omega\tau_d)}\left(\frac{N_\nu(1-2i\omega\tau)}{N(1-i\omega\tau)^2} - \delta_{\mu\nu}\right)\\ &\quad + \mathcal{O}(N^{-1}),\end{aligned} \tag{4.1.7}$$

where $\tau^{-1} = \tau_d^{-1} + 2e^2N/hC$ is the RC time. The $\mathcal{O}(N)$ term in the r.h.s. of Eq. (4.1.7) is the classical admittance, the β-dependent $\mathcal{O}(1)$ term is the weak-localization correction.

[1] For a justification of the extended circular ensemble from the Hamiltonian approach to chaotic scattering [37], the reader is referred to App. A. A similar extension of the circular ensemble to model the magnetic-field dependence of S is discussed Sec. 7.3.

Notice the almost complete formal similarity between the fully screened result (4.1.7) and the unscreened result (4.1.6): Up to one term, screening results in the replacement of the dwell time τ_d by the RC-time τ. The fact that the similarity is not complete is the key result of this section which we discuss below in more detail.

The first two terms in the small-ω expansion of $\langle G_{\mu\nu}(\omega)\rangle$ yield the average d.c. conductance $\langle G_{\mu\nu}\rangle$ and emittance $\langle E_{\mu\nu}\rangle$,

$$\langle G_{\mu\nu}\rangle = N_\mu\left(\delta_{\mu\nu} - N_\nu/N\right) + (2-\beta)(N_\mu/\beta N)\left(N_\nu/N - \delta_{\mu\nu}\right), \qquad (4.1.8)$$

$$\langle E_{\mu\nu}\rangle = N_\mu N_\nu \tau/N - (2-\beta)(N_\mu\tau_d/\beta N)\left(N_\nu/N - \delta_{\mu\nu}\right). \qquad (4.1.9)$$

Eq. (4.1.8) was previously obtained in Ref. [4]. For $C \to 0$, the RC-time τ vanishes. For $\beta = 2$ we then find $\langle E_{\mu\nu}\rangle = 0$, for $\beta = 1$ the weak-localization contribution $\langle E_{11}\rangle = -\langle E_{12}\rangle = N_1 N_2 \langle dn/d\varepsilon\rangle/N^3 h$ leads to a positive emittance, while for $\beta = 4$ the emittance is negative. For comparison we mention that for complete screening, a ballistic conductor has an inductive emittance $E = -(1/4h)\langle dn/d\epsilon\rangle$, whereas a metallic diffusive conductor behaves capacitively as $E = (1/6h)\langle dn/d\epsilon\rangle$ [9].

For simplicity, we restrict our presentation of the admittance fluctuations to the d.c. conductance $G_{\mu\nu}$ and the emittance $E_{\mu\nu}$ at zero temperature. As before, we use the diagrammatic technique of Ch. 6. The leading ω-behavior of the admittance fluctuations is determined by the cross-correlator $\mathrm{cov}\,(G_{\mu\nu}, E_{\mu\nu})$ [Recall that $\mathrm{cov}\,(x,y) = \langle xy\rangle - \langle x\rangle\langle y\rangle$]. We find that $\mathrm{cov}\,(G_{\mu\nu}, E_{\mu\nu})$ is unaffected by the capacitive interaction with the gate,

$$\mathrm{cov}\,(G_{\mu\nu}, E_{\rho\sigma}) = \mathrm{cov}\,(G_{\mu\nu}, E^u_{\rho\sigma}) = -\frac{N_\mu N_\nu\,\tau_d}{N^2}\left(\frac{N_\rho}{N} - \delta_{\mu\rho}\right)\left(\frac{N_\sigma}{N} - \delta_{\nu\sigma}\right). \qquad (4.1.10)$$

For the autocorrelator of the emittance we find

$$\begin{aligned}\mathrm{cov}\,(E_{\mu\nu}, E_{\rho\sigma}) &= \frac{3\,N_\mu N_\nu \tau_d^2}{2\,N^2}\left(\frac{N_\rho}{N} - \delta_{\mu\rho}\right)\left(\frac{N_\sigma}{N} - \delta_{\nu\sigma}\right) \qquad (4.1.11)\\ &\quad + \frac{N_\mu N_\nu \tau^2}{N^3}\left(\delta_{\mu\rho}N_\sigma + \delta_{\nu\sigma}N_\rho\right) + \frac{2\,N_\mu N_\nu N_\rho N_\sigma \tau^2}{\tau_d^2 N^4}(\tau^2 - \tau_d^2).\end{aligned}$$

Eqs. (4.1.10) and (4.1.11) are valid for $\beta = 2$. In zero magnetic field ($\beta = 1, 4$), the permutation $\rho \leftrightarrow \sigma$ must be added; in the presence of spin-orbit scattering ($\beta = 4$), Eqs. (4.1.10) and (4.1.11) are multiplied by $1/4$.

The relevant time scales for the low-frequency response of a chaotic quantum dot are obtained from Eqs. (4.1.9) and (4.1.10). The relevant time scale for the classical admittance is the charge-relaxation time τ, while the weak-localization correction $\delta G_{\mu\nu}(\omega)$ and the admittance fluctuations are governed by the dwell time τ_d. Hence, to leading order in ω, *the manifestation of quantum phase coherence on a.c. transport is unaffected by the Coulomb interactions.* For a macroscopic quantum dot, the density of states $dn/d\varepsilon \gg C/e^2$, so that the two characteristic time scales τ and τ_d differ considerably.

To explain this result, we first consider the weak-localization correction $\delta E_{\mu\nu}$ to the average emittance. A screening contribution to $\delta E_{\mu\nu}$ requires a magnetic-field dependent quantum interference correction to the charge accumulated in the cavity. To first

order in ω, the (unscreened) charge accumulation at a point $\vec{r}$ in the dot due to the external potential change $\delta U_\mu(\omega)$ is determined by the injectivity $d\overline{n}_\mu(\vec{r})/d\varepsilon$ and emissivity $d\underline{n}_\mu(\vec{r})/d\varepsilon$ [8, 9]. For symmetry reasons, the ensemble averages $\langle d\overline{n}_\mu(\vec{r})/d\varepsilon\rangle$ and $\langle d\underline{n}_\mu(\vec{r})/d\varepsilon\rangle$ both equal N_μ/N times the average local density of states $\langle dn(\vec{r})/d\varepsilon\rangle$, and have no magnetic-field dependent weak-localization correction. Hence weak localization affects how current is distributed into the different leads, but it does not lead to charging of the sample (to leading order in ω). This explains why the relevant time scale is the dwell time τ_d, characteristic of the non-interacting system, and not the charge-relaxation time τ.

Similarly, the screening correction to $\mathrm{cov}\,(G_{\mu\nu}, E_{\mu\nu})$ requires correlations between the d.c. conductance $G_{\mu\nu}$ and the injectivity $d\overline{n}_\rho(\vec{r})/d\varepsilon$ or emissivity $d\underline{n}_\rho(\vec{r})/d\varepsilon$ [8, 9]. For a chaotic cavity, we have

$$\begin{aligned}\mathrm{cov}\,(G_{\mu\nu}, d\overline{n}_\rho(\vec{r})/d\varepsilon) &= \mathrm{cov}\,(G_{\mu\nu}, d\underline{n}_\rho(\vec{r})/d\varepsilon)\\ &= N_\rho\,\mathrm{cov}\,(G_{\mu\nu}, dn(\vec{r})/d\varepsilon)/N. \qquad (4.1.12)\end{aligned}$$

The correlator of the d.c. conductance and the local density of states vanishes for ideal leads, which is easily verified by computation of $\kappa_{ij} = \mathrm{cov}\left(|S_{ij}|^2, dn(\vec{r})/d\varepsilon\right)$. For $\beta = 2$ both $dn(\vec{r})/d\varepsilon$ and the distribution of S are invariant under multiplication of S with a unitary matrix. It follows that κ_{ij} is independent of i and j, hence $\kappa_{ij} = 0$. For $\beta = 1, 4$ a similar argument holds. The absence of correlations between the density of states and the d.c. conductance is special for the case of ideal point contacts. Correlations between $G_{\mu\nu}$ and $dn(\vec{r})/d\varepsilon$ are common for point contacts with tunnel barriers, when the scattering matrix has no uniform distribution.

The average and variance of the admittance of a chaotic quantum dot with only one point contact is obtained from our results by setting $N_1 = N$, $N_2 = 0$. Denoting the admittance of this system by $G(\omega) = G_{11}(\omega)$, we thus obtain

$$\langle G(\omega)\rangle = \frac{-Ni\omega\tau}{1 - i\omega\tau} + \frac{(2-\beta)\omega^2\tau^2}{\beta(1 - i\omega\tau_d)(1 - i\omega\tau)^2}, \qquad (4.1.13)$$

$$\mathrm{var}\,G(\omega) = \frac{4\tau^4}{\beta\tau_d^2}(i\omega)^2 + \mathcal{O}(\omega^3). \qquad (4.1.14)$$

Note that for a single point contact (see also Ref. [5]) the leading contribution to the variance of the admittance is proportional to ω^2. Since the a.c. response of such a system is purely capacitive, the absence of a linear term in $\mathrm{var}\,G(\omega)$ and the weak localization correction $\delta G(\omega)$ agrees with our previous result that quantum interference corrections to the low-frequency admittance of a two-probe quantum dot are unaffected by the Coulomb interactions. The variance given by Eq. (4.1.14) agrees with Fyodorov and Sommers [13] who have used a different approach.

In conclusion, we have calculated the average and variance of the admittance of a chaotic quantum dot which is coupled to two electron reservoirs via multichannel point contacts. The quantum dot is capacitively coupled to a gate. In the universal regime of multichannel point contacts, phase coherent a.c. transport is characterized by weak localization and admittance fluctuations. The relevant time scale for the quantum-interference effects at

low frequencies ω is the dwell time τ_d, while the classical admittance depends on the RC time τ. Since these two time scales differ several orders of magnitude for a macroscopic quantum dot ($\tau \ll \tau_d$), this effect should be clearly visible in a measurement of the a.c. response of a chaotic quantum dot.

4.2 Quantum mechanical time-delay matrix in chaotic scattering

Eisenbud [14] and Wigner [15] introduced the notion of time delay in a quantum mechanical scattering problem. Wigner's one-dimensional analysis was generalized to an $N \times N$ scattering matrix S by Smith [16], who studied the Hermitian energy derivative $Q = -i\hbar S^{-1}\partial S/\partial E$ and interpreted its diagonal elements as the delay time for a wave packet incident in one of the N scattering channels. The matrix Q is called the Wigner-Smith time-delay matrix and its eigenvalues $\tau_1, \tau_2, \ldots, \tau_N$ are called proper delay times.

Recently, interest in the time-delay problem was revived in the context of chaotic scattering [17]. There is considerable theoretical [17–19] and experimental [20–22] evidence that an ensemble of chaotic billiards containing a small opening (through which N modes can propagate at energy E) has a uniform distribution of S in the group of $N \times N$ unitary matrices — restricted only by fundamental symmetries (see Ch. 2). This universal distribution is the circular ensemble of random-matrix theory [6], introduced by Dyson for its mathematical simplicity [23]. The eigenvalues $e^{i\phi_n}$ of S in the circular ensemble are distributed according to

$$P(\phi_1, \phi_2, \ldots, \phi_N) \propto \prod_{n<m} |e^{i\phi_n} - e^{i\phi_m}|^\beta, \tag{4.2.1}$$

with the Dyson index $\beta = 1, 2, 4$ depending on the presence or absence of time-reversal and spin-rotation symmetry.

No formula of such generality is known for the time-delay matrix, although many authors have worked on this problem [13, 19, 24–33]. An early result, $\langle \mathrm{tr}\, Q \rangle = \tau_H$, is due to Lyuboshits [24], who equated the ensemble average of the sum of the delay times $\mathrm{tr}\, Q = \sum_{n=1}^{N} \tau_n$ to the Heisenberg time $\tau_H = 2\pi\hbar/\Delta$ (with Δ the mean level spacing of the closed system). The second moment of $\mathrm{tr}\, Q$ was computed by Lehmann et al. [29] and by Fyodorov and Sommers [13, 30]. The distribution of Q itself is not known, except for $N = 1$ [30, 32]. The trace of Q determines the density of states [34], and is therefore sufficient for most thermodynamic applications [32]. For applications to quantum transport, however, the distribution of all individual eigenvalues τ_n of Q is needed, as well as the distribution of the eigenvectors (see e.g. next subsection).

The solution of this 40 year old problem is presented here. We have found that the eigenvalues of Q are independent of S. [2] The distribution of the inverse delay times

[2] The absence of correlations between the τ_n's and the ϕ_n's is a special property of the proper delay times. In contrast, the derivatives $\partial\phi_n/\partial E$ considered in Refs. [30, 31] are correlated with the ϕ_n's.

$\gamma_n = 1/\tau_n$ turns out to be the Laguerre ensemble of random-matrix theory,

$$P(\gamma_1, \ldots, \gamma_N) \propto \prod_{i<j} |\gamma_i - \gamma_j|^\beta \prod_k \gamma_k^{\beta N/2} e^{-\beta \tau_H \gamma_k/2}, \tag{4.2.2}$$

but with an unusual N-dependent exponent. (The function P is zero if any one of the τ_n's is negative.) The correlation functions of the τ_n's consist of series over (generalized) Laguerre polynomials [35], hence the name "Laguerre ensemble". The eigenvectors of Q are not independent of S, unless $\beta = 2$ (which is the case of broken time-reversal symmetry). However, for any β the correlations can be transformed away if we replace Q by the symmetrized matrix

$$Q_E = -i\hbar\, S^{-1/2} \frac{\partial S}{\partial E} S^{-1/2}, \tag{4.2.3}$$

which has the same eigenvalues as Q. The matrix of eigenvectors U which diagonalizes $Q_E = U \mathrm{diag}(\tau_1, \ldots, \tau_N) U^\dagger$ is independent of S and the τ_n's, and uniformly distributed in the orthogonal, unitary, or symplectic group (for $\beta = 1$, 2, or 4, respectively). The distribution (4.2.2) confirms the conjecture by Fyodorov and Sommers [13, 30] that the distribution of tr Q has an algebraic tail $\propto (\mathrm{tr}\, Q)^{-2-\beta N/2}$.

Although the time-delay matrix was interpreted by Smith as a representation of the "time operator", this interpretation is ambiguous [13]. The ambiguity arises because a wavepacket has no well-defined energy. There is no ambiguity in the application of Q to transport problems where the incoming wave can be regarded monochromatic, like the low-frequency response of a chaotic cavity [7, 32] (see also the previous section) or the Fermi-energy dependence of the conductance (see next subsection). In the first problem, time delay is described by complex reflection (or transmission) coefficients $R_{mn}(\omega)$,

$$\begin{aligned} R_{mn}(\omega) &= R_{mn}(0)[1 + i\omega\tau_{mn} + \mathcal{O}(\omega^2)], \\ R_{mn}(0) &= |S_{mn}|^2, \quad \tau_{mn} = \mathrm{Im}\, \hbar S_{mn}^{-1} \partial S_{mn}/\partial E. \end{aligned} \tag{4.2.4}$$

The delay time τ_{mn} determines the phase shift of the a.c. signal and goes back to Eisenbud [14]. With respect to a suitably chosen basis, we may require that both the matrices $R_{mn}(0)$ and τ_{mn} are diagonal. Then we have

$$R_{mn}(\omega) = \delta_{mn}[1 + i\omega\tau_m + \mathcal{O}(\omega^2)], \tag{4.2.5}$$

where the τ_m ($m = 1, \ldots, N$) are the proper delay times (eigenvalues of the Wigner-Smith time-delay matrix Q). For electronic systems, the $\mathcal{O}(\omega)$ term of $R_{mn}(\omega)$ is the capacitance. Hence, in this context, the proper delay times have the physical interpretation of "capacitance eigenvalues". [3]

[3] For an electronic system (with capacitance C), Coulomb interactions need to be taken into account self-consistently, see e.g. Refs. [7, 32] or the previous section. The result is

$$R_{mn}(\omega) = \delta_{mn}(1 + i\omega\tau_m) - \frac{i\omega\tau_m\tau_n}{hC/2e^2 + \sum_j \tau_j} + \mathcal{O}(\omega^2).$$

We now describe the derivation of our results. We start with some general considerations about the invariance properties of the ensemble of energy-dependent scattering matrices $S(E)$, following Wigner [36], and Gopar, Mello, and Büttiker [32]. The $N \times N$ matrix S is unitary for $\beta = 2$ (broken time-reversal symmetry), unitary symmetric for $\beta = 1$ (unbroken time-reversal and spin-rotation symmetry), and unitary self-dual for $\beta = 4$ (unbroken time-reversal and broken spin-rotation symmetry). The distribution functional $P[S(E)]$ of a chaotic system is assumed to be invariant under a transformation

$$S(E) \to V S(E) V', \tag{4.2.6}$$

where V and V' are arbitrary unitary matrices which do not depend on E ($V' = V^{\mathrm{T}}$ for $\beta = 1$, $V' = V^{\mathrm{R}}$ for $\beta = 4$, where T denotes the transpose and R the dual of a matrix). This invariance property is manifest in the random-matrix model for the E-dependence of the scattering matrix given in Sec. 4.1. A microscopic justification starting from the Hamiltonian approach to chaotic scattering [37] is given in the appendix. Eq. (4.2.6) implies with $V = V' = iS^{-1/2}$ that

$$P(S, Q_E) = P(-\mathbb{1}, Q_E). \tag{4.2.7}$$

Here $P(S, Q_E)$ is the joint distribution of S and Q_E, defined with respect to the standard (flat) measure dQ_E for the Hermitian matrix Q_E and the invariant measure dS for the unitary matrix S. From Eq. (4.2.7) we conclude that S and Q_E are statistically uncorrelated; Their distribution is completely determined by its form at the special point $S = -\mathbb{1}$.

The distribution of S and Q_E at $S = -\mathbb{1}$ is computed using established methods of random-matrix theory [6, 37]. The $N \times N$ scattering matrix S is expressed in terms of the eigenvalues E_α and the eigenfunctions $\psi_{n\alpha}$ of the $M \times M$ Hamiltonian matrix $\mathcal{H}$ of the closed chaotic cavity [19],

$$S = \frac{1 - iK}{1 + iK}, \quad K_{mn} = \frac{\Delta M}{\pi} \sum_{\alpha=1}^{M} \frac{\psi_{m\alpha} \psi_{n\alpha}^*}{E - E_\alpha}. \tag{4.2.8}$$

The Hermitian matrix $\mathcal{H}$ is taken from the Gaussian orthogonal (unitary, symplectic) ensemble [6], $P(\mathcal{H}) \propto \exp(-\beta \pi^2 \mathrm{tr}\, \mathcal{H}^2 / 4\Delta^2 M)$. This implies that the eigenvector elements $\psi_{j\alpha}$ are Gaussian distributed real (complex, quaternion) numbers for $\beta = 1$ (2, 4), with zero mean and with variance M^{-1}, and that the eigenvalues E_α have distribution

$$P(\{E_\alpha\}) \propto \prod_{\mu<\nu} |E_\mu - E_\nu|^\beta \prod_\mu e^{-\beta \pi^2 E_\mu^2 / 4\Delta^2 M}. \tag{4.2.9}$$

The limit $M \to \infty$ is taken at the end of the calculation.

The probability $P(-\mathbb{1}, Q_E)$ is found by inspection of Eq. (4.2.8) near $S = -\mathbb{1}$. The case $S = -\mathbb{1}$ is special, because S equals $-\mathbb{1}$ only if the energy E is an (at least) N-fold degenerate eigenvalue of $\mathcal{H}$. For matrices S in a small neighborhood of $-\mathbb{1}$, we may restrict the summation in Eq. (4.2.8) to those N energy levels E_α, $\alpha = 1, \ldots, N$, that are (almost) degenerate with E (i.e. $|E - E_\alpha| \ll \Delta$). The remaining $M - N$ eigenvalues of $\mathcal{H}$ do not contribute to the scattering matrix. This enormous reduction of the number of

energy levels involved provides the simplification that allows us to compute the complete distribution of the matrix Q_E.

We arrange the eigenvector elements $\psi_{n\alpha}$ into an $N \times N$ matrix $\Psi_{j\alpha} = \psi_{j\alpha} M^{1/2}$. Its distribution $P(\Psi) \propto \exp(-\beta \mathrm{tr}\, \Psi\Psi^\dagger/2)$ is invariant under a transformation $\Psi \to \Psi O$, where O is an orthogonal (unitary, symplectic) matrix. We use this freedom to replace Ψ by the product ΨO, and choose a uniform distribution for O. We finally define the $N \times N$ Hermitian matrix $H_{ij} = \sum_{\alpha=1}^{N} O_{i\alpha}(E_\alpha - E) O^*_{j\alpha}$. Since the distribution of the energy levels E_α close to E is given by $\prod_{\mu<\nu} |E_\mu - E_\nu|^\beta$ [cf. Eq. (4.2.9)], it follows that the matrix H has a uniform distribution near $H = 0$. We then find

$$S = -\mathbb{1} + (i\tau_H/\hbar)\Psi^{\dagger -1} H \Psi^{-1}, \quad Q_E = \tau_H \Psi^{\dagger -1}\Psi^{-1}. \tag{4.2.10}$$

Hence the joint distribution of S and Q_E at $S = -\mathbb{1}$ is given by

$$\begin{aligned} P(-\mathbb{1}, Q_E) \;&\propto\; \int d\Psi\, dH\, e^{-\beta\, \mathrm{tr}\, \Psi\Psi^\dagger/2} \\ &\quad \times \delta(\Psi^{\dagger -1} H \Psi^{-1})\, \delta(Q_E - \tau_H \Psi^{\dagger -1}\Psi^{-1}) \\ &= \int d\Psi\, e^{-\beta\, \mathrm{tr}\, \Psi\Psi^\dagger/2} \left(\det \Psi\Psi^\dagger\right)^{(\beta N + 2 - \beta)/2} \\ &\quad \times \delta(Q_E - \tau_H \Psi^{\dagger -1}\Psi^{-1}). \end{aligned} \tag{4.2.11}$$

The remaining integral in Eq. (4.2.11) depends entirely on the positive-definite Hermitian matrix $\Gamma = \Psi\Psi^\dagger$. In Refs. [35] and [38] it is shown that

$$\int d\Psi f(\Psi\Psi^\dagger) = \int d\Gamma\, (\det \Gamma)^{(\beta-2)/2}\, f(\Gamma)\Theta(\Gamma), \tag{4.2.12}$$

where $\Theta(\Gamma) = 1$ if all eigenvalues of Γ are positive and 0 otherwise, and f is an arbitrary function of $\Gamma = \Psi\Psi^\dagger$. Integration of Eq. (4.2.11) with the help of Eq. (4.2.12) finally yields the distribution (4.2.2) for the inverse delay times and the uniform distribution of the eigenvectors, as advertised.

In addition to the energy derivative of the scattering matrix, one may also consider the derivative with respect to an external parameter X, such as the shape of the system, or the magnetic field [13, 30, 31]. In random-matrix theory, the parameter dependence of energy levels and wavefunctions is described through a parameter dependent $M \times M$ Hermitian matrix ensemble,

$$\mathcal{H}(X) = \mathcal{H} + M^{-1/2} X\, \mathcal{H}', \tag{4.2.13}$$

where $\mathcal{H}$ and $\mathcal{H}'$ are taken from the same Gaussian ensemble. We characterize $\partial S/\partial X$ through the symmetrized derivative

$$Q_X = -i S^{-1/2} \frac{\partial S}{\partial X} S^{-1/2}, \tag{4.2.14}$$

by analogy with the symmetrized time-delay matrix Q_E in Eq. (4.2.3). To calculate the distribution of Q_X, we assume that the invariance (4.2.6) also holds for the X-dependent

ensemble of scattering matrices. (A random-matrix model with this invariance property is given in Sec. 7.3). Then it is sufficient to consider the special point $S = -\mathbb{1}$. From Eqs. (4.2.10) and (4.2.13) we find

$$Q_X = \Psi^{\dagger -1} H' \Psi^{-1}, \quad P(H') \propto \exp(-\beta \mathrm{tr}\, H'^2/16), \tag{4.2.15}$$

where $H'_{\mu\nu} = -(\tau_H/\hbar) M^{-1/2} \sum_{i,j} \psi^*_{i\mu} \mathcal{H}'_{ij} \psi_{j\nu}$. A calculation similar to that of the distribution of the time-delay matrix shows that the distribution of Q_X is a Gaussian, with a width set by Q_E,

$$\begin{aligned} P(S, Q_E, Q_X) &\propto (\det Q_E)^{-2\beta N - 3 + 3\beta/2} \\ &\times \exp\left[-\frac{\beta}{2} \mathrm{tr} \left(\tau_H Q_E^{-1} + \frac{1}{8} (\tau_H Q_E^{-1} Q_X)^2 \right) \right]. \end{aligned} \tag{4.2.16}$$

The fact that delay times set the scale for the sensitivity to an external perturbation in an open system is well understood in terms of classical trajectories [39], in the semiclassical limit $N \to \infty$. Eq. (4.2.16) makes this precise in the fully quantum-mechanical regime of a finite number of channels N. Correlations between parameter dependence and delay time were also obtained in Refs. [13, 30, 31], for the phase shift derivatives $\partial \phi_j / \partial X$.

In summary, we have calculated the distribution of the Wigner-Smith time-delay matrix for chaotic scattering. This is relevant for experiments on frequency and parameter-dependent transmission through chaotic microwave cavities [21, 22] or semiconductor quantum dots with ballistic point contacts [40]. The distribution (4.2.1) has been known since Dyson's 1962 paper as the circular ensemble [23]. It is remarkable that the Laguerre ensemble (4.2.2) for the (inverse) delay times was not discovered earlier.

4.3 Distribution of parametric conductance derivatives of a quantum dot

Parametric fluctuations in quantum systems with a chaotic classical dynamics are of fundamental importance for the characterization of mesoscopic systems. The fluctuating dependence of an energy level $E_j(X)$ on an external parameter X, such as the magnetic field, has received considerable attention [41]. A key role is played by the "level velocity" dE_j/dX, describing the response to a small perturbation [42–44]. In open systems, the role of the level velocity is played by the "conductance velocity" dG/dX. Remarkably little is known about its distribution.

The interest in this problem was stimulated by experiments on semiconductor microstructures known as quantum dots, in which the electron motion is ballistic and chaotic [40]. A typical quantum dot is confined by gate electrodes, and connected to two electron reservoirs by ballistic point contacts, through which only a few modes can propagate at the Fermi level. The parametric dependence of the conductance has been measured by several groups [45–47]. In the single-mode limit, parametric fluctuations are of the same order as the average, so that one needs the complete distribution of G and dG/dX to characterize the system. Knowing the average and variance is not sufficient. Analytical results are

available for point contacts with a large number of modes [1, 48–53]. In this section, we present the complete distribution in the opposite limit of two single-mode point contacts and show that it differs strikingly from the multi-mode case considered previously.

The main differences which we have found are the following. We consider the joint distribution of the conductance G and the derivatives $\partial G/\partial V$, $\partial G/\partial X$ with respect to the gate voltage V and an external parameter X (typically the magnetic field). If the point contacts contain a large number of modes, $P(G, \partial G/\partial V, \partial G/\partial X)$ factorizes into three independent Gaussian distributions [1,48–50]. In the single-mode case, in contrast, we find that this distribution does not factorize and decays algebraically rather than exponentially. By integrating out G and one of the two derivatives, we obtain the conductance velocity distributions $P(\partial G/\partial V)$ and $P(\partial G/\partial X)$ plotted in Fig. 4-2. Both distributions have a singularity at zero velocity, and algebraic tails. A remarkable prediction of our theory is that the correlations between G, on the one hand, and $\partial G/\partial V$ and $\partial G/\partial X$, on the other hand, can be transformed away by the change of variables $G = (2e^2/h)\sin^2\theta$, where θ is the polar coordinate introduced in Ref. [51]. The derivatives $\partial\theta/\partial V$ and $\partial\theta/\partial X$ are statistically independent of θ. There exists no change of variables that transforms away the correlations between $\partial G/\partial V$ and $\partial G/\partial X$.

Another new feature of the single-mode case concerns the effect of Coulomb interactions [8, 9]. In the simplest model, the strength of the Coulomb repulsion is measured by the ratio of the charging energy e^2/C (with C the capacitance of the quantum dot) and the mean level spacing Δ. In the regime $e^2/C \gg \Delta$, where most experiments are done, Coulomb interactions suppress fluctuations of the charge Q on the quantum dot as a function of V or X, at the expense of fluctuations in the electrical potential U. Since the Fermi level μ in the quantum dot is pinned by the reservoirs, the kinetic energy $E = \mu - U$ at the Fermi level fluctuates as well. Fluctuations of E can not be ignored, because the conductance is determined by E, and not by μ. An ensemble of quantum dots with fixed Q and fluctuating E behaves effectively as a canonical ensemble — rather than a grand-canonical ensemble. In the opposite regime $e^2/C \ll \Delta$, the energy E does not fluctuate on the scale of the level spacing. The ensemble is now truly grand-canonical. Fluctuations of E on the scale of Δ can be neglected in the multi-mode case, so that the distinction between canonical and grand-canonical averages is irrelevant. In the single-mode case the distinction becomes important. We will see that the distribution of the conductance velocities is different in the two ensembles. (The distribution of the conductance itself is the same.) The difference between grand-canonical and canonical averages has been studied extensively in connection with the problem of the persistent current [54–56], which is a thermodynamic property. Here we find a difference in the case of a transport property, which is more unusual [57].[4]

To derive these results, we combine a scattering formalism with random-matrix theory [58]. The 2×2 scattering matrix S determines the conductance

$$G = |S_{12}|^2, \tag{4.3.1}$$

[4]The difference between canonical and grand-canonical averages which we find is related, but not identical, to the effects of the Coulomb blockade predicted by I. L. Aleiner and L. I. Glazman (preprint, cond-mat/9612138).

and the (unscreened) compressibilities [9]

$$\frac{\partial Q}{\partial E} = \frac{1}{2\pi i}\mathrm{tr}\, S^\dagger \frac{\partial S}{\partial E}, \quad \frac{\partial Q}{\partial X} = \frac{1}{2\pi i}\mathrm{tr}\, S^\dagger \frac{\partial S}{\partial X}. \tag{4.3.2}$$

(We measure G in units of $2e^2/h$ and Q in units of e.) Grand-canonical averages $\langle\cdots\rangle_{GC}$ and canonical averages $\langle\cdots\rangle_C$ are related by

$$\langle\cdots\rangle_C = \Delta\langle\cdots\times dQ/dE\rangle_{GC}. \tag{4.3.3}$$

The factor dQ/dE is the Jacobian to go from an average over Q in the canonical ensemble to an average over E in the grand-canonical ensemble. Conductance velocities in the two ensembles are related by

$$\left.\frac{\partial G}{\partial X}\right|_Q = \left.\frac{\partial G}{\partial X}\right|_E - \frac{\partial G}{\partial E}\frac{\partial Q}{\partial X}\left(\frac{\partial Q}{\partial E}\right)^{-1}, \tag{4.3.4}$$

where $|_Q$ and $|_E$ indicate, respectively, derivatives at constant Q (canonical) and constant E (grand-canonical). Derivatives $\partial G/\partial V$ with respect to the gate voltage are proportional to $\partial G/\partial Q$ in the canonical ensemble and to $\partial G/\partial E$ in the grand-canonical ensemble. (The proportionality coefficients contain elements of the capacitance matrix of the quantum dot plus gates.) The two derivatives are related by

$$\frac{\partial G}{\partial Q} = \frac{\partial G}{\partial E}\left(\frac{\partial Q}{\partial E}\right)^{-1}. \tag{4.3.5}$$

The problem that we face is the calculation of the joint distribution of S, $\partial S/\partial E$, and $\partial S/\partial X$. In view of the relations (4.3.3)–(4.3.5) it is sufficient to consider the grand-canonical ensemble. This problem is closely related to the old problem [15, 16] of the distribution of the Wigner-Smith delay times $\tau_1, \ldots, \tau_N$, which are the eigenvalues of the $N \times N$ matrix $-iS^\dagger \partial S/\partial E$. (The eigenvalues are real positive numbers.) Interest in this problem has revived in connection with chaotic scattering [5, 13, 30, 31]. In Sec. 4.2 it has been shown that the rates $\gamma_n = 1/\tau_n$ are distributed according to

$$P(\{\gamma_n\}) \propto \prod_{i<j}|\gamma_i - \gamma_j|^\beta \prod_k \gamma_k^{\beta N/2} e^{-\pi\beta\gamma_k/\Delta}. \tag{4.3.6}$$

This distribution is known in random-matrix theory as the Laguerre ensemble, because the correlation functions can be written as series over (generalized) Laguerre polynomials [35]. For $N = 1$ we recover the result of Refs. [30] and [5]. In our case $N = 2$.

To compute the conductance velocities it is not sufficient to know the delay times τ_n, but we also need to know the distribution of the eigenvectors of the Wigner-Smith time-delay matrix $-iS^\dagger \partial S/\partial E$. Furthermore, we need the distribution of $-iS^\dagger \partial S/\partial X$. The general result containing this information is (see Sec. 4.2)

$$P(S, \tau_E, \tau_X) \propto \exp\left[-\beta\,\mathrm{tr}\left(\frac{\pi}{\Delta}\tau_E^{-1} + \frac{\pi^2 X_0^2}{4\Delta^2}(\tau_E^{-1}\tau_X)^2\right)\right] \times (\det\tau_E)^{-2\beta N + 3(\beta-2)/2}, \tag{4.3.7}$$

$$\tau_E = -iS^{-1/2}\frac{\partial S}{\partial E}S^{-1/2}, \quad \tau_X = -iS^{-1/2}\frac{\partial S}{\partial X}S^{-1/2}. \tag{4.3.8}$$

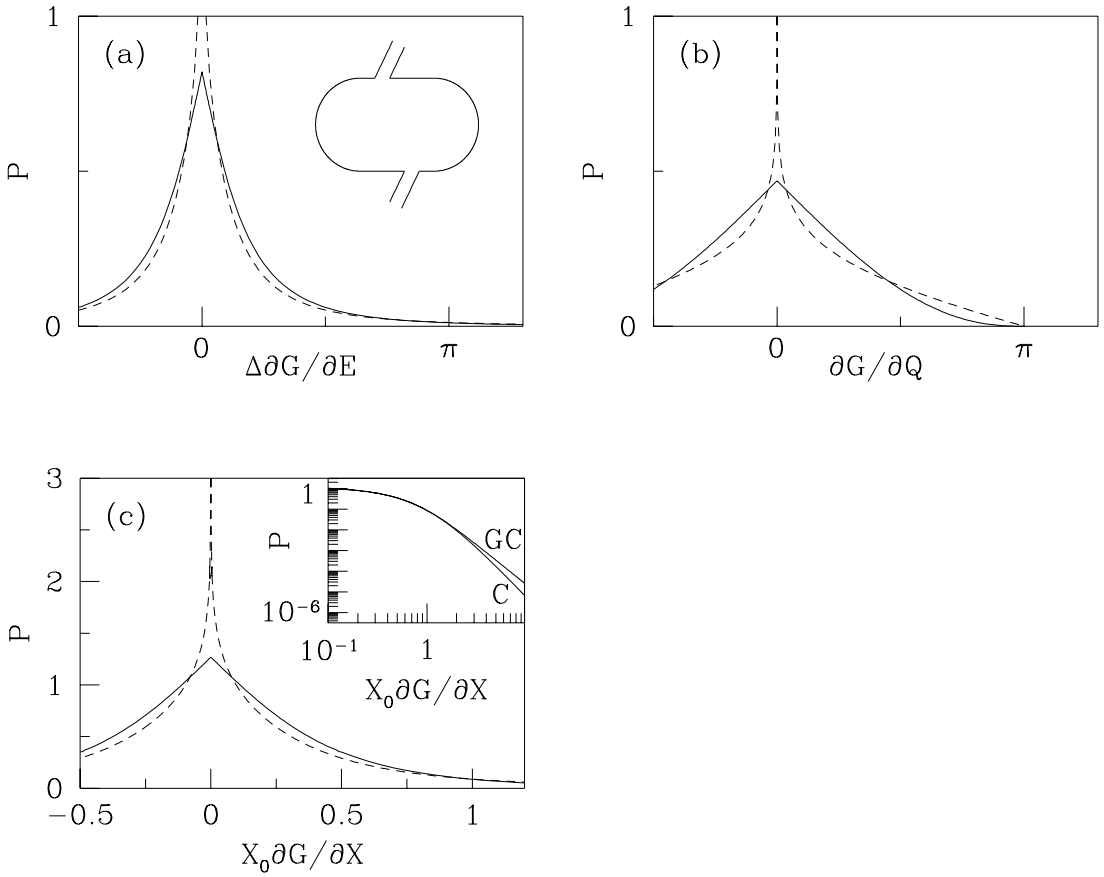

Figure 4-2. Distributions of conductance velocities in a chaotic cavity with two single-mode point contacts [inset in (a)], computed from Eq. (4.3.13). Dashed curves are for $\beta = 1$ (time-reversal symmetry), solid curves for $\beta = 2$ (no time-reversal symmetry). (The case $\beta = 4$, which is similar to $\beta = 2$, is omitted for clarity.) The distribution of $\Delta\partial G/\partial E$ (grand-canonical ensemble) is shown in (a) and the distribution of $\partial G/\partial Q$ (canonical ensemble) is shown in (b). (The conductance G is measured in units of $2e^2/h$, the charge Q in units of e.) In (c) the distribution of $X_0\partial G/\partial X$ is shown for the grand-canonical ensemble (the canonical case being nearly identical on a linear scale). The inset compares the canonical (C) and grand-canonical (GC) results for $\beta = 2$ on a logarithmic scale.

The matrix τ_E has the same eigenvalues as the time-delay matrix, but it is more convenient because it is uncorrelated with S, while the time-delay matrix is not. By integrating out τ_E and τ_X from Eq. (4.3.7), we obtain a uniform distribution for S, as expected for a chaotic cavity [17, 18]. The resulting distribution of the conductance [4], $P(G) \propto G^{-1+\beta/2}$, is the same in the canonical and grand-canonical ensembles, because S and dQ/dE are uncorrelated [cf. Eq. (4.3.3)]. By integrating out S, τ_X, and the eigenvectors of τ_E, we obtain the distribution (4.3.6) of the delay times. The distribution of τ_X at fixed τ_E is a Gaussian. The scale of this Gaussian is set by the parameter X_0, which has no universal value.[5]

We are now ready to compute the distribution of the conductance velocities. Derivatives with respect to E and Q are related to the delay times by

$$\frac{\partial G}{\partial E} = c(\tau_1 - \tau_2)\sqrt{G(1-G)}, \tag{4.3.9}$$

$$\frac{\partial G}{\partial Q} = 2\pi c \frac{\tau_1 - \tau_2}{\tau_1 + \tau_2}\sqrt{G(1-G)}, \tag{4.3.10}$$

where $c \in [-1, 1]$ is a number that depends on the phases of the matrix elements of S and on the eigenvectors of τ_E. Its distribution $P(c) \propto (1-c^2)^{-1+\beta/2}$ is independent of τ_1, τ_2, and G. The derivative $\partial G/\partial X$ has a Gaussian distribution at a given value of S and τ_E, with zero mean and with variance

$$\left\langle \left(\left.\frac{\partial G}{\partial X}\right|_E \right)^2 \right\rangle = \alpha \left[G(1-G)\tau_1\tau_2 + \frac{1}{2}\left(\frac{\partial G}{\partial E}\right)^2 \right], \tag{4.3.11}$$

$$\left\langle \left(\left.\frac{\partial G}{\partial X}\right|_Q \right)^2 \right\rangle = \alpha\tau_1\tau_2 \left[G(1-G) - \frac{1}{4\pi^2}\left(\frac{\partial G}{\partial Q}\right)^2 \right], \tag{4.3.12}$$

where we have abbreviated $\alpha = 4\Delta^2/\pi^2 X_0^2 \beta$. Because the variance of $\partial G/\partial X$ depends on $\partial G/\partial E$ or $\partial G/\partial Q$, these conductance velocities are correlated.

From the distribution (4.3.6) of τ_1, τ_2, and the independent distributions of G and c, we calculate the joint distribution of G and its (dimensionless) derivatives $G_X = X_0 \partial G/\partial X$, $G_E = (\Delta/2\pi)\partial G/\partial E$, and $G_Q = (1/2\pi)\partial G/\partial Q$. The result in the grand-canonical and canonical ensembles is

$$P_{GC}(G, G_E, G_X) = \frac{1}{Z}\int_0^\infty dx \int_{\frac{G_E^2}{G(1-G)}}^\infty dy \frac{\left[yG - G_E^2/(1-G)\right]^{-1+\beta/2} x^{-2-2\beta}}{\sqrt{\pi(x+y)G(1-G)\,f(x)}} \times \exp\left[-\frac{2\beta}{x}\sqrt{x+y} - \frac{G_X^2}{f(x)} \right], \tag{4.3.13}$$

$$P_C(G, G_Q, G_X) = \frac{2}{Z}\int_0^\infty dx \int_{\frac{G_Q^2}{G(1-G)}}^1 dy \frac{\left[yG - G_Q^2/(1-G)\right]^{-1+\beta/2} x^{3\beta}}{(1-y)^{(\beta+3)/2}\sqrt{\pi G(1-G)g(x)}}$$

[5] If X represents the magnetic flux through the quantum dot, then $X_0 \simeq (h/e)(\tau_{\rm ergodic}/\tau_{\rm dwell})^{1/2}$, where $\tau_{\rm dwell}$ is the mean dwell time in the quantum dot and $\tau_{\rm ergodic} \ll \tau_{\rm dwell}$ is the time scale for ergodic exploration of the available phase space.

$$\times \exp\left[-\frac{2\beta x}{\sqrt{1-y}} - \frac{G_X^2}{g(x)}\right], \tag{4.3.14}$$

where

$$\begin{aligned} f(x) &= 8\beta^{-1}[xG(1-G) + 2G_E^2], \\ g(x) &= 8(x^2\beta)^{-1}[G(1-G) - G_Q^2], \\ Z &= 3\beta^{-3\beta-1}\Gamma(\beta/2)\Gamma(\beta)\Gamma(3\beta/2). \end{aligned}$$

By integrating out G and one of the two derivatives from Eq. (4.3.13), we obtain the conductance velocity distributions of Fig. 4-2. (The case $\beta = 4$ is close to $\beta = 2$ and is omitted from the plot for clarity.) The distributions have a singularity at zero derivative: A cusp for $\beta = 2$ and 4, and a logarithmic divergence for $\beta = 1$. The tails of the distributions of $\partial G/\partial X$ are algebraic in both ensembles, but with a different exponent,

$$P_{GC}(\partial G/\partial X) \propto (\partial G/\partial X)^{-\beta-2}, \tag{4.3.15}$$

$$P_{C}(\partial G/\partial X) \propto (\partial G/\partial X)^{-2\beta-1}. \tag{4.3.16}$$

The distribution of $\partial G/\partial E$ (grand-canonical ensemble) also has an algebraic tail [proportional to $(\partial G/\partial E)^{-\beta-2}$], while the distribution of $\partial G/\partial Q$ (canonical ensemble) is identically zero for $|\partial G/\partial Q| \geq \pi$. In both ensembles, the second moment of the conductance velocities is finite for $\beta = 2$ and 4, but infinite for $\beta = 1$.

In conclusion, we have calculated the joint distribution of the conductance G and its parametric derivatives for a chaotic cavity, coupled to electron reservoirs by two single-mode ballistic point contacts. The distribution is fundamentally different from the multi-mode case, being highly non-Gaussian and with correlated derivatives. (Correlations between G and the parametric derivatives can be transformed away by a change of variables.) We account for Coulomb interactions by using a canonical ensemble instead of a grand-canonical ensemble. Our results for the canonical ensemble are relevant for the analysis of recent experiments on chaotic quantum dots, where the conductance G is measured as a function of both the magnetic field and the shape of the quantum dot [47]. The grand-canonical results are relevant for experiments on microwave cavities [21, 22]. Together with the theory provided here, such experiments can yield information on the distribution of delay times in chaotic scattering that can not be obtained by other means.

Appendix A: Stub model versus Hamiltonian approach

In this appendix we consider the extended circular ensemble of Sec. 4.1 for the energy dependence of the scattering matrix in more detail. We compare the extended circular ensemble with the Hamiltonian approach and show that they are equivalent in the limit that the number of modes in the stub $N_s \to \infty$.

In the extended circular ensemble of Sec. 4.1, a fictitious stub (a closed lead) is attached to the cavity (see Fig. 4-1b) . The stub has N_s propagating modes. The total number of

modes in the real leads is N. The $N \times N$ scattering matrix $S(\varepsilon)$ of the quantum dot is expressed in terms of the $(N+N_s)\times(N+N_s)$ scattering matrix U of the dot with the stub replaced by a regular open lead and the $N_s \times N_s$ reflection matrix $r_s(\varepsilon)$ of the stub,

$$S(\varepsilon) \;=\; U_{ll} + U_{ls}\,[1 - r_s U_{ss}]^{-1}\, r_s U_{sl}, \quad U = \begin{pmatrix} U_{ll} & U_{ls} \\ U_{sl} & U_{ss} \end{pmatrix}. \tag{A.1}$$

Here we decomposed the matrix U into four blocks U_{ij}, which describe transmission and reflection from and to the stub (s) or the two leads (l). In the model of Sec. 4.1, the energy dependence of U is neglected, while the ε-dependence of r_s is taken into account via a simple ansatz,

$$r_s(\varepsilon) = -e^{-i\varepsilon\Phi}, \tag{A.2}$$

where Φ is a (symmetric) positive definite matrix. We assume that all eigenvalues of Φ are comparable, so that $N_s \mathrm{tr}\,\Phi^2 \sim (\mathrm{tr}\,\Phi)^2$. We further set

$$\mathrm{tr}\,\Phi = 2\pi/\Delta, \tag{A.3}$$

where Δ is the mean level spacing of the closed quantum dot. The unitary matrix U is taken from the appropriate circular ensemble (depending on whether time-reversal symmetry and/or spin-rotation symmetry are present). If the point contacts to the real leads contain tunnel barriers, U is distributed according to the Poisson kernel (cf. Sec. 2.2; we assume that the stub contains no tunnel barriers). In the end, the limit $N_s \to \infty$ is taken. This ensures that particles are reflected from the stub many times before they exit through one of the real point contacts. The extended circular ensemble is defined by Eqs. (A.1)—(A.3). To avoid confusion with other extensions of the circular ensemble, we call it the "stub model" for the energy dependence of the scattering matrix.

In the Hamiltonian approach, the scattering matrix $S(\varepsilon)$ is expressed in terms of an $M \times M$ random Hermitian matrix H, modeling the Hamiltonian of the closed cavity, and a $M \times N$ rectangular matrix W, describing the coupling between the states in the closed dot and the scattering states in the lead [37],

$$S(\varepsilon) = \mathbb{1} - 2\pi i W^\dagger (\varepsilon - H + i\pi W W^\dagger)^{-1} W. \tag{A.4}$$

In the end, the limit $M \to \infty$ is taken. For a chaotic cavity, the matrix H is a random matrix, usually taken from the Gaussian ensemble. However, the precise distribution of H is not important, and we are free to take a different distribution.

In Sec. 2.2 it was shown that the scattering matrix approach and the Hamiltonian approach are equivalent at a fixed energy ε. Moreover, it was shown that if the Hamiltonian H is distributed according to the Lorentzian ensemble, the equivalence between the two approaches even holds if the scattering matrix and the Hamiltonian have the same size. We use this equivalence to write the scattering matrix U in terms of a hermitian matrix H and a coupling matrix W,

$$U = 1 + 2\pi i W^\dagger (H - i\pi W W^\dagger)^{-1} W, \tag{A.5}$$

where the matrices W and H have the same size as U. The matrix H is distributed according to the Lorentzian ensemble,

$$P(H) \propto \det\left(M\Delta^2 + \pi^2 H^2\right)^{-(\beta M+2-\beta)/2}, \tag{A.6}$$

where we have set $M = N + N_\mathrm{s}$. The coupling matrix W is a square matrix, which we separate into two rectangular blocks describing the coupling with the lead and the stub,

$$W = (W_\mathrm{l}, W_\mathrm{s}). \tag{A.7}$$

The matrix W_l is an $M \times N$ rectangular matrix with elements

$$(W_\mathrm{l})_{\mu n} = \pi^{-1}\delta_{\mu n}(\Delta M)^{1/2}\left(2\Gamma_n^{-1} - 1 - 2\Gamma_n^{-1}\sqrt{1-\Gamma_n}\right)^{1/2}, \tag{A.8}$$

where Γ_n ($n = 1, \ldots, N$) is the transmission probability of mode n in the leads. Since the stub contains no tunnel barrier, the $M \times N_\mathrm{s}$ matrix W_s has elements $(W_\mathrm{l})_{\mu n} = \delta_{\mu,N+n}\pi^{-1}(M\Delta)^{1/2}$.

Substitution of Eq. (A.5) into Eq. (A.1) yields

$$S(\varepsilon) = 1 - 2\pi i W_\mathrm{l}^\dagger G(\varepsilon)^{-1} W_\mathrm{l}, \tag{A.9}$$

$$\begin{aligned} G(\varepsilon) &= i\pi W_\mathrm{s}[1 + r_\mathrm{s}(\varepsilon)][1 - r_\mathrm{s}(\varepsilon)]^{-1} W_\mathrm{s}^\dagger - H + i\pi W_\mathrm{l} W_\mathrm{l}^\dagger \\ &= \pi^{-1}\Delta M \tan[\tilde{\Phi}\varepsilon/2] - H + i\pi W_\mathrm{l} W_\mathrm{l}^\dagger, \end{aligned} \tag{A.10}$$

where the $M \times M$ matrix $\tilde{\Phi}$ is defined as

$$\tilde{\Phi} = \begin{pmatrix} 0 & 0 \\ 0 & \Phi \end{pmatrix}. \tag{A.11}$$

We expand G to first order in ε. This is allowed, because the eigenvalues of $\varepsilon\Phi$ are of order N_s^{-1}. The result is

$$G(\varepsilon) = \varepsilon - H - \delta H + i\pi W_1 W_1^\dagger, \quad \delta H = (1 - M\tilde{\Phi}\Delta/2\pi)\varepsilon. \tag{A.12}$$

Apart from the term δH, this is precisely the expression for the ε-dependent scattering matrix in the Hamiltonian approach, cf. Eq. (A.4). The correction δH, which is absent in the Hamiltonian approach, is not relevant for energies $\varepsilon \sim \Delta$ and in the limit $M, N_\mathrm{s} \to \infty$, because $\mathrm{tr}\,\delta H = 0$ and $\mathrm{tr}\,\delta H^2 \sim M\varepsilon^2$. (A perturbation δH with a vanishing trace is only relevant if $\mathrm{tr}\,\delta H^2 \sim M^2\Delta^2$ [59]). This proves equivalence of the stub model and the Hamiltonian approach for the energy dependence of the scattering matrix.

In Sec. 7.3, a stub model is formulated for the dependence on an external parameter X, such as the magnetic field or the shape of the quantum dot. One can also show that this stub model is equivalent to the Hamiltonian approach. In the Hamiltonian approach, the parameter dependent Hamiltonian $H(X)$ is modeled through the hermitian matrix

$$H(X) = H + (X/\sqrt{M})H', \tag{A.13}$$

where H and H' are both random hermitian $M \times M$ matrices with the same mean level spacing. The factor $\sqrt{M}$ is added in Eq. (A.13) to remove the M-dependence from the relevant scale for the parameter X. If X describes the shape of the cavity, H' is real and symmetric. If X describes the magnetic field, H' is antisymmetric.

In the stub model of Sec. 7.3, the X-dependence is modeled through an X-dependent reflection matrix $r_s(X)$ of the stub, which has the form

$$r_s(X) = -\exp\left(-\frac{2\pi i X A}{M^{3/2}\Delta}\right), \tag{A.14}$$

where A is a (random) matrix taken from the same ensemble as H'. Repeating the same steps as above, we find that the scattering matrix $S(X)$ reads

$$\begin{aligned} S(X) &= 1 - 2\pi i W_1^\dagger G(X)^{-1} W_1, \\ G(X) &= -H - \pi^{-1} M\Delta \tan[\pi \tilde{A} X / M^{3/2}\Delta] + i\pi W_1 W_1^\dagger, \end{aligned} \tag{A.15}$$

where $\tilde{A}_{\mu\nu} = A_{\mu-N,\nu-N}$ if $\mu, \nu > N$ and $\tilde{A}_{\mu\nu} = 0$ else. As before, we expand to first order in X and find

$$G(X) = -H(X) + i\pi W_1 W_1^\dagger, \quad H(X) = H + (X/\sqrt{M})\tilde{A}. \tag{A.16}$$

The Hamiltonian $H(X)$ is formally equivalent to Eq. (A.13). The only difference is that the matrix $\tilde{A}$ has zeros for indices $\mu, \nu \leq N$, while the elements of H_1 are nonzero everywhere. Since typical matrix elements of H' are of order $\Delta\sqrt{M}$, the difference is not relevant for $X \sim 1$ and $M \to \infty$. This completes the proof of the equivalence of the stub models for the ε and X dependence of the scattering matrix and the Hamiltonian approach.

References

[1] R. A. Jalabert, H. U. Baranger, and A. D. Stone, Phys. Rev. Lett. **65**, 2442 (1990); H. U. Baranger, R. A. Jalabert, and A. D. Stone, Phys. Rev. Lett. **70**, 3876 (1993).

[2] V. N. Prigodin, K. B. Efetov and S. Iida, Phys. Rev. Lett. **71**, 1230 (1993); K. B. Efetov, Phys. Rev. Lett. **74**, 2299 (1995).

[3] V. N. Prigodin, B. L. Altshuler, K. B. Efetov and S. Iida, Phys. Rev. Lett. **72**, 546 (1994); V. N. Prigodin, K. B. Efetov and S. Iida, Phys. Rev. B **51**, 17223 (1995).

[4] H. U. Baranger and P. A. Mello, Phys. Rev. Lett. **73**, 142 (1994); R. A. Jalabert, J.-L. Pichard, and C. W. J. Beenakker, Europhys. Lett. **27**, 255 (1994).

[5] V. A. Gopar, P. A. Mello, and M. Büttiker, Phys. Rev. Lett. **77**, 3005 (1996).

[6] J. Wang and H. Guo, Phys. Rev. B54, R11090 (1996); Y. Cohen and Y. Avishai, J. Phys. Condens. Matter **7**, L121 (1995); D. Z. Liu, B. Y. K. Hu, C. A. Stafford, and S. Das Sarma, Phys. Rev. B**50**, 5799 (1994); N. Kumar and A. M. Jayannavar, preprint (cond-mat/9607042).

[7] M. Büttiker, A. Prêtre, and H. Thomas, Phys. Rev. Lett. **70**, 4114 (1993).

[8] M. Büttiker, J. Phys.: Condens. Matter **5**, 9361, (1993); M. Büttiker, H. Thomas, and A. Prêtre, Z. Phys. B **94**, 133 (1994).

[9] T. Christen and M. Büttiker, Phys. Rev. Lett. **77**, 143 (1996); M. Büttiker and T. Christen, in *Quantum Transport in Semiconductor Submicron Structures*, edited by B. Kramer, NATO ASI Series Vol. **326**, (Kluwer, Dordrecht, 1996). For a discussion of dwell times, injectivities and emissivities in open structures see also V. Gasparian, T. Christen, and M. Büttiker, Phys. Rev. A **54**, 4022 (1996).

[10] P. W. Anderson, E. Abrahams, and T. V. Ramakrishnan, Phys. Rev. Lett. **43**, 718 (1979); L. P. Gor'kov, A. I. Larkin, and D. E. Khmel'nitskiĭ, Pis'ma Zh. Eksp. Teor. Fiz. **30**, 248 (1979) [JETP Lett. **30**, 228 (1979)].

[11] B. L. Al'tshuler, Pis'ma Zh. Eksp. Teor. Fiz. **41**, 530 (1985) [JETP Lett. **41**, 648 (1985)]; P. A. Lee and A. D. Stone, Phys. Rev. Lett. **55**, 1622 (1985).

[12] M. L. Mehta, *Random Matrices* (Academic, New York, 1991).

[13] Y. V. Fyodorov and H.-J. Sommers, J. Math. Phys. **38**, 1918 (1997).

[14] L. Eisenbud, PhD thesis (Princeton, 1948).

[15] E. P. Wigner, Phys. Rev. **98**, 145 (1955).

[16] F. T. Smith, Phys. Rev. **118**, 349 (1960).

[17] U. Smilansky, in *Chaos and Quantum Physics*, edited by M.-J. Giannoni, A. Voros, and J. Zinn-Justin (North-Holland, Amsterdam, 1991).

[18] R. Blümel and U. Smilansky, Phys. Rev. Lett. **60**, 477 (1988); **64**, 241 (1990).

[19] C. H. Lewenkopf and H. A. Weidenmüller, Ann. Phys. **212**, 53 (1991).

[20] E. Doron, U. Smilansky, and A. Frenkel, Phys. Rev. Lett. **65**, 3072 (1990).

[21] J. Stein, H.-J. Stöckmann, and U. Stoffregen, Phys. Rev. Lett. **75**, 53 (1995).

[22] A. Kudrolli, V. Kidambi, and S. Sridhar, Phys. Rev. Lett. **75**, 822 (1995).

[23] F. J. Dyson, J. Math. Phys. **3**, 140 (1962).

[24] V. L. Lyuboshits Phys. Lett. B **72**, 41 (1977); Yad. Fiz. **27**, 948 (1978); **37**, 292 (1983) [Sov. J. Nucl. Phys. **27**, 502 (1978)]; **37**, 174 (1983)].

[25] M. Bauer, P. A. Mello, and K. W. McVoy, Z. Phys. A **293**, 151 (1979).

[26] H. L. Harney, F.-M. Dittes, and A. Müller, Ann. Phys. **220**, 159 (1992).

[27] B. Eckhardt, Chaos **3**, 613 (1993)

[28] F. Izrailev, D. Saher, and V. V. Sokolov, Phys. Rev. E **49**, 130 (1994).

[29] N. Lehmann, D. V. Savin, V. V. Sokolov, and H.-J. Sommers, Physica D **86**, 572 (1995).

[30] Y. V. Fyodorov and H.-J. Sommers, Phys. Rev. Lett. **76**, 4709 (1996); Y. V. Fyodorov, D. V. Savin, and H.-J. Sommers (preprint cond-mat/9701108).

[31] P. Šeba, K. Życzkowski, and J. Zakrewski, Phys. Rev. E **54**, 2438 (1996).

[32] V. A. Gopar, P. A. Mello, and M. Büttiker, Phys. Rev. Lett. **77**, 3005 (1996).

[33] E. R. Mucciolo, R. A. Jalabert, and J.-L. Pichard (preprint, cond-mat/9703178).

[34] E. Akkermans, A. Auerbach, J. E. Avron, and B. Shapiro, Phys. Rev. Lett. **66**, 76 (1991).

[35] K. Slevin and T. Nagao, Phys. Rev. B **50**, 2380 (1994); T. Nagao and K. Slevin, J. Math. Phys. **34**, 2075 (1993); T. Nagao and P. J. Forrester, Nucl. Phys. B **435**, 401 (1995).

[36] E. P. Wigner, Ann. Math. **53**, 36 (1951); Proc. Cambridge Phil. Soc. **47**, 790 (1951); Ann. Math. **55**, 7 (1952).

[37] J. J. M. Verbaarschot, H. A. Weidenmüller, and M. R. Zirnbauer, Phys. Rep. **129**, 367 (1985).

[38] E. Brézin, S. Hikami, and A. Zee, Nucl. Phys. B **464**, 411 (1996).

[39] R. A. Jalabert, H. U. Baranger and A. D. Stone, Phys. Rev. Lett. **65**, 2442 (1990).

[40] R. M. Westervelt, in *Nano-Science and Technology*, edited by G. Timp (American Institute of Physics, New York, 1996).

[41] B. L. Altshuler and B. D. Simons, in *Mesoscopic Quantum Physics*, edited by E. Akkermans, G. Montambaux, J.-L. Pichard, and J. Zinn-Justin (North-Holland, Amsterdam, 1995).

[42] B. D. Simons and B. L. Altshuler, Phys. Rev. B **48**, 5422 (1993).

[43] Y. V. Fyodorov, Phys. Rev. Lett. **73**, 2688 (1994); Y. V. Fyodorov and A. D. Mirlin, Phys. Rev. B **51**, 13403 (1995).

[44] N. Taniguchi, A. Hashimoto, B. D. Simons, and B. L. Altshuler, Europhys. Lett. **27**, 335 (1994).

[45] C. M. Marcus, A. J. Rimberg, R. M. Westervelt, P. F. Hopkins, and A. C. Gossard, Phys. Rev. Lett. **69**, 506 (1992).

[46] A. M. Chang, H. U. Baranger, L. N. Pfeiffer, and K. W. West, Phys. Rev. Lett. **73**, 2111 (1994).

[47] I. H. Chan, R. M. Clarke, C. M. Marcus, K. Campman, and A. C. Gossard, Phys. Rev. Lett. **74**, 3876 (1995).

[48] Z. Pluhař, H. A. Weidenmüller, J. A. Zuk, and C. H. Lewenkopf, Phys. Rev. Lett. **73**, 2115 (1994).

[49] K. B. Efetov, Phys. Rev. Lett. **74**, 2299 (1995).

[50] K. Frahm, Europhys. Lett. **30**, 457 (1995).

[51] K. Frahm and J.-L. Pichard, J. Phys. I France **5**, 877 (1995).

[52] J. Rau, Phys. Rev. B **51**, 7734 (1995).

[53] A. M. S. Macêdo, Phys. Rev. B **53**, 8411 (1996).

[54] H.-F. Cheung, Y. Gefen, E. K. Riedel, and W.-H. Shih, Phys. Rev. B **37**, 6050 (1988).

[55] H. Bouchiat and G. Montambaux, J. Phys. (Paris) **50**, 2695 (1989).

[56] B. L. Altshuler, Y. Gefen, and Y. Imry, Phys. Rev. Lett. **66**, 88 (1991).

[57] A. Kamenev and Y. Gefen, Phys. Rev. B **49**, 14474 (1994).

[58] C. W. J. Beenakker, Rev. Mod. Phys. (July 1997, cond-mat/9612179).

[59] A. Pandey and M. L. Mehta, Commun. Math. Phys. **87**, 449 (1983).

5 Localization in disordered wires

5.1 Equivalence of the one-dimensional σ model and the Dorokhov-Mello-Pereyra-Kumar equation

There are two known approaches to the theory of phase-coherent conduction and localization in disordered wires: The first is the Fokker-Planck approach of Dorokhov, Mello, Pereyra, and Kumar [1–5]. The second is the field-theoretic approach of Efetov and Larkin, which leads to a supersymmetric nonlinear σ model [6, 7]. Both approaches provide a description of quantum transport that is independent of microscopic details of the disordered wire. The only properties which enter are its length L, the elastic mean free path ℓ, the number N of propagating transverse modes at the Fermi level (referred to as "channels"), and the symmetry index $\beta \in \{1, 2, 4\}$ (depending on the presence or absence of time-reversal and/or spin-rotational symmetry). In the first approach, the transfer matrix is expressed as a product of a large number of random matrices. As more matrices are added to this product, the transmission eigenvalues T_n execute a Brownian motion. (The T_n are the N eigenvalues of the transmission matrix product $t^\dagger t$.) The resulting Fokker-Planck equation for the L-dependence of the distribution $P(T_1, \ldots, T_N)$ is known as the Dorokhov-Mello-Pereyra-Kumar (DMPK) equation. In the second approach, one starts from the random Hamiltonian of the disordered wire and then expresses averages of Green's functions [6, 7] or moments of the transmission eigenvalues [8–11] as integrals over matrices Q containing both commuting and anticommuting variables. These so-called supermatrices are restricted by the nonlinear constraint $Q^2 = 1$ and give rise to a field theory known as the one-dimensional nonlinear σ model.

In the last decade, research on the Fokker-Planck and field-theoretic approach has proceeded quite independently. Recently, exact results for the average conductance $\langle G \rangle$, its variance $\mathrm{var}\, G$, and the density $\rho(T) = \langle \sum_n \delta(T - T_n) \rangle$ of transmission eigenvalues were obtained from both approaches. For the unitary symmetry class (no time-reversal symmetry; $\beta = 2$), the DMPK equation was solved exactly by Beenakker and Rejaei [12]. The construction of a set of biorthogonal polynomials for this exact solution then allowed for the exact computation of $\langle G \rangle$, $\mathrm{var}\, G$, and $\rho(T)$ for arbitrary N and L in the case $\beta = 2$ [13]. Although there exists a formal solution for the other two symmetry classes [orthogonal class (time-reversal symmetry without spin-orbit scattering; $\beta = 1$) and symplectic class (time-reversal symmetry with spin-orbit scattering; $\beta = 4$)] [14], no exact results for $\langle G \rangle$, $\mathrm{var}\, G$, and $\rho(T)$ have been obtained. Concerning the σ model, an important and substantial progress was the development of "super Fourier analysis" by Zirnbauer [10]. This allowed the exact calculation [10, 11] of $\langle G \rangle$ and $\mathrm{var}\, G$ for all β in the thick-wire limit $N \to \infty$, $L/\ell \to \infty$ at fixed ratio $N\ell/L$. The eigenvalue density $\rho(T)$ was computed from the σ model by Rejaei [15], in the thick-wire limit and for the case $\beta = 2$.

If one takes the thick-wire limit of the $\beta = 2$ results for $\langle G \rangle$, $\mathrm{var}\, G$, and $\rho(T)$ from the

DMPK equation, they agree precisely with those from the σ model [13,15]. For $\beta = 1$ and 4, a comparison of the two approaches has only been possible in the metallic regime $\ell \ll L \ll N\ell$, where the results for $\langle G \rangle$ and $\mathrm{var}\, G$ from the DMPK equation [3–5] and from the σ model [9,11,16] agree with conventional diagrammatic perturbation theory [17–20]. The equivalence of the two approaches outside the perturbative regime has been questioned [13] as a result of recent work by Zirnbauer [10], and by Mirlin, Müller-Groeling, and Zirnbauer [11]. Starting from the σ model in the thick-wire limit, they obtained a finite limit $\langle G \rangle \to e^2/2h$ as $L/N\ell \to \infty$ in the case $\beta = 4$. On the other hand, one can prove rigorously [13] that the DMPK equation gives $\lim_{L\to\infty}\langle G \rangle = 0$ for all β. It was this puzzling contradiction which motivated us to search for a general proof of equivalence of the DMPK equation and the σ model, without the restriction to $\beta = 2$.

In this chapter, we present a general proof of the equivalence of the two approaches, which applies to all three symmetry classes β, to all length scales L, and to the complete distribution of transmission eigenvalues described by the p-point functions $\rho_p(T_1, \ldots, T_p) = (N!/(N-p)!) \int dT_{p+1} \ldots \int dT_N \; P(T_1, \ldots, T_N)$ for arbitrary p. We cannot relax the assumption that the number N of propagating channels in the disordered wire is $\gg 1$, since it is needed for the derivation of the one-dimensional σ model [11]. However, we can consider the σ model formulation of a thick disordered wire which is coupled to the leads by means of a point contact with $N_1 \leq N$ transmitted modes [9], and show that it is mathematically equivalent to a DMPK equation for a wire with N_1 propagating channels. The equivalence proof demonstrates that $\lim_{L\to\infty}\langle G \rangle = 0$ in the σ model, in apparent contradiction with Zirnbauer's work. We have reexamined the calculation of Refs. 10 and 11, and argue that for $\beta = 4$ the Kramers degeneracy of the transmission eigenvalues was not taken into account properly in the super Fourier analysis. This leads to a spurious "zero-mode", which does not decay as $L \to \infty$. Restoring Kramers degeneracy, we obtain modified expressions for $\langle G \rangle$ and $\mathrm{var}\, G$ which decrease exponentially in the localized regime and moreover agree well with numerical simulations [21].

Both the σ model and the DMPK equation were derived from a number of different models for a disordered wire. The original derivation of the DMPK equation by Dorokhov [1], which started from a model of N coupled chains with defects, was followed by the random-matrix formulation of Mello, Pereyra, and Kumar [2]. These authors considered a product of random transfer matrices, drawn from an ensemble of maximum entropy. Later it was shown that the DMPK equation is insensitive to the choice of the ensemble, the only relevant assumptions being weak scattering (mean free path ℓ much greater than the Fermi wave length λ_F) and equivalence of the scattering channels [22,23]. It is this latter assumption which restricts the DMPK equation to a wire geometry. From the mathematical point of view, the DMPK equation is the diffusion equation on a certain coset-space of transfer matrices [24]. The one-dimensional σ model was originally derived by Efetov and Larkin [6,7] from a white noise model for the disorder potential. Two later derivations used random-matrix models for the Hamiltonian of the disordered wire. Iida, Weidenmüller, and Zuk (IWZ) adapted Wegner's n-orbital model [25] to the study of transport properties [9]. In this description, the wire is modeled by a large number of disordered segments in series, each segment having a random Hamiltonian drawn from the Gaussian ensemble.

An alternative derivation of the σ model, due to Fyodorov and Mirlin [26], uses a random band matrix to model the Hamiltonian of the disordered wire. In the present chapter we follow Ref. 11 and use the IWZ formulation of the σ model.

Our proof of equivalence of the DMPK equation and the σ model builds on the ideas which were used by Rejaei [15] to calculate $\rho(T)$ from the σ model for $\beta = 2$. Inspired by Nazarov's diagrammatic calculation of $\rho(T)$ in the metallic regime [27], Rejaei introduced a generating function F which depends both on the transmission eigenvalues T_n and on the radial parameters θ_i of the supermatrices in the unitary σ model. Rejaei was able to solve the $1d$ σ model exactly for $\beta = 2$ and thus obtained the density $\rho(T)$ as a function of L by taking derivatives of F with respect to the θ_i's. The resulting $\rho(T)$ could then be compared with the result from the DPMK equation [13]. We introduce a more general generating function which allows us to establish the equivalence of the σ model and the DMPK equation at the level of p-point functions $\rho_p(T_1, \ldots, T_p)$, without actually having to compute this function. This approach works also for $\beta = 1$ and 4, where no explicit solution of the σ model is available.

The outline of the chapter is as follows: In Sec. 5.1.1, an outline of the equivalence proof is given. The full proof for the σ model with 8×8 supermatrices follows in Secs. 5.1.2 and 5.1.3, with technical material in Apps. A – C. For the p-point functions $\rho_p(T_1, \ldots, T_p)$, we have to consider the σ model with $8p \times 8p$ supermatrices. This extension is described in App. D. In section 5.1.4, we discuss the symplectic symmetry class ($\beta = 4$) in relation to Refs. 10 and 11. By accounting for Kramers degeneracy, we obtain modified expressions for $\langle G \rangle$ and $\operatorname{var} G$, which we compare with numerical simulations of the IWZ model by Mirlin and Müller-Groeling [21]. We conclude in Sec. 5.1.5.

5.1.1 Outline of the equivalence proof

Although our equivalence proof is technically rather involved, the basic idea can be described in a few paragraphs. In this section, we present an outline of the equivalence proof for the small σ model (8×8 supermatrices). The details are given in the following two sections and in the appendices A — C. Appendix D contains the necessary modifications to extend the proof to σ models with supermatrices of arbitrary size.

Part of the complexity of the problem is that the σ model and the DMPK equation focus on totally different objects. In the σ model, transport properties are expressed as functional integrals over supermatrices Q [9, 11]. (A supermatrix is a matrix containing an equal number of commuting and anticommuting elements. We follow the notation and conventions of Refs. 8, 9, and 11.) For the small σ model the 8×8 supermatrices are parameterized as [7, 8]

$$Q = T^{-1} \Lambda T, \quad \Lambda = \begin{pmatrix} 1 & 0 \\ 0 & -1 \end{pmatrix}, \tag{5.1.1}$$

$$T = \begin{pmatrix} u^{-1} & 0 \\ 0 & v^{-1} \end{pmatrix} \exp \begin{pmatrix} 0 & \frac{1}{2}\hat{\theta} \\ \frac{1}{2}\hat{\theta} & 0 \end{pmatrix} \begin{pmatrix} u & 0 \\ 0 & v \end{pmatrix}, \tag{5.1.2}$$

where u and v are pseudo-unitary 4×4 supermatrices. Notice that Q satisfies the non-linear constraint $Q^2 = 1$, hence the name "non-linear" σ model. (The letter σ is used for historical reasons.) The 4×4 supermatrix $\hat{\theta}$ is called the radial part of Q. It has the form

$$\hat{\theta} = \begin{pmatrix} \theta_1 & \theta_2 & 0 & 0 \\ \theta_2 & \theta_1 & 0 & 0 \\ 0 & 0 & i\theta_3 & i\theta_4 \\ 0 & 0 & i\theta_4 & i\theta_3 \end{pmatrix}, \tag{5.1.3}$$

with the symmetry restrictions

$$\begin{aligned} &\theta_4 = 0 && \text{if } \beta = 1, \\ &\theta_2 = \theta_4 = 0 && \text{if } \beta = 2, \\ &\theta_2 = 0 && \text{if } \beta = 4. \end{aligned} \tag{5.1.4}$$

While the σ model works with the radial part of a supermatrix, the DMPK equation works with the radial part of an ordinary matrix (containing only commuting elements). This is the transfer matrix X. The radial part of X is an $N \times N$ diagonal matrix $\hat{\lambda}$, related to the eigenvalues of $XX^\dagger$. The eigenvalues of $XX^\dagger$ come in N inverse pairs $e^{\pm x_n}$, related to the diagonal elements λ_n of $\hat{\lambda}$ by $\lambda_n = \sinh^2 x_n$. For $\beta = 4$ the eigenvalues are twofold degenerate (Kramers degeneracy). The matrix $\hat{\lambda}$ then contains only the N independent eigenvalues. The conductance G is directly related to the λ_n's by the Landauer formula [2, 28]

$$G = \frac{2e^2}{h} \sum_{n=1}^{N} T_n = \frac{2e^2}{h} \sum_{n=1}^{N} \frac{1}{1+\lambda_n}, \tag{5.1.5}$$

since the N independent transmission eigenvalues T_n are related to the λ_n's by $T_n = (1 + \lambda_n)^{-1}$.

We connect both approaches by considering a generating function $F(\hat{\theta}, \hat{\lambda})$ which depends on both radial matrices:

$$F(\hat{\theta}, \hat{\lambda}) = \prod_{n=1}^{N} f(\hat{\theta}, \lambda_n), \tag{5.1.6}$$

$$f(\hat{\theta}, \lambda) = \mathrm{Sdet}^{-d/2} \left[\lambda + \cosh^2(\hat{\theta}/2) \right] \tag{5.1.7}$$

$$= \left[\frac{(1 + 2\lambda + \cos(\theta_3 + \theta_4))\ (1 + 2\lambda + \cos(\theta_3 - \theta_4))}{(1 + 2\lambda + \cosh(\theta_1 + \theta_2))\ (1 + 2\lambda + \cosh(\theta_1 - \theta_2))} \right]^{d/2},$$

$$d = 1 \text{ if } \beta = 1, 2; \quad d = 2 \text{ if } \beta = 4. \tag{5.1.8}$$

The symbol Sdet stands for the superdeterminant of a supermatrix. For $\beta = 2$ this is the generating function introduced by Rejaei.

An ensemble of disordered wires of length L provides a distribution of $\hat{\lambda}$. The ensemble average $\langle F(\hat{\theta}, \hat{\lambda}) \rangle$ contains all statistical properties that are accessible from the small σ

model. These include the average conductance $\langle G\rangle$, its variance $\mathrm{var}\, G$ and the density of transmission eigenvalues $\rho(T)$. We explain in appendix A how to extract these quantities by taking derivatives of $\langle F(\hat\theta,\hat\lambda)\rangle$. The average $\langle F(\hat\theta,\hat\lambda)\rangle$ can be determined by each of the two approaches independently, in terms of a partial differential equation for the L-dependence and an initial condition at $L = 0$. For the σ model on the one hand, the evolution equation reads

$$\frac{\partial}{\partial L}\left\langle F(\hat\theta,\hat\lambda)\right\rangle = \frac{2}{\xi}\Delta_{\hat\theta}\left\langle F(\hat\theta,\hat\lambda)\right\rangle, \tag{5.1.9}$$

where $\Delta_{\hat\theta}$ is the (radial part of the) Laplacian on the σ model space, and where $\xi = \beta N\ell$ is the localization length. The explicit form of $\Delta_{\hat\theta}$ is given by [7]

$$\Delta_{\hat\theta} = \frac{\beta}{2d}\sum_i J^{-1}(\hat\theta)\,\frac{\partial}{\partial\theta_i}\,J(\hat\theta)\,\frac{\partial}{\partial\theta_i}, \tag{5.1.10}$$

where the sum runs over the independent coordinates θ_i [see Eq. (5.1.4)] and $J(\hat\theta)$ is the integration measure for the radial decomposition (5.1.1),

$$\begin{aligned}
J(\theta_1,\theta_2,\theta_3) &= \sinh\theta_1\,\sinh\theta_2\,\sin^3\theta_3\prod_{s_1,s_2=\pm1}\sinh^{-2}\left(\tfrac12(\theta_1+s_1\theta_2+is_2\theta_3)\right) \text{ if } \beta=1,\\
J(\theta_1,\theta_3) &= \sinh\theta_1\,\sin\theta_3\prod_{s_1=\pm1}\sinh^{-2}\left(\tfrac12(\theta_1+is_1\theta_3)\right), \qquad \text{if } \beta=2,\\
J(\theta_1,\theta_3,\theta_4) &= \sin\theta_3\,\sin\theta_4\,\sinh^3\theta_1\prod_{s_1,s_2=\pm1}\sinh^{-2}\left(\tfrac12(\theta_1+is_1\theta_3+is_2\theta_4)\right) \text{ if } \beta=4.
\end{aligned}$$

The DMPK equation on the other hand, yields the evolution equation

$$\frac{\partial}{\partial L}\left\langle F(\hat\theta,\hat\lambda)\right\rangle = \frac{2}{\xi}\left\langle D_{\hat\lambda}\,F(\hat\theta,\hat\lambda)\right\rangle, \tag{5.1.11}$$

where $D_{\hat\lambda}$ is a second order differential operator in the parameters λ_n,

$$D_{\hat\lambda} = J^{-1}(\hat\lambda)\sum_{n=1}^{N}\frac{\partial}{\partial\lambda_n}\,J(\hat\lambda)\,\lambda_n(1+\lambda_n)\,\frac{\partial}{\partial\lambda_n}, \tag{5.1.12}$$

$$J(\hat\lambda) = \prod_{n>m}|\lambda_n-\lambda_m|^\beta. \tag{5.1.13}$$

The key ingredient of the equivalence proof is the identity

$$\Delta_{\hat\theta}F(\hat\theta,\hat\lambda) = D_{\hat\lambda}\,F(\hat\theta,\hat\lambda), \tag{5.1.14}$$

which shows that the evolution with L of $\langle F(\hat\theta,\hat\lambda)\rangle$ is the same in both approaches. Showing that the initial conditions at $L = 0$ coincide as well, completes the equivalence proof.

5.1.2 One-dimensional σ model

We begin the detailed exposition of the equivalence proof with a formulation of the σ model. As in Ref. 11, we use the formulation of Iida-Weidenmüller-Zuk (IWZ) [9].

The IWZ model

The IWZ model [9, 16] applies Wegner's n-orbital model [25] to a wire geometry and supplements it by a coupling to ideal (not disordered) leads, as in Landauer's approach to conduction [29]. The left and right leads (labeled by indices 1 and 2) contain N_1 and N_2 propagating modes each (per spin direction for $\beta = 1, 2$, or per Kramers doublet for $\beta = 4$). The disordered wire of length L is assumed to consist of K segments in series (Fig. 5-1). The Hamiltonian H of the disordered wire without leads is represented by a matrix $H^{ij}_{\mu\nu}$, where the upper indices i, j label the segments $1 \le i, j \le K$ and the lower indices μ, ν label the M states (per spin direction or Kramers doublet) within each segment. The elements of H are real ($\beta = 1$), complex ($\beta = 2$) or quaternion ($\beta = 4$) numbers. The coupling between the states inside one segment is described by the matrices $H^{ii}_{\mu\nu}$, which are distributed according to the Gaussian ensemble

$$P(H^{ii}) = \text{const.} \times \exp\left(-\tfrac{1}{4}\beta M v_1^{-2} \mathrm{Tr}\,(H^{ii})^2\right). \tag{5.1.15}$$

Here v_1 is a parameter which governs the level density at the Fermi level ($E = 0$). The coupling between the states of adjacent segments is given by another set of Gaussian distributed random matrices $H^{ij} = (H^{ji})^\dagger$ (with coupling parameter v_2),

$$P(H^{ij}) = \text{const.} \times \exp\left(-\tfrac{1}{2}\beta M^2 v_2^{-2} \mathrm{Tr}\, H^{ij} H^{ji}\right),$$
$$j = i \pm 1. \tag{5.1.16}$$

Segments which are not adjacent are uncoupled, $H^{ij} = 0$ if $|i - j| \ge 2$. The coupling to the ideal leads is described by a fixed $KM \times (N_1 + N_2)$ rectangular matrix $W = W_1 + W_2$ with real ($\beta = 1$), complex ($\beta = 2$) or quaternion ($\beta = 4$) elements. The matrix W has elements $W^i_{\mu n}$, where i labels the segment, μ the states in the segment, and n the modes in the leads. The elements of W_1 (which describes the coupling to lead 1) are nonzero only for $i = 1$ and $1 \le n \le N_1$; the elements of W_2 (coupling to lead 2) are nonzero only for $i = K$ and $N_1 < n \le N_1 + N_2$.

The scattering matrix S (matrix elements S_{nm}) of the system at energy E is given by [9]

$$S = 1 - 2\pi i W^\dagger (E - H + i\pi W W^\dagger)^{-1} W. \tag{5.1.17}$$

The indices n, m correspond to lead 1 if $1 \le n, m \le N_1$ and to lead 2 if $N_1 < n, m \le N_1 + N_2$. The reflection and transmission matrices r, r', t, t' are submatrices of S,

$$S = \begin{pmatrix} r & t' \\ t & r' \end{pmatrix}. \tag{5.1.18}$$

Since S is unitary, the products $t^\dagger t$ and $t'^\dagger t'$ have the same set of non-zero eigenvalues, denoted by $T_n = (1 + \lambda_n)^{-1}$. (If $N_2 > N_1$ there are also $N_2 - N_1$ transmission eigenvalues which are zero, and can therefore be disregarded.)

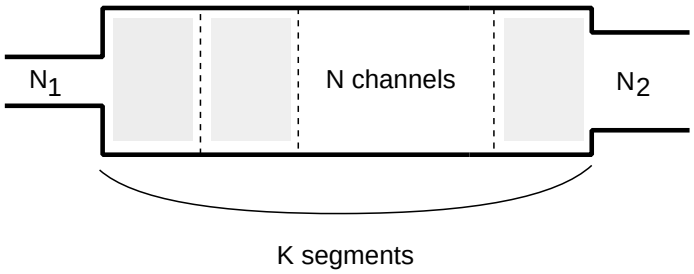

Figure 5-1. Schematic drawing of the disordered wire and the leads according to the IWZ model description. The left lead (lead 1) contains N_1, the right lead (lead 2) N_2 propagating channels. The number of propagating channels in the disordered wire is N. In the IWZ model, the disordered wire is divided into K segments, each having a random Hamiltonian drawn drom the Gaussian ensemble. The derivation of the $1d$ σ model from the IWZ model assumes $N \gg 1$, but allows for finite N_1 and N_2.

The generating function

We now define the generating function $F(\hat{\theta}, \hat{\lambda})$ introduced in the previous section. We start from the the relationship (5.1.17) between the scattering matrix and the Hamiltonian in the IWZ model. We consider the generating function

$$F = \mathrm{Sdet}^{-\frac{1}{2}}(E - \mathcal{H} + i\pi W_1 W_1^\dagger Q + i\pi W_2 W_2^\dagger \Lambda), \tag{5.1.19}$$

$$\mathcal{H} = H 1_8 \ \text{ if } \beta = 1, 4; \quad \mathcal{H} = (\mathrm{Re}H)1_8 + i(\mathrm{Im}H)\tau_3 \ \text{ if } \beta = 2. \tag{5.1.20}$$

Here 1_8 is the 8×8 supersymmetric unit matrix and τ_3 is a diagonal matrix with elements $(1, -1, 1, -1, 1, -1, 1, -1)$. The matrix Λ was defined in Eq. (5.1.1). Note that Q is an arbitrary supermatrix as in Eq. (5.1.1) and that it replaces the matrix Λ in the coupling term of lead 1. In App. B we show that F depends only on the radial part $\hat{\theta}$ of the matrix Q and that the only dependence on H is through the transmission eigenvalues $T_n = (1 + \lambda_n)^{-1}$. We also show that Eq. (5.1.19) reduces to the function $F(\hat{\theta}, \hat{\lambda})$ defined in Eq. (5.1.6) of the previous section.

In the following, we evaluate the ensemble average $\langle F \rangle$ using the supersymmetric formalism. We first express $\langle F \rangle$ as a Gaussian integral over an $8MK$-dimensional supervector ψ:

$$\langle F \rangle = \left\langle \int \mathcal{D}\psi \ \exp\left(\tfrac{1}{2} i \ \psi^\dagger \Lambda (E - \mathcal{H} + i\pi W_1 W_1^\dagger Q + i\pi W_2 W_2^\dagger \Lambda + i\epsilon\Lambda)\psi\right)\right\rangle. \tag{5.1.21}$$

The convergence of the Gaussian integral is assured by the parameterization (5.1.1) of the matrix Q. Performing the standard steps, described in Refs. 9 and 11, we obtain in the relevant limit $M \to \infty$

$$\langle F \rangle = \int dQ_1 \int dQ_K \ f_1(Q, Q_1) \ f_2(\Lambda, Q_K) \, W(Q_1, Q_K), \tag{5.1.22}$$

$$W(Q_1, Q_K) = \int dQ_2 \ldots \int dQ_{K-1} \ \exp\left(-\frac{d\, v_2^2}{2 v_1^2} \sum_{i=1}^{K-1} \mathrm{Str}(Q_i \, Q_{i+1}),\right) \tag{5.1.23}$$

$$f_1(Q, Q_1) = \exp\left(-\frac{1}{2}d\sum_{n=1}^{N_1}\mathrm{Str}\,\ln(1+x_n\,QQ_1)\right), \tag{5.1.24}$$

$$f_2(Q, Q_K) = \exp\left(-\frac{1}{2}d\sum_{n=N_1+1}^{N_1+N_2}\mathrm{Str}\,\ln(1+x_n\,QQ_K)\right). \tag{5.1.25}$$

The numbers x_n denote the eigenvalues of the matrices $(\pi/v_1)W_1^\dagger W_1$ (if $1 \le n \le N_1$) or $(\pi/v_1)W_2^\dagger W_2$ (if $N_1 < n \le N_1 + N_2$). The integer d was defined in Eq. (5.1.8).

Following Ref. 11, we consider the limit $v_1^2 \ll v_2^2$. Then the sum in (5.1.23) can be replaced by an integral and the Q_i-integrals yield a path integral. The discrete number of segments K becomes the continuous (dimensionless) variable s. The propagator (5.1.23) can be identified with the heat kernel of the supersymmetric space, determined by the heat equation [11]

$$\begin{aligned} 2\beta(v_2/v_1)^2\frac{\partial}{\partial s}W(Q', Q'') &= \Delta_{Q'}W(Q', Q''), \\ \lim_{s\to 0} W(Q', Q'') &= \delta(Q', Q''). \end{aligned} \tag{5.1.26}$$

The precise definition of the Laplacian Δ_Q and the detailed justification of Eq. (5.1.26) are contained in Ref. 11 (Δ_Q in Eq. (5.1.26) differs by an additional factor $\beta/(8d)$ with respect to the notations of Ref. 11). We thus arrive at the expression

$$\langle F\rangle = \int dQ' \int dQ''\; f_1(Q, Q')\, W(Q', Q'')\; f_2(\Lambda, Q''). \tag{5.1.27}$$

The next step is to notice that $f_1(Q, Q')$ has the same symmetry as the heat kernel, i.e. $f_1(T^{-1}QT, T^{-1}Q'T) = f_1(Q, Q')$ where T is an arbitrary element as described in (5.1.1). This implies $\Delta_{Q'} f_1(Q, Q') = \Delta_Q f_1(Q, Q')$ and hence $\langle F\rangle$ also satisfies the heat equation

$$2\beta(v_2/v_1)^2\frac{\partial}{\partial s}\langle F\rangle = \Delta_Q\langle F\rangle. \tag{5.1.28}$$

Since $\langle F\rangle$ only depends on the radial part $\hat{\theta}$ of Q, it is sufficient to consider the radial part $\Delta_{\hat{\theta}}$ of the Laplacian Δ_Q. This radial part $\Delta_{\hat{\theta}}$ can be written as in Eq. (5.1.10). We thus find that the ensemble average $\langle F(\hat{\theta}, \hat{\lambda})\rangle$ of the generating function defined in Eq. (5.1.6) satisfies the partial differential equation

$$2\beta(v_2/v_1)^2\frac{\partial}{\partial s}\langle F(\hat{\theta}, \hat{\lambda})\rangle = \Delta_{\hat{\theta}}\langle F(\hat{\theta}, \hat{\lambda})\rangle, \tag{5.1.29}$$

with the initial condition implied by Eq. (5.1.26),

$$\lim_{s\to 0}\left\langle F(\hat{\theta}, \hat{\lambda})\right\rangle = \int dQ'\, f_1(Q, Q')\, f_2(\Lambda, Q'). \tag{5.1.30}$$

Together, Eqs. (5.1.29) and (5.1.30) determine the ensemble average of the generating function $F(\hat{\theta}, \hat{\lambda})$ evaluated in the framework of the nonlinear σ model.

The two limits of the IWZ model which were needed for the derivation of Eq. (5.1.30), $M \to \infty$ and $v_1^2/v_2^2 \to 0$, restrict the validity of Eq. (5.1.30) to the case of weak disorder ($\ell \gg \lambda_F$) and thick wires ($N \gg 1$) respectively [9, 11]. Whereas the requirement of weak disorder is also needed for the DMPK equation, the requirement that the number of channels in the disordered wire be large is not. To see how the latter requirement follows from the condition $v_1^2 \ll v_2^2$, we consider the expression for the average conductance $\langle G \rangle$ in the diffusive metallic regime ($\ell \ll L \ll N\ell$) [9, 11],

$$\langle G \rangle = \frac{2e^2}{h} \frac{N\ell}{L} = \frac{2e^2}{h} \frac{4v_2^2}{v_1^2 s}. \tag{5.1.31}$$

Taking the linear dimension of a segment of the disordered wire in the IWZ model of order ℓ (i.e. $s \approx L/\ell$, see Ref. 9), we find that $v_1^2 \ll v_2^2$ corresponds to $N \gg 1$. However, no restriction has been put to the numbers N_1 and N_2 of propagating channels in the leads in the above derivation of the σ model, which allows us to consider finite values of N_1 and N_2. This situation corresponds to the case in which the thick disordered wire is coupled to the leads 1 and 2 by means of point contacts, with N_1, N_2 open channels. As in Ref. 11, the case of a disordered wire without point contacts is recovered in the limit $N_1, N_2 \to \infty$.

We conclude this section with some remarks about the choice of initial conditions. In usual σ model calculations [10, 11, 15], one considers the case ideal coupling ($x_n = 1$, $n = 1, \ldots, N_1 + N_2$) and identifies $N = N_1 = N_2$ (equal number of channels in the leads and in the wire). In the thick-wire limit $N \to \infty$ the function $f_i(Q, Q')$ is just the delta function [11] $\delta(Q, Q')$, and $\langle F \rangle$ becomes identical to the heat kernel itself [cf. Eq. (5.1.27)]:

$$\langle F \rangle = W(Q, \Lambda), \;\; N_1 = N_2 = N \gg 1. \tag{5.1.32}$$

For $\beta = 2$, this result was derived by Rejaei [15]. In this case $\langle F \rangle$ has the delta-function initial condition $\lim_{s\to 0}\langle F \rangle = \delta(Q, \Lambda)$. To make contact with the DMPK equation, we need a different "ballistic" initial condition, such that all T_n's are unity in the limit of zero wire length. To achieve this, we take ideal coupling and assume that one of the leads has many more channels than the other. To be specific, we fix N_1 and take the limit $N_2 \to \infty$. One then finds the initial condition

$$\begin{aligned} \lim_{s\to 0}\langle F \rangle &= \exp\left(-\tfrac{1}{2} N_1 d \;\mathrm{Str}\; \ln(1 + Q\Lambda)\right) \\ &= \left(\frac{\cos\theta_3 + \cos\theta_4}{\cosh\theta_1 + \cosh\theta_2}\right)^{N_1 d}, \; 1 \le N_1 \ll N_2. \end{aligned} \tag{5.1.33}$$

In the next section, we will see that this is precisely the ballistic initial condition of the DMPK equation.

5.1.3 DMPK equation

Let us now evaluate the ensemble average of the generating function (5.1.6) from the DMPK equation. The DMPK equation is a Fokker-Planck-type equation for the

L-evolution of the probability distribution $P(\hat{\lambda})$ of the λ_n's: [1–5]

$$\frac{1}{2}(\beta N + 2 - \beta)\ell \frac{\partial}{\partial L} P(\hat{\lambda}) = \sum_{n=1}^{N} \frac{\partial}{\partial \lambda_n} \lambda_n (1+\lambda_n) J(\hat{\lambda}) \frac{\partial}{\partial \lambda_n} J^{-1}(\hat{\lambda}) P(\hat{\lambda}), \tag{5.1.34}$$

$$J(\hat{\lambda}) = \prod_{n>m} |\lambda_n - \lambda_m|^{\beta}, \tag{5.1.35}$$

where ℓ denotes the mean free path in the disordered wire and N the number of propagating modes. There is *no* restriction to $N \gg 1$ in the DMPK approach. We take the ballistic initial condition

$$\lim_{L\to 0} P(\hat{\lambda}) = \prod_{n=1}^{N} \delta(\lambda_n - 0^+). \tag{5.1.36}$$

The DMPK equation implies for $F(\hat{\theta}, \hat{\lambda})$ the evolution equation [2, 4]

$$\begin{aligned} \frac{\partial}{\partial L}\langle F(\hat{\theta},\hat{\lambda})\rangle &= \frac{\partial}{\partial L}\int d\lambda_1 \ldots \int d\lambda_N F(\hat{\theta},\hat{\lambda})\, P(\hat{\lambda}) \\ &= \frac{2}{\ell}(\beta N + 2 - \beta)^{-1} \left\langle D_{\hat{\lambda}}\, F(\hat{\theta},\hat{\lambda}) \right\rangle, \end{aligned} \tag{5.1.37}$$

with the differential operator $D_{\hat{\lambda}}$ given by Eq. (5.1.12). In Appendix C we prove the algebraic identity between the two different types of Laplacians (5.1.10) and (5.1.12) applied to $F(\hat{\theta}, \hat{\lambda})$,

$$\Delta_{\hat{\theta}} F(\hat{\theta},\hat{\lambda}) = D_{\hat{\lambda}}\, F(\hat{\theta},\hat{\lambda}). \tag{5.1.38}$$

From Eqs. (5.1.37), and (5.1.38) we conclude that that the average $\langle F(\hat{\theta}, \hat{\lambda})\rangle$, calculated in the framework of the DMPK equation, also fulfills the evolution equation (5.1.29) of the nonlinear σ model, provided we identify [cf. Eq. (5.1.31)]

$$\frac{4}{s}(v_2/v_1)^2 = \frac{N\ell}{L} = \frac{\xi}{\beta L}, \quad N \gg 1. \tag{5.1.39}$$

Here we introduced the localization length $\xi = \beta N \ell$ (notice that the definition of ξ in Ref. 11 differs by a factor $2/\beta$).

It remains to compare the initial conditions. The ballistic initial condition for the DMPK equation implies

$$\lim_{L\to 0}\langle F(\hat{\theta},\hat{\lambda})\rangle = f(\hat{\theta}, \lambda = 0)^N = \left(\frac{\cos\theta_3 + \cos\theta_4}{\cosh\theta_1 + \cosh\theta_2}\right)^{Nd}, \tag{5.1.40}$$

which equals the initial condition (5.1.33) for the nonlinear σ model. (The thick-wire limit $\lim_{L\to 0}\langle F\rangle = \delta(Q,\Lambda)$ is obtained by letting $N \to \infty$ in the above expression). This proves the equivalence of both approaches, as far as the generating function (5.1.6) is concerned. In Appendix D of this chapter we extend the equivalence proof to p-point functions $\rho_p(T_1, \ldots, T_p)$ for arbitrary p.

5.1.4 The controversial symplectic ensemble

The main motivation of this section was to resolve a controversy between the DMPK equation and the one-dimensional σ model in the symplectic symmetry class ($\beta = 4$). On the one hand, the DMPK equation implies [13] $\langle G\rangle \to 0$ as $L \to \infty$. On the other hand, Zirnbauer [10] finds from the σ model that $\langle G\rangle \to \frac{1}{2}e^2/h$ as $L \to \infty$.

The equivalence proof presented in this chapter has as a logical consequence that $\langle G\rangle \to 0$ as $L \to \infty$ if $\langle G\rangle$ is evaluated in the framework of the σ model. To demonstrate this, we apply the argument of Ref. 13. The DMPK equation implies for the average dimensionless conductance $g = \sum_n (1+\lambda_n)^{-1}$ the evolution equation [4]

$$\xi \frac{\partial\langle g\rangle}{\partial L} = -\beta\langle g^2\rangle - (2-\beta)\langle g_2\rangle, \tag{5.1.41}$$

with $g_2 = \sum_n (1+\lambda_n)^{-2}$. This relation also follows from the evolution equation (5.1.29) of the σ model (expanding the generating function for small θ_i and applying the results of appendix A). Since $0 \le g_2 \le g^2$, we have

$$\xi \frac{\partial\langle g\rangle}{\partial L} \le -\frac{1}{2}\beta\langle g^2\rangle \le 0. \tag{5.1.42}$$

We suppose that $\lim_{L\to\infty}\langle g\rangle$ exists. Since $\partial\langle g\rangle/\partial L \le 0$ [Eq. (5.1.42)] this implies that $\lim_{L\to\infty}\partial\langle g\rangle/\partial L = 0$. Hence $\lim_{L\to\infty}\langle g^2\rangle = 0$ by Eq. (5.1.42). Since $\langle g\rangle^2 \le \langle g^2\rangle$ this implies that also $\lim_{L\to\infty}\langle g\rangle = 0$.

Where does the non-zero limit in Refs. 10 and 11 come from? The ground-breaking contribution of Zirnbauer was to use a "super-Fourier expansion" of the heat kernel $W(Q, Q')$ in terms of eigenfunctions of the Laplacian in the space of the σ model. This type of Fourier analysis is well understood for classical symmetric spaces [30]. The development and application of the supersymmetric analogue for the σ model enabled Zirnbauer, Mirlin, and Müller-Groeling to compute non-perturbatively the first two moments of the conductance for any β. The non-zero limiting value $\lim_{L\to\infty}\langle g\rangle = 1/4$ for $\beta = 4$ resulted from a "zero mode", a non-trivial eigenfunction of the Laplacian with zero eigenvalue. Since this zero mode does not decay as $L \to \infty$, it led to the surprising conclusion of absence of localization in a wire with spin-orbit scattering in zero magnetic field [10].

An explicit expression for the zero-mode was not obtained in Refs. 10 and 11, but only its contribution to the moments of the conductance was computed. By inspecting the initial condition (5.1.33) of the generating function for the σ model we have been able to construct a zero mode for $\beta = 4$, but only if we ignore the Kramers degeneracy of the transmission eigenvalues. This unphysical zero mode, given by

$$\phi_0(\theta_1, \theta_3, \theta_4) = \frac{\cos\theta_3 + \cos\theta_4}{2 + 2\cosh\theta_1}, \tag{5.1.43}$$

arises by taking the initial condition (5.1.33) with $N_1 = 1$ and $\beta = 4$, but *without* the extra factor two in the exponent, required by Kramers degeneracy. This unphysical initial condition solves the evolution equation (5.1.29) for the ensemble average of the generating

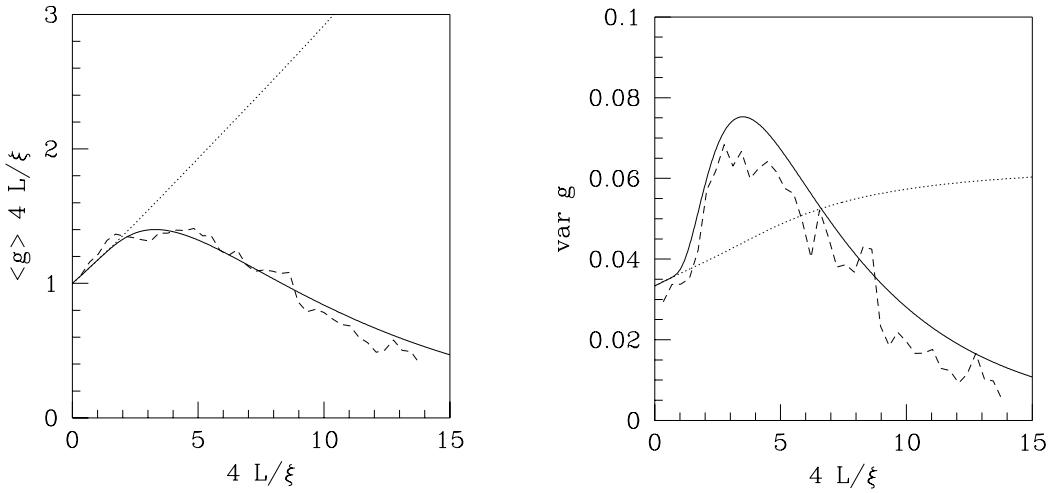

Figure 5-2. Left: The average conductance $\langle g\rangle$ multiplied by $4L/\xi = L/N\ell$ (left) and the variance $\mathrm{var}\, g$ of the conductance (right) for the symplectic symmetry class as a function of $4L/\xi$ for $N \gg 1$. Shown are our result (5.1.48) (solid), the numerical simulation of Ref. 21 ($M = 100$, $N = 25$) (dashed), and the result of Ref. 11 (dotted).

function and implies an L-independent average conductance $\langle g\rangle = 1/4$. Although we can not prove that Eq. (5.1.43) is Zirnbauer's zero mode, the coincidence with the limiting value $\lim_{L\to\infty}\langle g\rangle = 1/4$, $\lim_{L\to\infty}\mathrm{var}\, g = 1/16$ is quite suggestive.

The reason why we have to exclude the zero mode (5.1.43) from the Fourier expansion of the heat kernel is that it is not single-valued on the σ model space of supermatrices Q, although it is a well-defined function of $\hat{\theta}$. The parameterization (5.1.1) of Q is 2π-periodic in the angles $\theta_\pm = \theta_3 \pm \theta_4$. We can then consider on the space of angles θ_3, θ_4 a parity operation P which consists of adding π to both of these angles. This parity operation does not change Q, but it changes the zero mode (5.1.43). The Laplacian (5.1.10) commutes with P and the eigenfunctions have therefore either even or odd parity (eigenvalues $+1$ or -1 of P, respectively). The physical modes of the σ model must have even parity, since only these functions are single-valued. For $\beta = 4$, it is the Kramers degeneracy which ensures that the initial condition (5.1.33) has even parity.

This observation led us to check the parity of the eigenfunctions $\phi_\nu(Q)$ of the Laplacian in the super Fourier analysis of Refs. 10 and 11. We consider the eigenvalue equation

$$\Delta_{\hat{\theta}}\phi_\nu(\theta_1,\theta_3,\theta_4) = -\varepsilon(\nu)\phi_\nu(\theta_1,\theta_3,\theta_4) \tag{5.1.44}$$

for $\beta = 4$ in the limit $\theta_1 \to \infty$ at fixed θ_3, θ_4. In this limit, the Laplace operator simplifies considerably

$$\Delta_{\hat{\theta}} \to e^{\theta_1}\frac{\partial}{\partial\theta_1}e^{-\theta_1}\frac{\partial}{\partial\theta_1} + \frac{1}{\sin\theta_3}\frac{\partial}{\partial\theta_3}\sin\theta_3\frac{\partial}{\partial\theta_3} + \frac{1}{\sin\theta_4}\frac{\partial}{\partial\theta_4}\sin\theta_4\frac{\partial}{\partial\theta_4}. \tag{5.1.45}$$

From this expression one may identify the set of quantum numbers $\nu = (\lambda, 1+2n_1, 1+2n_2)$, where λ is a real number and n_1, n_2 are non-negative integers. The asymptotic behavior of the eigenfunctions $\phi_\nu(\theta_1, \theta_3, \theta_4)$ is given by

$$\phi_\nu(\theta_1,\theta_3,\theta_4) \sim \exp\left[\tfrac{1}{2}(1+i\lambda)\theta_1\right]\Big(P_{n_1}(\cos\theta_3)P_{n_2}(\cos\theta_4) + P_{n_2}(\cos\theta_3)P_{n_1}(\cos\theta_4)\Big), \tag{5.1.46}$$

with the Legendre polynomials $P_n(x)$ and the eigenvalues

$$\varepsilon(\lambda, 1+2n_1, 1+2n_2) = \frac{1}{4}\Big(\lambda^2 + (1+2n_1)^2 + (1+2n_2)^2 - 1\Big). \tag{5.1.47}$$

The parity of this eigenfunction is just $(-1)^{n_1+n_2}$ and we have to restrict ourselves to those n_1 and n_2 with n_1+n_2 even. Applying this selection rule to the expressions for $\langle g\rangle$ and $\langle g^2\rangle$ of Refs. 10 and 11, omitting the zero mode [and the subsidiary series with quantum numbers $\nu = (i, l, l\pm 2)$ of Refs. 10 and 11, for which the asymptotic behavior (5.1.46) is also valid], and multiplying the surviving terms with a factor of 2 to account for Kramers degeneracy, yields for $\beta = 4$ and in the limit $N_1 = N_2 = N \to \infty$ the expression

$$\begin{aligned}\langle g^n\rangle &= 2^{5-n} \sum_{\substack{l_1,l_2=1,3,5,\ldots,\\ l_1+l_2\equiv 2 \,(\mathrm{mod}\,4)}} \int_0^\infty d\lambda\ \lambda(\lambda^2+1)\tanh(\pi\lambda/2) l_1 l_2 p_n(\lambda, l_1, l_2) \\ &\quad\times \prod_{\sigma,\sigma_1,\sigma_2=\pm 1} (-1 + i\sigma\lambda + \sigma_1 l_1 + \sigma_2 l_2)^{-1} \exp\Big[-(\lambda^2 + l_1^2 + l_2^2 - 1)L/(2\xi)\Big],\end{aligned} \tag{5.1.48}$$

where $n = 1, 2$ and

$$\begin{aligned} p_1(\lambda, l_1, l_2) &= \lambda^2 + l_1^2 + l_2^2 - 1, \\ p_2(\lambda, l_1, l_2) &= \tfrac{1}{4}\Big[2\lambda^4 + l_1^4 + l_2^4 + 3\lambda^2(l_1^2 + l_2^2) - 2\lambda^2 + l_1^2 + l_2^2 - 2\Big]. \end{aligned}$$

Note that in our notations the dimensionless conductance g is by a factor 2 smaller than g in the notations of Ref. 11. Comparison of Eq. (5.1.48) with the $\beta = 4$ result of Ref. 11, where the parity selection rule was not implemented, shows that the perturbation expansion around $L/\xi = 0$ is the same. (We checked this numerically up to order $(L/\xi)^3$.) Outside the perturbative regime, the two expressions are completely different. Instead of a non-zero limit $\langle g\rangle = 1/4$ for $L/\xi \gg 1$, we find from Eq. (5.1.48) the exponential decay

$$\langle g\rangle \approx \frac{16}{9}\,(2L/\pi\xi)^{-3/2} e^{-L/2\xi}. \tag{5.1.49}$$

To test our result, we have compared it with a direct numerical simulation of the IWZ model by Mirlin and Müller-Groeling [21] (with $M = 100$, $N = 25$ and an average over 100 different samples). The comparison is shown in Fig. 5-2. It is clear that our Eq. (5.1.48) (solid curve) agrees quite well with the simulation, while the result of Ref. 11 does not (dotted curve).

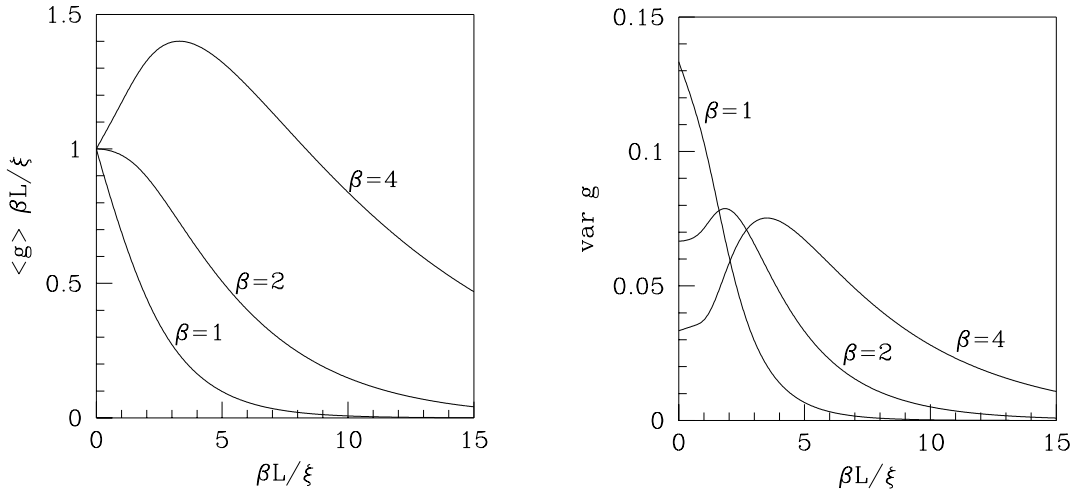

Figure 5-3. The average conductance $\langle g \rangle$ multiplied by $\beta L/\xi = L/N\ell$ (left) and the variance $\mathrm{var}\, g$ of the conductance (right) for the three symmetry classes as a function of $\beta L/\xi$ for $N \gg 1$. The curves for $\beta = 1, 2$ are taken from Refs. 10 and 11 and the curve for $\beta = 4$ is calculated from Eq. (5.1.48). Notice that $\xi = \beta N\ell$ is proportional to β, so that the scaling of the axes is β-independent.

Notice that this issue of the parity of the eigenfunctions does not occur for $\beta = 1, 2$, since there is only one compact angle (θ_3) in those cases. The parity operation on the $\hat{\theta}$-matrices exists only for $\beta = 4$. For completeness we collect in Fig. 5-3 the results for $\langle g \rangle$ and $\mathrm{var}\, g$ for all three symmetry classes. The $\beta = 1, 2$ results are from Ref. 11, the $\beta = 4$ result is our Eq. (5.1.48).

5.1.5 Conclusion

We have established the exact mathematical equivalence of the two non-perturbative theoretical approaches to phase-coherent transport and localization in disordered wires: The Fokker-Planck equation of Dorokhov, Mello, Pereyra, and Kumar [1–5] and the one-dimensional supersymmetric nonlinear σ model [6, 7, 9, 11, 26]. The equivalence has the logical consequence that the absence of localization in the symplectic symmetry class, obtained by Zirnbauer by super-Fourier analysis of the σ model, is not correct. By applying a selection rule enforced by Kramers degeneracy to the eigenfunctions of Refs. 10 and 11, we have obtained modified expressions for $\langle G \rangle$ and $\mathrm{var}\, G$, which decay exponentially as $L \to \infty$ and which agree well with existing numerical simulations [21].

Our equivalence proof has both conceptual and practical implications. The DMPK equation and the $1d$ σ model originated almost simultaneously in the early eighties, and at the same institute. [1, 6] Nevertheless, work on both approaches proceeded independently in the next decade. Knowing that, instead of two theories, there is only one, seems to us a considerable conceptual simplification of the field. It implies that the microscopic

derivations and random-matrix models developed for the σ model apply as well to the DMPK equation, and vice versa. (we see only the restriction, that the σ model requires the thick-wire limit $N \to \infty$, while the DMPK equation applies to any number of channels N.) Practically, each of the two approaches has its own advantages, and now that we know that they are equivalent, we can choose the approach which is best suited to our needs and skills.

Appendix A: Transport properties determined by the generating function

We list the transport properties of interest that can be generated from $F(\hat{\theta}, \hat{\lambda})$, following Rejaei [15]. Let us consider the function

$$f(z_1, z_2) = \left\langle \frac{\det(1 + z_2\, t^\dagger t)}{\det(1 + z_1\, t^\dagger t)} \right\rangle, \tag{A.1}$$

which equals $\langle F(\hat{\theta}, \hat{\lambda})\rangle$ at $z_2 = -\sin^2(\frac{1}{2}\theta_3)$, $z_1 = \sinh^2(\frac{1}{2}\theta_1)$, and $\theta_2 = \theta_4 = 0$. We write Eq. (A.1) in the form

$$f(z_1, z_2) = \left\langle \exp\left[\mathrm{Tr}\, \ln(1 + z_2\, t^\dagger t) - \mathrm{Tr}\, \ln(1 + z_1\, t^\dagger t)\right]\right\rangle. \tag{A.2}$$

The standard expansion [8, 9] with respect to small z_1 and z_2 yields the first two moments of the dimensionless conductance $g = (1/d)\,\mathrm{Tr}\, t^\dagger t$ (with $d = 1 + \delta_{4,\beta}$),

$$\begin{aligned} \langle g\rangle &= \frac{1}{d}\frac{\partial}{\partial z_2} f(z_1, z_2)\Big|_{z_1=0=z_2} \\ &= -\frac{1}{d}\frac{\partial}{\partial z_1} f(z_1, z_2)\Big|_{z_1=0=z_2}, \qquad \text{(A.3)} \\ \langle g^2\rangle &= -\frac{1}{d^2}\frac{\partial}{\partial z_1}\frac{\partial}{\partial z_2} f(z_1, z_2)\Big|_{z_1=0=z_2}. \qquad \text{(A.4)} \end{aligned}$$

We may also consider [15, 27] derivatives of $f(z_1, z_2)$ at $z_1 = z_2$. This may require the analytic continuation of θ_1, θ_3 to complex values if $z_1 < 0$, $z_2 > 0$ or $z_2 < -1$. Therefore, we introduce the function $f(z_1)$ as

$$\begin{aligned} f(z_1) &= \frac{\partial}{\partial z_2} f(z_1, z_2)\Big|_{z_2=z_1} \\ &= \left\langle \mathrm{Tr}\left[(1 + z_1\, t^\dagger t)^{-1}\, t^\dagger t\right]\right\rangle \\ &= \sum_{n=0}^{\infty} (-z_1)^n \langle \mathrm{Tr}\,(t^\dagger t)^{n+1}\rangle \\ &= z_1^{-1}\left(\mathrm{Tr}(1) - \left\langle \mathrm{Tr}\left[(1 + z_1\, t^\dagger t)^{-1}\right]\right\rangle\right). \qquad \text{(A.5)} \end{aligned}$$

The average density of transmission eigenvalues now follows from:

$$\begin{aligned}\rho(T) &= \langle \mathrm{Tr}\,\delta(T - t^\dagger t)\rangle \\ &= -\frac{1}{\pi T^2}\mathrm{Im}\; f\left(-(T+i0^+)^{-1}\right). \end{aligned} \tag{A.6}$$

The application of Eq. (A.6) requires the analytical continuation of both variables z_1 and z_2 to values < -1.

Appendix B: The generating function in terms of the transmission matrix

In this appendix, we show that Eq. (5.1.19) for the generating function in the IWZ model equals Eq. (5.1.6). We first consider the two cases $\beta = 1, 4$ of time reversal symmetry, when $\mathcal{H} = H1_8$ in Eq. (5.1.19). The necessary modifications for $\beta = 2$ are described at the end.

We make use of the folding identity

$$\mathrm{Sdet}\begin{pmatrix} 1_n & A \\ B & 1_m \end{pmatrix} = \mathrm{Sdet}(1_n - AB) = \mathrm{Sdet}(1_m - BA). \tag{B.1}$$

We abbreviate $G_\pm = (E - H \pm i\pi WW^\dagger)^{-1}$. Taking out the factor $(E - \mathcal{H} + i\pi WW^\dagger\Lambda)$ (with unit superdeterminant), we may rewrite Eq. (5.1.19) as

$$\begin{aligned} F &= \mathrm{Sdet}^{-\frac{1}{2}}\left(1 + \begin{pmatrix} G_+ & 0 \\ 0 & G_- \end{pmatrix} i\pi W_1 W_1^\dagger (Q - \Lambda)\right) \\ &= \mathrm{Sdet}^{-\frac{1}{2}}\left(1 + i\pi \begin{pmatrix} W_1^\dagger G_+ W_1 & 0 \\ 0 & W_1^\dagger G_- W_1 \end{pmatrix}(Q - \Lambda)\right), \end{aligned} \tag{B.2}$$

where we have applied Eq. (B.1) on $B = W_1^\dagger$. We now insert the reflection matrix $r = 1 - 2\pi i W_1^\dagger G_+ W_1$ [see Eqs. (5.1.18) and (5.1.17)] into Eq. (B.2) and obtain

$$F = \mathrm{Sdet}^{-\frac{1}{2}}\left(\frac{1}{2}(1 + \Lambda Q) + \frac{1}{2}\begin{pmatrix} r & 0 \\ 0 & r^\dagger \end{pmatrix}(1 - \Lambda Q)\right). \tag{B.3}$$

Now we use the parameterization (5.1.1) for Q. Notice that Eq. (B.3) does not depend on the angular part of Q [the matrices u, v in (5.1.2)]. Hence we may choose Q as

$$Q = T^{-1}\Lambda T,\;\; T = \exp(\tfrac{1}{2}\Theta),\;\; \Theta = \begin{pmatrix} 0 & \hat{\theta} \\ \hat{\theta} & 0 \end{pmatrix}, \tag{B.4}$$

which leads to

$$\tfrac{1}{2}(1 + \Lambda Q) = \cosh(\tfrac{1}{2}\Theta)\, T, \quad \tfrac{1}{2}(1 - \Lambda Q) = -\sinh(\tfrac{1}{2}\Theta)\, T.$$

Inserting this in Eq. (B.3) and taking out the factor T (with unit superdeterminant), we get

$$\begin{aligned} F &= \mathrm{Sdet}^{-1/2} \begin{pmatrix} \cosh(\frac{1}{2}\hat{\theta}) & -r\sinh(\frac{1}{2}\hat{\theta}) \\ -r^\dagger \sinh(\frac{1}{2}\hat{\theta}) & \cosh(\frac{1}{2}\hat{\theta}) \end{pmatrix} \\ &= \mathrm{Sdet}^{-1/2} \left(\cosh^2(\tfrac{1}{2}\hat{\theta}) - \sinh^2(\tfrac{1}{2}\hat{\theta}) r^\dagger r \right) \\ &= \mathrm{Sdet}^{-1/2} \left(1 + \sinh^2(\tfrac{1}{2}\hat{\theta}) t^\dagger t \right), \end{aligned} \tag{B.5}$$

where we have again used (B.1) and the relation $r^\dagger r = 1 - t^\dagger t$ imposed by unitarity of the scattering matrix.

The matrix $t^\dagger t$ has eigenvalues $T_n = (1+\lambda_n)^{-1}$ ($n = 1, \ldots, N_1$), which are twofold degenerate for $\beta = 4$, hence

$$\begin{aligned} F &= \prod_{n=1}^{N_1} \mathrm{Sdet}^{-d/2} (1 + \sinh^2(\tfrac{1}{2}\hat{\theta})\, T_n) \\ &= \prod_{n=1}^{N_1} \mathrm{Sdet}^{-d/2} \left(\lambda_n + \cosh^2(\tfrac{1}{2}\hat{\theta}) \right). \end{aligned} \tag{B.6}$$

Here $d = 1 + \delta_{\beta,4}$. Eq. (B.6) establishes the connection between the two expressions (5.1.6) and (5.1.19) for the generating function.

The above calculation assumes $\mathcal{H} = H 1_8$, hence $\beta = 1$ or $\beta = 4$. In the case $\beta = 2$, one has instead $\mathcal{H} = \mathrm{Re}(H) 1_8 + i\,\mathrm{Im}(H)\tau_3$. Instead of two subblocks with r and $r^\dagger$ [see Eq. (B.3)], one now needs four subblocks with r, r^T, $r^\dagger$, and r^*. Repeating the calculation one finds that the final result (B.6) remains the same.

Appendix C: Identity of Laplacians

The goal of this appendix is to prove Eq. (5.1.14). Hereto we first analyze the structure of the l.h.s. of Eq. (5.1.14) in more detail.

The derivatives of $F(\hat{\theta}, \hat{\lambda})$ with respect to θ_j are calculated using

$$\frac{\partial F(\hat{\theta}, \hat{\lambda})}{\partial \theta_j} = \left(\sum_{n=1}^{N} \frac{1}{f(\hat{\theta}, \lambda_n)} \frac{\partial f(\hat{\theta}, \lambda_n)}{\partial \theta_j} \right) F(\hat{\theta}, \hat{\lambda}), \tag{C.1}$$

$$\begin{aligned} \frac{\partial^2 F(\hat{\theta}, \hat{\lambda})}{\partial \theta_j^2} &= \left(\sum_{n=1}^{N} \frac{1}{f(\hat{\theta}, \lambda_n)} \frac{\partial^2 f(\hat{\theta}, \lambda_n)}{\partial \theta_j^2} \right) F(\hat{\theta}, \hat{\lambda}) + \\ &\quad \left(\sum_{n \neq m}^{N} \frac{1}{f(\hat{\theta}, \lambda_n) f(\hat{\theta}, \lambda_m)} \frac{\partial f(\hat{\theta}, \lambda_n)}{\partial \theta_j} \frac{\partial f(\hat{\theta}, \lambda_m)}{\partial \theta_j} \right) F(\hat{\theta}, \hat{\lambda}). \end{aligned} \tag{C.2}$$

Inspection of Eqs. (5.1.10), (C.1) and (C.2) shows that $\Delta_{\hat{\theta}} F(\hat{\theta}, \hat{\lambda})$ has two contributions, one involving a single summation over the channel indices n, and another one involving a double summation over channel indices $n \neq m$,

$$\Delta_{\hat{\theta}} F(\hat{\theta}, \hat{\lambda}) = \left(\sum_{n=1}^{N} g_1(\hat{\theta}, \lambda_n) \right) F(\hat{\theta}, \hat{\lambda}) + \left(\sum_{n \neq m}^{N} g_2(\hat{\theta}, \lambda_n, \lambda_m) \right) F(\hat{\theta}, \hat{\lambda}). \qquad \text{(C.3)}$$

Using the definition (5.1.7) of $f(\hat{\theta}, \hat{\lambda})$ one may straightforwardly calculate the functions g_1 and g_2. The expressions are rather lengthy and will not be given here.

The r.h.s. of Eq. (5.1.14) contains the differential operator $D_{\hat{\lambda}}$, which is given by Eq. (5.1.12). Simple algebra yields

$$\begin{aligned} D_{\hat{\lambda}} \;=\; & \sum_{n=1}^{N} \left(\lambda_n(1+\lambda_n) \frac{\partial^2}{\partial \lambda_n^2} + (1+2\lambda_n) \frac{\partial}{\partial \lambda_n} \right) + \\ & \frac{\beta}{2} \sum_{n \neq m}^{N} (\lambda_n - \lambda_m)^{-1} \left(\lambda_n(1+\lambda_n) \frac{\partial}{\partial \lambda_n} - \lambda_m(1+\lambda_m) \frac{\partial}{\partial \lambda_m} \right). \qquad \text{(C.4)} \end{aligned}$$

As a consequence, $D_{\hat{\lambda}} F(\hat{\theta}, \hat{\lambda})$ has again the structure of Eq. (C.3), with g_1 and g_2 now given by

$$g_1(\hat{\theta}, \lambda) \;=\; \frac{1}{f(\hat{\theta}, \lambda)} \left[\lambda(1+\lambda) \frac{\partial^2 f(\hat{\theta}, \lambda)}{\partial \lambda^2} + (1+2\lambda) \frac{\partial f(\hat{\theta}, \lambda)}{\partial \lambda} \right], \qquad \text{(C.5)}$$

$$g_2(\hat{\theta}, \lambda_1, \lambda_2) \;=\; \frac{\beta/2}{\lambda_1 - \lambda_2} \left[\frac{\lambda_1(1+\lambda_1)}{f(\hat{\theta}, \lambda_1)} \frac{\partial f(\hat{\theta}, \lambda_1)}{\partial \lambda_1} - \frac{\lambda_2(1+\lambda_2)}{f(\hat{\theta}, \lambda_2)} \frac{\partial f(\hat{\theta}, \lambda_2)}{\partial \lambda_2} \right]. \qquad \text{(C.6)}$$

Comparison of Eqs. (C.3) and (C.5) shows that the two definitions of the functions g_1 and g_2 are identical. This completes the proof of Eq. (5.1.14).

Appendix D: Extension to higher dimensional supermatrices

The argumentation presented in Secs. 5.1.2 and 5.1.3 can be generalized to σ models with Q matrices of arbitrary dimension $8p$ with $p \geq 1$. This generalized equivalence proof applies to the p-point functions $\rho_p(T_1, \ldots, T_p)$ instead to the limited number of statistical quantities that can be generated by the "small" σ model with $p = 1$ (compare appendix A). Here, we briefly present the modifications with respect to the $p = 1$ case. The modifications concern the parameterization (5.1.1) and the generating function (5.1.7).

The main technical difficulty in such a generalization is due to the radial part of the Laplace operator. The procedure to calculate it on conventional symmetric spaces is standard [30] and is carried over to the supersymmetric σ models as described in appendix B of

Ref. 11. It is now more convenient to use a slightly modified form of the parameterization of the Q-matrices, where $\hat{\theta}$ in Eq. (5.1.1) is fully diagonal (rather than block-diagonal):

$$\hat{\theta} = \begin{pmatrix} \hat{x} & 0 \\ 0 & i\hat{y} \end{pmatrix},$$
$$(\hat{x})_{nm} = x_n \delta_{nm}, (\hat{y})_{nm} = y_n \delta_{nm}, 1 \leq n, m \leq 2p. \tag{D.1}$$

The symmetry restrictions are [cf. Eq. (5.1.4)]

$$\begin{aligned} y_i &= y_{i+p} && \text{if } \beta = 1, \\ x_i &= x_{i+p},\ y_i = y_{i+p} && \text{if } \beta = 2, \\ x_i &= x_{i+p} && \text{if } \beta = 4, \end{aligned} \tag{D.2}$$

for $i = 1, \ldots, p$. In the case $p = 1$, we have the relations $x_1 = \theta_1 + \theta_2$, $x_2 = \theta_1 - \theta_2$, $y_1 = \theta_3 + \theta_4$, and $y_2 = \theta_3 - \theta_4$ between these parameters and the θ_i used in (5.1.3).

We can directly apply the results of appendix B in Ref. 11 which are given in terms of the so-called *roots* $\alpha(\Theta)$ [with Θ given as in (B.4)]. The roots are linear functions of Θ which are the eigenvalues of the linear mapping $\mathrm{ad}(\Theta)(X_\alpha) := [\Theta, X_\alpha] = \alpha(\Theta)X_\alpha$, defined on a certain super-Lie algebra [11]. The eigenvectors X_α of the mapping are the *root vectors*, which do not depend on Θ. The radial integration measure $J(\hat{\theta})$ in Eq. (5.1.10) can be expressed as [30]

$$J(\hat{\theta}) = \prod_{\alpha > 0} \sinh^{m_\alpha}[\tfrac{1}{2}\alpha(\Theta)], \tag{D.3}$$

where the integer m_α is the multiplicity of the root α (the dimension of the root space). Both positive and negative values of m_α can occur. The factor $\frac{1}{2}$ is due to the difference between the normalization (5.1.1) of Θ and the one used in Ref. 11. In appendix A of Ref. 11, explicit formulas for the roots as well as for the root vectors are given for the case $\beta = 1$, $p = 1$.

We have calculated the roots and the root vectors for all β and arbitrary dimension $8p$ of the Q matrices. For simplicity, we only present the results for the roots and their multiplicities. Let us denote with p_x (p_y) the number of independent x_i (y_i) parameters, i.e.: $p_x = 2p$, p, p and $p_y = p$, p, $2p$ for $\beta = 1, 2, 4$, respectively. Note that $\beta p_x = 2p_y$. We find 8 different types of (positive) roots:

$$\begin{aligned} &\alpha(\Theta) = x_j - x_l && (1 \leq j < l \leq p_x), && m_\alpha = \beta, \\ &\alpha(\Theta) = x_j - iy_l && (1 \leq j \leq p_x,\ 1 \leq l \leq p_y), && m_\alpha = -2, \\ &\alpha(\Theta) = i(y_j - y_l) && (1 \leq j < l \leq p_y), && m_\alpha = 4/\beta, \\ &\alpha(\Theta) = 2x_j && (1 \leq j \leq p_x), && m_\alpha = \beta - 1, \\ &\alpha(\Theta) = 2iy_j && (1 \leq j \leq p_y), && m_\alpha = 4/\beta - 1, \\ &\alpha(\Theta) = x_j + x_l && (1 \leq j < l \leq p_x), && m_\alpha = \beta, \\ &\alpha(\Theta) = x_j + iy_l && (1 \leq j \leq p_x,\ 1 \leq l \leq p_y), && m_\alpha = -2, \\ &\alpha(\Theta) = i(y_j + y_l) && (1 \leq j < l \leq p_y), && m_\alpha = 4/\beta. \end{aligned} \tag{D.4}$$

The radial part of the Laplacian takes the form

$$\Delta_{\hat\theta} = \sum_{j=1}^{p_x} J^{-1}(\hat\theta)\,\frac{\partial}{\partial x_j}\,J(\hat\theta)\,\frac{\partial}{\partial x_j} + \frac{\beta}{2}\sum_{j=1}^{p_y} J^{-1}(\hat\theta)\,\frac{\partial}{\partial y_j}\,J(\hat\theta)\,\frac{\partial}{\partial y_j}. \tag{D.5}$$

The expressions (5.1.6) and (5.1.19) for the generating function now remain valid with the modified $\hat\theta$ of Eq. (D.1), and with Eq. (5.1.7) replaced by

$$f(\hat\theta,\lambda) = \prod_{i=1}^{p_y}[1+2\lambda+\cos(y_i)]\prod_{i=1}^{p_x}[1+2\lambda+\cosh(x_i)]^{-\beta/2}. \tag{D.6}$$

It is convenient to use the variables $u_i = \sinh^2(\frac{1}{2}x_i)$ and $v_i = -\sin^2(\frac{1}{2}y_i)$ in terms of which the Laplacian has the form

$$\Delta_{\hat\theta} = \sum_{j=1}^{p_x}\tilde J^{-1}\,\frac{\partial}{\partial u_j}\,u_j(1+u_j)\,\tilde J\,\frac{\partial}{\partial u_j} - \frac{\beta}{2}\sum_{j=1}^{p_y}\tilde J^{-1}\,\frac{\partial}{\partial v_j}\,v_j(1+v_j)\,\tilde J\,\frac{\partial}{\partial v_j}, \tag{D.7}$$

$$\begin{aligned}\tilde J \;=\; & \prod_{1\le i<j\le p_x}(u_i-u_j)^{\beta}\prod_{1\le i<j\le p_y}(v_i-v_j)^{4/\beta}\prod_{i=1}^{p_x}\prod_{j=1}^{p_y}(u_i-v_j)^{-2} \\ & \times\prod_{i=1}^{p_x}\Big(u_i(1+u_i)\Big)^{\beta/2-1}\prod_{i=1}^{p_y}\Big(v_i(1+v_i)\Big)^{2/\beta-1}.\end{aligned} \tag{D.8}$$

The generating function $F(\hat\theta,\hat\lambda)$ is given by

$$F(\hat\theta,\hat\lambda) = \prod_{n=1}^{N}\left(\prod_{i=1}^{p_y}(1+\lambda_n+v_i)\prod_{i=1}^{p_x}(1+\lambda_n+u_i)^{-\beta/2}\right). \tag{D.9}$$

We have verified that the identity of Laplacians [Eq. 5.1.14)] remains true for the modified expressions (D.7) and (D.9). The calculations goes in a similar way as shown in App. C for $p = 1$. Now, we have to keep track of 7 different types of contributions with double and triple sums over functions of λ_n, u_i, v_j.

In App. A we have shown that the average density of transmission eigenvalues $\rho(T)$ can be obtained from the generating function (5.1.6). Using the corresponding function for the higher-dimensional σ model considered here, it is straightforward to get the p-point correlation functions $\rho_p(T_1,\ldots,T_p)$.

References

[1] O. N. Dorokhov, Pis'ma Zh. Eksp. Teor. Fiz. **36**, 259 (1982) [JETP Lett. **36**, 318 (1982)].

[2] P. A. Mello, P. Pereyra, and N. Kumar, Ann. Phys. (NY) **181**, 290 (1988).

[3] P. A. Mello, Phys. Rev. Lett. **60**, 1089 (1988).

[4] P. A. Mello and A. D. Stone, Phys. Rev. B **44**, 3559 (1991).

[5] A. M. S. Macêdo and J. T. Chalker, Phys. Rev. B **46**, 14985 (1992).

[6] K. B. Efetov and A. I. Larkin, Zh. Eksp. Theor. Fiz. **85**, 764 (1983) [Sov. Phys. JETP **58**, 444 (1983)].

[7] K. B. Efetov, Adv. in Phys. **32**, 53 (1983).

[8] J. J. M. Verbaarschot, H. A. Weidenmüller, and M. R. Zirnbauer, Phys. Rep. **129**, 367 (1985).

[9] S. Iida, H. A. Weidenmüller, and J. A. Zuk, Ann. Phys. (NY) **200**, 219 (1990).

[10] M. R. Zirnbauer, Phys. Rev. Lett. **69**, 1584 (1992).

[11] A. D. Mirlin, A. Müller-Groeling, and M. R. Zirnbauer, Ann. Phys. (NY) **236**, 325 (1994).

[12] C. W. J. Beenakker and B. Rejaei, Phys. Rev. Lett. **71**, 3689 (1993); Phys. Rev. B **49**, 7499 (1994).

[13] K. Frahm, Phys. Rev. Lett. **74**, 4706 (1995); K. Frahm and J.-L. Pichard, J. Phys. I France **5**, 877 (1995).

[14] M. Caselle, Phys. Rev. Lett. **74**, 2776 (1995).

[15] B. Rejaei, Phys. Rev. B, to be published.

[16] A. Altland, Z. Phys. B **82**, 105 (1991).

[17] P. W. Anderson, E. Abrahams, and T. V. Ramakrishnan, Phys. Rev. Lett. **43**, 718 (1979).

[18] L. P. Gor'kov, A. I. Larkin, and D. E. Khmel'nitskiĭ, Pis'ma Zh. Eksp. Teor. Fiz. **30**, 248 (1979) [JETP Lett. **30**, 228 (1979)].

[19] B. L. Al'tshuler, Pis'ma Zh. Eksp. Teor. Fiz. **41**, 530 (1985) [JETP Lett. **41**, 648 (1985)].

[20] P. A. Lee and A. D. Stone, Phys. Rev. Lett. **55**, 1622 (1985); P. A. Lee, A. D. Stone and H. Fukuyama, Phys. Rev. B **35**, 1039 (1987).

[21] A. D. Mirlin and A. Müller-Groeling, unpublished calculations.

[22] P. A. Mello and B. Shapiro, Phys. Rev. B **37**, 5860 (1988).

[23] P. A. Mello and S. Tomsovic, Phys. Rev. Lett. **67**, 342 (1991); Phys. Rev. B **46**, 15963 (1992).

[24] A. Hüffmann, J. Phys. A **23**, 5733 (1990).

[25] F. J. Wegner, Phys. Rev. B **19**, 783 (1979).

[26] Y. V. Fyodorov and A. D. Mirlin, Phys. Rev. Lett. **67**, 2405 (1991).

[27] Yu. V. Nazarov, Phys. Rev. Lett. **73**, 134 (1994).

[28] A. D. Stone, P. A. Mello, K. A. Muttalib, and J.-L. Pichard in *Mesoscopic Phenomena in Solids*, edited by B. L. Altshuler, P. A. Lee, and R. A. Webb (North Holland, Amsterdam, 1991).

[29] R. Landauer, Phil. Mag. **21**, 863 (1970).

[30] S. Helgason, *Groups and Geometric Analysis* (Academic, Orlando, 1984).

6 Diagrammatic technique for integration over the unitary group

The random-matrix theory of quantum transport describes the statistics of transport properties of phase-coherent (mesoscopic) systems in terms of the statistics of random matrices (for reviews, see Refs. [1–4]). There exist two separate (but equivalent) approaches: Either the random matrix is used to model the Hamiltonian of the closed system, or it is used to model the scattering matrix of the open system. The second approach is more direct than the first, because the scattering matrix directly determines the conductance through the Landauer formula,

$$G = \frac{2e^2}{h} \mathrm{tr}\, tt^\dagger. \tag{6.0.1}$$

(The transmission matrix t is a submatrix of the scattering matrix.)

Random-matrix theory has been applied successfully to two types of mesoscopic systems: chaotic cavities and disordered wires. Baranger and Mello [5] and Jalabert, Pichard, and Beenakker [6] studied conduction through a chaotic cavity on the assumption that the scattering matrix S is uniformly distributed in the unitary group, restricted only by symmetry. This is the circular ensemble, introduced by Dyson [7], and shown to apply to a chaotic cavity by Blümel and Smilansky [8]. The symmetry restriction is that $SS^* = 1$ in the presence of time-reversal symmetry. (The superscript $*$ indicates complex conjugation if the elements of S are complex numbers; in the presence of spin-orbit scattering, S is a matrix of quaternions, and S^* denotes the quaternion complex conjugate.) For the disordered wire, the circular ensemble applies not to the scattering matrix itself, but to the unitary matrices v, w, v', and w' in the polar decomposition,

$$S = \begin{pmatrix} v & 0 \\ 0 & w \end{pmatrix} \begin{pmatrix} \sqrt{1-T} & i\sqrt{T} \\ i\sqrt{T} & \sqrt{1-T} \end{pmatrix} \begin{pmatrix} v' & 0 \\ 0 & w' \end{pmatrix}. \tag{6.0.2}$$

The matrix T is a diagonal matrix containing the transmission eigenvalues $T_n \in [0,1]$ on the diagonal. (The T_n's are the eigenvalues of the matrix product $tt^\dagger$.) The distribution of the transmission eigenvalues is governed by a Fokker-Planck equation, the Dorokhov-Mello-Pereyra-Kumar (DMPK) equation [9, 10]. The isotropy assumption [10] states that v, v', w, and w' are uniformly and independently distributed in the unitary group, with the restriction $v^*v' = 1$, $w^*w' = 1$ in the presence of time-reversal symmetry.

The role of the circular ensemble of unitary matrices in the scattering matrix approach is comparable to the role of the Gaussian ensemble of Hermitian matrices in the Hamiltonian approach. However, whereas many computational techniques have been developed for averaging over the Gaussian ensemble [11–18], the circular ensemble has received less attention. If the dimension N of the unitary matrices is small, the average over the circular ensemble can be done exactly, see e.g. Secs. 2.1 and 3.1 or Ref. [19]. For some applications

in the regime of large N, one may regard the elements of the unitary matrix as independent Gaussian variables [20], and then use the known diagrammatic perturbation theory for the Gaussian ensemble [12, 17]. In other applications the Gaussian approximation breaks down.

In this chapter we present a diagrammatic technique for integration over the unitary group, which is not restricted to the Gaussian approximation. We discuss two applications: A chaotic cavity coupled to the outside via a tunnel barrier, and a disordered wire attached to a superconductor. In both cases, we calculate the mean and variance of the conductance up to and including terms of order 1. We point out the analogy between the diagrams contributing to the average over the circular ensemble and the diffuson and cooperon diagrams which appear in the theory of weak localization [33, 34] and universal conductance fluctuations [23, 24] in disordered metals. In the presence of the superconductor a third type of diagrams shows up, which gives rise to the coexistence of weak localization with a magnetic field (see also Sec. 7.2 and Ref. [25]), and to anomalous conductance fluctuations (see also Sec. 7.1.

This chapter starts in Sec. 6.1 with a summary of known results [26–28] for the integration over the unitary group of a polynomial function of matrix elements. The diagrammatic technique is explained in Sec. 6.2. Generalizations to unitary symmetric matrices and to unitary quaternion matrices are given in Secs. 6.3 and 6.4, respectively. We then apply the technique to the chaotic cavity (Sec. 6.5) and the normal-metal–superconductor junction (Sec. 6.6). Some of the results of Sec. 6.5 have been obtained previously by Iida, Weidenmüller, and Zuk, who used the Hamiltonian approach to quantum transport and the supersymmetry technique [1, 15]. The results of Sec. 6.6 have some overlap with Secs. 7.1 and 7.2. There is also some overlap between Sec. 6.6 and a recent work by Argaman and Zee [29].

6.1 Integration of polynomials of unitary matrices

In this section we summarize known results [26–28] for the integration of a polynomial function $f(U)$ of the matrix elements of an $N \times N$ unitary matrix U over the unitary group $\mathcal{U}(N)$. We refer to the integration as an "average", which we denote by brackets $\langle \cdots \rangle$,

$$\langle f \rangle \equiv \int dU \; f(U). \tag{6.1.1}$$

Here dU is the invariant measure (Haar measure) on $\mathcal{U}(N)$, normalized to unity ($\int dU = 1$). The ensemble of unitary matrices that corresponds to this average is known as the circular unitary ensemble (CUE) [7, 30].

We consider a polynomial function $f(U) = U_{a_1 b_1} \ldots U_{a_n b_n} U^*_{\alpha_1 \beta_1} \ldots U^*_{\alpha_m \beta_m}$. The average $\langle f(U) \rangle$ is zero unless $n = m$, $\alpha_1, \ldots, \alpha_n$ is a permutation P of $a_1, \ldots, a_n$, and $\beta_1, \ldots, \beta_n$ is a permutation P' of $b_1, \ldots, b_n$. The general structure of the average is

$$\left\langle U_{a_1 b_1} \ldots U_{a_m b_m} U^*_{\alpha_1 \beta_1} \ldots U^*_{\alpha_n \beta_n} \right\rangle = \delta_{nm} \sum_{P, P'} V_{P, P'} \prod_{j=1}^{n} \delta_{a_j \alpha_{P(j)}} \delta_{b_j \beta_{P'(j)}}, \tag{6.1.2}$$

where the summation is over all permutations P and P' of the numbers $1, \ldots, n$. The coefficients $V_{P,P'}$ depend only on the *cycle structure* of the permutation $P^{-1}P'$ [27]. Recall that each permutation of $1, \ldots, n$ has a unique factorization in disjoint cyclic permutations ("cycles") of lengths $c_1, \ldots, c_k$ (where $n = \sum_{j=1}^{k} c_k$). The statement that $V_{P,P'}$ depends only on the cycle structure of $P^{-1}P'$ means that $V_{P,P'}$ depends only on the lengths $c_1, \ldots, c_k$ of the cycles in the factorization of $P^{-1}P'$. One may therefore write $V_{c_1,\ldots,c_k}$ instead of $V_{P,P'}$.

As an example, we consider the case $n = m = 2$ explicitly. The summation over the permutations P and P' extends over the identity permutation $id = [(1,2) \to (1,2)]$ and the exchange permutation $ex = [(1,2) \to (2,1)]$. Hence Eq. (6.1.2) reads

$$\begin{aligned}\left\langle U_{a_1b_1} U_{a_2b_2} U^*_{\alpha_1\beta_1} U^*_{\alpha_2\beta_2} \right\rangle &= V_{id,id}\, \delta_{a_1\alpha_1}\delta_{b_1\beta_1}\delta_{a_2\alpha_2}\delta_{b_2\beta_2} + V_{ex,id}\, \delta_{a_1\alpha_2}\delta_{b_1\beta_1}\delta_{a_2\alpha_1}\delta_{b_2\beta_2} \\ &\quad + V_{id,ex}\, \delta_{a_1\alpha_1}\delta_{b_1\beta_2}\delta_{a_2\alpha_2}\delta_{b_2\beta_1} + V_{ex,ex}\, \delta_{a_1\alpha_2}\delta_{b_1\beta_2}\delta_{a_2\alpha_1}\delta_{b_2\beta_1}. \end{aligned} \tag{6.1.3}$$

The permutation $P^{-1}P'$ that corresponds to $P = P' = id$ [the first term on the r.h.s. of Eq. (6.1.3)] is again the identity permutation: $P^{-1}P' = id = [(1,2) \to (1,2)]$. Its factorization in cyclic permutations is $id = (1 \to 1)(2 \to 2)$, so that $P^{-1}P'$ factorizes in two cyclic permutations of unit length. Hence the cycle structure of $P^{-1}P'$ is $\{1,1\}$, and $V_{id,id} = V_{1,1}$. The second term on the r.h.s. of Eq. (6.1.3), corresponding to $P = ex$, $P' = id$, has $P^{-1}P' = ex = [(1,2) \to (2,1)]$, which factorizes in a single cyclic permutation of length two, $ex = (1 \to 2 \to 1)$. Hence the cycle structure of $P^{-1}P'$ is $\{2\}$, and $V_{ex,id} = V_2$. Treating the remaining two terms of Eq. (6.1.3) similarly, we obtain

$$\begin{aligned}\left\langle U_{a_1b_1} U_{a_2b_2} U^*_{\alpha_1\beta_1} U^*_{\alpha_2\beta_2} \right\rangle &= V_{1,1}\, \delta_{a_1\alpha_1}\delta_{b_1\beta_1}\delta_{a_2\alpha_2}\delta_{b_2\beta_2} + V_2\, \delta_{a_1\alpha_2}\delta_{b_1\beta_1}\delta_{a_2\alpha_1}\delta_{b_2\beta_2} \\ &\quad + V_2\, \delta_{a_1\alpha_1}\delta_{b_1\beta_2}\delta_{a_2\alpha_2}\delta_{b_2\beta_1} + V_{1,1}\, \delta_{a_1\alpha_2}\delta_{b_1\beta_2}\delta_{a_2\alpha_1}\delta_{b_2\beta_1}. \end{aligned}$$

In general, the coefficient $V_{1,\ldots,1}$ refers to equal permutations $P = P'$, corresponding to a pairwise (Gaussian) contraction of the matrices U and U^*. Coefficients $V_{c_1,\ldots,c_k}$ with some $c_j \neq 1$ give non-Gaussian contributions.

The coefficients V are determined by the recursion relation [27]

$$N V_{c_1,\ldots,c_k} + \sum_{p+q=c_1} V_{p,q,c_2,\ldots,c_k} + \sum_{j=2}^{k} c_j\, V_{c_1+c_j,c_2,\ldots,c_{j-1},c_{j+1},\ldots,c_k} = \delta_{c_1 1} V_{c_2,\ldots,c_k}, \tag{6.1.4}$$

with $V_0 \equiv 1$. One can show that the solution $V_{c_1,\ldots,c_k}$ does not depend on the order of the indices $c_1, \ldots, c_k$. Results for V up to $n = 5$ are given in App. A. The large-N expansion of V is

$$V_{c_1,\ldots,c_k} = \prod_{j=1}^{k} V_{c_j} + \mathcal{O}(N^{k-2n-2}), \tag{6.1.5}$$

$$V_c = \frac{1}{c} N^{1-2c} (-1)^{c-1} \binom{2c-2}{c-1} + \mathcal{O}(N^{-1-2c}). \tag{6.1.6}$$

(The numbers $c^{-1}\binom{2c-2}{c-1}$ are the Catalan numbers.) For example, the coefficient $V_{1,\ldots,1} = N^{-n} + \mathcal{O}(N^{-n-2})$. The Gaussian approximation amounts to setting all V's equal to zero except $V_{1,\ldots,1}$, which is set to N^{-n}.

The coefficients $V_{c_1,\ldots,c_k}$ determine moments of U. Similarly, the coefficients $W_{c_1,\ldots,c_k}$ determine cumulants of U. The cumulants are obtained from the moments by subsequent subtraction of all possible factorizations in cumulants of lower degree. For example,

$$\begin{aligned} W_{c_1} &= V_{c_1}, \\ W_{c_1,c_2} &= V_{c_1,c_2} - W_{c_1} W_{c_2}, \\ W_{c_1,c_2,c_3} &= V_{c_1,c_2,c_3} - W_{c_1} W_{c_2,c_3} - W_{c_2} W_{c_1,c_3} - W_{c_3} W_{c_1,c_2} - W_{c_1} W_{c_2} W_{c_3}. \end{aligned}$$

The recursion relation (6.1.4) for V implies a recursion relation for W,

$$\begin{aligned} N W_{c_1,\ldots,c_k} + \sum_{p+q=c_1} W_{p,q,c_2,\ldots,c_k} + \sum_{j=2}^{k} c_j \, W_{c_1+c_j,c_2,\ldots,c_{j-1},c_{j+1},\ldots,c_k} \\ + \sum_{p+q=c_1} \sum_{l=1}^{k} \frac{1}{(l-1)!(k-l)!} \sum_{P} W_{p,c_{P(2)},\ldots,c_{P(l)}} W_{q,c_{P(l+1)},c_{P(k)}} &= 0, \end{aligned} \tag{6.1.7}$$

with $W_0 \equiv 1$ and P a permutation of $2, \ldots, k$. To leading order in $1/N$ this equation has the solution,

$$W_{c_1,\ldots,c_k} = 2^k N^{-2n-k+2} (-1)^{n+k} \frac{(2n+k-3)!}{(2n)!} \prod_{j=1}^{k} \frac{(2c_j-1)!}{(c_j-1)!^2} + \mathcal{O}(N^{-2n-k}). \tag{6.1.8}$$

Notice that $W_{c_1,\ldots,c_k}$ decreases with increasing number of cycles k, opposite to the behavior of $V_{c_1,\ldots,c_k}$.

In principle, the recursion relations permit an exact evaluation of the average of any polynomial function of U. In practice, as the number of U's and U^*'s increases, keeping track of the indices and of the Kronecker delta's which connect them becomes more and more cumbersome. It is by the introduction of a diagrammatic technique that one can carry out this bookkeeping problem in a controlled and systematic way.

6.2 Diagrammatic technique

The usefulness of diagrams for the bookkeeping problem is well-established for averages over the Gaussian ensemble of Hermitian matrices [12]. Brézin and Zee [17] have developed a diagrammatic method which can be applied to non-Gaussian ensembles as well, as a perturbation expansion in a small parameter multiplying the non-Gaussian terms in the distribution. No such small parameter exists for the circular ensemble. The method presented here deals with non-Gaussian contributions to all orders. Creutz [26] has given a diagrammatic algorithm for integrals over SU(N). Because of the more complicated structure of SU(N), we could not effectively apply his method to integrals over $\mathcal{U}(N)$ in the case of a large number of U's.

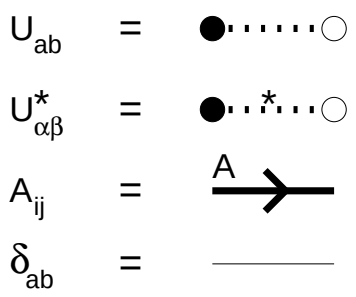

Figure 6-1. Substitution rules for the unitary matrices U and U^*, the fixed matrix A and the Kronecker delta.

The diagrams consist of the building blocks shown in Fig. 6-1. We represent matrix elements U_{ab} or $U^*_{\alpha\beta}$ by thick dotted lines. The first index (a or α) is a black dot, the second index (b or β) a white dot. A fixed matrix A_{ij} is represented by a directed thick solid line, pointed from the first to the second index. Summation over an index is indicated by attachment of the solid line to a dot. As an example, the functions $f(U) = \mathrm{tr}\, AUBU^\dagger$ and $g(U) = \mathrm{tr}\, AUBUCU^\dagger DU^\dagger$ are represented in Fig. 6-2.

The average over the matrix U consists of summing over all permutations P and P' in Eq. (6.1.2). Permutations are generated by drawing thin lines (representing Kronecker deltas) between all black dots attached to U and black dots attached to U^* (one line per dot). Black dots connect to black dots and white dots to white dots. To find the contribution of the permutations P and P' to $\langle f(U)\rangle$, we need (i) to determine the cycle structure of the permutation $P^{-1}P'$, and (ii) to sum over the indices of the fixed matrices A.

(i) The cycle structure can be read off from the diagrams. A cycle of the permutation $P^{-1}P'$ gives rise to a closed circuit in the diagram consisting of alternating dotted and thin lines. The length c_k of the cycle is half the number of dotted lines contained in the circuit. We call such circuits U-cycles of length c_k.

(ii) The trace over the elements of A is done by inspection of the closed circuits in the diagram which consist of alternating thick and thin lines. We call such circuits T-cycles. A T-cycle containing the matrices $A^{(1)}$, $A^{(2)}$, ..., $A^{(k)}$ (in this order) gives rise to $\mathrm{tr}\, A^{(1)}A^{(2)}\ldots A^{(k)}$. If the thick line corresponding to a matrix A is traversed opposite to its direction, the matrix should be replaced by its transpose A^{T}.

As an example, let us consider the average of the functions $f(U) = \mathrm{tr}\, AUBU^\dagger$ and $g(U) = \mathrm{tr}\, AUBUCU^\dagger DU^\dagger$. Connecting the dots by thin lines, we arrive at the diagrams of Fig. 6-3. For f, there is only one diagram. It contains a single U-cycle of length 1 (weight V_1) and two T-cycles (which generate $\mathrm{tr}\, A$ and $\mathrm{tr}\, B$). We look up the value of $V_1 = 1/N$ in App. A, and find

$$\langle f(U)\rangle = V_1 \mathrm{tr}\, A\, \mathrm{tr}\, B = N^{-1}\mathrm{tr}\, A\, \mathrm{tr}\, B, \tag{6.2.1}$$

Four diagrams contribute to g. The first diagram contains two U-cycles of length 1, and three T-cycles. Its contribution is $V_{1,1}\,\mathrm{tr}\, A\,\mathrm{tr}\, BD\,\mathrm{tr}\, C$. The second diagram contains two U-cycles of length 1 and a single T-cycle. Its contribution is $V_{1,1}\mathrm{tr}\, ADCB$. The third

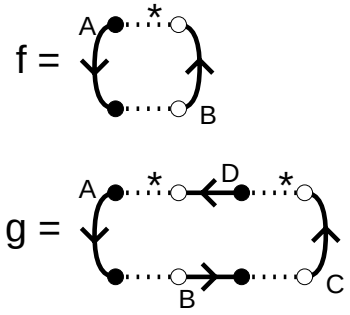

Figure 6-2. Diagrammatic representation of the functions $f(U) = \mathrm{tr}\, AUBU^\dagger$ and $g(U) = \mathrm{tr}\, AUBUCU^\dagger DU^\dagger$.

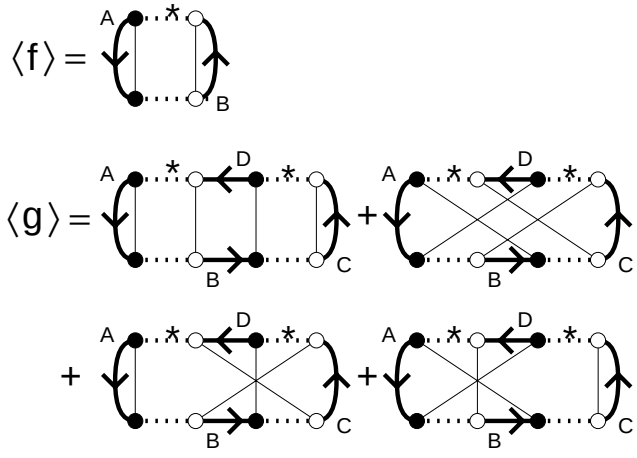

Figure 6-3. Diagrammatic representation of the averages of the functions f and g in Fig. 6-2.

and fourth diagram each contain a single U-cycle of length 2 and two T-cycles. Their contributions are $V_2\,\mathrm{tr}\,A\,\mathrm{tr}\,BDC$ and $V_2\,\mathrm{tr}\,ADB\,\mathrm{tr}\,C$. In total we find

$$\begin{aligned}\langle g(U)\rangle &= V_{1,1}(\mathrm{tr}\,A\,\mathrm{tr}\,BD\,\mathrm{tr}\,C + \mathrm{tr}\,ADCB) + V_2(\mathrm{tr}\,A\,\mathrm{tr}\,BDC + \mathrm{tr}\,ADB\,\mathrm{tr}\,C)\\ &= (N^2-1)^{-1}(\mathrm{tr}\,A\,\mathrm{tr}\,BD\,\mathrm{tr}\,C + \mathrm{tr}\,ADCB)\\ &\quad -[N(N^2-1)]^{-1}(\mathrm{tr}\,A\,\mathrm{tr}\,BDC + \mathrm{tr}\,ADB\,\mathrm{tr}\,C)\,. \qquad (6.2.2)\end{aligned}$$

Whereas each individual T-cycle gives rise to a trace of matrices, it is only the combination of *all* U-cycles together that determines the coefficient $V_{c_1,\ldots,c_k}$. The evaluation of a diagram would be more efficient, if we could attribute a weight to an *individual* U-cycle. We introduced the cumulant expansion of the coefficients V in the coefficients W for this purpose. The leading term $V_{c_1,\ldots,c_k} = \prod_{p=1}^k W_{c_p}$ of the cumulant expansion attributes a weight W_{c_p} to each individual U-cycle of length c_p. This is sufficient for the calculation of the large-N limit of the average $\langle f\rangle$. The next term $\sum_{i<j}^k W_{c_i,c_j}\prod_{p\neq i,j}^k W_{c_p}$ attributes a weight W_{c_i,c_j} to the pair (i,j) of U-cycles, and the weight W_{c_p} to all others individually. This is sufficient for the variance of f. The general rule is that the jth order cumulant

of f in the large-N limit requires the jth order term in the cumulant expansion of the coefficients V, and hence requires consideration of groups of j U-cycles.

Let us summarize the diagrammatic rules:

1. Draw the diagrams according to the substitution rules of Fig. 6-1.

2. Draw thin lines to pair black dots attached to U to black dots attached to U^*. Do the same for the white dots.

3. Every closed circuit of alternating thick solid lines and thin solid lines (a T-cycle) corresponds to a trace of the matrices A appearing in the circuit. If a thick line is traversed opposite to its direction, the transpose of the matrix appears in the trace.

4. Every closed circuit of alternating dotted and thin solid lines (a U-cycle) corresponds to a cycle of length c_k equal to half the number of dotted lines. The set of U-cycles in a diagram defines the coefficient $V_{c_1,\ldots,c_k}$, which is the weight of the diagram. The coefficient V can be factorized into cumulants. To determine the cumulant coefficients W, partition the U-cycles into groups. Every group of p U-cycles of lengths $c_1, \ldots, c_p$ contributes a weight $W_{c_1,\ldots,c_p}$.

The diagrammatic rules are exact. In the large-N limit, we may reduce the number of diagrams and partitions that is involved. Let us determine the order in N of a diagram with l T-cycles and k U-cycles of total length n partitioned into g groups. Counting every trace as an order N and using the large-N result (6.1.8) for the coefficients W, we find a contribution of order $N^{2g+l-k-2n}$. Since $g \leq k$ the order is maximal if $g = k$ and the total number of cycles $k + l$ is maximal. Thus, for large N, we may restrict ourselves to diagrams with as many cycles as possible and with a partition of the U-cycles in groups of a single cycle (i.e. we may approximate $V_{c_1,\ldots,c_k} \approx W_{c_1} \ldots W_{c_k}$).

We conclude this section with one more example, which is the calculation of the variance $\mathrm{var}\, f = \langle f^2 \rangle - \langle f \rangle^2$ of the function $f(U) = \mathrm{tr}\, AUBU^\dagger$. Diagrammatically, we calculate $\langle f^2 \rangle$ as in Fig. 6-4a, resulting in

$$\begin{aligned} \langle f^2 \rangle &= V_{1,1} \left[(\mathrm{tr}\, A)^2 (\mathrm{tr}\, B)^2 + \mathrm{tr}\, A^2\, \mathrm{tr}\, B^2 \right] + W_2 \left[\mathrm{tr}\, A^2 (\mathrm{tr}\, B)^2 + (\mathrm{tr}\, A)^2\, \mathrm{tr}\, B^2 \right], \\ \Longrightarrow \mathrm{var}\, f &= W_{1,1} \left[(\mathrm{tr}\, A)^2 (\mathrm{tr}\, B)^2 + \mathrm{tr}\, A^2\, \mathrm{tr}\, B^2 \right] + W_1^2\, \mathrm{tr}\, A^2\, \mathrm{tr}\, B^2 \\ &\quad + W_2 \left[\mathrm{tr}\, A^2 (\mathrm{tr}\, B)^2 + (\mathrm{tr}\, A)^2\, \mathrm{tr}\, B^2 \right]. \end{aligned}$$

If we now consider the order in N of the various contributions, we see that the leading $\mathcal{O}(N^2)$ term of $\langle f^2 \rangle$ ($l = 4$, $g = k = 2$, corresponding to 6 cycles and a partition of the U-cycles into two groups of a single cycle), is exactly canceled by $\langle f \rangle^2$. This exact cancelation is possible because the leading contribution of $\langle f^2 \rangle$ is *disconnected*: Each T-cycle, and each group of U-cycles belongs entirely to one of the two factors $\mathrm{tr}\, AUBU^\dagger$ of f^2. Only connected diagrams contribute to the variance of f. The connected diagrams are

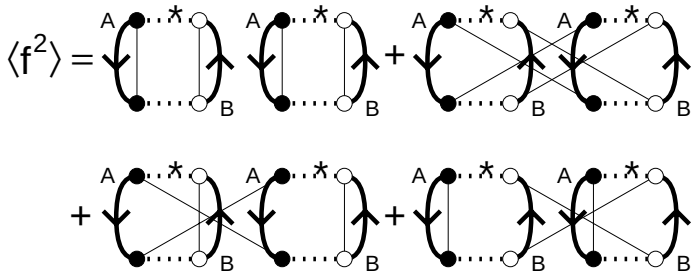

Figure 6-4. Diagrammatic representation of $\langle f^2 \rangle$.

of order 1 ($k + l = 4$ and $g = k$ or $k + l = 6$ and $g = k - 1$). They give the variance

$$\begin{aligned} \text{var } f &= W_{1,1}(\text{tr } A)^2 (\text{tr } B)^2 + W_1^2 \text{tr } A^2 \text{ tr } B^2 \\ &\quad + W_2 \left[\text{tr } A^2 (\text{tr } B)^2 + (\text{tr } A)^2 \text{ tr } B^2 \right] + \mathcal{O}(N^{-1}). \end{aligned} \tag{6.2.3}$$

6.3 Integration of unitary symmetric matrices

In the presence of time-reversal symmetry the scattering matrix S is both unitary and symmetric: $SS^\dagger = 1$, $S = S^{\mathrm{T}}$. The elements of S are complex numbers. (The case of a quaternion S, corresponding to spin-orbit scattering, is treated in the next section.) The ensemble of uniformly distributed unitary symmetric matrices is known as the circular orthogonal ensemble (COE) [7, 30]. Averages of the unitary symmetric matrix U over the COE can be computed in two ways. One way is to substitute $U = VV^{\mathrm{T}}$, with the matrix V uniformly distributed over the unitary group. This has the advantage that one can use the same formulas as for averages over the CUE, but the disadvantage that the number of unitary matrices is doubled. A more efficient way is to use specific formulas for the COE, as we now discuss.

The average of a polynomial in U and U^* over the COE has the general structure

$$\langle U_{a_1 a_2} \dots U_{a_{2n-1} a_{2n}} U^*_{\alpha_1 \alpha_2} \dots U^*_{\alpha_{2m-1} \alpha_{2m}} \rangle = \delta_{nm} \sum_P V_P \prod_{j=1}^{2n} \delta_{a_j \alpha_{P(j)}}. \tag{6.3.1}$$

The summation is over permutations P of the numbers $1, \dots, 2n$. We can decompose P as

$$P = \left(\prod_{j=1}^{n} T_j \right) P_{\mathrm{e}} P_{\mathrm{o}} \left(\prod_{j=1}^{n} T'_j \right), \tag{6.3.2}$$

where T_j and T'_j permute the numbers $2j - 1$ and $2j$, and P_{e} (P_{o}) permutes n even (odd) numbers. Because $U_{ab} = U_{ba}$, the moment coefficient V_P depends only on the cycle structure $\{c_1, \dots, c_k\}$ of $P_{\mathrm{e}}^{-1} P_{\mathrm{o}}$ [31], so that we may write $V_{c_1,\dots,c_k}$ instead of V_P.

The moment coefficients obey the recursion relation

$$(N+c_1)V_{c_1,\ldots,c_k} + \sum_{p+q=c_1} V_{p,q,c_2,\ldots,c_k} + 2\sum_{j=2}^{k} c_j\, V_{c_1+c_j,c_2,\ldots,c_{j-1},c_{j+1},\ldots,c_k} = \delta_{c_1 1} V_{c_2,\ldots,c_k},$$

with $V_0 \equiv 1$. The large-N expansion of V is

$$V_{c_1,\ldots,c_k} = \prod_{j=1}^{k} V_{c_j} + \mathcal{O}(N^{k-2n-2}), \tag{6.3.3}$$

$$V_c = \frac{1}{c} N^{1-2c}(-1)^{c-1}\binom{2c-2}{c-1} - N^{-2c}(-4)^{c-1} + \mathcal{O}(N^{-1-2c}). \tag{6.3.4}$$

Compared with Eq. (6.1.5) an extra term of order N^{-2c} appears in V_c because of the symmetry restriction. The recursion relation for the cumulant coefficients W is

$$(N+c_1)W_{c_1,\ldots,c_k} + \sum_{p+q=c_1} W_{p,q,c_2,\ldots,c_k} + 2\sum_{j=2}^{k} c_j\, W_{c_1+c_j,c_2,\ldots,c_{j-1},c_{j+1},\ldots,c_k} + \\ + \sum_{p+q=c_1}\sum_{l=1}^{k} \frac{1}{(l-1)!(k-l)!}\sum_{P} W_{p,c_{P(2)},\ldots,c_{P(l)}} W_{q,c_{P(l+1)},c_{P(k)}} = 0,$$

with $W_0 \equiv 1$ and P a permutation of the numbers $2,\ldots,k$. The solution for large N is

$$W_{c_1,\ldots,c_k} = 2^{2k-1} N^{-2n-k+2}(-1)^{n+k}\frac{(2n+k-3)!}{(2n)!}\prod_{j=1}^{k}\frac{(2c_j-1)!}{(c_j-1)!^2} + \mathcal{O}(N^{-2n-k+1}). \tag{6.3.5}$$

The coefficients $V_{c_1,\ldots,c_k}$ and $W_{c_1,\ldots,c_k}$ are listed in App. A for $n = c_1 + \ldots + c_k \le 5$.

For the diagrammatic representation, we again use the substitution rules of Fig. 6-1. The symmetry of U is taken into account by allowing thin lines between black and white dots. Therefore, rule 2 is replaced by

2. Pair the dots attached to U to the dots attached to U^* by connecting them with thin lines.

As examples, we compute the averages of $f(U) = \operatorname{tr} AUBU^\dagger$ and $g(U) = \operatorname{tr} AUBUCU^\dagger DU^\dagger$ over the COE. The diagrams for $\langle f(U)\rangle$ are shown in Fig. 6-5, with the result

$$\langle f(U)\rangle = V_1(\operatorname{tr} A \operatorname{tr} B + \operatorname{tr} A^{\mathrm{T}} B) = (N+1)^{-1}(\operatorname{tr} A \operatorname{tr} B + \operatorname{tr} A^{\mathrm{T}} B). \tag{6.3.6}$$

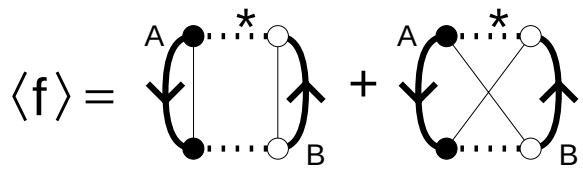

Figure 6-5. Diagrammatic representation of $\langle f(U)\rangle$ for $f(U) = \mathrm{tr}\, AUBU^\dagger$, where U is a unitary symmetric matrix. The second term arises because of the symmetry constraint.

Similarly, we find that

$$\begin{aligned}\langle g(U)\rangle \;=\; & [(N+1)(N+3)]^{-1} \\ & \times (\mathrm{tr}\,A\,\mathrm{tr}\,BD\,\mathrm{tr}\,C \;+\mathrm{tr}\,AD^{\mathrm{T}}B^{\mathrm{T}}\,\mathrm{tr}\,C \;+\mathrm{tr}\,A\,\mathrm{tr}\,BC^{\mathrm{T}}D \;+\mathrm{tr}\,AD^{\mathrm{T}}CB^{\mathrm{T}} \\ & +\mathrm{tr}\,ADCB \;+\mathrm{tr}\,AC^{\mathrm{T}}D^{\mathrm{T}}B + \mathrm{tr}\,ADB^{\mathrm{T}}C^{\mathrm{T}} + \mathrm{tr}\,AC^{\mathrm{T}}\,\mathrm{tr}\,BD^{\mathrm{T}}) \\ & -[(N(N+1)(N+3)]^{-1} \\ & \times (\mathrm{tr}\,A\,\mathrm{tr}\,BDC \;+\mathrm{tr}\,AC^{\mathrm{T}}D^{\mathrm{T}}B^{\mathrm{T}} \;+\mathrm{tr}\,A\,\mathrm{tr}\,BD^{\mathrm{T}}C \;+\mathrm{tr}\,AC^{\mathrm{T}}DB^{\mathrm{T}} \\ & +\mathrm{tr}\,ADB\,\mathrm{tr}\,C + \mathrm{tr}\,AD^{\mathrm{T}}B\,\mathrm{tr}\,C \;+\mathrm{tr}\,ADBC^{\mathrm{T}} + \mathrm{tr}\,AD^{\mathrm{T}}BC^{\mathrm{T}} \\ & +\mathrm{tr}\,AD^{\mathrm{T}}B^{\mathrm{T}}C^{\mathrm{T}} \;+\mathrm{tr}\,AC^{\mathrm{T}}\,\mathrm{tr}\,BD \;+\mathrm{tr}\,AD^{\mathrm{T}}CB \;+\mathrm{tr}\,AC^{\mathrm{T}}DB \\ & +\mathrm{tr}\,A\,\mathrm{tr}\,BC^{\mathrm{T}}D^{\mathrm{T}} \;+\mathrm{tr}\,ADCB^{\mathrm{T}} \;+\mathrm{tr}\,A\,\mathrm{tr}\,BD^{\mathrm{T}}\,\mathrm{tr}\,C \;+\mathrm{tr}\,ADB^{\mathrm{T}}\,\mathrm{tr}\,C).\end{aligned}$$

6.4 Integration of matrices of quaternions

We extend the results of the previous sections for integrals over unitary matrices of complex numbers to integrals over unitary matrices of quaternions. This is relevant to the case that spin-rotation symmetry is broken by spin-orbit scattering.

Let us first recall the definition and basic properties of quaternions [30]. A quaternion q is represented by a 2×2 matrix,

$$q = a_0\mathbb{1} + ia_1\sigma_1 + ia_2\sigma_2 + ia_3\sigma_3, \tag{6.4.1}$$

where $\mathbb{1}$ is the 2×2 unit matrix and σ_i is a Pauli matrix,

$$\sigma_1 = \begin{pmatrix} 0 & 1 \\ 1 & 0 \end{pmatrix}, \quad \sigma_2 = \begin{pmatrix} 0 & -i \\ i & 0 \end{pmatrix}, \quad \sigma_3 = \begin{pmatrix} 1 & 0 \\ 0 & -1 \end{pmatrix}. \tag{6.4.2}$$

The coefficients a_j are complex numbers. The complex conjugate q^* and Hermitian conjugate $q^\dagger$ of a quaternion q are defined as

$$q^* = a_0^*\mathbb{1} + ia_1^*\sigma_1 + ia_2^*\sigma_2 + ia_3^*\sigma_3, \quad q^\dagger = a_0^*\mathbb{1} - ia_1^*\sigma_1 - ia_2^*\sigma_2 - ia_3^*\sigma_3. \tag{6.4.3}$$

The complex conjugate of a quaternion differs from the complex conjugate of a 2×2 matrix, whereas the Hermitian conjugate equals the Hermitian conjugate of a 2×2 matrix.

Let Q be an $N \times N$ matrix of quaternions with elements $Q_{kl} = Q_{kl}^{(0)} \mathbb{1} + i Q_{kl}^{(1)} \sigma_1 + i Q_{kl}^{(2)} \sigma_2 + i Q_{kl}^{(3)} \sigma_3$. The complex conjugate Q^* and Hermitian conjugate $Q^\dagger$ are defined by $(Q^*)_{kl} = Q_{kl}^*$ and $(Q^\dagger)_{kl} = Q_{lk}^\dagger$. The dual matrix Q^{R} is defined by $Q^{\mathrm{R}} = (Q^\dagger)^* = (Q^*)^\dagger$. We call Q unitary if $QQ^\dagger = 1$ and self-dual if $Q = Q^{\mathrm{R}}$. A unitary self-dual matrix is defined by $QQ^\dagger = QQ^* = 1$. The trace $\mathrm{tr}\, Q$ is defined by $\mathrm{tr}\, Q = \sum_j Q_{jj}^{(0)}$, which equals $1/2$ the trace of the $2N \times 2N$ complex matrix corresponding to Q. The scattering matrix in zero magnetic field is a unitary self-dual matrix, because of time-reversal symmetry. The ensemble of quaternion matrices which is uniformly distributed over the unitary group is called the circular unitary ensemble (CUE). If the ensemble is restricted to self-dual matrices it is called the circular symplectic ensemble (CSE) [7, 30].

The integration of a polynomial function $f(U)$ of an $N \times N$ quaternion matrix U over the CUE or CSE can be related to the integration of a function $\hat{f}(U)$ of an $N \times N$ complex matrix U over the CUE or COE. The translation rule is as follows (a similar rule has been formulated for Gaussian ensembles in Refs. [32, 33]):

1. $\hat{f}(U)$ is constructed from $f(U)$ by replacing, respectively, the complex conjugates, Hermitian conjugates, and duals of quaternion matrices by complex conjugates, Hermitian conjugates, and transposes of complex matrices. Furthermore, every trace is replaced by $-\frac{1}{2}\mathrm{tr}$, and numerical factors N are replaced by $-\frac{1}{2}N$.

2. The average $\langle \hat{f}(U) \rangle$ is calculated using the rules for integration of $N \times N$ complex matrices over the CUE or COE.

3. The average $\langle f(U) \rangle$ over the CUE or CSE is found by replacing, respectively, the complex conjugates, Hermitian conjugates, and transposes of complex matrices by the complex conjugates, Hermitian conjugates, and duals of quaternion matrices. Traces are replaced by $-2\,\mathrm{tr}$ and numerical factors N by $-2N$.

As examples, we compute the averages of the functions $f(U) = \mathrm{tr}\, AUBU^\dagger$ and $g(U) = \mathrm{tr} AUBUCU^\dagger DU^\dagger$ of $N \times N$ quaternion matrices over the CUE and CSE. The first step is to construct the functions $\hat{f}(U)$ and $\hat{g}(U)$ of $N \times N$ complex matrices,

$$\hat{f}(U) = -\tfrac{1}{2}\,\mathrm{tr} AUBU^\dagger, \quad \hat{g}(U) = -\tfrac{1}{2}\,\mathrm{tr} AUBUCU^\dagger DU^\dagger. \tag{6.4.4}$$

The second step is to average $\hat{f}$ and $\hat{g}$ over the CUE. The result is in Eqs. (6.2.1) and (6.2.2),

$$\begin{aligned} \langle \hat{f} \rangle_{\mathrm{CUE}} &= -\tfrac{1}{2} N^{-1} \mathrm{tr}\, A\, \mathrm{tr}\, B, & (6.4.5) \\ \langle \hat{g} \rangle_{\mathrm{CUE}} &= -\tfrac{1}{2}(N^2-1)^{-1} (\mathrm{tr}\, A\, \mathrm{tr}\, BD\, \mathrm{tr}\, C + \mathrm{tr}\, ADCB) \\ &\quad + \tfrac{1}{2}[N(N^2-1)]^{-1} (\mathrm{tr}\, A\, \mathrm{tr}\, BDC + \mathrm{tr}\, ADB\, \mathrm{tr}\, C)\,. & (6.4.6) \end{aligned}$$

The third step is to translate back to quaternion matrices,

$$\begin{aligned} \langle f \rangle_{\mathrm{CUE}} &= N^{-1} \mathrm{tr}\, A\, \mathrm{tr}\, B, & (6.4.7) \\ \langle g \rangle_{\mathrm{CUE}} &= (4N^2-1)^{-1} (4\,\mathrm{tr}\, A\, \mathrm{tr}\, BD\, \mathrm{tr}\, C + \mathrm{tr}\, ADCB) \\ &\quad - [N(4N^2-1)]^{-1} (\mathrm{tr}\, A\, \mathrm{tr}\, BDC + \mathrm{tr}\, ADB\, \mathrm{tr}\, C)\,. & (6.4.8) \end{aligned}$$

Figure 6-6. Chaotic cavity (grey) connected to two leads containing tunnel barriers (black).

Similarly, to compute the average of f and g over the CSE we need the average of $\hat{f}$ and $\hat{g}$ over the COE given by Eq. (6.3.6), and then translate back to quaternion matrices. For $\langle f(U)\rangle$ we find

$$\begin{aligned} \langle \hat{f}\rangle_{\rm COE} &= -\tfrac{1}{2}(N+1)^{-1}(\mathrm{tr}\, A\,\mathrm{tr}\, B + \mathrm{tr}\, A^{\rm T}B), \\ \Longrightarrow \langle f\rangle_{\rm CSE} &= (2N-1)^{-1}(2\,\mathrm{tr}\, A\,\mathrm{tr}\, B - \mathrm{tr}\, A^{\rm R}B). \end{aligned} \tag{6.4.9}$$

Similarly, we find for $\langle g(U)\rangle$ the final result

$$\begin{aligned} \langle g\rangle_{\rm CSE} \;=\; & [(2N-1)(2N-3)]^{-1} \\ & \times (4\,\mathrm{tr}\, A\,\mathrm{tr}\, BD\,\mathrm{tr}\, C \;-2\,\mathrm{tr}\, AD^{\rm R}B^{\rm R}\,\mathrm{tr}\, C \;-2\,\mathrm{tr}\, A\,\mathrm{tr}\, BC^{\rm R}D \;+\mathrm{tr}\, AD^{\rm R}CB^{\rm R} \\ & +\mathrm{tr}\, ADCB \;+\mathrm{tr}\, AC^{\rm R}D^{\rm R}B + \mathrm{tr}\, ADB^{\rm R}C^{\rm R} - 2\,\mathrm{tr}\, AC^{\rm R}\,\mathrm{tr}\, BD^{\rm R}) \\ & -[(2N(2N-1)(2N-3)]^{-1} \\ & \times (2\,\mathrm{tr}\, A\,\mathrm{tr}\, BDC \;-\mathrm{tr}\, AC^{\rm R}D^{\rm R}B^{\rm R} \;+2\,\mathrm{tr}\, A\,\mathrm{tr}\, BD^{\rm R}C \;-\mathrm{tr}\, AC^{\rm R}DB^{\rm R} \\ & +2\,\mathrm{tr}\, ADB\,\mathrm{tr}\, C + 2\,\mathrm{tr}\, AD^{\rm R}B\,\mathrm{tr}\, C \;-\mathrm{tr}\, ADBC^{\rm R} - \mathrm{tr}\, AD^{\rm R}BC^{\rm R} \\ & +2\,\mathrm{tr}\, A\,\mathrm{tr}\, BC^{\rm R}D^{\rm R} \;-\mathrm{tr}\, ADCB^{\rm R} \;-4\,\mathrm{tr}\, A\,\mathrm{tr}\, BD^{\rm R}\,\mathrm{tr}\, C \;+2\,\mathrm{tr}\, ADB^{\rm R}\,\mathrm{tr}\, C \\ & -\mathrm{tr}\, AD^{\rm R}B^{\rm R}C^{\rm R} \;+2\,\mathrm{tr}\, AC^{\rm R}\,\mathrm{tr}\, BD \;-\mathrm{tr}\, AD^{\rm R}CB \;-\mathrm{tr}\, AC^{\rm R}DB). \end{aligned}$$

6.5 Application to a chaotic cavity

We consider the system shown in Fig. 6-6, consisting of a chaotic cavity attached to two leads, containing tunnel barriers. The $M \times M$ scattering matrix S is decomposed into $N_i \times N_j$ submatrices s_{ij},

$$S = \begin{pmatrix} s_{11} & s_{12} \\ s_{21} & s_{22} \end{pmatrix}, \tag{6.5.1}$$

which describe scattering from lead j into lead i ($M = N_i + N_j$). The conductance G is given by the Landauer formula,

$$G/G_0 = \mathrm{tr}\, s_{12}s_{12}^\dagger = \mathrm{tr}\, C_1 S C_2 S^\dagger, \quad G_0 = 2e^2/h. \tag{6.5.2}$$

The projection matrices C_1 and $C_2 = 1 - C_1$ are defined by $(C_1)_{ij} = 1$ if $i = j \le N_1$ and 0 otherwise.

In the absence of tunnel barriers in the leads, S is distributed according to the circular ensemble. The symmetry index $\beta \in \{1, 2, 4\}$ distinguishes the COE ($\beta = 1$), CUE ($\beta = 2$), and CSE ($\beta = 4$). Calculation of the average and variance of G is straightforward [5,6],

$$\langle G/G_0 \rangle = \frac{\beta N_1 N_2}{\beta M + 2 - \beta}, \tag{6.5.3}$$

$$\operatorname{var} G/G_0 = \frac{2\beta N_1 N_2 (\beta N_1 + 2 - \beta)(\beta N_2 + 2 - \beta)}{(\beta M + 2 - 2\beta)(\beta M + 2 - \beta)^2 (\beta M + 4 - \beta)}. \tag{6.5.4}$$

In Sec. 2.2, we have shown that in the presence of a tunnel barrier in lead i with reflection matrix r_i, the distribution of S is given by the Poisson kernel [34–36],

$$P(S) \propto \left|\det(1 - \bar{S}^\dagger S)\right|^{-(\beta M + 2 - \beta)}, \quad \bar{S} = \begin{pmatrix} r_1 & 0 \\ 0 & r_2 \end{pmatrix}. \tag{6.5.5}$$

The sub-unitary matrix $\bar{S}$ is the ensemble average of S: $\int dS P(S) S = \bar{S}$. The eigenvalues Γ_j of $1 - \bar{S}\bar{S}^\dagger$ are the transmission eigenvalues of the tunnel barriers. The fluctuating part $\delta S \equiv S - \bar{S}$ of S can be decomposed as

$$\delta S = T'(1 - UR')^{-1} UT, \tag{6.5.6}$$

where T, T', and R' are $M \times M$ matrices such that the $2M \times 2M$ matrix

$$\Sigma = \begin{pmatrix} \bar{S} & T' \\ T & R' \end{pmatrix} \tag{6.5.7}$$

is unitary. The usefulness of the decomposition (6.5.6) is that U is distributed according the circular ensemble (cf. Sec. 2.2) [20,34]. In the presence of time-reversal symmetry, we further have $\bar{S} = \bar{S}^{\mathrm{T}}$, $T' = T^{\mathrm{T}}$, $R' = R'^{\mathrm{T}}$, and $U = U^{\mathrm{T}}$. Physically, U corresponds to the scattering matrix of the cavity without the tunnel barriers in the leads and Σ corresponds to the scattering matrix of the tunnel barriers in the absence of the cavity, cf. Ch. 2.

The decomposition (6.5.6) reduces the problem of averaging S with the Poisson kernel to integrating U over the unitary group. Because the conductance G is a rational function of U, this average can not be done in closed form for all M. For $N_1, N_2 \gg 1$ a perturbative calculation is possible. In this section we will compute the mean and variance of the conductance in the large-N limit, using the diagrammatic technique of the previous sections.

6.5.1 Average conductance

According to the Landauer formula (6.5.2) the average conductance is given by

$$\langle G/G_0 \rangle = \langle \operatorname{tr} C_1 \delta S C_2 \delta S^\dagger \rangle, \tag{6.5.8}$$

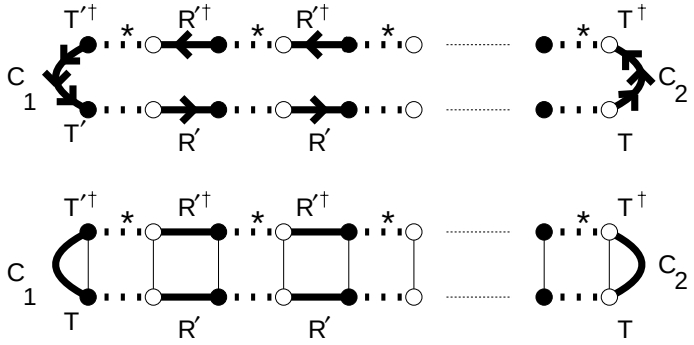

Figure 6-7. Top: Diagrammatic representation of the function $f_n(U)$ in Eq. (6.5.9); Bottom: Ladder diagram with the largest number of cycles, which gives the $\mathcal{O}(N)$ contribution to the average conductance. The arrows are omitted if the direction of the diagram is not ambiguous.

where we have used that $\langle \delta S \rangle = 0$. Expansion of the denominator in the decomposition (6.5.6) of δS yields the series

$$\langle G/G_0 \rangle = \sum_{n=1}^{\infty} \langle f_n(U) \rangle, \tag{6.5.9}$$

$$f_n(U) = \mathrm{tr}\, C_1 T' (U R')^{n-1} U T C_2 T^\dagger U^\dagger (R'^\dagger U^\dagger)^{n-1} T'^\dagger. \tag{6.5.10}$$

The average of the polynomial function $f_n(U)$ can be calculated diagrammatically. We represent $f_n(U)$ by the top diagram in Fig. 6-7. The average over the matrix U is done as follows.

The leading contribution, which is of order M, comes from the diagrams with the largest number of T- and U-cycles. For a polynomial of the type (6.5.8) (all U's are on one side of the $U^\dagger$'s), these diagrams have a "ladder" structure (see bottom diagram in Fig. 6-7). The ladder diagrams contain n U-cycles and $n+1$ T-cycles. Their weight is $W_1^n = M^{-n} + \mathcal{O}(M^{-n-1})$, resulting in

$$\langle f_n(U) \rangle = M^{-n}\, \mathrm{tr}\, T'^\dagger C_1 T'\, (\mathrm{tr}\, R' R'^\dagger)^{n-1}\, \mathrm{tr}\, T C_2 T^\dagger + \mathcal{O}(1). \tag{6.5.11}$$

Summation of the series (6.5.9) yields $\langle G \rangle$ to leading order in M,

$$\begin{aligned} \langle G/G_0 \rangle &= \frac{(\mathrm{tr}\, T'^\dagger C_1 T')(\mathrm{tr}\, T C_2 T^\dagger)}{M - \mathrm{tr}\, R' R'^\dagger} + \mathcal{O}(1) \\ &= \frac{(N_1 - \mathrm{tr}\, \bar{S}^\dagger C_1 \bar{S})(N_2 - \mathrm{tr}\, \bar{S} C_2 \bar{S}^\dagger)}{M - \mathrm{tr}\, \bar{S}\bar{S}^\dagger} + \mathcal{O}(1). \end{aligned} \tag{6.5.12}$$

In the second equality we have used the unitarity of the matrix Σ defined in Eq. (6.5.7).

The weak-localization correction is the $\mathcal{O}(1)$ contribution to $\langle G \rangle$. In general, an $\mathcal{O}(1)$ contribution to the average conductance can have two sources: (i) a higher order contribution to the weight $W_{c_1,\ldots,c_k}$ of the leading-order diagrams, and (ii) higher order diagrams.

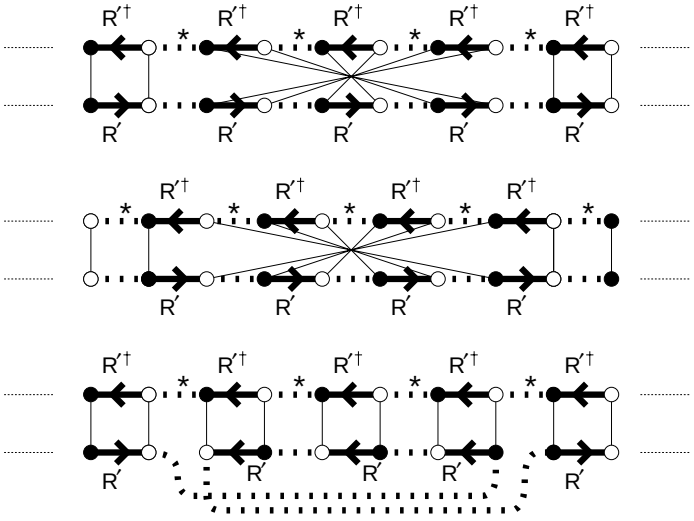

Figure 6-8. Top and middle: Two maximally crossed diagrams contributing to the weak-localization correction to the average conductance. The right and left parts of the diagram have a ladder structure; Bottom: The maximally crossed part of the top diagram redrawn as a ladder diagram.

In the absence of time-reversal symmetry both contributions are absent: (i) $W_1 = M^{-1}$ has no $\mathcal{O}(M^{-2})$ term, and (ii) there are no diagrams of order 1.

The situation is different in the presence of time-reversal symmetry. We discuss the case $\beta = 1$ in which there is no spin-orbit scattering. The case $\beta = 4$ then follows from the translation rule of Sec. 6.4. In the presence of time-reversal symmetry, (i) the coefficient $W_1 = M^{-1} - M^{-2} + \ldots$ has an $\mathcal{O}(M^{-2})$ term, and (ii) there are diagrams of order 1. The first contribution is a correction nM^{-n-1} to the weight M^{-n} in Eq. (6.5.11). Summation over n yields the first correction to Eq. (6.5.12),

$$\delta G_1 \;=\; -\frac{(\mathrm{tr}\, T'^{\dagger} C_1 T')(\mathrm{tr}\, T C_2 T^{\dagger})}{(M - \mathrm{tr}\, R' R'^{\dagger})^2}. \tag{6.5.13}$$

The second contribution is from diagrams which are obtained from the ladder diagrams by reversing the order of the contractions in a part of the diagram. The central part of the diagram is "maximally crossed", the left and right ends are ladders (see Fig. 6-8). In disordered systems, the ladder diagrams are known as diffusons, while the maximally crossed diagrams are known as cooperons. The maximally crossed diagrams are not allowed in the absence of time-reversal symmetry, because dots of different color are connected by thin lines (violating rule 2 in Sec. 6.2). A maximally crossed diagram can be redrawn as a ladder diagram by flipping one of the horizontal lines along a vertical axis (bottom diagram in Fig. 6-8).

In the maximally crossed diagrams all cycles but one have minimum length. The cycle with the exceptional length can be a U-cycle (top diagram in Fig. 6-8), or a T-cycle (middle diagram). To evaluate these diagrams, we need to introduce some more notation (see Fig.

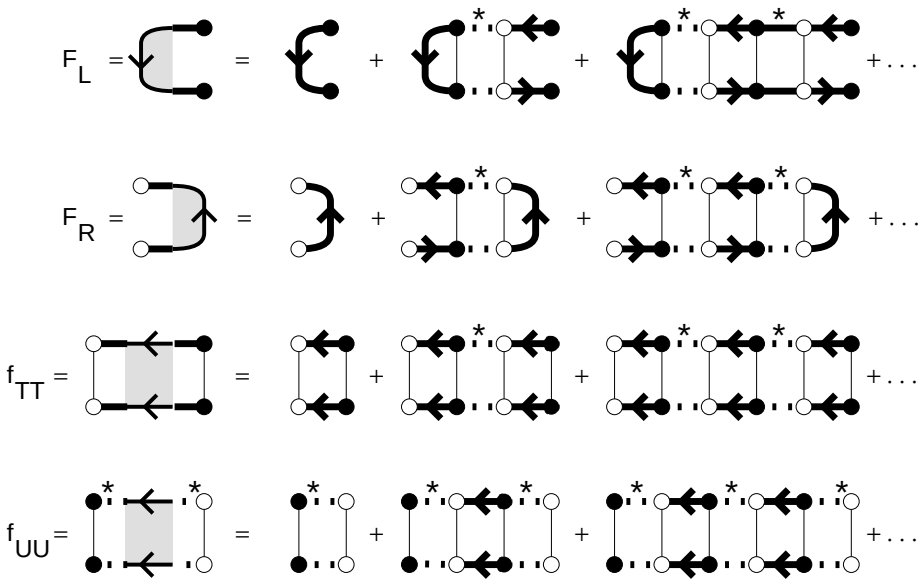

Figure 6-9. Diagrammatic representation of Eqs. (6.5.14) and (6.5.16).

6-9). We denote the left and right ladder diagrams by matrices $F_{\rm L}$ and $F_{\rm R}$,

$$\begin{aligned} F_{\rm L} &= T'^{\dagger} C_1 T' + \sum_{n=1}^{\infty} M^{-n} (\mathrm{tr}\, T'^{\dagger} C_1 T') (\mathrm{tr}\, R'^{\dagger} R')^{n-1} R'^{\dagger} R' \\ &= T'^{\dagger} C_1 T' + \left(\frac{\mathrm{tr}\, T'^{\dagger} C_1 T'}{M - \mathrm{tr}\, R' R'^{\dagger}} \right) R'^{\dagger} R', \end{aligned} \tag{6.5.14}$$

$$\begin{aligned} F_{\rm R} &= T C_2 T^{\dagger} + \sum_{n=1}^{\infty} M^{-n} R' R'^{\dagger} (\mathrm{tr}\, R' R'^{\dagger})^{n-1} (\mathrm{tr}\, T C_2 T^{\dagger}) \\ &= T C_2 T^{\dagger} + R' R'^{\dagger} \left(\frac{\mathrm{tr}\, T C_2 T^{\dagger}}{M - \mathrm{tr}\, R' R'^{\dagger}} \right). \end{aligned} \tag{6.5.15}$$

The scalars f_{UU} and f_{TT} represent the maximally crossed part of the diagram,

$$f_{TT} = \sum_{n=0}^{\infty} M^{-n} (\mathrm{tr}\, R' R'^{\dagger})^{n+1} = \frac{M\, \mathrm{tr}\, R R'^{\dagger}}{M - \mathrm{tr}\, R' R'^{\dagger}}, \tag{6.5.16}$$

$$f_{UU} = \sum_{n=0}^{\infty} M^{-n-1} (\mathrm{tr}\, R' R'^{\dagger})^{n} = \frac{1}{M - \mathrm{tr}\, R' R'^{\dagger}}. \tag{6.5.17}$$

We used the symmetry of R' to replace $R'^{\rm T}$ by R'. With this notation we may draw the contribution δG_2 to the weak-localization correction from the maximally crossed diagrams as in Fig. 6-10. It evaluates to

$$\delta G_2 = -M^{-3}\, \mathrm{tr}\, F_{\rm L}\, f_{TT}\, \mathrm{tr}\, F_{\rm R} + \mathrm{tr}\, F_{\rm L}\, f_{UU} F_{\rm R}^{\rm T}. \tag{6.5.18}$$

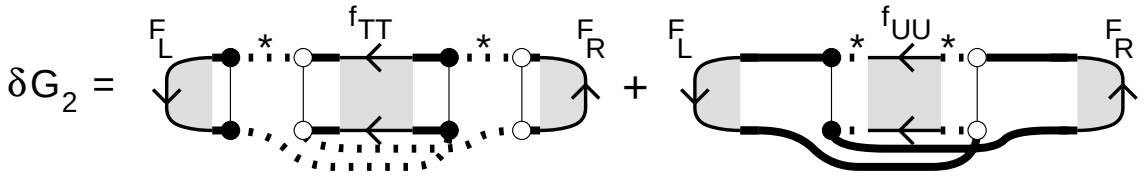

Figure 6-10. Diagrammatic representation of the weak-localization correction δG_2 from the maximally crossed diagrams. The total correction $\delta G = \delta G_1 + \delta G_2$ contains also a contribution δG_1 from the weight factors [Eq. (6.5.13)]

The total weak-localization correction $\delta G = \delta G_1 + \delta G_2$ becomes

$$\delta G = -(\mathrm{tr}\, T^\dagger T)^{-3} \left[(\mathrm{tr}\, C_2 T^\dagger T)^2 \,\mathrm{tr}\, C_1 (T^\dagger T)^2 \; + (\mathrm{tr}\, C_1 T^\dagger T)^2 \,\mathrm{tr}\, C_2 (T^\dagger T)^2 \right]. \quad (6.5.19)$$

Since $T^\dagger T = 1 - \bar{S}^\dagger \bar{S}$ has eigenvalues Γ_n, we may write the final result for the average conductance in the form

$$\langle G/G_0 \rangle = \frac{g_1 g_1'}{g_1 + g_1'} + \left(1 - \frac{2}{\beta}\right) \frac{g_2 g_1'^2 + g_2' g_1^2}{(g_1 + g_1')^3} + \mathcal{O}(M^{-1}), \quad (6.5.20)$$

$$g_p = \sum_{n=1}^{N_1} \Gamma_n^p, \;\; g_p' = \sum_{n=1+N_1}^{M} \Gamma_n^p. \quad (6.5.21)$$

(The $\beta = 4$ result follows from the translation rule of Sec. 6.4.) The first term in Eq. (6.5.20) is the series conductance of the two tunnel conductances $G_0 g_1$ and $G_0 g_1'$. The term proportional to $1 - 2/\beta$ is the weak-localization correction. In the absence of tunnel barriers one has $g_p = N_1$, $g_p' = N_2$, and the large-M limit of Eq. (6.5.3) is recovered. In the case of two identical tunnel barriers ($N_1 = N_2 = M/2 \equiv N$, $\Gamma_n = \Gamma_{n+N}$ for $j = 1, \ldots, N$), Eq. (6.5.20) simplifies to

$$\langle G/G_0 \rangle \;\; = \;\; \frac{1}{2} g_1 + \left(1 - \frac{2}{\beta}\right) \frac{g_2}{4\, g_1} + \mathcal{O}(M^{-1}). \quad (6.5.22)$$

Eq. (6.5.22) was previously obtained by Iida, Weidenmüller and Zuk [15]. If all Γ_n's are equal to Γ, Eq. (6.5.22) simplifies further to $\langle G/G_0 \rangle = \frac{1}{2} N\Gamma + \frac{1}{4}(1 - 2/\beta)\Gamma$.

6.5.2 Conductance fluctuations

We seek the effect of tunnel barriers on the variance of the conductance, $\mathrm{var}\, G = \langle G^2 \rangle - \langle G \rangle^2$. We consider $\beta = 1$ and 2 first, and translate to $\beta = 4$ in the end. Using the decomposition (6.5.6) we write the variance in the form

$$\mathrm{var}\, G/G_0 = \mathrm{var}\, (\mathrm{tr}\, C_1 \delta S C_2 \delta S^\dagger) = \sum_{k,l,m,n \geq 1} \mathrm{covar}\, (f_{kl},\, f_{mn}), \quad (6.5.23)$$

$$f_{kl} = \mathrm{tr}\, C_1 T' (U R')^{k-1} U T C_2 T^\dagger U^\dagger (R'^\dagger U^\dagger)^{l-1} T'^\dagger. \quad (6.5.24)$$

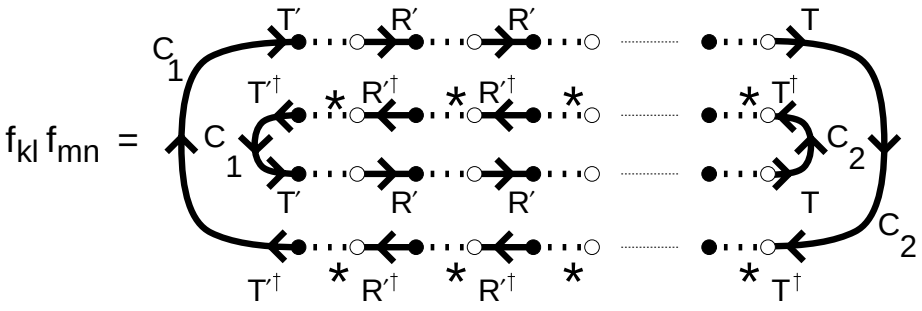

Figure 6-11. Diagrammatic representation of a term contributing to G^2, and hence to the variance (6.5.23) of the conductance.

Since the number U's and U^*'s must be equal for a non-zero average, covar$(f_{kl}, f_{mn}) \equiv \langle f_{kl} f_{mn}\rangle - \langle f_{kl}\rangle\langle f_{mn}\rangle = 0$ unless $k+m = l+n$. Diagrammatically, we represent $f_{kl} f_{mn}$ by Fig. 6-11. The diagram consists of an inner loop, corresponding to f_{kl}, and an outer loop, corresponding to f_{mn}. The covariance of f_{kl} and f_{mn} is given by the connected diagrams. We call a diagram "connected" if (i) the partition of the U-cycles contains a group which consists of U-cycles from the inner and the outer part, or (ii) the diagram contains a cycle (a U-cycle or a T-cycle) connecting the inner and outer loops.

We first compute the contribution from diagrams which are connected only because of (i), i.e. diagrams in which all U-cycles and T-cycles belong either to the inner or outer loop. The contribution from such a diagram is maximal, if the U-cycles are partitioned in groups which are as small as possible. The optimal partition consists of groups of size 1, except for a single group of size 2, which contains one U-cycle from the inner and one from the outer loop. Furthermore, the total number of cycles is maximal if both the inner and outer loops are ladder diagrams. This requires $k = l$ and $m = n$. The covariance from this diagram is

$$\begin{aligned}\text{covariance} \;&=\; km\,\delta_{kl}\delta_{mn} W_{1,1} W_1^{k+m-2} \\ &\quad\times (\mathrm{tr}\, T'^{\dagger} C_1 T')^2\, (\mathrm{tr}\, R' R'^{\dagger})^{k+m-2} (\mathrm{tr}\, T C_2 T^{\dagger})^2 + \mathcal{O}(M^{-1}). \quad (6.5.25)\end{aligned}$$

Summing over k and m we obtain the first contribution to var G/G_0,

$$\text{variance} \;=\; M^{-4}\,(\mathrm{tr}\, F_{\mathrm{L}}\,\mathrm{tr}\, F_{\mathrm{R}})^2. \quad (6.5.26)$$

The second contribution, consisting of diagrams in which the inner and outer loops are connected by T- or U-cycles, is of maximal order if the partition of the U-cycles involves only groups of size 1. For $\beta = 2$ there are 16 connected diagrams of maximal order. They are shown in Fig. 6-12, and their contribution to var G/G_0 is tabulated in Table 6-1. The shaded areas indicate ladder parts of the diagram (see Figs. 6-9 and 6-13). The matrices F_{L} and F_{R}, and the scalars f_{UU} and f_{TT} are defined in Eqs. (6.5.14) and (6.5.16). The definitions of the matrix H and of the scalars f_{UT} and f_{TU} are

$$f_{UT} \;=\; f_{TU} = \sum_{n=1}^{\infty} M^{-n} (\mathrm{tr}\, R' R'^{\dagger})^n = \frac{\mathrm{tr}\, R' R'^{\dagger}}{M - \mathrm{tr}\, R' R'^{\dagger}}, \quad (6.5.27)$$

diagram	$\beta = 1, 2$	$\beta = 1$
a	$W_2^2\,(\mathrm{tr}\,F_\mathrm{L})^2\;f_{TT}^2\,(\mathrm{tr}\,F_\mathrm{R})^2$	$W_2^2\,\mathrm{tr}\,F_\mathrm{R}\,\mathrm{tr}\,R_\mathrm{L}\;f_{TT}^2\,\mathrm{tr}\,F_\mathrm{L}\,\mathrm{tr}\,F_\mathrm{R}$
b	$W_3\,(\mathrm{tr}\,F_\mathrm{L})^2\;f_{TT}\,(\mathrm{tr}\,F_\mathrm{R})^2$	$W_3\,\mathrm{tr}\,F_\mathrm{R}\,\mathrm{tr}F_\mathrm{L}\;f_{TT}\,\mathrm{tr}\,F_\mathrm{L}\,\mathrm{tr}\,F_\mathrm{R}$
c	$W_2\,(\mathrm{tr}\,F_\mathrm{L})^2\;f_{TU}^2\,\mathrm{tr}\,F_\mathrm{R}^2$	$W_2\,\mathrm{tr}\,F_\mathrm{R}\,\mathrm{tr}\,F_\mathrm{L}\;f_{TU}^2\,\mathrm{tr}\,F_\mathrm{L}^\mathrm{T}F_\mathrm{R}$
d	$\mathrm{tr}\,H\,H^\dagger\;f_{UU}$	$\mathrm{tr}\,H^\mathrm{T}H^\dagger\;f_{UU}$
e	$W_2\,\mathrm{tr}\,F_\mathrm{L}^2\;f_{UT}^2\,(\mathrm{tr}\,F_\mathrm{R})^2$	$W_2\,\mathrm{tr}\,F_\mathrm{R}^\mathrm{T}F_\mathrm{L}\,f_{UT}^2\,\mathrm{tr}\,F_\mathrm{L}\,\mathrm{tr}\,F_\mathrm{R}$
f	$W_3\,(\mathrm{tr}\,F_\mathrm{L})^2\;f_{TT}\,(\mathrm{tr}\,F_\mathrm{R})^2$	$W_3\,\mathrm{tr}\,F_\mathrm{R}\,\mathrm{tr}F_\mathrm{L}\;f_{TT}\,\mathrm{tr}\,F_\mathrm{L}\,\mathrm{tr}\,F_\mathrm{R}$
g	$\mathrm{tr}\,F_\mathrm{L}^2\;f_{UU}^2\,\mathrm{tr}\,F_\mathrm{R}^2$	$\mathrm{tr}\,F_\mathrm{R}^\mathrm{T}F_\mathrm{L}\;f_{UU}^2\,\mathrm{tr}\,F_\mathrm{L}^\mathrm{T}F_\mathrm{R}$
h	$\mathrm{tr}\,H^\dagger H\;f_{UU}$	$\mathrm{tr}\,H^*H\;f_{UU}$
i	$W_2^2\,\mathrm{tr}\,F_\mathrm{L}\,\mathrm{tr}\,F_\mathrm{R}\;f_{TT}^2\,\mathrm{tr}\,F_\mathrm{L}\,\mathrm{tr}\,F_\mathrm{R}$	$W_2^2\,\mathrm{tr}\,F_\mathrm{R}\,\mathrm{tr}\,F_\mathrm{L}\;f_{TT}^2\,\mathrm{tr}\,F_\mathrm{L}\,\mathrm{tr}\,F_\mathrm{R}$
j	$W_2^2\,\mathrm{tr}\,F_\mathrm{L}\,\mathrm{tr}\,F_\mathrm{R}\;f_{TT}^2\,\mathrm{tr}\,F_\mathrm{L}\,\mathrm{tr}\,F_\mathrm{R}$	$W_2^2\,\mathrm{tr}\,F_\mathrm{L}\,\mathrm{tr}\,F_\mathrm{R}\;f_{TT}^2\,\mathrm{tr}\,F_\mathrm{R}\,\mathrm{tr}\,F_\mathrm{L}$
k	$W_2\,\mathrm{tr}\,H\,R'^\dagger\;f_{TU}\,f_{UT}\,\mathrm{tr}\,F_\mathrm{L}\,\mathrm{tr}\,F_\mathrm{R}$	$W_2\,\mathrm{tr}\,H^\mathrm{T}R'^\dagger\;f_{TU}\,f_{UT}\,\mathrm{tr}\,F_\mathrm{L}\,\mathrm{tr}\,F_\mathrm{R}$
l	$W_2\,\mathrm{tr}\,F_\mathrm{L}\,\mathrm{tr}\,F_\mathrm{R}\;f_{TU}\,f_{UT}\,\mathrm{tr}\,H^\dagger R'$	$W_2\,\mathrm{tr}\,F_\mathrm{L}\,\mathrm{tr}\,F_\mathrm{R}\;f_{TU}\,f_{UT}\,\mathrm{tr}\,H^*R'$
m	$W_2\,\mathrm{tr}\,F_\mathrm{L}\,\mathrm{tr}\,F_\mathrm{R}\;f_{TU}\,f_{UT}\,\mathrm{tr}\,R'H^\dagger$	$W_2\,\mathrm{tr}\,F_\mathrm{R}\,\mathrm{tr}\,F_\mathrm{L}\;f_{TU}\,f_{UT}\,\mathrm{tr}\,R'^\mathrm{T}H^\dagger$
n	$W_2\,\mathrm{tr}\,R'^\dagger H\;f_{TU}\,f_{UT}\,\mathrm{tr}\,F_\mathrm{L}\,\mathrm{tr}\,F_\mathrm{R}$	$W_2\,\mathrm{tr}\,R'^*H\;f_{TU}\,f_{UT}\,\mathrm{tr}\,F_\mathrm{L}\,\mathrm{tr}\,F_\mathrm{R}$
o	$\mathrm{tr}\,H\,R'^\dagger\;f_{UU}^2\,\mathrm{tr}\,R'H^\dagger$	$\mathrm{tr}\,H^\mathrm{T}R'^\dagger\;f_{UU}^2\,\mathrm{tr}\,R'^\mathrm{T}H^\dagger$
p	$\mathrm{tr}\,R'^\dagger H\;f_{UU}^2\mathrm{tr}\,H^\dagger R'$	$\mathrm{tr}\,R'^*H\,f_{UU}^2\,\mathrm{tr}\,H^*R'$

Table 6-1. Contribution to $\mathrm{var}\,G/G_0$ from the connected diagrams of Fig. 6-12.

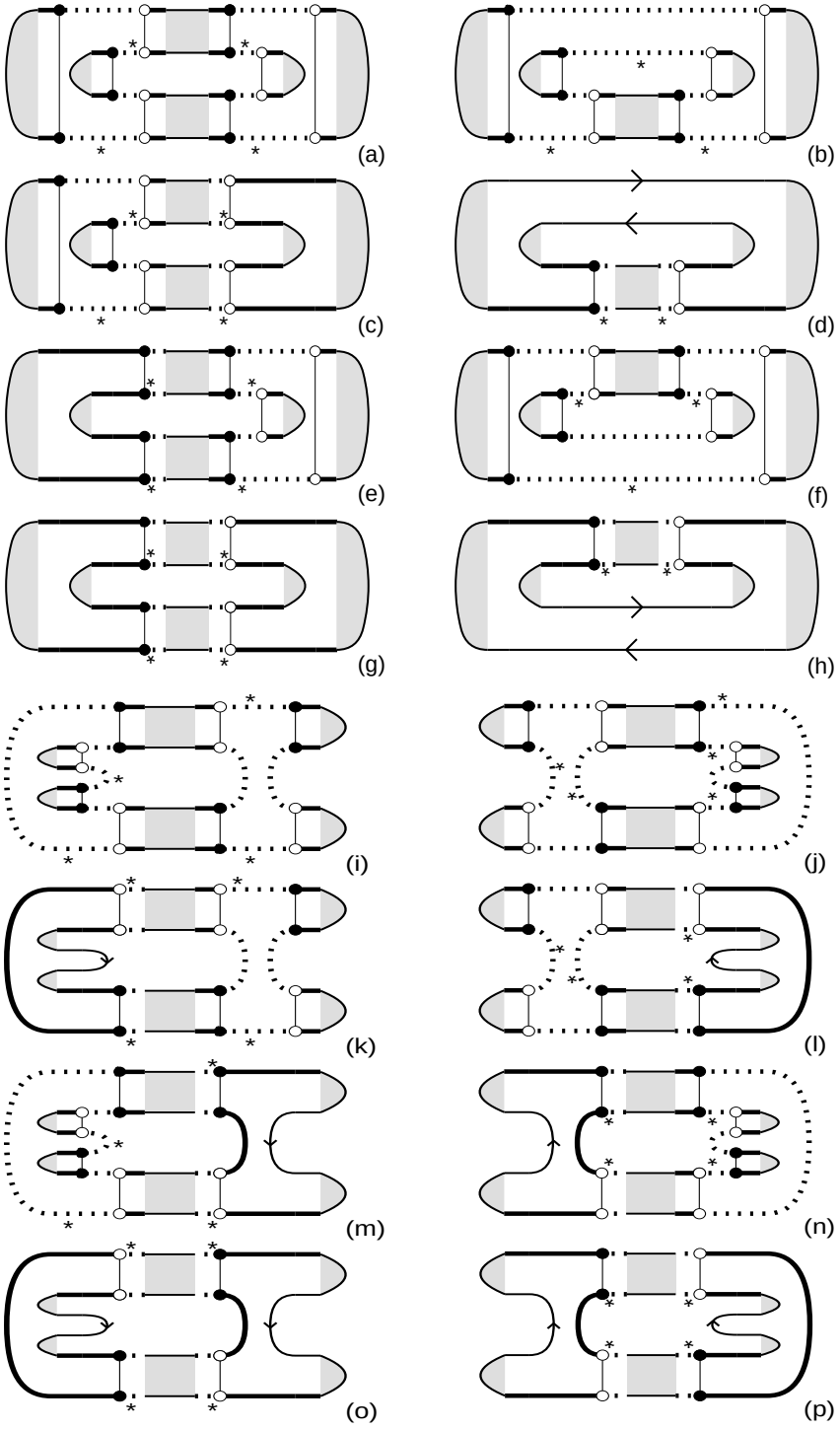

Figure 6-12. The 16 connected diagrams which contribute to the variance of the conductance. The shaded parts are defined in Figs. 6-9 and 6-13. These diagrams contribute for $\beta = 1$ and 2. For $\beta = 1$ there are 16 more diagrams, obtained by flipping the inner loop around a vertical axis (diagram a–h) or around a horizontal axis (i–p), so that ladders become maximally crossed.

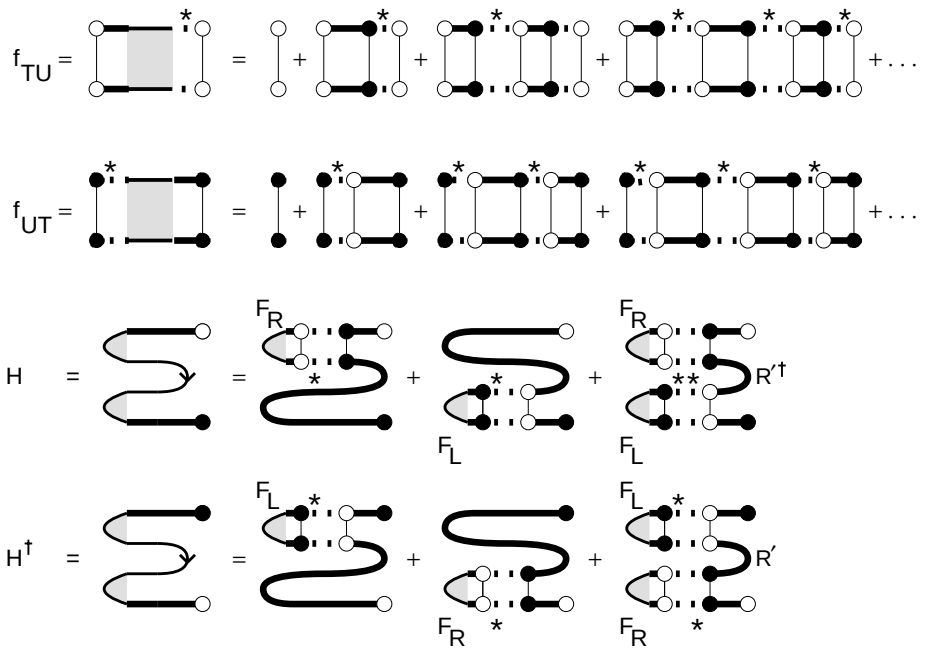

Figure 6-13. Diagrammatic representation of Eq. (6.5.27).

$$H \;=\; M^{-1}(\mathrm{tr}\,F_{\mathrm{R}})R'T'^{\dagger}C_1T' + M^{-1}(\mathrm{tr}\,F_{\mathrm{L}})TC_2T^{\dagger}R' + M^{-2}(\mathrm{tr}\,F_{\mathrm{L}})(\mathrm{tr}\,F_{\mathrm{R}})R'R'^{\dagger}R'.$$

In the presence of time-reversal symmetry ($\beta = 1$), the matrix U is symmetric. Diagrammatically, this means that no distinction is made between black and white dots. In addition to the 16 diffuson-like diagrams of Fig. 6-12, 16 more cooperon-like diagrams contribute. These are obtained from the diagrams of Fig. 6-12 by flipping the inner loop around a vertical (Fig. 6-12a–h) or horizontal (Fig. 6-12i–p) axis, so that segments with a ladder structure become maximally crossed. Their contributions are listed in Table 6-1. The contributions from the individual diffuson-like and cooperon-like diagrams are different. The total contribution to $\mathrm{var}\,G$ from diffuson-like and cooperon-like diagrams is the same.

The final result for the variance of G is

$$\begin{aligned}\mathrm{var}\,G/G_0 \;=\; & 2\beta^{-1}\left(g_1+g_1'\right)^{-6}\Big(2g_1^4g_1'^2+4g_1^3g_1'^3-4g_1^2g_2g_1'^3+2g_1^2g_1'^4-2g_1g_2g_1'^4\\ & +3g_2^2g_1'^4-2g_1g_3g_1'^4+2g_2g_1'^5-2g_3g_1'^5+2g_1^5g_2'-2g_1^4g_1'g_2'\\ & -4g_1^3g_1'^2g_2'+6g_1^2g_2g_1'^2g_2'+3g_1^4g_2'^2-2g_1^5g_3'-2g_1^4g_1'g_3'\Big). \qquad (6.5.28)\end{aligned}$$

One verifies that the large-N limit of Eq. (6.5.4) is recovered in the absence of tunnel barriers. For the special case of identical tunnel barriers ($g_p = g_p'$), this simplifies to

$$\mathrm{var}\,G/G_0 \;=\; (8\beta\, g_1^2)^{-1}\left(2g_1^2-2g_1g_2+3g_2^2-2g_1g_3\right), \qquad (6.5.29)$$

in agreement with Ref. [15]. If all transmission eigenvalues $\Gamma_n \equiv \Gamma$ are equal, one has $\mathrm{var}\,G/G_0 = (8\beta)^{-1}[1+(1-\Gamma)^2]$. A high tunnel barrier ($\Gamma \ll 1$) thus doubles the variance.

6.5.3 Density of transmission eigenvalues

The transmission eigenvalues $T_n \in [0,1]$ are the N_1 eigenvalues of the matrix product $s_{12}s_{12}^\dagger$. Without loss of generality we may assume that $N_1 \leq N_2$. The matrix product $s_{21}s_{21}^\dagger$ then has the same N_1 eigenvalues as $s_{12}s_{12}^\dagger$, plus $N_2 - N_1$ eigenvalues equal to zero. The N_1 non-zero transmission eigenvalues appear as the diagonal elements of the diagonal matrix T in the polar decomposition of the scattering matrix

$$S = \begin{pmatrix} s_{11} & s_{12} \\ s_{21} & s_{22} \end{pmatrix} = \begin{pmatrix} v & 0 \\ 0 & w \end{pmatrix} \begin{pmatrix} \sqrt{1-T} & 0 & i\sqrt{T} \\ 0 & \mathbb{1} & 0 \\ i\sqrt{T} & 0 & \sqrt{1-T} \end{pmatrix} \begin{pmatrix} v' & 0 \\ 0 & w' \end{pmatrix}. \quad (6.5.30)$$

Here v and v' (w and w') are $N_1 \times N_1$ ($N_2 \times N_2$) unitary matrices and $\mathbb{1}$ is the $N_2 - N_1$ dimensional unit matrix. If $N_1 = N_2$, Eq. (6.5.30) simplifies to Eq. (6.0.2).

Sofar we have only studied the conductance $G = G_0 \sum_n T_n$. The leading contribution to the average conductance comes from ladder diagrams. If we wish to average transport properties of the form $A = \sum_n a(T_n)$ (so-called linear statistics on the transmission eigenvalues), we need to know the density $\rho(T)$ of the transmission eigenvalues T_n. The leading-order contribution to the transmission-eigenvalue density is given by a larger class of diagrams, as we now discuss.

The density $\rho(T) = \langle \sum_{n=1}^{N_1} \delta(T - T_n) \rangle$ of the transmission eigenvalues follows from the matrix Green function $F(z)$:

$$F(z) = \left\langle C_1 (z - SC_2S^\dagger C_1)^{-1} \right\rangle, \quad (6.5.31)$$

$$\rho(T) = -\pi^{-1} \mathrm{Im}\, \mathrm{tr}\, F(T + i\epsilon), \quad (6.5.32)$$

where ϵ is a positive infinitesimal. We first compute $\rho(T)$ in the absence of tunnel barriers, when the result is known from other methods [4–6,37]. Then we include the tunnel barriers, when the result is not known.

In the absence of tunnel barriers, the scattering matrix S is distributed according to the circular ensemble, so that averaging amounts to integrating over the unitary group. We compute $F(z)$ as an expansion in powers of $1/z$,

$$F(z) = \sum_{n=0}^{\infty} \langle C_1 z^{-1} (SC_2S^\dagger C_1 z^{-1})^n \rangle. \quad (6.5.33)$$

We will also need the Green function

$$F'(z) = \langle C_2 (z - S^\dagger C_1 S C_2)^{-1} \rangle = \sum_{n=0}^{\infty} \langle C_2 z^{-1} (S^\dagger C_1 S C_2 z^{-1})^n \rangle. \quad (6.5.34)$$

The two Green functions F and F' are represented diagrammatically in Fig. 6-14. A diagram contributes to leading order [which is $\mathcal{O}(1)$] if the number of T-and U-cycles is

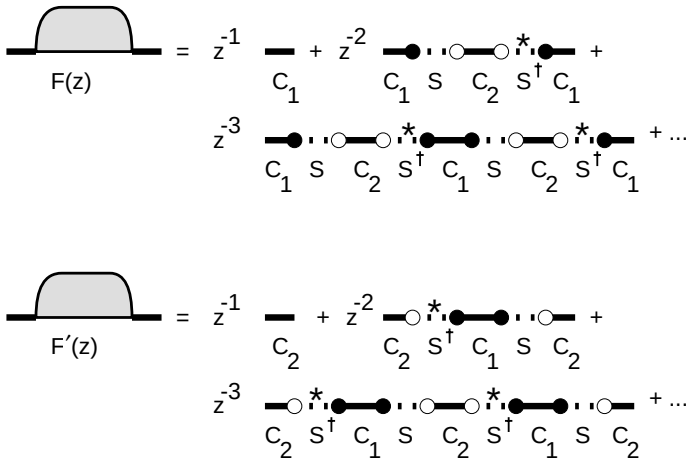

Figure 6-14. Diagrammatic representation of the Green functions for the density of transmission eigenvalues.

maximal. That is the case if the diagram is *planar*, meaning that the thin lines do not cross. The ladder diagrams are a subset of the planar diagrams. Planar diagrams have been studied in the context of the diagrammatic evaluation of integrals over Hermitian matrices, in particular for the Gaussian ensemble [12, 17]. For the Gaussian ensemble, only planar diagrams with U-cycles of unit length have to be taken into account. Summation over all these diagrams results in a self-consistency or Dyson equation for $F(z)$, which solves the problem [17]. For an integral of unitary matrices, U-cycles of arbitrary length need to be taken into account, as is shown diagrammatically in Fig. 6-15. The corresponding Dyson equation is

$$F(z) = z^{-1}C_1 + z^{-1}C_1\Sigma(z)F(z), \qquad \Sigma(z) = \sum_{n=1}^{\infty} W_n \left[z \operatorname{tr} F'(z)\right]^n [\operatorname{tr} F(z)]^{n-1}, \tag{6.5.35}$$

$$F'(z) = z^{-1}C_2 + z^{-1}C_2\Sigma'(z)F'(z), \quad \Sigma'(z) = \sum_{n=1}^{\infty} W_n [z \operatorname{tr} F(z)]^n [\operatorname{tr} F'(z)]^{n-1}. \tag{6.5.36}$$

In terms of the generating function

$$h(z) \;=\; \sum_{n=1}^{\infty} W_n z^{n-1} = \frac{1}{2z}\left(\sqrt{M^2+4z} - M\right), \tag{6.5.37}$$

we may rewrite Eq. (6.5.35) as

$$F(z) = C_1(z - \Sigma(z)C_1)^{-1}, \qquad \Sigma(z) = h\left(z \operatorname{tr} F(z) \operatorname{tr} F'(z)\right) z \operatorname{tr} F'(z), \tag{6.5.38}$$

$$F'(z) = C_2(z - \Sigma(z)C_2)^{-1}, \qquad \Sigma'(z) = h\left(z \operatorname{tr} F(z) \operatorname{tr} F'(z)\right) z \operatorname{tr} F(z). \tag{6.5.39}$$

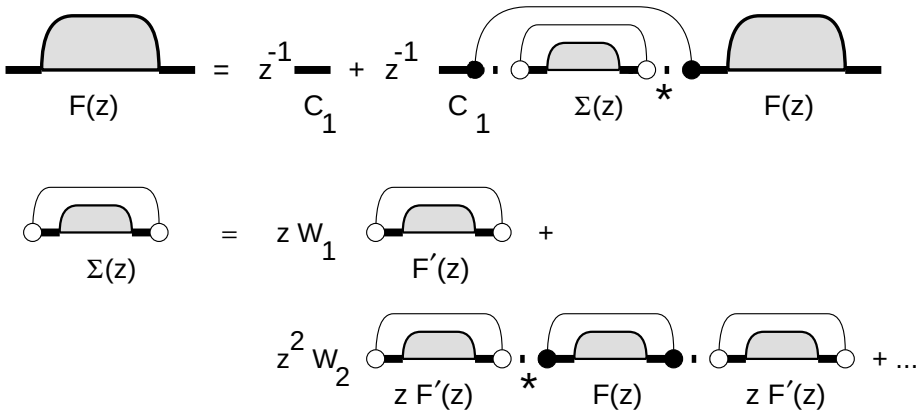

Figure 6-15. Diagrammatic representation of the Dyson equation (6.5.35) for $F(z)$.

In the derivation of Eq. (6.5.38) we did not use the particular form of the matrices C_1 and C_2. As a check we may choose $C_1 = C_2 = 1$, so that $F(z) = F'(z) = (z-1)^{-1}$, and verify that Eq. (6.5.38) holds.

The solution of Eq. (6.5.38) is

$$\operatorname{tr} F(z) = \frac{N_1 - N_2}{2z} + \frac{\sqrt{M^2 z - (N_1 - N_2)^2}}{2z\sqrt{z-1}}, \tag{6.5.40}$$

$$\operatorname{tr} F'(z) = \frac{N_2 - N_1}{2z} + \frac{\sqrt{M^2 z - (N_2 - N_1)^2}}{2z\sqrt{z-1}}. \tag{6.5.41}$$

The resulting density of transmission eigenvalues is

$$\rho(T) = \frac{M\sqrt{T - T_{\min}}}{2\pi T\sqrt{1-T}}\theta(T - T_{\min}), \quad T_{\min} = \frac{(N_1 - N_2)^2}{M^2}, \tag{6.5.42}$$

in agreement with Refs. [5, 6, 37]. (The function $\theta(x) = 1$ if $x > 0$ and 0 if $x < 0$.)

The weak-localization correction to $\rho(T)$ follows from the $\mathcal{O}(M^{-1})$ term in the large-M expansion of $F(z)$. As in Sec. 6.5.1, it has two contributions: $\delta F_1(z)$, which is due to the sub-leading order term in the large-M expansion of W_n, and $\delta F_2(z)$, which is due to diagrams of order $\mathcal{O}(M^{-1})$. In the absence of time-reversal symmetry, both contributions are absent. In the presence of time-reversal symmetry, the sub-leading order term $\delta W_n = -M^{-2n}(-4)^{n-1}$ in the large-M expansion of W_n [cf. Eq. (6.3.3)] yields a sub-leading order contribution δh to the generating function h,

$$\delta h(z) = \sum_{n=1}^{\infty} \delta W_n z^{n-1} = -(M^2 + 4z)^{-1}, \tag{6.5.43}$$

from which we obtain

$$\operatorname{tr} \delta F_1(z) = \tfrac{1}{4}(z - T_{\min})^{-1} - \tfrac{1}{4}(z-1)^{-1}. \tag{6.5.44}$$

The contribution $\delta F_2(z)$ comes from diagrams in which thin lines connect black and white dots. Each such diagram contains the product C_1C_2, which vanishes. Hence, the $\mathcal{O}(M^{-1})$ contribution to $F(z)$ consists of $\delta F_1(z)$ only. The resulting weak-localization correction to the transmission eigenvalue density is

$$\delta\rho(T) = \frac{2-\beta}{4\beta}\left[\delta(T - T_{\min} - \epsilon) - \delta(T - 1 + \epsilon)\right], \tag{6.5.45}$$

in agreement with Refs. [4, 6].

We now include tunnel barriers in the leads. Motivated by Nazarov's calculation of the density of transmission eigenvalues in a disordered metal [38], we introduce the $2M \times 2M$ matrices

$$\boldsymbol{S} = \begin{pmatrix} S & 0 \\ 0 & S^\dagger \end{pmatrix}, \quad \boldsymbol{C} = \begin{pmatrix} 0 & C_2 \\ C_1 & 0 \end{pmatrix}, \quad \boldsymbol{F}(z) = \begin{pmatrix} 0 & F'(z) \\ F(z) & 0 \end{pmatrix}, \tag{6.5.46}$$

$$\boldsymbol{T} = \begin{pmatrix} T & 0 \\ 0 & T^\dagger \end{pmatrix}, \quad \boldsymbol{T'} = \begin{pmatrix} T' & 0 \\ 0 & T'^\dagger \end{pmatrix}, \quad \boldsymbol{R'} = \begin{pmatrix} R' & 0 \\ 0 & R'^\dagger \end{pmatrix}. \tag{6.5.47}$$

Analogous to Eq. (6.5.6), we decompose $\boldsymbol{S} = \bar{\boldsymbol{S}} + \boldsymbol{\delta S}$, where $\bar{\boldsymbol{S}} = \langle \boldsymbol{S} \rangle$ and

$$\boldsymbol{\delta S} = \boldsymbol{T}'(1 - \boldsymbol{U}\boldsymbol{R}')^{-1}\boldsymbol{U}\boldsymbol{T}, \quad \boldsymbol{U} = \begin{pmatrix} U & 0 \\ 0 & U^\dagger \end{pmatrix} \tag{6.5.48}$$

is given in terms of a matrix U which is distributed according to the circular ensemble. Because $\bar{S}$, C_1, and C_2 commute and $C_1C_2 = 0$, we may replace S by δS in the expression (6.5.31) for $F(z)$. The result for the matrix Green function $\boldsymbol{F}(z)$ is

$$\begin{aligned} \boldsymbol{F}(z) &= (2z)^{-1} \sum_{\pm} \left\langle \boldsymbol{C} \pm \boldsymbol{C}\boldsymbol{T}' \left[1 - \boldsymbol{U}(\boldsymbol{R}' \pm \boldsymbol{T}\boldsymbol{C}\boldsymbol{T}' z^{-1/2})\right]^{-1} \boldsymbol{U}\boldsymbol{T}\boldsymbol{C} z^{-1/2} \right\rangle \\ &= (2z)^{-1} \sum_{\pm} \left[\boldsymbol{C} \pm \boldsymbol{A}_\pm (\boldsymbol{F}_\pm - \boldsymbol{X}_\pm)\boldsymbol{B}_\pm\right]. \end{aligned} \tag{6.5.49}$$

In the second equation we abbreviated $\boldsymbol{X}_\pm = \boldsymbol{R}' \pm \boldsymbol{T}\boldsymbol{C}\boldsymbol{T}' z^{-1/2}$, $\boldsymbol{F}_\pm = \langle \boldsymbol{X}_\pm (1 - \boldsymbol{U}\boldsymbol{X}_\pm)^{-1} \rangle$, and defined $\boldsymbol{A}_\pm$ and $\boldsymbol{B}_\pm$ such that $\boldsymbol{A}_\pm \boldsymbol{X}_\pm = \boldsymbol{C}\boldsymbol{T}'$, $\boldsymbol{X}_\pm \boldsymbol{B}_\pm = \boldsymbol{T}\boldsymbol{C} z^{-1/2}$.

After these algebraic manipulations we are ready to compute $\boldsymbol{F}_\pm$ by expanding in planar diagrams. The result is a Dyson equation similar to Eq. (6.5.35),

$$\boldsymbol{F}_\pm = \boldsymbol{X}_\pm \left(1 + \boldsymbol{\Sigma}_\pm \boldsymbol{F}_\pm\right), \quad \boldsymbol{\Sigma}_\pm = \sum_{n=1}^{\infty} W_n \left(\mathcal{P}\boldsymbol{F}_\pm\right)^{2n-1}, \tag{6.5.50}$$

where the projection operator $\mathcal{P}$ acts on a $2M \times 2M$ matrix $\boldsymbol{A}$ as

$$\boldsymbol{A} = \begin{pmatrix} A_{11} & A_{12} \\ A_{21} & A_{22} \end{pmatrix}, \quad \mathcal{P}\boldsymbol{A} = \begin{pmatrix} 0 & \mathbb{1}_M \operatorname{tr} A_{12} \\ \mathbb{1}_M \operatorname{tr} A_{21} & 0 \end{pmatrix}, \tag{6.5.51}$$

$\mathbb{1}_M$ being the $M \times M$ unit matrix. The presence of the projection operator $\mathcal{P}$ in Eq. (6.5.50) ensures that the planar diagrams contain only contractions between U (the 1, 1 block of $\boldsymbol{U}$) and $U^\dagger$ (the 2, 2 block of $\boldsymbol{U}$). In terms of the generating function h we obtain the result

$$\boldsymbol{F} = (2z)^{-1} \sum_{\pm} \left(\boldsymbol{C} \pm \boldsymbol{C}\boldsymbol{T}'(1 - \boldsymbol{\Sigma}_\pm \boldsymbol{X}_\pm)^{-1} \boldsymbol{\Sigma}_\pm \boldsymbol{T}\boldsymbol{C} z^{-1/2} \right), \tag{6.5.52}$$

$$\boldsymbol{\Sigma}_\pm = \left(\mathcal{P}\boldsymbol{X}_\pm (1 - \boldsymbol{\Sigma}_\pm \boldsymbol{X}_\pm)^{-1} \right) h \left(\left(\mathcal{P}\boldsymbol{X}_\pm (1 - \boldsymbol{\Sigma}_\pm \boldsymbol{X}_\pm)^{-1} \right)^2 \right). \tag{6.5.53}$$

It remains to solve the 2×2 matrix equation (6.5.53). We could not do this analytically for arbitrary Γ_j, but only for the case of two identical tunnel barriers: $N_1 = N_2 = \frac{1}{2}M \equiv N$, $\Gamma_j = \Gamma_{j+N}$ ($j = 1, 2, \ldots, N$). The solution of Eq. (6.5.53) in that case is

$$\boldsymbol{\Sigma}_\pm = \pm \left(\sqrt{z} - \sqrt{z-1} \right) \begin{pmatrix} 0 & \mathbb{1}_M \\ \mathbb{1}_M & 0 \end{pmatrix}, \tag{6.5.54}$$

independent of the Γ_j's. The trace of the Green function is

$$\operatorname{tr} F(z) = \sum_{j=1}^{N} \frac{2(1-\Gamma_j)(\sqrt{z} - \sqrt{z-1}) + \Gamma_j / \sqrt{z-1}}{2z(1-\Gamma_j)(\sqrt{z} - \sqrt{z-1}) + \Gamma_j \sqrt{z}}, \tag{6.5.55}$$

and the corresponding density of transmission eigenvalues is

$$\rho(T) = \sum_{j=1}^{N} \frac{\Gamma_j (2 - \Gamma_j)}{\pi (\Gamma_j^2 - 4\Gamma_j T + 4T) \sqrt{T(1-T)}}. \tag{6.5.56}$$

As a check, we note that $\rho(T) \to N\delta(T)$ if $\Gamma_j \to 0$ for all j, and $\rho(T) \to N\pi^{-1}[T(1-T)]^{-1/2}$ if $\Gamma_j \to 1$ for all j [in agreement with Eq. (6.5.42)].

6.6 Application to a Normal-metal–superconductor junction

As an altogether different application of the diagrammatic technique, we consider a junction between a normal metal (N) and a superconductor (S) (see Fig. 6-16). At temperatures and voltages below the excitation gap Δ in S, conduction takes place via the mechanism of Andreev reflection [39]: An electron coming from N with an energy ε (relative to the Fermi energy E_F) is reflected at the NS interface as a hole with energy $-\varepsilon$. The missing charge of $2e$ is absorbed by the superconducting condensate. We calculate the average and variance of the conductance, for the two cases that the NS junction consists of a disordered wire or of a chaotic cavity.

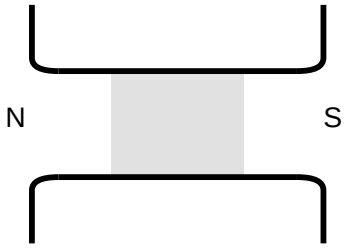

Figure 6-16. Conductor consisting of a normal metal (grey) coupled to one normal-metal reservoir (N) and one superconducting reservoir (S). The conductor may consist of a disordered segment or of a quantum dot.

Starting point of the calculation is the relationship between the differential conductance $G_{\rm NS}(eV) = dI/dV$ of the NS junction and the transmission and reflection matrices of the normal region [40],

$$\begin{aligned} G_{\rm NS}(\varepsilon) &= \frac{4e^2}{h}\,\mathrm{tr}\left(t'(\varepsilon)\left[1 + r'(-\varepsilon)^* r'(\varepsilon)\right]^{-1} t(-\varepsilon)^*\right) \\ &\quad \times \left(t'(\varepsilon)\left[1 + r'(-\varepsilon)^* r'(\varepsilon)\right]^{-1} t(-\varepsilon)^*\right)^\dagger . \end{aligned} \tag{6.6.1}$$

This formula requires $eV \ll \Delta \ll E_F$ and zero temperature. The reflection and transmission matrices are $N \times N$ matrices, which together constitute the $2N \times 2N$ scattering matrix S. Using the polar decomposition (6.0.2) we may rewrite the conductance formula (6.6.1) as

$$\begin{aligned} G_{\rm NS}(\varepsilon) &= \frac{4e^2}{h}\mathrm{tr}\left[T_+\left(1 + u_+\sqrt{1-T_-}u_-^*\sqrt{1-T_+}\right)^{-1} u_+\right. \\ &\quad \left. \times\, T_- u_+^\dagger\left(1 + \sqrt{1-T_+}u_-^{\rm T}\sqrt{1-T_-}u_+^\dagger\right)^{-1}\right], \end{aligned} \tag{6.6.2}$$

where $T_\pm = T(\pm\varepsilon)$ and $u_\pm = w'(\pm\varepsilon)w(\mp\varepsilon)^*$. In the presence of spin-orbit scattering, S is a matrix of quaternions, and the transpose should be replaced by the dual. In what follows, we will consider the case of no spin-orbit scattering. Spin-orbit scattering (considered by Slevin, Pichard, and Mello [41]) will be included at the end by means of the translation rule of Sec. 6.4.

Averages are computed in two steps: first over the unitary matrix u, then over the matrix of transmission eigenvalues T. Four cases can be distinguished, depending on the magnitude of the magnetic field B and voltage V relative to the characteristic field B_c for breaking time-reversal symmetry ($\mathcal{T}$) and characteristic voltage E_c/e for breaking electron-hole degeneracy ($\mathcal{D}$):[1]

[1] In a disordered wire (length L, width W, mean free path ℓ), one has $B_c = h/eLW$, $E_c = \hbar v_F \ell/L^2$. In a chaotic cavity (area A, mean dwell time τ, mean time to cross the cavity τ') one has $B_c = (h/eA)(\tau'/\tau)^{1/2}$, $E_c = \hbar/\tau$).

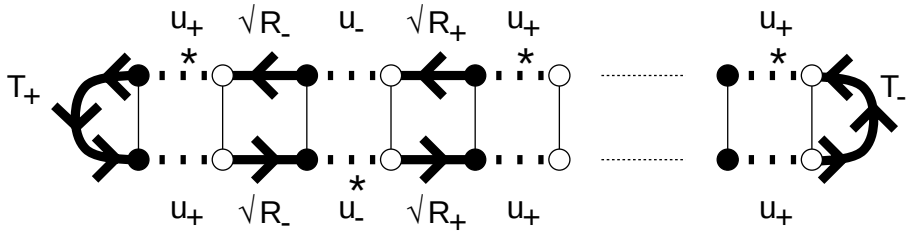

Figure 6-17. Ladder diagram for the $\mathcal{O}(N)$ contribution to $\langle G_{\rm NS}\rangle$. We defined $R_\pm = 1 - T_\pm$.

0. $eV \ll E_c$, $B \ll B_c \Longleftrightarrow \mathcal{T}$ and $\mathcal{D}$ are both present: Then $u_\pm$ may be approximated by the unit matrix, so that one only needs to average over the transmission eigenvalues. This case has been studied extensively [42] and does not concern us here.

1. $eV \ll E_c$, $B \gg B_c \Longleftrightarrow \mathcal{D}$ is present, but $\mathcal{T}$ is broken: Then we may neglect the ε-dependence of S, so that $u_+ = u_- \equiv u$. According to the isotropy assumption, u is uniformly distributed in $\mathcal{U}(N)$.

2. $eV \gg E_c$, $B \ll B_c \Longleftrightarrow \mathcal{T}$ is present, but $\mathcal{D}$ is broken: Then we may consider $S(\varepsilon)$ and $S(-\varepsilon)$ as independent unitary symmetric matrices. Hence $u_+ = u_-^\dagger \equiv u$ is uniformly distributed in $\mathcal{U}(N)$.

3. $eV \gg E_c$, $B \gg B_c \Longleftrightarrow$ both $\mathcal{T}$ and $\mathcal{D}$ are broken: Then u_+ and u_- are independent, both uniformly distributed in $\mathcal{U}(N)$.

We compute the average and variance of the conductance for cases 1, 2, and 3.

6.6.1 Average conductance

We start with the computation of the average conductance $\langle G_{\rm NS}\rangle$. We first perform the average $\langle\cdots\rangle_u$ over $u_\pm$ and then over $T_\pm$. To leading order only ladder diagrams contribute, see Fig. 6-17. The result is the same for cases 1, 2, and 3:

$$\langle G_{\rm NS}/G_0\rangle_u = 2N\frac{\tau_{1+}\tau_{1-}}{\tau_{1+}+\tau_{1-}-\tau_{1+}\tau_{1-}} + \mathcal{O}(1), \tag{6.6.3}$$

$$\tau_{k\pm} = \frac{1}{N}\,\mathrm{tr}\,T_\pm^k = \frac{1}{N}\sum_{j=1}^{N} T_j^k(\pm\varepsilon). \tag{6.6.4}$$

The $\mathcal{O}(1)$ contribution $\delta G_{\rm NS}$ is different for the three cases.

Case 1, absence of $\mathcal{T}$ and presence of $\mathcal{D}$. We put $u_\pm = u$, $\tau_{k\pm} = \tau_k$. For normal metals, the $\mathcal{O}(1)$ contribution δG to $\langle G\rangle$ vanishes if $\mathcal{T}$ is broken. However, in the NS junction an $\mathcal{O}(1)$ contribution remains. The diagrams which contribute to $\delta G_{\rm NS}$ have a maximally crossed central part, with contractions between U's and U^*'s on the same side

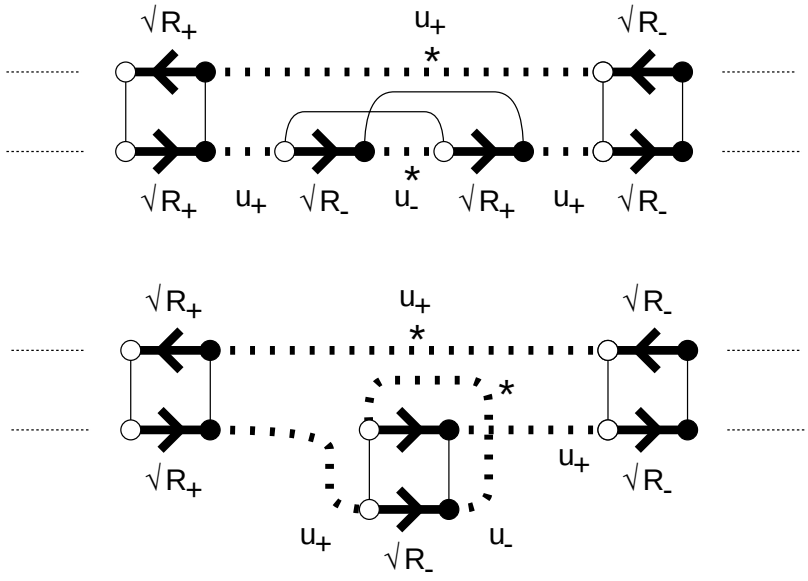

Figure 6-18. Maximally crossed diagram for the $\mathcal{O}(1)$ correction to $\langle G_{\rm NS}\rangle$ in the absence of time-reversal symmetry and presence of electron-hole degeneracy (top). The right and left parts of the diagram have a ladder structure. The central part may be redrawn as a ladder diagram (bottom).

of the diagram (Fig. 6-18, top). The left and right ends have a ladder structure. In the Hamiltonian approach, a similar maximally crossed diagram has been studied by Altland and Zirnbauer [25], who call it a "symplecton". In total four diagrams contribute to $\delta G_{\rm NS}$, see Fig. 6-19. The building blocks of the diagram have the algebraic expressions

$$\begin{aligned}
F_\pm &= T_\pm + (1-T_\pm)\,\mathrm{tr}\,T_\pm\,\mathrm{tr}\,(1-T_\mp)\sum_{j=0}^{\infty} N^{-2j-2}\left[\mathrm{tr}\,(1-T_+)\,\mathrm{tr}\,(1-T_-)\right]^j \\
&= (\tau_{1\pm} + T_\pm\tau_{1\mp} - \tau_{1+}\tau_{1-})\,(\tau_{1+}+\tau_{1-}-\tau_{1+}\tau_{1-})^{-1}\,, \qquad (6.6.5)\\
F'_\pm &= -(1-T_\mp)\,\mathrm{tr}\,T_\pm\sum_{j=0}^{\infty} N^{-2j-1}\left[\mathrm{tr}\,(1-T_+)\,\mathrm{tr}\,(1-T_-)\right]^j \\
&= -(\tau_{1\pm} - \tau_{1\pm}T_\mp)\,(\tau_{1+}+\tau_{1-}-\tau_{1+}\tau_{1-})^{-1}\,, \qquad (6.6.6)\\
H_\pm &= i\,N^{-1}T_\pm\sqrt{1-T_\pm}\,\mathrm{tr}\,F_\mp - i\,N^{-2}(1-T_\pm)\sqrt{1-T_\pm}\,\mathrm{tr}\,F_\mp\,\mathrm{tr}\,F'_\pm, \qquad (6.6.7)\\
f_{TT\pm} &= -\mathrm{tr}\,(1-T_\pm)\sum_{j=0}^{\infty} N^{-2j}\left[\mathrm{tr}\,(1-T_+)\,\mathrm{tr}\,(1-T_-)\right]^j \\
&= -N(1-\tau_{1\pm})\,(\tau_{1+}+\tau_{1-}-\tau_{1+}\tau_{1-})^{-1}\,, \qquad (6.6.8)\\
f_{UU\pm} &= -\mathrm{tr}\,(1-T_\pm)\sum_{j=0}^{\infty} N^{-2j-2}\left[\mathrm{tr}\,(1-T_+)\,\mathrm{tr}\,(1-T_-)\right]^j \\
&= -N^{-1}(1-\tau_{1\pm})\left[\tau_{1+}+\tau_{1-}-\tau_{1+}\tau_{1-}\right]^{-1}\,, \qquad (6.6.9)
\end{aligned}$$

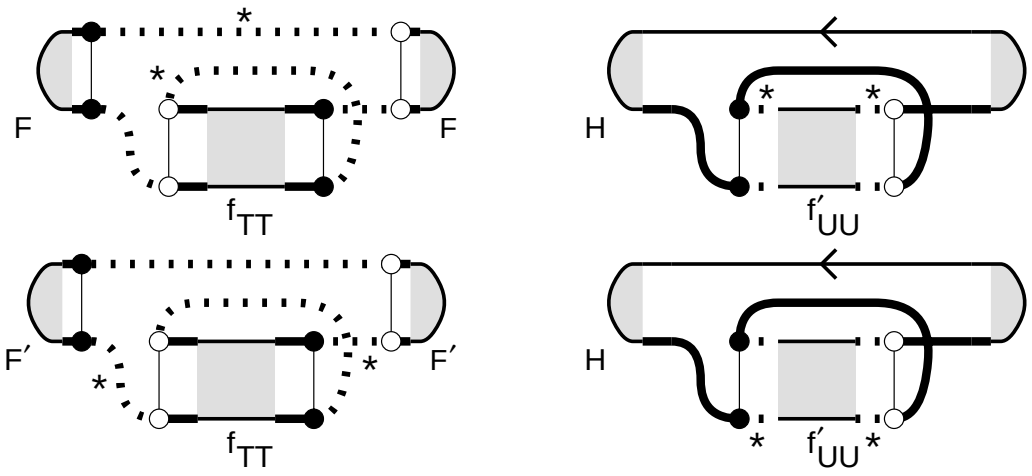

Figure 6-19. Diagrams for the $\mathcal{O}(1)$ correction to $\langle G_{\rm NS}\rangle$ in the absence of time-reversal symmetry and presence of electron-hole degeneracy.

$$\begin{aligned} f'_{UU\pm} &= \sum_{j=0}^{\infty} N^{-2j-1}\left[\mathrm{tr}\,(1-T_+)\,\mathrm{tr}\,(1-T_-)\right]^j \\ &= N^{-1}\left(\tau_{1+}+\tau_{1-}-\tau_{1+}\tau_{1-}\right)^{-1}. \end{aligned} \tag{6.6.10}$$

Capital letters indicate matrices, lower-case letters indicate scalars. The subscripts $\pm$ are omitted from Fig. 6-19 because of electron-hole degeneracy. The $\mathcal{O}(1)$ correction $\delta G_{\rm NS}$ represented in Fig. 6-19 equals

$$\begin{aligned} \delta G_{\rm NS}/G_0 &= 8\, f'_{UU}\,\mathrm{tr}\, iH\sqrt{1-T}\; + 4W_2\, f_{TT}[(\mathrm{tr}\,F)^2+(\mathrm{tr}\,F')^2] \\ &= -\frac{8\tau_1-4\tau_1^2+4\tau_1^3-8\tau_2}{\tau_1(2-\tau_1)^3}. \end{aligned} \tag{6.6.11}$$

We still have to average over the transmission eigenvalues. We use that the sample-to-sample fluctuations $\tau_k-\langle\tau_k\rangle$ are an order $1/N$ smaller than the average. (This is a general property of a linear statistics, i.e. of quantities of the form $A=\sum_n a(T_n)$, see Ref. [4].) Hence

$$\langle\, f(\tau_k)\rangle = f(\langle\tau_k\rangle)[1+\mathcal{O}(N^{-2})], \tag{6.6.12}$$

which implies that we may replace the average of the rational functions (6.6.3) and (6.6.11) of the τ_k's by the rational functions of the average $\langle\tau_k\rangle$. This average has the $1/N$ expansion

$$\langle\tau_k\rangle = \langle\tau_k\rangle_0 + \mathcal{O}(N^{-2}), \tag{6.6.13}$$

where $\langle\tau_k\rangle_0$ is $\mathcal{O}(N^0)$. There is no term of order N^{-1} in the absence of $\mathcal{T}$. The average over T of Eqs. (6.6.3) and (6.6.11) becomes

$$\langle G_{\rm NS}/G_0\rangle = \frac{2N\langle\tau_1\rangle_0}{2-\langle\tau_1\rangle_0} - \frac{8\langle\tau_1\rangle_0-4\langle\tau_1\rangle_0^2+4\langle\tau_1\rangle_0^3-8\langle\tau_2\rangle_0}{\langle\tau_1\rangle_0(2-\langle\tau_1\rangle_0)^3}+\mathcal{O}(N^{-1}). \tag{6.6.14}$$

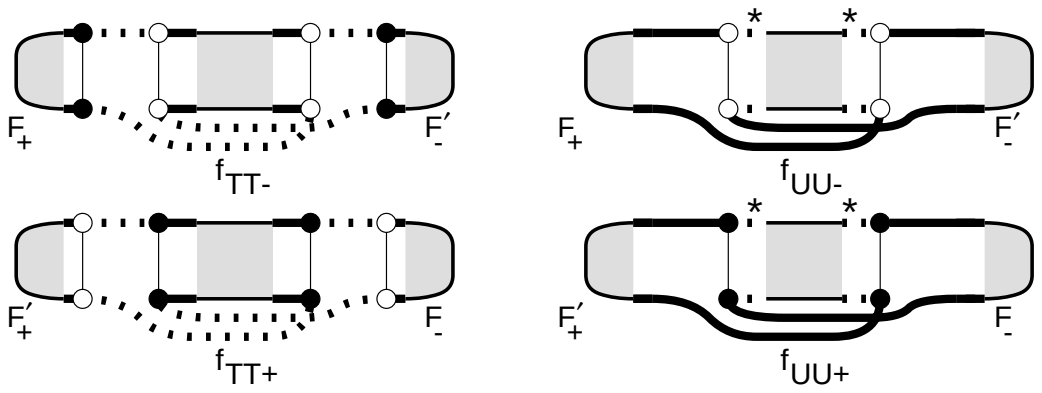

Figure 6-20. Diagrams for the $\mathcal{O}(1)$ correction to $\langle G_{\rm NS}\rangle$ in the absence of electron-hole degeneracy and presence of time-reversal symmetry.

Case 2, presence of $\mathcal{T}$ and absence of $\mathcal{D}$. We put $u_+ = u_-^\dagger \equiv u$. The $\mathcal{O}(1)$ correction comes from the maximally crossed diagrams of Fig. 6-20,

$$\begin{aligned}\delta G_{\rm NS}/G_0 &= 2\,W_2\,\mathrm{tr}\,F_+\,f_{TT-}\,\mathrm{tr}\,F'_- + 2\,W_2\,\mathrm{tr}\,F'_+\,f_{TT+}\,\mathrm{tr}\,F_- \\ &\quad + 2\,\mathrm{tr}\,F_+\,f_{UU-}F_-^{\prime\rm T} + 2\,\mathrm{tr}\,F'_+\,f_{UU+}F_-^{\rm T}. \end{aligned} \tag{6.6.15}$$

Averaging over the transmission eigenvalues amounts to replacing $\tau_{k\pm}$ by its average, i.e. $\tau_{k\pm} \to \langle\tau_k\rangle_0 + N^{-1}\delta\tau_k + \mathcal{O}(N^{-2})$. (The average of $\tau_{k\pm}$ is the same for $+\varepsilon$ and $-\varepsilon$.) Because $\mathcal{T}$ is not broken there is a term of $\mathcal{O}(N^{-1})$ in this expression. We find for the average conductance

$$\begin{aligned}\langle G_{\rm NS}/G_0\rangle &= \frac{2N\langle\tau_1\rangle_0}{2-\langle\tau_1\rangle_0} + \frac{4\,\delta\tau_1}{(2-\langle\tau_1\rangle_0)^2} \\ &\quad + \frac{4\,\langle\tau_1\rangle_0^2 - 4\,\langle\tau_1\rangle_0^3 - 4\,\langle\tau_2\rangle_0 + 4\,\langle\tau_1\rangle_0\langle\tau_2\rangle_0}{\langle\tau_1\rangle_0\,(2-\langle\tau_1\rangle_0)^3} + \mathcal{O}(N^{-1}). \end{aligned} \tag{6.6.16}$$

Case 3, both $\mathcal{T}$ and $\mathcal{D}$ broken. Because u_+ and u_- are independent, there are no diagrams which contribute to order 1. The average conductance is obtained by averaging Eq. (6.6.3) over the transmission eigenvalues,

$$\langle G_{\rm NS}/G_0\rangle = \frac{2N\langle\tau_1\rangle_0}{2-\langle\tau_1\rangle_0} + \mathcal{O}(N^{-1}). \tag{6.6.17}$$

From the translation rule of Sec. 6.4 one deduces that in the presence of spin-orbit scattering, the leading $\mathcal{O}(N)$ term of the average conductance is unchanged, while the $\mathcal{O}(1)$ correction is multiplied by $-1/2$, in agreement with what was found by Slevin, Pichard and Mello [41].

The formulas given above apply to any system for which the isotropy assumption holds. We discuss two examples:

(a) A disordered wire (length L, mean free path ℓ, number of transverse modes N), connected to a superconductor. We use the results [43]

$$\begin{aligned} \langle\tau_1\rangle_0 &= (1+L/\ell)^{-1}, && (6.6.18)\\ \langle\tau_2\rangle_0 &= \tfrac{2}{3}(1+L/\ell)^{-1}+\tfrac{1}{3}(1+L/\ell)^{-4}, && (6.6.19)\\ \delta\tau_1 &= -\tfrac{1}{3}(1+\ell/L)^{-3}. && (6.6.20)\end{aligned}$$

We assume $\ell \ll L \ll N\ell$ and neglect terms of order $L/N\ell$ and ℓ/L but retain terms of order 1 and $N\ell^p/L^p$ ($p \geq 1$). Substitution of Eq. (6.6.18) into Eqs. (6.6.14), (6.6.16), and (6.6.17) yields

$$\langle G_{\rm NS}/G_0\rangle = \begin{cases} N(1+L/\ell)^{-1}-1+4/\pi^2 & (\mathcal{D},\mathcal{T}),\\ N(1/2+L/\ell)^{-1}-1/3 & (\mathcal{D},\text{no }\mathcal{T}),\\ N(1/2+L/\ell)^{-1}-2/3 & (\text{no }\mathcal{D},\mathcal{T}),\\ N(1/2+L/\ell)^{-1} & (\text{no }\mathcal{D},\text{no }\mathcal{T}).\end{cases} \qquad (6.6.21)$$

The result in the presence of both $\mathcal{T}$ and $\mathcal{D}$ has been taken from Refs. [44, 45]. In the presence of spin-orbit scattering, the $\mathcal{O}(N)$ term is unchanged, while the $\mathcal{O}(1)$ term is multiplied by $-1/2$.

(b) A chaotic cavity without tunnel barriers in the leads. Lead 1 (with N_1 modes) is connected to a normal metal, lead 2 (with N_2 modes) to a superconductor. An asymmetry between N_1 and N_2 appears because the dimension of $u_\pm$ in the polar decomposition (6.5.30) is $N_2 \times N_2$. The $N_2 \times N_2$ matrix $T_\pm$ contains the $\min(N_1, N_2)$ non-zero transmission eigenvalues on the diagonal (remaining diagonal elements being zero). We denote $N_{\rm tot} = N_1 + N_2$ and $N_A = (N_1^2 + 6N_1N_2 + N_2^2)^{1/2}$. The averages $\langle\tau_1\rangle_0$ and $\langle\tau_2\rangle_0$ and the correction $\delta\tau_1$ can be computed from the density of transmission eigenvalues [Eqs. (6.5.42) and (6.5.45)]. The results are

$$\delta\tau_1 = -N_1N_2N_{\rm tot}^{-2},\quad \langle\tau_1\rangle_0 = N_1N_{\rm tot}^{-1},\quad \langle\tau_2\rangle_0 = N_1(N_{\rm tot}^2 - N_1N_2)N_{\rm tot}^{-3}. \qquad (6.6.22)$$

Substitution into Eqs. (6.6.14), (6.6.16), and (6.6.17) gives

$$\langle G_{\rm NS}/G_0\rangle = \begin{cases} N_{\rm tot}(1-N_{\rm tot}/N_A) - 8N_1N_2N_{\rm tot}^2/N_A^4 & (\mathcal{D},\mathcal{T}),\\ 2N_1N_2/(N_{\rm tot}+N_2) - 4N_1N_2N_{\rm tot}/(N_{\rm tot}+N_2)^3 & (\mathcal{D},\text{no }\mathcal{T}),\\ 2N_1N_2/(N_{\rm tot}+N_2) - 4N_2N_{\rm tot}^2/(N_{\rm tot}+N_2)^3 & (\text{no }\mathcal{D},\mathcal{T}),\\ 2N_1N_2/(N_{\rm tot}+N_2) & (\text{no }\mathcal{D},\text{no }\mathcal{T}).\end{cases} \qquad (6.6.23)$$

The leading order term in Eq. (6.6.23) has also been obtained by Argaman and Zee [29]. (The case $N_1 = N_2$ was given in Ref. [6]).

6.6.2 Conductance fluctuations

To compute the variance of the conductance, we average in two steps: $\langle\cdots\rangle = \langle\langle\cdots\rangle_u\rangle_T$, where $\langle\cdots\rangle_u$ and $\langle\cdots\rangle_T$ are, respectively, the average over the unitary matrices $u_\pm$ and

over the matrices of transmission eigenvalues $T_\pm$. It is convenient to add and subtract $\langle\langle G_{\rm NS}\rangle_u^2\rangle_T$, so that the variance splits up into two parts,

$$\mathrm{var}\, G_{\rm NS} \;=\; \Big\langle \langle G_{\rm NS}\rangle_u^2 \Big\rangle_T - \Big\langle \langle G_{\rm NS}\rangle_u \Big\rangle_T^2 + \Big\langle \langle G_{\rm NS}^2\rangle_u - \langle G_{\rm NS}\rangle_u^2 \Big\rangle_T \,, \qquad (6.6.24)$$

which we evaluate separately.

The first two terms of Eqs. (6.6.24) give the variance of $\langle G_{\rm NS}\rangle_u$ over the distribution of transmission eigenvalues. We calculated $\langle G_{\rm NS}\rangle_u$ in Eq. (6.6.3). Since $\langle G_{\rm NS}\rangle_u$ is a function of the linear statistic $\tau_{1\pm}$ only, we know that its fluctuations are an order $1/N$ smaller than the average. This implies that, to leading order in $1/N$,

$$\begin{aligned}\Big\langle \langle G_{\rm NS}\rangle_u^2 \Big\rangle_T - \Big\langle \langle G_{\rm NS}\rangle_u \Big\rangle_T^2 \;&=\; \sum_{\sigma,\sigma'=\pm} \left\langle \frac{\partial \langle G_{\rm NS}\rangle_u}{\partial\, \tau_{1\sigma}} \right\rangle_T \left\langle \frac{\partial \langle G_{\rm NS}\rangle_u}{\partial\, \tau_{1\sigma'}} \right\rangle_T \mathrm{covar}\,(\tau_{1\sigma}\,,\, \tau_{1\sigma'}) \\ &=\; 8\, G_0^2\, N^2\, (2-\langle\tau_1\rangle_0)^{-4}\, \mathrm{var}\,\tau_1 \;\times \begin{cases} 1 & (\text{without } \mathcal{D}), \\ 2 & (\text{with } \mathcal{D}). \end{cases}\end{aligned} \qquad (6.6.25)$$

We now turn to the third and fourth term of Eq. (6.6.24). These terms involve the variance $\langle G_{\rm NS}^2\rangle_u - \langle G_{\rm NS}\rangle_u^2$ of $G_{\rm NS}$ over $\mathcal{U}(N)$ and subsequently an average over the T_n's. The calculation is similar to that of Sec. 6.5.2. We represent $G_{\rm NS}^2$ by the diagram in Fig. 6-21. The variance with respect to $u_\pm$ is given by the connected diagrams. We distinguish between two types of connected diagrams: (i) diagrams in which the inner and the outer loop are connected by a T-cycle or by a U-cycle, and (ii) diagrams in which the partition of the U-cycles involves a group which consists of a U-cycle from the inner loop and a U-cycle from the outer loop. The diagrams are similar to those of Fig. 6-12, and are omitted. The final result is

$$\begin{aligned}\Big\langle \langle G_{\rm NS}^2\rangle_u - \langle G_{\rm NS}\rangle_u^2 \Big\rangle_T \;&=\; 8\, G_0^2\, (2-\langle\tau_1\rangle_0)^{-6}\, \langle\tau_1\rangle_0^{-2} \Big(4\langle\tau_1\rangle_0^2 - 8\langle\tau_1\rangle_0^3 + 9\langle\tau_1\rangle_0^4 \\ &\quad - 4\langle\tau_1\rangle_0^5 + 2\langle\tau_1\rangle_0^6 - 4\langle\tau_1\rangle_0\langle\tau_2\rangle_0 + 2\langle\tau_1\rangle_0^2\langle\tau_2\rangle_0 \\ &\quad - 2\langle\tau_1\rangle_0^3\langle\tau_2\rangle_0 - 2\langle\tau_1\rangle_0^4\langle\tau_2\rangle_0 + 6\langle\tau_2\rangle_0^2 - 6\langle\tau_1\rangle_0\langle\tau_2\rangle_0^2 \\ &\quad + 3\langle\tau_1\rangle_0^2\langle\tau_2\rangle_0^2 - 4\langle\tau_1\rangle_0\langle\tau_3\rangle_0 + 6\langle\tau_1\rangle^2\langle\tau_3\rangle_0 - 2\langle\tau_1\rangle_0^3\langle\tau_3\rangle_0 \Big) \\ &\quad \times \begin{cases} 2 & (\mathcal{D},\, \text{no } \mathcal{T}), \\ 2 & (\mathcal{T},\, \text{no } \mathcal{D}), \\ 1 & (\text{no } \mathcal{D},\, \text{no } \mathcal{T}). \end{cases}\end{aligned} \qquad (6.6.26)$$

The sum of Eqs. (6.6.25) and (6.6.26) equals $\mathrm{var}\, G_{\rm NS}$, according to Eq. (6.6.24).

In the presence of spin-orbit scattering $\mathrm{var}\, G_{\rm NS}$ is four times as small, according to the translation rule of Sec. 6.4.

We give explicit results for the disordered wire and the chaotic cavity.

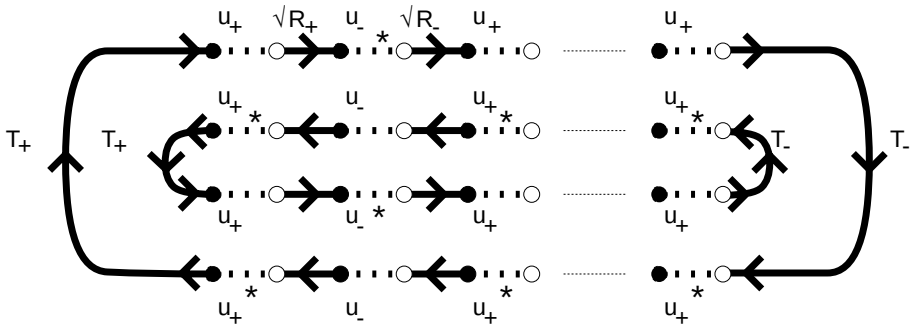

Figure 6-21. Diagrammatic representation of $G_{\rm NS}^2$.

(a) For the disordered wire one has [43, 46]

$$\operatorname{var}\tau_1 = \tfrac{1}{15}N^{-2}, \quad \langle\tau_k\rangle_0 = \tfrac{1}{2}(\ell/L)\Gamma(\tfrac{1}{2})\Gamma(k)/\,\Gamma(k+\tfrac{1}{2}).$$

Substitution into Eqs. (6.6.25) and (6.6.26) yields the variance

$$\operatorname{var} G_{\rm NS}/G_0 = \begin{cases} 16/15 - 48/\pi^4 & \approx 0.574 \quad (\mathcal{D}, \mathcal{T}), \\ 8/15 & \approx 0.533 \quad (\mathcal{D}, \text{no } \mathcal{T}), \\ 8/15 & \approx 0.533 \quad (\mathcal{T}, \text{no } \mathcal{D}), \\ 4/15 & \approx 0.267 \quad (\text{no } \mathcal{D}, \text{no } \mathcal{T}). \end{cases} \tag{6.6.27}$$

The result in the presence of both $\mathcal{T}$ and $\mathcal{D}$ has been taken from Ref. [45, 47]. If both $\mathcal{D}$ and $\mathcal{T}$ are present, breaking $\mathcal{T}$ (or $\mathcal{D}$) reduces the variance by less than 10% [48].

(b) For the chaotic cavity one has the variance $\operatorname{var}\tau_1 = 2N_1^2/\beta N_{\rm tot}^4$ and the third moment $\langle\tau_3\rangle_0 = N_1(N_{\rm tot}^4 - 2N_{\rm tot}^2 N_1 N_2 + 2N_1^2 N_2^2)/N_{\rm tot}^5$ [see Eqs. (6.5.4) and (6.5.42)]. In combination with Eq. (6.6.22) this gives

$$\operatorname{var} G_{\rm NS}/G_0 = \begin{cases} 128N_1^2N_2^2(N_{\rm tot}^4 + 2N_1^2N_2^2)(N_{\rm tot}^2 + 4N_1N_2)^{-4} & (\mathcal{D}, \mathcal{T}), \\ 32N_2^2N_{\rm tot}^2(N_{\rm tot}^2 - N_1N_2)(N_{\rm tot} + N_2)^{-6} & (\mathcal{D}, \text{no } \mathcal{T}), \\ 32N_2^2N_{\rm tot}^2(N_{\rm tot}^2 - N_1N_2)(N_{\rm tot} + N_2)^{-6} & (\mathcal{T}, \text{no } \mathcal{D}), \\ 16N_2^2N_{\rm tot}^2(N_{\rm tot}^2 - N_1N_2)(N_{\rm tot} + N_2)^{-6} & (\text{no } \mathcal{D}, \text{no } \mathcal{T}). \end{cases} \tag{6.6.28}$$

If the coupling between the cavity and the normal metal is weak compared to the coupling to the superconductor ($N_2 \gg N_1$), one finds

$$\operatorname{var} G_{\rm NS}(\mathcal{D}, \mathcal{T})/\operatorname{var} G_{\rm NS}(\mathcal{D}, \text{no } \mathcal{T}) = \mathcal{O}(N_1/N_2)^2.$$

In this case breaking $\mathcal{T}$ greatly enhances the conductance fluctuations. In the opposite case, if the couplings are equal ($N_1 = N_2$), one finds

$$\operatorname{var} G_{\rm NS}(\mathcal{D}, \mathcal{T})/\operatorname{var} G_{\rm NS}(\mathcal{D}, \text{no } \mathcal{T}) = 2187/2084 \approx 1.07.$$

In this case breaking $\mathcal{T}$ has almost no effect on the conductance fluctuations.

6.7 Summary

We developed a diagrammatic technique for the evaluation of integrals of polynomial functions of unitary matrices over the unitary group $\mathcal{U}(N)$. In the large-N limit the number of relevant diagrams is restricted, which allows for the evaluation of integrals over rational functions. We also considered integrals of unitary symmetric matrices, by means of a slight modification of the diagrammatic rules. A translation rule was given to relate integrals of (self-dual) unitary matrices of quaternions to integrals over (symmetric) unitary matrices of complex numbers.

We discussed two applications: A chaotic cavity (quantum dot) with tunnel barriers in the leads and a normal-metal–superconductor (NS) junction. In both cases, the conductance is a rational function of a unitary matrix. In the large-N limit the average conductance is given by a series of ladder diagrams. The weak-localization correction consists of maximally-crossed diagrams. These two types of diagrams are analogous to the diffuson and cooperon diagrams in the diagrammatic perturbation theory for disordered systems [21, 22]. We computed the density of transmission eigenvalues, where the leading order term is given by planar diagrams. Resummation of the diagrams leads to a Dyson equation for the Green function, similar to that encountered in the theory of integrals over Hermitian matrices [12, 17].

For the NS junction, the $\mathcal{O}(1)$ correction to the average conductance is non-zero in the presence of a magnetic field, because of a different type of maximally crossed diagrams. These diagrams are suppressed by a sufficiently large voltage to break electron-hole degeneracy. The new type of maximally crossed diagrams explains the coexistence of weak localization with a magnetic field (see also Sec. 7.2 and the insensitivity of the conductance fluctuations to a magnetic field [48].

Appendix A: Weight factors for polynomial integrals

In Tables 6-2 – 6-5 we list the weight factors $V_{c_1,\ldots,c_k}$ and $W_{c_1,\ldots,c_k}$ for $n = c_1 + \ldots + c_k \leq 5$ for the CUE and the COE. (Tables of V are also given in Refs. [27, 28] for the CUE and in Ref. [31] for the COE.) The weight factors are rational functions of the dimension N of the unitary matrix. The denominators A_n and B_n of, respectively, $V_{c_1,\ldots,c_k}$ and $W_{c_1,\ldots,c_k}$ depend only on n. They are tabulated in Tables 6-2 and 6-3. The numerators $A_n V_{c_1,\ldots,c_k}$ and $B_n W_{c_1,\ldots,c_k}$ are tabulated in Tables 6-4 and 6-5.

n	A_n (CUE)	A_n (COE)
1	N	$N+1$
2	$N(N^2-1)$	$N(N+1)(N+3)$
3	$N(N^2-1)(N^2-4)$	$(N-1)N(N+1)(N+3)(N+5)$
4	$N^2(N^2-1)(N^2-4)(N^2-9)$	$(N-2)(N-1)N(N+1)(N+2)(N+3)$ $\times (N+5)(N+7)$
5	$N^2(N^2-1)(N^2-4)(N^2-9)$ $\times (N^2-16)$	$(N-3)(N-2)(N-1)N(N+1)(N+2)$ $\times (N+3)(N+5)(N+7)(N+9)$

Table 6-2. Denominators A_n of the coefficients $V_{c_1,\ldots,c_k}$ for $n = c_1 + \ldots + c_k \leq 5$.

n	B_n (CUE)	B_n (COE)
1	N	$N+1$
2	$N^2(N^2-1)$	$N(N+1)^2(N+3)$
3	$N^3(N^2-1)(N^2-4)$	$(N-1)N(N+1)^3(N+3)(N+5)$
4	$N^4(N^2-1)^2(N^2-4)(N^2-9)$	$(N-2)(N-1)N^2(N+1)^4(N+2)$ $\times (N+3)^2(N+5)(N+7)$
5	$N^5(N^2-1)^2(N^2-4)(N^2-9)$ $\times (N^2-16)$	$(N-3)(N-2)(N-1)N^2(N+1)^5(N+2)$ $\times (N+3)^2(N+5)(N+7)(N+9)$

Table 6-3. Denominators B_n of the coefficients $W_{c_1,\ldots,c_k}$ for $n = c_1 + \ldots + c_k \leq 5$.

$c_1, \ldots, c_k$	$A_n V_{c_1,\ldots,c_k}$ (CUE)	$A_n V_{c_1,\ldots,c_k}$ (COE)
1	1	1
1, 1	N	$2+N$
2	-1	-1
1, 1, 1	$-2+N^2$	$2+5\,N+N^2$
2, 1	$-N$	$-3-N$
3	2	2
1, 1, 1, 1	$6-8\,N^2+N^4$	$-32-8\,N+28\,N^2+11\,N^3+N^4$
2, 1, 1	$4\,N-N^3$	$-4-18\,N-9\,N^2-N^3$
2, 2	$6+N^2$	$24+7\,N+N^2$
3, 1	$-3+2\,N^2$	$10+12\,N+2\,N^2$
4	$-5\,N$	$-11-5\,N$
1, 1, 1, 1, 1	$78\,N-20\,N^3+N^5$	$128-408\,N-84\,N^2+59\,N^3+16\,N^4+N^5$
2, 1, 1, 1	$-24+14\,N^2-N^4$	$92+38\,N-43\,N^2-14\,N^3-N^4$
2, 2, 1	$-2\,N+N^3$	$56+43\,N+12\,N^2+N^3$
3, 1, 1	$-18\,N+2\,N^3$	$-52+40\,N+22\,N^2+2\,N^3$
3, 2	$-24-2\,N^2$	$-88-18\,N-2\,N^2$
4, 1	$24-5\,N^2$	$-7-36\,N-5\,N^2$
5	$14\,N$	$38+14\,N$

Table 6-4. Numerators $A_n V_{c_1,\ldots,c_k}$ of the coefficients $V_{c_1,\ldots,c_k}$ for $n = c_1 + \ldots + c_k \leq 5$. The denominators A_n are given Table 6-2.

$c_1, \ldots, c_k$	$B_n W_{c_1,\ldots,c_k}$ (CUE)	$B_n W_{c_1,\ldots,c_k}$ (COE)
1	1	1
1, 1	1	2
2	$-N$	$-1-N$
1, 1, 1	8	32
2, 1	$-4\,N$	$-8-8\,N$
3	$2\,N^2$	$2+4\,N+2\,N^2$
1, 1, 1, 1	$-216+144\,N^2$	$-1680+6720\,N+6096\,N^2+1152\,N^3$
2, 1, 1	$72\,N-48\,N^3$	$280-840\,N-2136\,N^2-1208\,N^3-192\,N^4$
2, 2	$-42\,N^2+18\,N^4$	$-140-116\,N+384\,N^2+592\,N^3$ $+268\,N^4+36\,N^5$
3, 1	$-15\,N^2+15\,N^4$	$198\,N+552\,N^2+540\,N^3+216\,N^4+30\,N^5$
4	$5\,N^3-5\,N^5$	$-33\,N-125\,N^2-182\,N^3-126\,N^4$ $-41\,N^5-5\,N^6$
1, 1, 1, 1, 1	$-13824+4224\,N^2$	$-483840+297984\,N+407040\,N^2+67584\,N^3$
2, 1, 1, 1	$3456\,N-1056\,N^3$	$60480+23232\,N-88128\,N^2-59328\,N^3$ $-8448\,N^4$
2, 2, 1	$-1248\,N^2+288\,N^4$	$-12096-21120\,N+1152\,N^2+18432\,N^3$ $+9408\,N^4+1152\,N^5$
3, 1, 1	$-480\,N^2+240\,N^4$	$-3024+192\,N+15072\,N^2+18432\,N^3$ $+7536\,N^4+960\,N^5$
3, 2	$312\,N^3-72\,N^5$	$1512+4152\,N+2496\,N^2-2448\,N^3$ $-3480\,N^4-1320\,N^5-144\,N^6$
4, 1	$56\,N^3-56\,N^5$	$-912\,N-3376\,N^2-4768\,N^3-3168\,N^4$ $-976\,N^5-112\,N^6$
5	$-14\,N^4+14\,N^6$	$114\,N+536\,N^2+1018\,N^3+992\,N^4$ $+518\,N^5+136\,N^6+14\,N^7$

Table 6-5. Numerators $B_n W_{c_1,\ldots,c_k}$ of the coefficients $W_{c_1,\ldots,c_k}$ for $n = c_1 + \ldots + c_k \leq 5$. The denominators B_n are given in Table 6-3.

References

[1] H. A. Weidenmüller, Physica A **167**, 28 (1990).

[2] A. D. Stone, P. A. Mello, K. A. Muttalib, and J.-L. Pichard, in *Mesoscopic Phenomena in Solids*, edited by B. L. Al'tshuler, P. A. Lee, and R. A. Webb (North–Holland, Amsterdam, 1991).

[3] P. A. Mello, in *Mesoscopic Quantum Physics*, edited by E. Akkermans, G. Montambaux, J.-L. Pichard, and J. Zinn-Justin (North-Holland, Amsterdam, 1995).

[4] C. W. J. Beenakker, Rev. Mod. Phys. (July 1997, cond-mat/9612179).

[5] H. U. Baranger and P. A. Mello, Phys. Rev. Lett. **73**, 142 (1994).

[6] R. A. Jalabert, J.-L. Pichard, and C. W. J. Beenakker, Europhys. Lett. **27**, 255 (1994).

[7] F. J. Dyson, J. Math. Phys. **3**, 140 (1962); **3**, 157 (1962).

[8] R. Blümel and U. Smilansky, Phys. Rev. Lett. **60**, 477 (1988); **64**, 241 (1990); U. Smilansky, in *Chaos and Quantum Physics*, edited by M.-J. Giannoni, A. Voros, and J. Zinn-Justin (North-Holland, Amsterdam, 1991).

[9] O. N. Dorokhov, Pis'ma Zh. Eksp. Teor. Fiz. **36**, 259 (1982) [JETP Lett. **36**, 318 (1982)].

[10] P. A. Mello, P. Pereyra, and N. Kumar, Ann. Phys. (N.Y.) **181**, 290 (1988).

[11] L. A. Pastur, Teoret. Mat. Fiz. **10**, 102 (1972) [Theoret. Math. Phys. **10**, 67 (1972)].

[12] A. Pandey, Ann. Phys. (N.Y.) **134**, 110 (1981).

[13] K. B. Efetov, Adv. Phys. **32**, 53 (1983).

[14] J. J. M. Verbaarschot, H. A. Weidenmüller, and M. R. Zirnbauer, Phys. Rep. **129**, 367 (1985).

[15] S. Iida, H. A. Weidenmüller, and J. A. Zuk, Phys. Rev. Lett. **64**, 583 (1990); Ann. Phys. (N.Y.) **200**, 219 (1990).

[16] V. N. Prigodin, K. B. Efetov and S. Iida, Phys. Rev. Lett. **71**, 1230 (1993); Phys. Rev. B **51**, 17223 (1995).

[17] E. Brézin and A. Zee, Phys. Rev. E **49**, 2588 (1994).

[18] A. D. Mirlin, A. Müller-Groeling, and M. R. Zirnbauer, Ann. Phys. (N.Y.) **236**, 325 (1994).

[19] H. U. Baranger and P. A. Mello, Phys. Rev. B **51**, 4703 (1995); Europhys. Lett. **33**, 465 (1996).

[20] W. A. Friedman and P. A. Mello, Ann. Phys. (N.Y.) **161**, 276 (1985).

[21] P. W. Anderson, E. Abrahams, and T. V. Ramakrishnan, Phys. Rev. Lett. **43**, 718 (1979).

[22] L. P. Gor'kov, A. I. Larkin, and D. E. Khmel'nitskiĭ, Pis'ma Zh. Eksp. Teor. Fiz. **30**, 248 (1979) [JETP Lett. **30**, 228 1979].

[23] B. L. Al'tshuler, Pis'ma Zh. Eksp. Teor. Fiz. **41**, 530 (1985) [JETP Lett. **41**, 648 (1985)].

[24] P. A. Lee and A. D. Stone, Phys. Rev. Lett. **55**, 1622 (1985); P. A. Lee, A. D. Stone, and H. Fukuyama, Phys. Rev. B **35**, 1039 (1987).

[25] A. Altland and M. R. Zirnbauer, Phys. Rev. Lett. **76**, 3420 (1996); Phys. Rev. B **55**, 1142 (1997).

[26] M. Creutz, J. Math. Phys. **19**, 2043 (1978).

[27] S. Samuel, J. Math. Phys. **21**, 2695 (1980).

[28] P. A. Mello, J. Phys. A **23**, 4061 (1990).

[29] N. Argaman and A. Zee, Phys. Rev. B **54**, 7406 (1996).

[30] M. L. Mehta, *Random Matrices* (Academic, New York, 1991).

[31] P. A. Mello and T. H. Seligman, Nucl. Phys. A **344**, 489 (1980).

[32] K. Jüngling and R. Oppermann, Z. Phys. B **38**, 93 (1980); R. Oppermann and K. Jüngling, Phys. Lett. A **76**, 449 (1980).

[33] F. Wegner, Z. Phys. B **94**, 297 (1983).

[34] L. K. Hua, *Harmonic Analysis of Functions of Several Complex Variables in the Classical Domains* (Amer. Math. Soc., Providence, 1963).

[35] P. A. Mello, P. Pereyra, and T. H. Seligman, Ann. Phys. (N.Y.) **161**, 254 (1985).

[36] E. Doron and U. Smilansky, Nucl. Phys. A **545**, 455 (1992).

[37] Yu. V. Nazarov, in *Quantum Dynamics of Submicron Structures*, edited by H. A. Cerdeira, B. Kramer, and G. Schön, NATO ASI Series E291 (Kluwer, Dordrecht, 1995).

[38] Yu. V. Nazarov, Phys. Rev. Lett. **73**, 134 (1994).

[39] A. F. Andreev, Zh. Eksp. Teor. Fiz. **46**, 1823 (1964) [Sov. Phys. JETP **19**, 1228 (1964)].

[40] C. W. J. Beenakker, Phys. Rev. B **46**, 12841 (1992).

[41] K. Slevin, J.-L. Pichard, and P. A. Mello, J. Phys. I (France) **6**, 529 (1996).

[42] For a review, see: C. W. J. Beenakker, in *Mesoscopic Quantum Physics*, edited by E. Akkermans, G. Montambaux, J.-L. Pichard, and J. Zinn-Justin (North-Holland, Amsterdam, 1995).

[43] P. A. Mello and A. D. Stone, Phys. Rev. B **44**, 3559 (1991).

[44] C. W. J. Beenakker, Phys. Rev. B **49**, 2205 (1994).

[45] A. M. S. Macêdo and J. T. Chalker, Phys. Rev. B **49**, 4695 (1994).

[46] C. W. J. Beenakker and M. Büttiker, Phys. Rev. B **46**, 1889 (1992).

[47] C. W. J. Beenakker and B. Rejaei, Phys. Rev. B **49**, 7499 (1994).

[48] I. K. Marmorkos, C. W. J. Beenakker, and R. A. Jalabert, Phys. Rev. B **48**, 2811 (1993).

7 Normal-metal–superconductor junctions

7.1 Insensitivity to time-reversal symmetry breaking of universal conductance fluctuations with Andreev reflection

Universal conductance fluctuations (UCF) are a fundamental manifestation of phase-coherent transport in disordered metals [1, 2]. The adjective "universal" describes two aspects of the sample-to-sample fluctuations of the conductance: (1) The variance var G is of order $(e^2/h)^2$, independent of sample size or disorder strength; (2) var G decreases precisely by a factor of two if time-reversal symmetry ($\mathcal{T}$) is broken by a magnetic field. The universality of this factor of two has been established both by diagrammatic perturbation theory [1, 2] and by random-matrix theory [3–6]. In the former approach, one has two classes of diagrams, cooperons and diffusons, which contribute equally to var G in the presence of $\mathcal{T}$. A magnetic field suppresses the cooperons but leaves the diffusons unaffected, hence var G is reduced by $\frac{1}{2}$. In the latter approach, the universality of the factor-of-two reduction follows from the Dyson-Mehta theorem [7], which applies to the variance var A of any observable $A = \sum_n a(T_n)$ which is a linear statistic on the transmission eigenvalues T_n [8]. The crossover from a linear to a quadratic eigenvalue repulsion upon breaking $\mathcal{T}$ directly leads to a reduction by $\frac{1}{2}$ of var A.[1]

The situation is qualitatively different if the normal-metal conductor (N) is attached at one end to a superconductor (S). At the NS interface the dissipative normal current is converted into a dissipationless supercurrent, via the scattering process of Andreev reflection: [9] An electron incident from N is reflected as a hole, with the addition of a Cooper pair to the superconducting condensate. The conversion from normal to supercurrent has essentially no effect on the average conductance, provided that the interface resistance is negligibly small [10]. However, the effect on the conductance fluctuations is striking: The variance is still universally of order $(e^2/h)^2$, but it has become *insensitive* to the breaking of $\mathcal{T}$. Numerical simulations by Marmorkos, Jalabert, and Beenakker [11] of a disordered wire attached to a superconductor have shown that the variance is unaffected by a $\mathcal{T}$-breaking magnetic field, within the 10% statistical uncertainty of the simulations. This does not contradict the Dyson-Mehta theorem, because the conductance $G_{\rm NS}$ of the NS junction is a linear statistic in the presence — but not in the absence of $\mathcal{T}$ [12]. One wonders whether there is some hidden symmetry principle which would constrain var $G_{\rm NS}$ to be the same, regardless of whether $\mathcal{T}$ is broken or not. No such symmetry principle has been found, and in fact we do not know of any successful generalization so far of the theory

[1] Here, and in the rest of the section, we assume that there is no spin-orbit interaction, and that spin-rotation symmetry is maintained both with and without $\mathcal{T}$.

of UCF to quantities which are not linear statistics.[2]

Here we wish to announce that we have succeeded in the analytical calculation of the variance of $G_{\rm NS}$ in the absence of $\mathcal{T}$, using techniques from random-matrix theory. We find that $\mathrm{var}\, G_{\rm NS}$ for a disordered wire attached to a superconductor is reduced by $(2-90/\pi^4)^{-1} \approx 0.929$ upon breaking $\mathcal{T}$. This number is sufficiently close to 1 to be consistent with the numerical simulations [11], and sufficiently different from 1 to explain why attempts to find a rigorous symmetry principle had failed. Still, we have been able to find an approximate symmetry argument, which explains in an intuitively appealing way why the number $(2-90/\pi^4)^{-1}$ is close to 1. Our theory is more generally applicable than to a disordered wire: It applies to any NS junction for which the probability distribution $P(S)$ of the scattering matrix S of the normal region depends only on the transmission eigenvalues T_n. (Such a distribution is called "isotropic" [6].) As two examples we consider a disordered metal grain and a ballistic constriction in a disordered wire. Our method can also be used to compute the effect of a magnetic field on weak-localization in an NS junction, as reported in Sec. 7.2.

Starting point of our calculation is the general relation between the conductance of the NS junction and the scattering matrix S of the normal region [12],

$$\begin{aligned} &G_{\rm NS} = 2G_0\, \mathrm{tr}\, mm^\dagger, \quad G_0 \equiv 2e^2/h, \\ &m = \sqrt{T}(1+u\sqrt{R}u^*\sqrt{R})^{-1}u\sqrt{T}, \quad u \equiv w_2 w_1^*. \end{aligned} \tag{7.1.1}$$

We used the polar decomposition

$$S = \begin{pmatrix} v_1 & 0 \\ 0 & w_1 \end{pmatrix} \begin{pmatrix} \mathrm{i}\sqrt{R} & \sqrt{T} \\ \sqrt{T} & \mathrm{i}\sqrt{R} \end{pmatrix} \begin{pmatrix} v_2 & 0 \\ 0 & w_2 \end{pmatrix}, \tag{7.1.2}$$

where v_1, v_2, w_1, and w_2 are $N \times N$ unitary matrices (N being the number of propagating modes at the Fermi level in each of the two leads attached to the sample). The matrix T is a diagonal matrix with the N transmission eigenvalues $T_i \in [0,1]$ on the diagonal, and $R = 1 - T$. In the presence of $\mathcal{T}$, one has $S = S^{\rm T}$, hence $w_2 = w_1^{\rm T}$, hence $u = 1$. (The superscript T denotes the transpose of the matrix.) Eq. (7.1.1) then simplifies to [12]

$$G_{\rm NS}(\mathcal{T}) = 2G_0 \textstyle\sum_n T_n^2 (2-T_n)^{-2}, \tag{7.1.3}$$

and $\mathrm{var}\, G_{\rm NS}$ follows directly from general formulas for the variance of a linear statistic on the transmission eigenvalues [8, 13]. In the absence of $\mathcal{T}$ no such simplification occurs.

To compute $\mathrm{var}\, G_{\rm NS} = \langle G_{\rm NS}^2 \rangle - \langle G_{\rm NS} \rangle^2$ in the absence of $\mathcal{T}$, we assume an isotropic distribution[3] of S, which implies that the average $\langle \cdots \rangle$ over the ensemble of scattering matrices can be performed in two steps: $\langle \cdots \rangle = \langle \langle \cdots \rangle_u \rangle_T$, where $\langle \cdots \rangle_u$ and $\langle \cdots \rangle_T$ are,

[2] A promising field-theoretic approach to this problem, based on the mapping onto a supersymmetric nonlinear σ-model, has so far not been successful [A. Altland, private communication]. The more conventional diagrammatic perturbation theory suffers form a proliferation of relevant diagrams, and has so far not been completed even in the presence of $\mathcal{T}$ [Y. Takane and H. Ebisawa, J. Phys. Soc. Japan **60**, 3130 (1991)].

[3] The assumption of an isotropic distribution of S is sufficient but not necessary. A weaker assumption which also ensures that the matrix u in Eq. (7.1.1) is uniformly distributed in $\mathcal{U}(N)$ is the so-called "equiv-

respectively, the average over the unitary matrices u and over the transmission eigenvalues T_i. It is convenient to add and subtract $\langle\langle G_{\rm NS}\rangle_u^2\rangle_T$, so that the variance of the conductance splits up into two parts,

$$\begin{aligned}\mathrm{var}\, G_{\rm NS} &= \left\langle \langle G_{\rm NS}\rangle_u^2 \right\rangle_T - \left\langle \langle G_{\rm NS}\rangle_u \right\rangle_T^2 + \\ &\quad \left\langle \langle G_{\rm NS}^2\rangle_u - \langle G_{\rm NS}\rangle_u^2 \right\rangle_T , \end{aligned} \tag{7.1.4}$$

which we evaluate separately.

The first part is the variance of $\langle G_{\rm NS}\rangle_u$ over the distribution of transmission eigenvalues. As a consequence of the isotropy assumption, the matrix u is uniformly distributed in the group $\mathcal{U}(N)$ of $N \times N$ unitary matrices [6]. To evaluate $\langle G_{\rm NS}\rangle_u$ we need to perform an integral over $\mathcal{U}(N)$ of a rational function of u, according to Eq. (7.1.1). Such matrix integrals are notoriously difficult to evaluate in closed form [14], but fortunately we only need the large-N limit. By applying the diagrammatic technique of Ch. 6 we find that

$$\begin{aligned}&\langle \mathrm{tr}\, T(u\sqrt{R}u^*\sqrt{R})^p u T u^\dagger (\sqrt{R}u^{\rm T}\sqrt{R}u^\dagger)^q\rangle_u = \\ &\quad \delta_{pq} N \tau_1^2 (1-\tau_1)^{2p} + \mathcal{O}(1), \end{aligned} \tag{7.1.5}$$

where we have defined the trace $\tau_k = N^{-1}\sum_i T_i^k$. It follows that, up to corrections of order unity,

$$\langle G_{\rm NS}\rangle_u = 2G_0 N \sum_{p=0}^{\infty} \tau_1^2 (1-\tau_1)^{2p} = \frac{2G_0 N \tau_1}{2-\tau_1}. \tag{7.1.6}$$

Since τ_k is a linear statistic, we know that its fluctuations are an order $1/N$ smaller than the average [6]. This implies that, to leading order in $1/N$, $\mathrm{var}\, f(\tau_k) = [f'(\tau_k)]^2 \times \mathrm{var}\,\tau_k$. The variance of Eq. (7.1.6) is therefore

$$\left\langle \langle G_{\rm NS}\rangle_u^2 \right\rangle_T - \left\langle \langle G_{\rm NS}\rangle_u \right\rangle_T^2 = \frac{16 G_0^2 N^2 \mathrm{var}\,\tau_1}{(2-\langle\tau_1\rangle)^4} + \mathcal{O}(1/N). \tag{7.1.7}$$

Note that the leading term in Eq. (7.1.7) is $\mathcal{O}(1)$.

We now turn to the second part of Eq. (7.1.4), which involves the variance $\langle G_{\rm NS}^2\rangle_u - \langle G_{\rm NS}\rangle_u^2$ of $G_{\rm NS}$ over $\mathcal{U}(N)$ at fixed transmission eigenvalues and subsequently an average over the T_i's. The calculation is similar in principle to that described in the preceding paragraph, but many more terms contribute to leading order in $1/N$. Here we only give the result,

$$\begin{aligned}&\left\langle \langle G_{\rm NS}^2\rangle_u - \langle G_{\rm NS}\rangle_u^2 \right\rangle_T \\ &\quad = 16 G_0^2 (2-\langle\tau_1\rangle)^{-6} \langle\tau_1\rangle^{-2} \Big\{ 4\langle\tau_1\rangle^2 - 8\langle\tau_1\rangle^3 + 9\langle\tau_1\rangle^4 - 4\langle\tau_1\rangle^5 + 2\langle\tau_1\rangle^6 - \end{aligned}$$

alent channel assumption" [P. A. Mello and S. Tomsovic, Phys. Rev. Lett. **67**, 342 (1991)]. Microscopic models which satisfy this assumption have been given by O. N. Dorokhov [Phys. Rev. B **37**, 10526 (1988)] and S. Iida, H. A. Weidenmüller, and J. A. Zuk [Ann. Phys. (NY) **200**, 219 (1990)]. See also Sec. 1.3 of this thesis.

$$4\langle\tau_1\rangle\langle\tau_2\rangle + 2\langle\tau_1\rangle^2\langle\tau_2\rangle - 2\langle\tau_1\rangle^3\langle\tau_2\rangle - 2\langle\tau_1\rangle^4\langle\tau_2\rangle + 6\langle\tau_2\rangle^2 - 6\langle\tau_1\rangle\langle\tau_2\rangle^2 + 3\langle\tau_1\rangle^2\langle\tau_2\rangle^2 - 4\langle\tau_1\rangle\langle\tau_3\rangle + 6\langle\tau_1\rangle^2\langle\tau_3\rangle - 2\langle\tau_1\rangle^3\langle\tau_3\rangle\Big\} + \mathcal{O}(1/N). \quad (7.1.8)$$

The sum of Eqs. (7.1.7) and (7.1.8) equals $\mathrm{var}\, G_{\mathrm{NS}}$, according to Eq. (7.1.4). The resulting expression contains only moments of the transmission eigenvalues. This solves the problem of the computation of $\mathrm{var}\, G_{\mathrm{NS}}$ in the absence of $\mathcal{T}$, since these moments are known.

For the application to a disordered wire (length L, mean free path ℓ) one has the variance [2, 5] $N^2 \mathrm{var}\,\tau_1 = \frac{1}{15}$, and averages [15] $\langle\tau_k\rangle = \frac{1}{2}(\ell/L)\Gamma(\frac{1}{2})\Gamma(k)/\,\Gamma(k+\frac{1}{2})$. Substitution into Eqs. (7.1.7) and (7.1.8) yields (in the diffusive limit $\ell/L \to 0$)

$$\mathrm{var}\, G_{\mathrm{NS}}(\text{no } \mathcal{T}) = \tfrac{8}{15} G_0^2 \approx 0.533\, G_0^2. \quad (7.1.9)$$

This is to be compared with the known result [13] in the presence of $\mathcal{T}$

$$\mathrm{var}\, G_{\mathrm{NS}}(\mathcal{T}) = (\tfrac{16}{15} - 48\pi^{-4}) G_0^2 \approx 0.574\, G_0^2. \quad (7.1.10)$$

Breaking $\mathcal{T}$ reduces the variance by less than 10%, as advertised.

We would like to obtain a more direct understanding of why the two numbers in Eqs. (7.1.9) and (7.1.10) are so close. To that end we return to the general expression (7.1.1) for the conductance G_{NS} of an NS junction, in terms of the scattering matrix S of the normal region. We compare G_{NS} with the conductance G_{NN} of an entirely normal metal consisting of two segments in series (see Fig. 7-1). The first segment has scattering matrix S, the second segment is the mirror image of the first. That is to say, the disorder potential is specularly reflected and the sign of the magnetic field is reversed. The system NN thus has a reflection symmetry (S), both in the presence and absence of $\mathcal{T}$. The scattering matrix of the second segment is $\Sigma S \Sigma$, where Σ is a $2N \times 2N$ matrix with zero elements, except for $\Sigma_{i,N+i} = \Sigma_{N+i,i} = 1$ ($i = 1, 2, \ldots, N$). (The matrix Σ interchanges scattering states incident from left and right.) The conductance G_{NN} follows from the transmission matrix through the two segments in series by means of the Landauer formula,

$$G_{\mathrm{NN}}(S) = G_0\, \mathrm{tr}\, m' m'^{\dagger}, \quad m' = \sqrt{T}(1 + u'\sqrt{R}u'\sqrt{R})^{-1}u'\sqrt{T}, \quad u' \equiv w_2 w_1. \quad (7.1.11)$$

The difference between Eqs. (7.1.1) and (7.1.11) is crucial in the presence of $\mathcal{T}$, when $w_2 = w_1^{\mathrm{T}}$, so that $u = 1$ while u' is some random (symmetric) unitary matrix. However, in the absence of $\mathcal{T}$, w_1 and w_2 are independent, so that both u and u' are randomly distributed unitary matrices. We have repeated the calculation of the variance starting from Eq. (7.1.11), and found that $\mathrm{var}\,\mathrm{tr}\, m m^{\dagger} = \mathrm{var}\,\mathrm{tr}\, m' m'^{\dagger}$, hence

$$\mathrm{var}\, G_{\mathrm{NS}}(\text{no } \mathcal{T}) = 4\, \mathrm{var}\, G_{\mathrm{NN}}(S, \text{no } \mathcal{T}). \quad (7.1.12)$$

The system NN is special because it possesses a reflection symmetry. Breaking the reflection symmetry S amounts to the replacement of the mirror-imaged segment by a different segment, with scattering matrix S' which is independent of S but drawn from the same ensemble. Breaking S reduces the variance of the conductance fluctuations by a factor of two, regardless of whether $\mathcal{T}$ is present or not,

$$\mathrm{var}\, G_{\mathrm{NN}}(S) = 2\, \mathrm{var}\, G_{\mathrm{NN}}(\text{no } S). \quad (7.1.13)$$

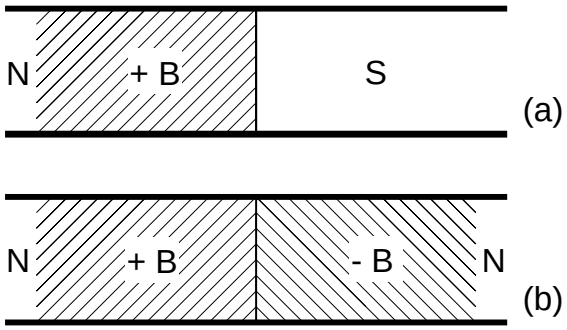

Figure 7-1. (a): Schematic drawing of a disordered normal metal (N) connected to a superconductor (S), in a time-reversal symmetry ($\mathcal{T}$) breaking magnetic field B. In (b) the normal region is connected in series with its mirror image. As indicated, the magnetic field B changes sign upon reflection. The variance of the conductance fluctuations in (a) is exactly four times the variance in (b). The variance in (b) is exactly two times the variance in the absence of the reflection symmetry (S). The exchange of $\mathcal{T}$ for S explains the insensitivity of the conductance fluctuations to a magnetic field, as discussed in the text.

We have checked this relation by an explicit calculation, but it seems intuitively obvious if one considers that the eigenstates separate into even and odd states which fluctuate independently. Since breaking $\mathcal{T}$ by itself reduces the variance of $G_{\rm NN}$ by a factor of two, we may write

$$\mathrm{var}\, G_{\rm NN}(S, \text{no } \mathcal{T}) = \mathrm{var}\, G_{\rm NN}(\mathcal{T}, \text{no } S). \tag{7.1.14}$$

Eqs. (7.1.12)–(7.1.14) are exact, and hold for any isotropic distribution of the scattering matrix. We need one more relationship, which is approximate and holds only for the case of a disordered wire: [12, 16]

$$\mathrm{var}\, G_{\rm NS}(\mathcal{T}) \approx 4\mathrm{var}\, G_{\rm NN}(\mathcal{T}, \text{no } S). \tag{7.1.15}$$

Taken together, Eqs. (7.1.12)–(7.1.15) imply the approximate relationship

$$\mathrm{var}\, G_{\rm NS}(\mathcal{T}) \approx \mathrm{var}\, G_{\rm NS}(\text{no } \mathcal{T}). \tag{7.1.16}$$

The exact calculation shows that the approximation is accurate within 10%. We now understand the insensitivity of the conductance fluctuations of a (disordered) NS-junction to a magnetic field as an *exchange of symmetries* in the related normal system NN: As $\mathcal{T}$ is broken, S is established, thereby compensating the reduction of $\mathrm{var}\, G_{\rm NS}$.[4]

We have emphasized the general applicability of equations (7.1.7), (7.1.8) and (7.1.12)–(7.1.14), which hold not just for a disordered wire, but for any isotropic distribution of the scattering matrix. We illustrate this by two examples. The first is an NS junction

[4]To avoid misunderstanding about the "exchange of symmetries", we stress that it refers to the related NN system and not to the NS junction itself. To be precise, the structure of the scattering matrix of the NS junction is such that the NS junction in the absence of $\mathcal{T}$ is related to an NN system *with* S, whereas in the presence of $\mathcal{T}$ it is related to an NN system *without* S. The first relationship is exact [Eq. (7.1.12)], the second one is approximate [Eq. (7.1.15)].

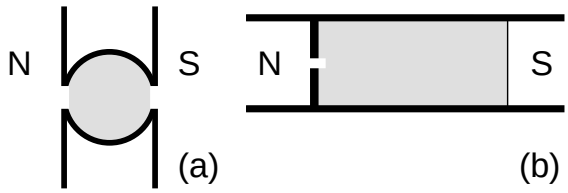

Figure 7-2. (a): Schematic drawing of an NS junction consisting of a disordered metal grain (shaded). (b): A disordered normal-metal wire (shaded) containing a point contact.

consisting of a disordered metal grain (see Fig. 7-2a). The coupling of N and S to the grain occurs via ballistic point contacts (width much smaller than the mean free path in the grain). Following Ref. [17], we may assume that the scattering matrix of the grain is distributed according to the circular ensemble of random-matrix theory. This is an isotropic distribution. The relevant moments of the transmission eigenvalues in the absence of $\mathcal{T}$ are [17] $\langle\tau_k\rangle = \pi^{-1/2}\Gamma(k+\frac{1}{2})/\,\Gamma(k+1)$, $N^2\mathrm{var}\,\tau_1 = \frac{1}{16}$. Substitution into the general formulas (7.1.7) and (7.1.8) yields

$$\mathrm{var}\,G_{\mathrm{NS}}(\text{no }\mathcal{T}) = \tfrac{128}{243}G_0^2 \approx 0.527\,G_0^2, \tag{7.1.17}$$

which is again close to the known result in the presence of $\mathcal{T}$ [17],

$$\mathrm{var}\,G_{\mathrm{NS}}(\mathcal{T}) = \tfrac{9}{16}G_0^2 \approx 0.563\,G_0^2. \tag{7.1.18}$$

The second example is a ballistic constriction (point contact) in a wire which is connected to a superconductor (see Fig. 7-6b). The point contact has conductance N_0G_0, which we assume to be much smaller than the conductance $N\ell/L$ of the disordered wire by itself. As discussed in Ref. [18], we may assume an isotropic distribution of the scattering matrix of the combined system (point contact plus disordered wire). The moments of the transmission eigenvalues are [18] $\langle\tau_k\rangle = N_0/N$, $N^2\mathrm{var}\,\tau_1 = \mathcal{O}(N_0L/N\ell)^2$. Substitution into Eqs. (7.1.7) and (7.1.8) yields, in the limit $N_0L/N\ell \to 0$,

$$\mathrm{var}\,G_{\mathrm{NS}}(\text{no }\mathcal{T}) = \tfrac{1}{2}G_0^2. \tag{7.1.19}$$

In contrast, if $\mathcal{T}$ is not broken, the conductance fluctuations are suppressed in this limit: [18, 19]

$$\mathrm{var}\,G_{\mathrm{NS}}(\mathcal{T}) = \mathcal{O}(N_0L/N\ell)^2 \ll G_0^2. \tag{7.1.20}$$

In this geometry a magnetic field greatly enhances the conductance fluctuations. The reason that a disordered wire with a constriction behaves so differently from an unconstricted wire, is that the relation (7.1.15) does not hold in the presence of a constriction. However, the general relationship (7.1.12) does hold, and indeed the result (7.1.19) is four times the variance of a structure consisting of two point contacts in series with a reflection symmetry.

In summary, we have solved the problem of universal conductance fluctuations in normal-metal–superconductor junctions in a magnetic field, under the assumption of an isotropic distribution of the scattering matrix of the normal region. We find that the structure of

the scattering matrix of the normal-metal–superconductor junction in the absence of time-reversal symmetry allows one to relate the conductance fluctuations to those of a normal system with reflection symmetry. This reflection symmetry is absent in the presence of time-reversal symmetry. It compensates the reduction of the conductance fluctuations due to breaking of time-reversal symmetry, and explains the anomalous insensitivity of the fluctuations in a magnetic field discovered in computer simulations [11].

7.2 Weak localization coexisting with a magnetic field in a normal-metal–superconductor microbridge

Weak localization is a quantum correction of order e^2/h to the classical conductance of a metal [20]. The word "localization" refers to the negative sign of the correction,[5] while the adjective "weak" indicates its smallness. In a wire geometry the weak-localization correction takes on the universal value [21] $\delta G = -\frac{2}{3}e^2/h$ at zero temperature, independent of the wire length L or mean free path ℓ.[6] The classical (Drude) conductance $G_0 \simeq (N\ell/L)\, e^2/h$ is much greater than δG in the metallic regime, where the number of scattering channels $N \gg L/\ell$. Theoretically, the weak-localization correction is the term of order N^0 in an expansion of the average conductance $\langle G\rangle = G_0 + \delta G + \mathcal{O}(N^{-1})$ in powers of N. Experimentally, δG is measured by application of a weak magnetic field B, which suppresses the weak-localization correction but leaves the classical conductance unaffected [22]. The suppression occurs because weak localization requires time-reversal symmetry ($\mathcal{T}$). In the absence of $\mathcal{T}$, quantum corrections to G_0 are of order N^{-1} and not of order N^0. As a consequence, the magnetoconductance has a dip around $B = 0$ of magnitude δG and width of order B_c (being the field at which one flux quantum penetrates the conductor).

What happens to weak localization if the normal-metal wire is attached at one end to a superconductor? This problem has been the subject of active research [11, 12, 23–27]. The term G_0 of order N is unaffected by the presence of the superconductor [12]. The $\mathcal{O}(N^0)$ correction δG is increased but remains universal [24, 25],

$$\delta G = -(2 - 8\pi^{-2})\, e^2/h \approx -1.19\, e^2/h. \tag{7.2.1}$$

In all previous analytical work zero magnetic field was assumed. It was surmised, either implicitly or explicitly [11], that $\delta G = 0$ in the absence of $\mathcal{T}$ — but this was never actually calculated analytically. We have now succeeded in doing this calculation and would like to report the result, which was entirely unexpected.

We find that a magnetic field by itself is not sufficient to suppress the weak-localization correction, but only reduces δG by about a factor of two. To achieve $\delta G = 0$ requires in addition the application of a sufficiently large voltage V to break the degeneracy in energy

[5] Spin-orbit scattering is assumed to be negligible, otherwise a positive quantum correction appears.

[6] The restriction to a wire geometry is essential for the universality. In a square or cube geometry, the weak-localization correction is L and ℓ-dependent.

$-\delta G\,[e^2/h]$	$\mathcal{T}$	no $\mathcal{T}$
$\mathcal{D}$	$2-8/\pi^2$	$2/3$
no $\mathcal{D}$	$4/3$	0

Table 7-1. Dependence of the weak-localization correction δG of a normal-metal wire attached to a superconductor on the presence or absence of time-reversal symmetry ($\mathcal{T}$) and electron hole-degeneracy ($\mathcal{D}$). The entry in the upper left corner was computed in Refs. [24, 25].

between the electrons (at energy eV above the Fermi energy E_F) and the Andreev-reflected holes (at energy eV below E_F). The electron-hole degeneracy ($\mathcal{D}$) is effectively broken when eV exceeds the Thouless energy $E_c = \hbar v_F \ell/L^2$ (with v_F the Fermi velocity). Weak localization coexists with a magnetic field as long as $eV \ll E_c$. Our analytical results are summarized in Table 7-1. These results disagree with the conclusions drawn in Ref. [11] on the basis of numerical simulations. We have found that the numerical data on the weak-localization effect was misinterpreted due to the presence of a magnetic-field dependent contact resistance, which was not understood at that time.

Starting point of our calculation is the general relation between the differential conductance $G = dI/dV$ of the normal-metal–superconductor (NS) junction and the transmission and reflection matrices of the normal region [12],

$$G = (4e^2/h)\,\mathrm{tr}\, m(eV)m^\dagger(eV), \quad m(\varepsilon) = t'(\varepsilon)\left[1-\alpha(\varepsilon)r^*(-\varepsilon)r(\varepsilon)\right]^{-1} t^*(-\varepsilon), \quad (7.2.2)$$

where $\alpha(\varepsilon) \equiv \exp[-2\mathrm{i}\arccos(\varepsilon/\Delta)]$. Eq. (7.2.2) holds for subgap voltages $V \leq \Delta/e$, and requires also $\Delta \ll E_F$ (Δ being the excitation gap in S). We assume that the length L of the disordered normal region is much greater than the superconducting coherence length $\xi = (\hbar v_F \ell/\Delta)^{1/2}$. This implies that the Thouless energy $E_c \ll \Delta$. In the voltage range $V \lesssim E_c/e$ we may therefore assume that $eV \ll \Delta$, hence $\alpha = -1$. The $N \times N$ transmission and reflection matrices t, t', r, and r' form the scattering matrix $S(\epsilon)$ of the disordered normal region (N being the number of propagating modes at the Fermi level, which corresponds to $\varepsilon = 0$). It is convenient to use the polar decomposition

$$\begin{pmatrix} r' & t' \\ t & r \end{pmatrix} = \begin{pmatrix} v_1 & 0 \\ 0 & w_1 \end{pmatrix} \begin{pmatrix} \mathrm{i}\sqrt{R} & \sqrt{T} \\ \sqrt{T} & \mathrm{i}\sqrt{R} \end{pmatrix} \begin{pmatrix} v_2 & 0 \\ 0 & w_2 \end{pmatrix}.$$

Here v_1, v_2, w_1, and w_2 are $N \times N$ unitary matrices, T is a diagonal matrix with the N transmission eigenvalues $T_i \in [0,1]$ on the diagonal, and $R = 1 - T$. Using this decomposition, and substituting $\alpha = -1$, Eq. (7.2.2) can be replaced by

$$\begin{aligned} m(\varepsilon) &= \sqrt{T(\varepsilon)}\left[1 + u(\varepsilon)\sqrt{R(-\varepsilon)}u^*(-\varepsilon)\sqrt{R(\varepsilon)}\right]^{-1} u(\varepsilon)\sqrt{T(-\varepsilon)}, \qquad (7.2.3)\\ u(\varepsilon) &\equiv w_2(\varepsilon)w_1^*(-\varepsilon). \end{aligned}$$

We perform our calculations in the general framework of random-matrix theory. The only assumption about the distribution of the scattering matrix that we make, is that it is

isotropic, i.e. that it depends only on the transmission eigenvalues [6]. In the presence of $\mathcal{T}$ (for $B \ll B_c$), $S = S^{\mathrm{T}}$, hence $w_1 = w_2^{\mathrm{T}}$. (The superscript T denotes the transpose of a matrix.) If $\mathcal{T}$ is broken, w_1 and w_2 are independent. In the presence of $\mathcal{D}$ (for $eV \ll E_c$), the difference between $S(eV)$ and $S(-eV)$ may be neglected. If $\mathcal{D}$ is broken, $S(eV)$ and $S(-eV)$ are independent. Of the four entries in Table 7-1, the case that both $\mathcal{T}$ and $\mathcal{D}$ are present is the easiest, because then $u = 1$ and Eq. (7.2.2) simplifies to [12]

$$G = (4e^2/h)\textstyle\sum_n T_n^2 (2 - T_n)^{-2}. \tag{7.2.4}$$

The conductance is of the form $G = \sum_n f(T_n)$, known as a linear statistic on the transmission eigenvalues. General formulas [24, 25] for the weak-localization correction to the average of a linear statistic lead directly to Eq. (7.2.1). The three other entries in Table 7-1, where either $\mathcal{T}$ or $\mathcal{D}$ (or both) are broken, are more difficult because G is no longer a linear statistic. We consider these three cases in separate paragraphs.

(1) $\mathcal{D}$, no $\mathcal{T}$ — Because of the isotropy assumption, w_1 and w_2, and hence u, are uniformly distributed in the unitary group $\mathcal{U}(N)$. We may perform the average $\langle\cdots\rangle$ over the ensemble of scattering matrices in two steps: $\langle\cdots\rangle = \langle\langle\cdots\rangle_u\rangle_T$, where $\langle\cdots\rangle_u$ and $\langle\cdots\rangle_T$ are, respectively, the average over the unitary matrix u and over the transmission eigenvalues T_i. We compute $\langle\cdots\rangle_u$ by an expansion in powers of N^{-1}. To integrate the rational function (7.2.2) of u over $\mathcal{U}(N)$, we first expand it into a geometric series and then use the diagrammatic technique of Ch. 6. The polynomials we need are

$$\begin{aligned} \langle G\rangle_u &= \frac{4e^2}{h} \sum_{p,q=0}^{\infty} M_{pq}(-1)^{p+q}, \\ M_{pq} &= \langle \mathrm{tr}\, T(u\sqrt{R}u^*\sqrt{R})^p u T u^\dagger (\sqrt{R}u^{\mathrm{T}}\sqrt{R}u^\dagger)^q\rangle_u. \end{aligned} \tag{7.2.5}$$

Neglecting terms of order N^{-1}, we find

$$M_{pq} = \begin{cases} N\tau_1^2(1-\tau_1)^{2p} \text{ if } p = q, \\ \tau_1(\tau_1^2 + \tau_1 - 2\tau_2)(1-\tau_1)^{p+q-1} - 2\min(p,q) \\ \quad \times \tau_1^2(\tau_1^2 - \tau_2)(1-\tau_1)^{p+q-2} \text{ if } |p-q| \text{ odd}, \\ 0 \text{ else}, \end{cases}$$

where we have defined the moment $\tau_k = N^{-1}\sum_i T_i^k$. The summation over p and q leads to

$$\frac{h}{4e^2}\langle G\rangle_u = \frac{N\tau_1}{2-\tau_1} - \frac{4\tau_1 - 2\tau_1^2 + 2\tau_1^3 - 4\tau_2}{\tau_1(2-\tau_1)^3}. \tag{7.2.6}$$

It remains to average over the transmission eigenvalues. Since τ_k is a linear statistic, we know that its sample-to-sample fluctuations $\delta\tau_k \equiv \tau_k - \langle\tau_k\rangle$ are an order $1/N$ smaller than the average [6]. Hence

$$\langle f(\tau_k)\rangle_T = f(\langle\tau_k\rangle)[1 + \mathcal{O}(N^{-2})], \tag{7.2.7}$$

which implies that we may replace the average of the rational function (7.2.6) of the τ_k's by the rational function of the average $\langle\tau_k\rangle$. This average has the $1/N$ expansion

$$\langle\tau_k\rangle = \langle\tau_k\rangle_0 + \mathcal{O}(N^{-2}), \tag{7.2.8}$$

where $\langle\tau_k\rangle_0$ is $\mathcal{O}(N^0)$. There is no term of order N^{-1} in the absence of $\mathcal{T}$. From Eqs. (7.2.6)–(7.2.8) we obtain the $1/N$ expansion of the average conductance,

$$\frac{h}{4e^2}\langle G\rangle = \frac{N\langle\tau_1\rangle_0}{2-\langle\tau_1\rangle_0} - \frac{4\langle\tau_1\rangle_0 - 2\langle\tau_1\rangle_0^2 + 2\langle\tau_1\rangle_0^3 - 4\langle\tau_2\rangle_0}{\langle\tau_1\rangle_0(2-\langle\tau_1\rangle_0)^3} + \mathcal{O}(N^{-1}). \tag{7.2.9}$$

Eq. (7.2.9) is generally valid for any isotropic distribution of the scattering matrix. We apply it to the case of a disordered wire in the limit $N\to\infty$, $\ell/L\to 0$ at constant $N\ell/L$. The moments $\langle\tau_k\rangle_0$ are given by [21]

$$\langle\tau_1\rangle_0 = \ell/L,\ \langle\tau_2\rangle_0 = \tfrac{2}{3}\ell/L. \tag{7.2.10}$$

Substitution into Eq. (7.2.9) yields the weak-localization correction $\delta G = -\frac{2}{3}e^2/h$, cf. Table 7-1.

(2) $\mathcal{T}$, no $\mathcal{D}$ — In this case one has $u^\dagger(-eV) = u(eV)$ and $u(eV)$ is uniformly distributed in $\mathcal{U}(N)$. A calculation similar to that in the previous paragraph yields for the average over u:

$$\begin{aligned}\frac{h}{4e^2}\langle G\rangle_u = {} & N\tau_{1+}\tau_{1-}(\tau_{1+}+\tau_{1-}-\tau_{1+}\tau_{1-})^{-1} + (\tau_{1+}+\tau_{1-}-\tau_{1+}\tau_{1-})^{-3} \\ & \times\Big[2\tau_{1+}^2\tau_{1-}^2 - \tau_{1+}^3\tau_{1-}^2 - \tau_{1+}^2\tau_{1-}^3 - \tau_{2+}\tau_{1-}^2 - \tau_{1+}^2\tau_{2-} + \tau_{2+}\tau_{1-}^3 + \tau_{1+}^3\tau_{2-}\Big],\end{aligned}$$

where we have abbreviated $\tau_{k\pm} = \tau_k(\pm eV)$. The next step is the average over the transmission eigenvalues. We may still use Eq. (7.2.7), and we note that $\langle\tau_k(\varepsilon)\rangle \equiv \langle\tau_k\rangle$ is independent of ε. (The energy scale for variations in $\langle\tau_k(\varepsilon)\rangle$ is E_F, which is much greater than the energy scale of interest E_c.) Instead of Eq. (7.2.8) we now have the $1/N$ expansion

$$\langle\tau_k\rangle = \langle\tau_k\rangle_0 + N^{-1}\delta\tau_k + \mathcal{O}(N^{-2}), \tag{7.2.11}$$

which contains also a term of order N^{-1} because of the presence of $\mathcal{T}$. The $1/N$ expansion of $\langle G\rangle$ becomes

$$\begin{aligned}\frac{h}{4e^2}\langle G\rangle \;=\; & \frac{N\langle\tau_1\rangle_0}{2-\langle\tau_1\rangle_0} + \frac{2\delta\tau_1}{(2-\langle\tau_1\rangle_0)^2} + \frac{2\langle\tau_1\rangle_0^2 - 2\langle\tau_1\rangle_0^3 - 2\langle\tau_2\rangle_0 + 2\langle\tau_1\rangle_0\langle\tau_2\rangle_0}{\langle\tau_1\rangle_0(2-\langle\tau_1\rangle_0)^3} \\ & + \mathcal{O}(N^{-1}).\end{aligned} \tag{7.2.12}$$

For the application to a disordered wire we use again Eq. (7.2.10) for the moments $\langle\tau_k\rangle_0$, which do not depend on whether $\mathcal{T}$ is broken or not. We also need $\delta\tau_1$, which in the presence of $\mathcal{T}$ is given by [21] $\delta\tau_1 = -\frac{1}{3}$. Substitution into Eq. (7.2.12) yields $\delta G = -\frac{4}{3}e^2/h$, cf. Table 7-1.

(3) no $\mathcal{T}$, no $\mathcal{D}$ — Now $u(eV)$ and $u(-eV)$ are independent, each with a uniform distribution in $\mathcal{U}(N)$. Carrying out the two averages over $\mathcal{U}(N)$ we find

$$\frac{h}{4e^2}\,\langle G\rangle_u = \frac{N\tau_{1+}\tau_{1-}}{\tau_{1+}+\tau_{1-}-\tau_{1+}\tau_{1-}}. \tag{7.2.13}$$

The average over the transmission eigenvalues becomes

$$\frac{h}{4e^2}\,\langle G\rangle = \frac{N\langle\tau_1\rangle_0}{2-\langle\tau_1\rangle_0} + \mathcal{O}(N^{-1}), \tag{7.2.14}$$

where we have used that $\delta\tau_1 = 0$ because of the absence of $\mathcal{T}$. We conclude that $\delta G = 0$ in this case, as indicated in Table 7-1.

This completes the calculation of the weak-localization correction to the average conductance. Our results, summarized in Table 7-1, imply a universal B and V-dependence of the conductance of an NS microbridge. Raising first B and then V leads to two subsequent increases of the conductance, while raising first V and then B leads first to a decrease and then to an increase.

So far we have only considered the $\mathcal{O}(N^0)$ correction δG to $\langle G\rangle = G_0 + \delta G$. What about the $\mathcal{O}(N)$ term G_0? From Eqs. (7.2.9), (7.2.12), and (7.2.14) we see that if either $\mathcal{T}$ or $\mathcal{D}$ (or both) are broken,

$$G_0 = \frac{4e^2}{h}\,\frac{N\langle\tau_1\rangle_0}{2-\langle\tau_1\rangle_0} = (2e^2/h)\,N\left(\tfrac{1}{2}+L/\ell\right)^{-1}. \tag{7.2.15}$$

In the second equality we substituted [21] $\langle\tau_1\rangle_0 = (1+L/\ell)^{-1}$, which in the limit $\ell/L \to 0$ reduces to Eq. (7.2.10). If both $\mathcal{T}$ and $\mathcal{D}$ are unbroken, then we have instead the result [28]

$$G_0 = (2e^2/h)\,N\,[1+L/\ell+\mathcal{O}(\ell/L)]^{-1}. \tag{7.2.16}$$

The difference between Eqs. (7.2.15) and (7.2.16) is a contact resistance, which has the value $h/4Ne^2$ in Eq. (7.2.15) but is twice as large in Eq. (7.2.16). In contrast, in a normal-metal wire the contact resistance is $h/2Ne^2$, independent of B or V. The B and V-dependent contact resistance in an NS junction is superimposed on the B and V-dependent weak-localization correction. Since the contribution to $\langle G\rangle$ from the contact resistance is of order $(e^2/h)N(\ell/L)^2$, while the weak-localization correction is of order e^2/h, the former can only be ignored if $N(\ell/L)^2 \ll 1$. This is an effective restriction to the diffusive metallic regime, where $\ell/L \ll 1$ and $N\ell/L \gg 1$. To measure the weak-localization effect without contamination from the contact resistance if $N(\ell/L)^2$ is not $\ll 1$, one has two options: (1) Measure the B-dependence at fixed $V \gg E_c/e$; (2) Measure the V-dependence at fixed $B \gg B_c$. In both cases we predict an increase of the conductance, by an amount $\frac{4}{3}e^2/h$ and $\frac{2}{3}e^2/h$, respectively. In contrast, in the normal state weak localization leads to a B-dependence, but not to a V-dependence.

We performed numerical simulations similar to those of Ref. [11] in order to test the analytical predictions. The disordered normal region was modeled by a tight-binding Hamiltonian on a square lattice (lattice constant a), with a random impurity potential at each site

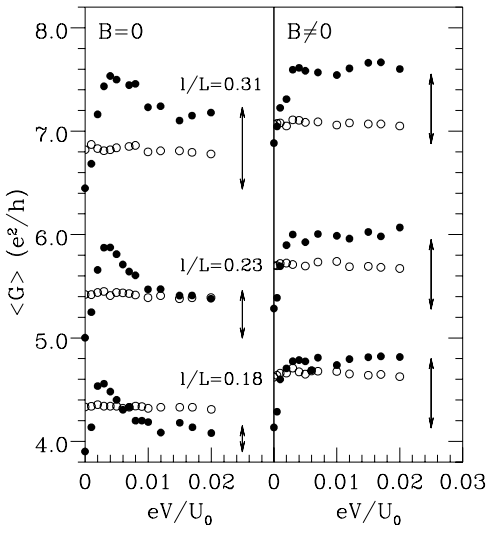

Figure 7-3. Numerical simulation of the voltage dependence of the average differential conductance for $B = 0$ (left panel) and for a flux $6\,h/e$ through the disordered normal region (right panel). The filled circles are for an NS junction; the open circles represent the V-independent conductance in the normal state. The three sets of data points correspond, from top to bottom, to $\ell/L = 0.31$, 0.23, and 0.18, respectively. The arrows indicate the theoretically predicted net increase of $\langle G\rangle$ between $V = 0$ and $V \gg E_c/e$.

(uniformly distributed between $\pm\frac{1}{2}U_d$). The Fermi energy was chosen at $E_F = 1.57U_0$ from the band bottom ($U_0 = \hbar^2/2ma^2$). The length L and width W of the disordered region are $L = 167a$, $W = 35a$, corresponding to $N = 15$ propagating modes at E_F. The mean free path is obtained from the conductance $G = (2e^2/h)N(1 + L/\ell)^{-1}$ of the normal region in the absence of $\mathcal{T}$. The scattering matrix of the normal region was computed numerically at $\varepsilon = \pm eV$, and then substituted into Eq. (7.2.2) to obtain the differential conductance.

In Fig. 7-3 we show the V-dependence of G (averaged over some 10^3 impurity configurations), for three values of ℓ. The left panel is for $B = 0$, the right panel for a flux of $6\,h/e$ through the disordered region. The V-dependence for $B = 0$ is mainly due to the contact resistance effect of order $N(\ell/L)^2$, and indeed one sees that the amount by which G increases depends significantly on ℓ.[7] The V-dependence in a $\mathcal{T}$-violating magnetic field is entirely due to the weak-localization effect, which should be insensitive to ℓ (as long as $\ell/L \ll 1 \ll N\ell/L$). This is indeed observed in the simulation. Quantitatively, we would expect that application of a voltage increases $\langle G\rangle$ by an amount $\frac{2}{3}e^2/h$ for the three curves in the right panel, which agrees very well with what is observed. In the absence of a magnetic field the analytical calculation predicts a net increase in $\langle G\rangle$ by 0.79, 0.46, and $0.25 \times e^2/h$ (from top to bottom), which is again in good agreement with the simulation.

[7] Our analytical calculation refers to the net increase of $\langle G\rangle$ between $V = 0$ and $V \gg E_c/e$. We can not describe the non-monotonic V-dependence at intermediate V, observed in the simulation for $B = 0$.

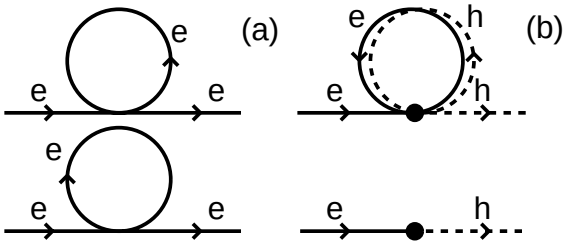

Figure 7-4. (a) Two Feynman paths interfering constructively in the presence of $\mathcal{T}$. (b) Two paths involving Andreev reflection (solid dot), which interfere destructively both in the presence and absence of $\mathcal{T}$.

In normal metals, the weak-localization correction δG is explained in terms of constructive interference of pairs of time-reversed Feynman paths (Fig. 7-4a) [22]. This interference is destroyed by a magnetic field. One might wonder what kind of interfering paths are responsible for δG in an NS junction without $\mathcal{T}$. Although our theory is not formulated in terms of Feynman paths, an interpretation of the quantity M_{pq} in Eq. (7.2.5) using Feynman paths is possible. The two simplest interfering paths are shown in Fig. 7-4b. Regardless of whether $\mathcal{T}$ is broken or not, there is an exact cancellation of the phase shifts accumulated by the electron and the hole which traverse the loop in the same direction. What remains is a phase shift of π due to the double Andreev reflection. As a consequence, the path with the double loop interferes destructively with the path without a loop, giving rise to a negative δG.

7.3 Phase-dependent magnetoconductance fluctuations in a chaotic Josephson junction

The conductance of a mesoscopic metal shows small fluctuations of universal size e^2/h as a function of magnetic field [1, 2]. These universal conductance fluctuations are sample-specific, which is why a plot of conductance G versus magnetic field B is called a "magnetofingerprint". The magnetoconductance is sample-specific because it depends sensitively on scattering phase shifts, and hence on the precise configuration of scatterers. Any agency which modifies phase shifts will modify the magnetoconductance. Altshuler and Spivak [29] first proposed to use a Josephson junction for this purpose. If the metal is connected to two superconductors with a phase difference ϕ of the order parameter, the conductance $G(B, \phi)$ contains two types of sample-specific fluctuations: aperiodic fluctuations as a function of B and 2π-periodic fluctuations as a function of ϕ. The magnetic field should be sufficiently large to break time-reversal symmetry, otherwise the sample-specific fluctuations will be obscured by a much stronger B- and ϕ-dependence of the ensemble-averaged conductance [10].[8]

[8] Sample-specific conductance fluctuations at zero magnetic field have been observed experimentally by P. G. N. de Vegvar, T. A. Fulton, W. H. Mallison, and R. E. Miller, Phys. Rev. Lett. **73**, 1416 (1994).

In a recent Letter, Den Hartog et al [30]. reported the experimental observation of phase-dependent magnetoconductance fluctuations in a T-shaped two-dimensional electron gas. The horizontal arm of the T is connected to two superconductors, the vertical arm to a normal metal reservoir. The observed magnitude of the fluctuations was much smaller than e^2/h, presumably because the motion in the T-junction was nearly ballistic. Larger fluctuations are expected if the arms of the T are closed, leaving only a small opening (a point contact) for electrons to enter or leave the junction. Motion in the junction can be ballistic or diffusive, as long as it is chaotic the statistics of the conductance fluctuations will only depend on the number of modes in the point contacts and not on the microscopic details of the junction.

In this section we present a theory for phase-dependent magnetoconductance fluctuations in a chaotic Josephson junction. We distinguish two regimes, depending on the relative magnitude of the number of modes M and N in the point contacts to the superconductors and normal metals respectively. For $M \gg N$ the ϕ-dependence of the conductance is strongly anharmonic. This is the regime studied by Altshuler and Spivak [29]. For $M \lesssim N$ the oscillations are nearly sinusoidal, as observed by Den Hartog et al [30]. The difference between the two regimes can be understood qualitatively in terms of interfering Feynman paths. In the regime $M \lesssim N$ only paths with a single Andreev reflection contribute to the conductance. Each such path depends on ϕ with a phase factor $e^{\pm i\phi/2}$. Interference of these paths yields a sinusoidal ϕ-dependence of the conductance. In the opposite regime $M \gg N$, quasiparticles undergo many Andreev reflections before leaving the junction. Hence higher harmonics appear, and the conductance becomes a random 2π-periodic function of ϕ.

The system under consideration is shown schematically in Fig. 7-5. It consists of a chaotic cavity in a time-reversal-symmetry breaking magnetic field B, which is coupled to two superconductors and to one or two normal metals by ballistic point contacts. The superconductors (S_1 and S_2) have the same voltage (defined as zero) and a phase difference ϕ. The conductance of this Josephson junction is measured in a three- or four-terminal configuration. In the three-terminal configuration (Fig. 7-5a), a current I flows from a normal metal N_1 into the superconductors. The conductance $G = I/V_1$ is the ratio of I and the voltage difference V_1 between N_1 and S_1, S_2. This corresponds to the experiment of Den Hartog et al [30]. In the four-terminal configuration (Fig. 7-5b), a current I flows from a normal metal N_1 into another metal N_2. The conductance $G = I/(V_1 - V_2)$ now contains the voltage difference between N_1 and N_2. This is the configuration studied by Altshuler and Spivak [29].

Following Ref. [30] we split the conductance $G(B,\phi) = G_0(B) + G_\phi(B,\phi)$ into a ϕ-independent background

$$G_0(B) \;=\; \int_0^{2\pi} \frac{d\phi}{2\pi}\, G(B,\phi), \tag{7.3.1}$$

plus 2π-periodic fluctuations G_ϕ. In the absence of time-reversal symmetry, the ensemble average $\langle G(B,\phi)\rangle \equiv \langle G\rangle$ is independent of B and ϕ. Hence $\langle G_0(B)\rangle = \langle G\rangle$ and

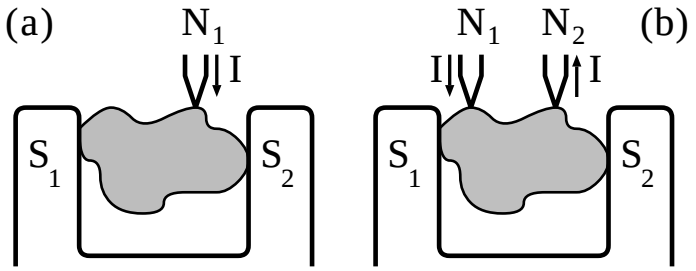

Figure 7-5. Josephson junction in a three-terminal (a) and four-terminal (b) configuration.

$\langle G_\phi(B,\phi)\rangle = 0$. The correlator of G is

$$C(\delta B,\delta\phi) = \langle G(B,\phi)G(B+\delta B,\phi+\delta\phi)\rangle - \langle G\rangle^2. \tag{7.3.2}$$

Fluctuations of the background conductance are described by the correlator of G_0,

$$\begin{aligned} C_0(\delta B) &= \langle G_0(B)G_0(B+\delta B)\rangle - \langle G\rangle^2 \\ &= \int_0^{2\pi}\frac{d\delta\phi}{2\pi}\,C(\delta B,\delta\phi). \end{aligned} \tag{7.3.3}$$

(In the second equality we used that $\langle G_\phi G_0\rangle = 0$.) The difference $C_\phi = C - C_0$ is the correlator of G_ϕ,

$$C_\phi(\delta B,\delta\phi) = \langle G_\phi(B,\phi)G_\phi(B+\delta B,\phi+\delta\phi)\rangle. \tag{7.3.4}$$

We compute these correlators for the three- and four-terminal configurations, beginning with the former.

In the three-terminal configuration, the cavity is connected to three point contacts (Fig. 7-5a). The contact to the normal metal has N propagating modes at the Fermi energy, the contacts to the superconductors have $M/2$ modes each. The $(N+M)\times(N+M)$ scattering matrix S of the cavity is decomposed into $M\times M$ ($N\times N$) reflection matrices r (r') and $N\times M$ ($M\times N$) transmission matrices t (t'),

$$S = \begin{pmatrix} r & t' \\ t & r' \end{pmatrix}. \tag{7.3.5}$$

The conductance at zero temperature is determined by the matrix s_{he} of scattering amplitudes from electron to hole [12, 16],

$$\begin{aligned} G &= 2\,\mathrm{tr}\, s_{he}s_{he}^\dagger, \\ s_{he} &= -i\,t^*\left(1+e^{i\Phi}re^{-i\Phi}r^*\right)^{-1}e^{i\Phi}t'. \end{aligned} \tag{7.3.6}$$

The diagonal matrix Φ has diagonal elements $\Phi_{nn} = \phi/2$ if $1 \le n \le M/2$ and $-\phi/2$ if $1+M/2 \le n \le M$. We measure G in units of $2e^2/h$.

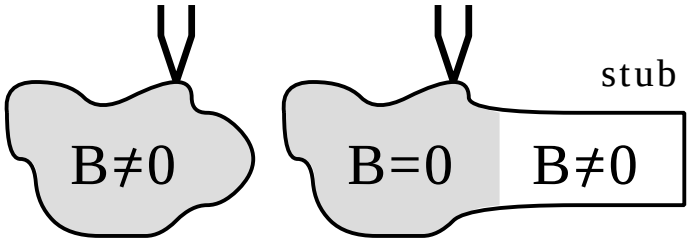

Figure 7-6. Schematic picture how the magnetic field is included in the scattering-matrix ensemble. A chaotic cavity with a spatially homogeneous magnetic field (left diagram) is statistically equivalent to a chaotic cavity in zero magnetic field (right diagram), which is coupled to a closed lead (a stub) having a non-symmetric reflection matrix.

For chaotic scattering without time-reversal symmetry, the matrix S is uniformly distributed in the unitary group [31]. This is the circular unitary ensemble (CUE) of random-matrix theory [32]. The CUE does not specify how S at different values of B is correlated. The technical innovation used in this section is an extension of the CUE, which includes the parametric dependence of the scattering matrix on the magnetic field. The method consists in replacing the magnetic field by a time-reversal-symmetry breaking stub (see Fig. 7-6). This idea is similar in spirit to Büttiker's method of modeling inelastic scattering by a phase-breaking lead [33]. The stub contains $N_{\rm stub}$ modes. The end of the stub is closed, so that it conserves the number of particles without breaking phase coherence. (Büttiker's lead, in contrast, is attached to a reservoir, which conserves the number of particles by matching currents, not amplitudes, and therefore breaks phase coherence.) We choose our scattering basis such that the $N_{\rm stub} \times N_{\rm stub}$ reflection matrix $r_{\rm stub}(B)$ of the stub equals the unit matrix at $B = 0$. For non-zero magnetic fields we take

$$r_{\rm stub}(B) = e^{BA}, \quad a^2 \equiv \sum_{n<m} A_{nm}^2, \tag{7.3.7}$$

where the matrix A is real and antisymmetric: $A_{nm} = A_{nm}^* = -A_{mn}$. Particle-number is conserved by the stub because $r_{\rm stub}$ is unitary, but time-reversal symmetry is broken, because $r_{\rm stub}$ is not symmetric if $B \neq 0$. In order to model a spatially homogeneous magnetic field, it is essential that $N_{\rm stub} \gg N + M$. The value of $N_{\rm stub}$ and the precise choice of A are irrelevant, all results depending only on the single parameter a.

The magnetic-field dependent scattering matrix $S(B)$ in this model takes the form

$$S(B) = U_{11} + U_{12}\,[1 - r_{\rm stub}(B)U_{22}]^{-1}\, r_{\rm stub}(B)\, U_{21}. \tag{7.3.8}$$

The matrices U_{ij} are the four blocks of a matrix U representing the scattering matrix of the cavity at $B = 0$, with the stub replaced by a regular lead. The distribution of U is the circular orthogonal ensemble (COE), which is the ensemble of uniformly distributed, unitary and symmetric matrices [32]. The distribution of $S(B)$ resulting from Eqs. (7.3.7) and (7.3.8) crosses over from the COE for $B = 0$ to the CUE for $B \to \infty$. One can show (see Ch. 4) that it is equivalent to the distribution of scattering matrices following from

the Pandey-Mehta Hamiltonian [34] $H = H_0 + iBH_1$ [where H_0 (H_1) is a real symmetric (antisymmetric) Gaussian distributed matrix].

It remains to relate the parameter a to microscopic properties of the cavity. We do this by computing the correlator $\Sigma_{mn}(\delta B) = \langle S_{mn}(B) S^*_{mn}(B+\delta B)\rangle$ from Eq. (7.3.8). Using the diagrammatic method of Ch. 6 to perform the average over the COE, we find (for $N+M \gg 1$)

$$\Sigma_{mn} = (N+M)^{-1}\left[1+(\delta B/B_c)^2\right]^{-1}, \quad n \neq m, \tag{7.3.9}$$

with $B_c \equiv a^{-1}\sqrt{N+M}$. This correlator of scattering matrix elements has also been computed by other methods [35–38]. Comparing results we can identify

$$a^2 = ce^2 v_F L^2 \min(\ell, L)/\hbar\delta, \tag{7.3.10}$$

with c a numerical coefficient of order unity depending on the shape of the cavity (linear dimension L, mean free path ℓ, Fermi velocity v_F, level spacing δ). For example, for a disordered disk or sphere (radius $L \gg \ell$) the coefficient $c = \pi/8$ for the disk and $\pi/15$ for the sphere.

We now proceed with the calculation of the correlator of the conductance. We consider broken time-reversal symmetry ($B \gg B_c$) and assume that N and M are both $\gg 1$. Using the method of Ch. 6 for the average over U, we obtain the average conductance $\langle G\rangle = 2NM/(N+2M)$ and the correlator

$$\begin{aligned} C(\delta B, \delta\phi) &= 16KN^2M^2(N+M)^2(N+2M)^{-4} \\ &\quad \times \frac{(N+M)^2 + (N^2+M^2K)\cos^2(\delta\phi/2)}{\left[(N+M)^2 - M^2K\cos^2(\delta\phi/2)\right]^2}, \end{aligned} \tag{7.3.11}$$

where we have abbreviated $K = \left[1+(\delta B/B_c)^2\right]^{-2}$. Eq. (7.3.11) simplifies considerably in the two limiting regimes $M \ll N$ and $M \gg N$. For $M \ll N$ we find

$$C_0(\delta B) = 24(M/N)^2 K, \tag{7.3.12}$$

$$C_\phi(\delta B, \delta\phi) = 8\,(M/N)^2\, K\cos\delta\phi, \tag{7.3.13}$$

whereas for $M \gg N$ we have (for $|\delta\phi| < \pi$)

$$C_0(\delta B) = \sqrt{\frac{N}{8M}}\left[1+\frac{M}{N}\left(\frac{\delta B}{B_c}\right)^2\right]^{-3/2}, \tag{7.3.14}$$

$$C_\phi(\delta B, \delta\phi) = \frac{1}{2}\left[1+\frac{M}{N}\left(\frac{\delta B}{B_c}\right)^2 + \frac{M}{8N}\delta\phi^2\right]^{-2}. \tag{7.3.15}$$

The two regimes differ markedly in several respects:

(1) The 2π-periodic conductance fluctuations are harmonic if $M \ll N$ and highly anharmonic if $M \gg N$. A small increment $\delta\phi \simeq \sqrt{N/M} \ll 2\pi$ of the phase difference

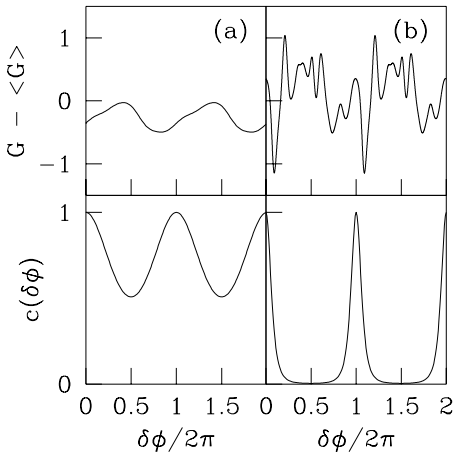

Figure 7-7. Top panels: conductance minus the ensemble average (in units of $2e^2/h$) as a function of the phase difference between the superconductors. Bottom panels: normalized correlator $c(\delta\phi) = C(0,\delta\phi)/C(0,0)$, computed from Eq. (7.3.11). (a) is for $N = 120$, $M = 60$; (b) is for $N = 10$, $M = 160$.

between the superconducting contacts is sufficient to decorrelate the conductance if $M \gg N$.

(2) The variance of the conductance $\mathrm{var}\, G = C_0(0) + C_\phi(0,0)$ has the universal magnitude $1/2$ if $M \gg N$, while it is reduced by a factor $(8M/N)^2$ if $M \ll N$.

(3) The variance $\mathrm{var}\, G_\phi = C_\phi(0,0)$ of the ϕ-dependent conductance is *larger* than the variance $\mathrm{var}\, G_0 = C_0(0)$ of the background conductance if $M \gg N$ (by a factor $\sqrt{M/8N}$), while it is *smaller* if $M \ll N$ (by a factor $1/3$).

(4) The correlators $C_\phi(\delta B, 0)$ and $C_0(\delta B)$ both decay as a squared Lorentzian in $\delta B/B_c$ if $M \ll N$. If $M \gg N$, on the contrary, $C_\phi(\delta B, 0)$ decays as a squared Lorentzian, while $C_0(\delta B)$ decays as a Lorentzian to the power $3/2$.

The difference between the two limiting regimes is illustrated in Fig. 7-7. The "sample-specific" curves in the upper panels were computed from Eq. (7.3.6) for a matrix S which was randomly drawn from the CUE. The correlators in the lower panels were computed from Eq. (7.3.11). The qualitative difference between $M \lesssim N$ (Fig. 7-7a) and $M \gg N$ (Fig. 7-7b) is clearly visible.

We now turn to the four-terminal configuration (Fig. 7-5b). The two point contacts to the superconductors have $M/2$ modes each, as before; The two point contacts to the normal metals have $N/2$ modes each. The conductance is given by the four-terminal generalization of Eq. (7.3.6) [39],

$$\begin{aligned} G &= R_{21}^{ee} + R_{21}^{he} + \frac{2(R_{11}^{he}R_{22}^{he} - R_{12}^{he}R_{21}^{he})}{R_{11}^{he} + R_{22}^{he} + R_{12}^{he} + R_{21}^{he}}, \\ R_{ij}^{he} &= \mathrm{tr}\, s_{he} c_j s_{he}^\dagger c_i, \quad R_{ij}^{ee} = \mathrm{tr}\, s_{ee} c_j s_{ee}^\dagger c_i, \end{aligned} \tag{7.3.16}$$

$$s_{ee} = r' - te^{-i\Phi}r^*\left(1 + e^{i\Phi}re^{-i\Phi}r^*\right)^{-1}e^{i\Phi}t'.$$

Here $(c_1)_{mn} = 1$ if $m = n \leq N/2$ and 0 otherwise, and $c_2 = 1 - c_1$. The matrix s_{he} was defined in Eq. (7.3.6). Performing the averages as before, we find $\langle G\rangle = N/4$ and

$$\begin{aligned} C(\delta B, \delta\phi) &= \tfrac{1}{16}N^2K[(N+M)^2 + M^2K\cos^2(\delta\phi/2)] \\ &\quad \times [(N+M)^2 - M^2K\cos^2(\delta\phi/2)]^{-2}. \end{aligned} \tag{7.3.17}$$

In the regime $M \ll N$ this simplifies to

$$C_0(\delta B) = \tfrac{1}{16}K, \tag{7.3.18}$$

$$C_\phi(\delta B, \delta\phi) = \tfrac{3}{32}(M/N)^2K^2\cos\delta\phi, \tag{7.3.19}$$

while in the regime $M \gg N$ we find again Eq. (7.3.14) (with an extra factor of $1/16$ on the r.h.s.).

The four-terminal configuration with $M \gg N$ is similar to the system studied by Altshuler and Spivak [29]. One basic difference is that they consider the high-temperature regime $k_BT \gg \hbar/\tau_{\rm dwell}$ (with $\tau_{\rm dwell}$ the mean dwell time of a quasiparticle in the junction), while we assume $T = 0$ (which in practice means $k_BT \ll \hbar/\tau_{\rm dwell}$). Because of this difference in temperature regimes we can not make a detailed comparison with the results of Ref. [29].

The features of the regime $M \lesssim N$ in the three-terminal configuration agree qualitatively with the experimental observations made by Den Hartog et al [30]. In particular, they find a nearly sinusoidal ϕ-dependence of the conductance, with $C_\phi(B, 0)$ being smaller than $C_0(B)$, while having the same B-dependence. The magnitude of the fluctuations which they observe is much smaller than what we find for a point-contact coupling with M and N of comparable magnitude. This brings us to the prediction, that the insertion of a point contact in the vertical arm of the T-junction of Ref. [30] (which is connected to a normal metal) would have the effect of (1) increasing the magnitude of the magnetoconductance fluctuations so that it would become of order e^2/h; (2) introducing higher harmonics in the ϕ-dependence of the conductance. This should be a feasible experiment which would probe an interesting new regime.

In conclusion, we have calculated the correlation function of the conductance of a chaotic cavity coupled via point contacts to two superconductors and one or two normal metals, as a function of the magnetic field through the cavity and the phase difference between the superconductors. If the superconducting point contacts dominate the conductance, the phase-dependent conductance fluctuations are harmonic, whereas they become highly anharmonic if the normal point contact limits the conductance. The harmonic regime has been observed in Ref. [30], and we have suggested a modification of the experiment to probe the anharmonic regime as well. We introduced a novel technique to compute the magnetoconductance fluctuations, consisting in the replacement of the magnetic field by a time-reversal-symmetry breaking stub. This extension of the circular ensemble is likely to be useful in other applications of random-matrix theory to mesoscopic systems.

References

[1] B. L. Al'tshuler, Pis'ma Zh. Eksp. Teor. Fiz. **41**, 530 (1985) [JETP Lett. **41**, 648 (1985)].

[2] P. A. Lee and A. D. Stone, Phys. Rev. Lett. **55**, 1622 (1985).

[3] Y. Imry, Europhys. Lett. **1**, 249 (1986).

[4] K. A. Muttalib, J.-L. Pichard, and A. D. Stone, Phys. Rev. Lett. **59**, 2475 (1987).

[5] P. A. Mello, Phys. Rev. Lett. **60**, 1089 (1988).

[6] A. D. Stone, P. A. Mello, K. A. Muttalib, and J.-L. Pichard, in *Mesoscopic Phenomena in Solids*, edited by B. L. Al'tshuler, P. A. Lee, and R. A. Webb (North–Holland, Amsterdam, 1991).

[7] F. J. Dyson and M. L. Mehta, J. Math. Phys. **4**, 701 (1963).

[8] C. W. J. Beenakker, Phys. Rev. Lett. **70**, 1155 (1993).

[9] A. F. Andreev, Zh. Eksp. Teor. Fiz. **46**, 1823 (1964) [Sov. Phys. JETP **19**, 1228 (1964)].

[10] For a review, see: C. W. J. Beenakker, in *Mesoscopic Quantum Physics*, edited by E. Akkermans, G. Montambaux, J.-L. Pichard, and J. Zinn-Justin (North-Holland, Amsterdam, 1995).

[11] I. K. Marmorkos, C. W. J. Beenakker, and R. A. Jalabert, Phys. Rev. B **48**, 2811 (1993).

[12] C. W. J. Beenakker, Phys. Rev. B **46**, 12841 (1992).

[13] C. W. J. Beenakker and B. Rejaei, Phys. Rev. Lett. **71**, 3689 (1993); J. T. Chalker and A. M. S. Macêdo, Phys. Rev. Lett. **71**, 3693 (1993).

[14] L. K. Hua, *Harmonic Analysis of Functions of Several Complex Variables in the Classical Domains* (Amer. Math. Soc., Providence, 1963).

[15] C. W. J. Beenakker and M. Büttiker, Phys. Rev. B **46**, 1889 (1992).

[16] Y. Takane and H. Ebisawa, J. Phys. Soc. Japan **61**, 2858 (1992).

[17] H. U. Baranger and P. A. Mello, Phys. Rev. Lett. **73**, 142 (1994); R. A. Jalabert, J.-L. Pichard, and C. W. J. Beenakker, Europhys. Lett. **27**, 255 (1994).

[18] C. W. J. Beenakker and J. A. Melsen, Phys. Rev. B **50**, 2450 (1994).

[19] D. L. Maslov, C. Barnes, and G. Kirczenow, Phys. Rev. Lett. **70**, 1984 (1993).

[20] P. W. Anderson, E. Abrahams, and T. V. Ramakrishnan, Phys. Rev. Lett. **43**, 718 (1979); L. P. Gor'kov, A. I. Larkin, and D. E. Khmel'nitskiĭ, Pis'ma Zh. Eksp. Teor. Fiz. **30**, 248 (1979) [JETP Lett. **30**, 228 1979].

[21] P. A. Mello and A. D. Stone, Phys. Rev. B **44**, 3559 (1991).

[22] G. Bergmann, Phys. Rep. **107**, 1 (1984).

[23] Y. Takane and H. Otani, J. Phys. Soc. Japan **63**, 3361 (1994).

[24] C. W. J. Beenakker, Phys. Rev. B **49**, 2205 (1994).

[25] A. M. S. Macêdo and J. T. Chalker, Phys. Rev. B **49**, 4695 (1994).

[26] K.-M. H. Lenssen et al., in *Coulomb and Interference Effects in Small Electronic Structures*, edited by D. C. Glattli, M. Sanquer, and J. Trân Thanh Vân (Editions Frontières, Gif-sur-Yvette, 1994).

[27] Yu. V. Nazarov, Phys. Rev. B **52**, 4720 (1995).

[28] C. W. J. Beenakker, B. Rejaei, and J. A. Melsen, Phys. Rev. Lett. **72**, 2470 (1994).

[29] B. L. Altshuler and B. Z. Spivak, Zh. Eksp. Teor. Fiz. **92**, 609 (1987) [Sov. Phys. JETP **65**, 343 (1987)].

[30] S. G. den Hartog, C. M. A. Kapteyn, B. J. van Wees, T. M. Klapwijk, W. van der Graaf, and G. Borghs, Phys. Rev. Lett. **76**, 4592 (1996).

[31] R. Blümel and U. Smilansky, Phys. Rev. Lett. **60**, 477 (1988).

[32] M. L. Mehta, *Random Matrices* (Academic, New York, 1991).

[33] M. Büttiker, Phys. Rev. B **33**, 3020 (1986).

[34] A. Pandey and M. L. Mehta, Commun. Math. Phys. **87**, 449 (1983).

[35] R. A. Jalabert, H. U. Baranger, and A. D. Stone, Phys. Rev. Lett. **65**, 1442 (1990).

[36] Z. Pluhař, H. A. Weidenmüller, J. A. Zuk, and C. H. Lewenkopf, Phys. Rev. Lett. **73**, 2115 (1994).

[37] K. B. Efetov, Phys. Rev. Lett. **74**, 2299 (1995).

[38] K. Frahm, Europhys. Lett. **30**, 457 (1995).

[39] C. J. Lambert, J. Phys. Condens. Matter **3**, 6579 (1991).

Samenvatting

Deze samenvatting bevat een beknopt overzicht van de in dit proefschrift behandelde onderwerpen uit de toevalsmatrixtheorie van quantumtransport.

In de quantummechanica leren we de beweging van elektronen te beschrijven door een golfvergelijking, met de bijbehorende golfverschijnselen als buiging en interferentie. In de vaste stof begint het quantummechanische karakter van de elektronen een rol te spelen bij kleine afstanden (een micrometer en kleiner) en bij lage temperaturen (een Kelvin en lager). Voor grotere afstanden en hogere temperaturen gaat het golfkarakter van de elektronen verloren en volstaat een beschrijving volgens de klassieke mechanica. De benaming quantumtransport wordt gebruikt in die gevallen waarin de elektrische geleiding in belangrijke mate bepaald wordt door het golfkarakter van de elektronen.

Het geleidingsvermogen van een metaal- of halfgeleiderdeeltje wordt bepaald door verstrooiing van elektronen aan verontreinigingen of roosterdefecten. Een geringe verschuiving van een verontreiniging of defect kan het quantummechanische interferentiepatroon, en dus het geleidingsvermogen, aanmerkelijk veranderen. Aangezien het in de praktijk onmogelijk is de plaats van alle defecten precies te kennen, is een statistische aanpak vereist voor een theorie van quantumtransport: niet de eigenschappen van één bepaald deeltje staan centraal, maar de kansverdeling voor deeltjes die macroscopisch equivalent zijn (eenzelfde afmeting en dichtheid van verontreinigingen), maar microscopisch verschillend (verontreinigingen op verschillende plaatsen). In dit proefschrift gebruiken we de toevalsmatrixtheorie als het wiskundige kader waarbinnen zo'n statistische beschrijving van quantumtransport gegeven wordt.

De toevalsmatrixtheorie werd in de zestiger jaren ontwikkeld in de kernfysica voor de beschrijving van verstrooiing aan zware atoomkernen. De toepasbaarheid voor quantumtransport is een recente ontdekking. De toevalsmatrixtheorie doet statistische uitspraken over matrices met toevallig gekozen elementen. De matrix waar het in ons probleem om gaat is de verstrooiingsmatrix, die de relatie tussen de amplitudes van de ingaande en uitgaande golven geeft. Als gevolg van ladingsbehoud is de verstrooiingsmatrix unitair. Verder voldoet hij aan symmetrie-eisen, opgelegd door de fundamentele symmetrieën van het systeem, zoals tijdsomkeersymmetrie of spin-rotatiesymmetrie. Als de verstrooiingsmatrix bekend is, dan weten we ook het geleidingsvermogen. Daarom is het belangrijk, de kansverdeling van de verstrooiingsmatrix te bestuderen.

In de hoofdstukken twee tot en met vier beschouwen we de kansverdeling van de verstrooiingsmatrix voor een verzameling van chaotische "quantumstippen". Een quantumstip is een metaal- of halfgeleiderdeeltje dat zo klein is, dat de afstand tussen de energieniveaus groter is dan de thermische energie. Dit betekent, dat het quantummechanische interferentiepatroon van de elektronen niet wordt uitgesmeerd door hun warmtebeweging (vandaar het voorvoegsel "quantum"). Men noemt een quantumstip "chaotisch" als de klassieke beweging van de elektronen chaotisch is. De stroom door een quantumstip loopt via twee

puntcontacten, die zo klein zijn dat een elektron eerst het hele volume doorloopt, alvorens door één van de puntcontacten te ontsnappen. Van buitenaf gezien heeft een quantumstip daardoor geen ruimtelijke structuur, en lijkt hij op een "nul-dimensionaal" systeem, hetgeen de benaming "stip" verklaart. Een verzameling van macroscopisch equivalente quantumstippen wordt verkregen door de vorm of de Fermi-energie te veranderen.

Volgens de toevalsmatrixtheorie is de verstrooiingsmatrix van een chaotische quantumstip met ballistische puntcontacten "zo toevallig mogelijk": zij is uniform verdeeld in de groep van unitaire matrices, slechts beperkt door de fundamentele symmetrieën van het systeem. Het is essentieel dat de puntcontacten ballistisch zijn. Dat wil zeggen, dat er in de contacten geen reflecties optreden. In hoofdstuk twee breiden we de theorie uit naar quantumstippen met niet-ballistische puntcontacten waarin reflectie optreedt aan een tunnelbarrière. Het belangrijkste resultaat van dit hoofdstuk is een bewijs van de geldigheid van de toevalsmatrixtheorie uitgaande van de bekende verdeling van de Hamiltoniaan van het systeem. Zo heeft de toevalsmatrixtheorie een microscopische grondslag gekregen.

In het derde hoofdstuk van dit proefschrift gaan we in op de gevolgen van het verbreken van de fasecoherentie door inelastische processen in quantumstippen. Bij eindige temperatuur treden dergelijke processen altijd op, voornamelijk ten gevolge van wisselwerking tussen de elektronen. Een gecontroleerde manier om fasecoherentie te verbreken is een meting van de elektrische spanning van een quantumstip. Omdat een spanningsmeter (bij benadering) geen stroom trekt, zal ieder elektron dat van de quantumstip naar de spanningsmeter gaat, door een ander elektron uit de spanningsmeter worden vervangen. De golffunctie van dit andere elektron heeft een willekeurige andere fase, en kan dus geen aanleiding meer geven tot quantuminterferentie. We berekenen de kansverdeling van het geleidingsvermogen voor een quantumstip met spanningsmeter, gebruikmakend van de toevalsmatrixtheorie van het vorige hoofdstuk. Vervolgens gebruiken we de spanningsmeter als een model voor inelastische processen bij eindige temperatuur.

In hoofdstuk vier staat de "vertragingstijd" in een chaotische quantumstip centraal. Dit is de tijd die een elektron in het deeltje doorbrengt, voordat het door een van de puntcontacten ontsnapt. De vertragingstijd hangt nauw samen met de energie-afgeleide van de logarithme van de verstrooiingsmatrix, de zogenaamde Wigner-Smith vertragingstijdmatrix. In tegenstelling tot de verstrooiingsmatrix zelf, was over de kansverdeling van de vertragingstijdmatrix weinig bekend. Wij zijn er in geslaagd de kansverdeling van de vertragingstijdmatrix te berekenen. Deze verdeling stelt ons in staat om de frequentie- en energieafhankelijkheid van het geleidingsvermogen van een quantumstip te bepalen.

In hoofdstuk vijf verschuift de aandacht van nuldimensionale systemen (stippen) naar ééndimensionale systemen (draden). Als een gevolg van destructieve interferentie, strekken de golffuncties zich in een wanordelijke draad slechts over een eindige afstand, de lokalisatielengte, uit. Bijgevolg is een draad die langer is dan de lokalisatielengte een isolator. Er zijn twee theoretische methoden om lokalisatie in wanordelijke draden te beschrijven: de veldentheorie van Efetov en Larkin, en de toevalsmatrixtheorie van Dorokhov, Mello, Pereyra, en Kumar. In de eerstgenoemde methode wordt het quantummechanische diffusieproces beschreven door het niet-lineaire σ-model, bekend uit de hoge-energiefysica. In de laatstgenoemde theorie wordt de draad opgebouwd uit dunne plakjes, die ieder een on-

afhankelijk gekozen verstrooiingsmatrix hebben. De kansverdeling van de verstrooiingsmatrix van de gehele draad volgt dan uit een Fokker-Planckvergelijking. Hoewel deze twee theorieën in het begin van de tachtiger jaren aan hetzelfde instituut (het Landau Instituut in Moskou) bedacht zijn, hebben ze zich sindsdien geheel los van elkaar ontwikkeld. In dit hoofdstuk laten we zien, dat ze wiskundig equivalent zijn.

In de voorgaande hoofdstukken hebben enkele basisprincipes van de toevalsmatrixtheorie van quantumtransport door chaotische quantumstippen en wanordelijke draden de revue gepasseerd. Om de toevalsmatrixtheorie daadwerkelijk toe te passen, is wiskundig gereedschap nodig om statistische gemiddelden van functies van toevalsmatrices te berekenen. Een veel voorkomend probleem is het nemen van een gemiddelde over de groep van unitaire matrices. Dit treedt bijvoorbeeld op als het gemiddelde geleidingsvermogen van een chaotische quantumstip berekend wordt. Voor kleine unitaire matrices (bijvoorbeeld de 2×2 verstrooiingsmatrix van een quantumstip met puntcontacten die slechts één mode doorlaten) kan dat door de matrix te parametriseren in Eulerhoeken. Als de matrices groter zijn, is dat praktisch niet meer mogelijk. Om toch over grote $N \times N$ unitaire matrices te kunnen middelen, hebben we een diagrammatische techniek ontwikkeld. Deze techniek stelt ons in staat om een integraal over de unitaire groep als een systematische ontwikkeling in $1/N$ uit te rekenen. Hoofdstuk zes bevat een beschrijving van de techniek en enkele toepassingen.

Tenslotte behandelen we in hoofdstuk zeven de toepassing van de toevalsmatrixtheorie op het geleidingsvermogen van een junctie tussen een normaal metaal en een supergeleider. Aan het grensvlak tussen het normale metaal (N) en de supergeleider (S) treedt Andreevreflectie op: elektronen worden gereflecteerd als gaten. (Een gat is een lege toestand onder het Ferminiveau, terwijl een elektron een volle toestand boven het Ferminiveau is). Door de combinatie met Andreevreflectie zijn allerlei quantuminterferentieverschijnselen in NS-juncties gevarieerder en verrassender dan in gewone metalen. De toevalsmatrixtheorie is uitermate geschikt om quantumtransport door NS-juncties te beschrijven, omdat alle transporteigenschappen van NS-juncties direct volgen uit de verstrooiingsmatrix van het normale metaal, en de toevalsmatrixtheorie een volledige beschrijving geeft van de kansverdeling van die matrix. In hoofdstuk zeven berekenen we de zwakke-lokalisatiecorrectie op het gemiddelde geleidingsvermogen en de fluctuaties rond het gemiddelde. Zwakke lokalisatie is een afname van het middelde geleidingsvermogen ten opzichte van de “klassieke” waarde. In tegenstelling tot een normaal metaal, waar de zwakke lokalisatie onderdrukt wordt als tijdsomkeersymmetrie wordt verbroken door een magneetveld, blijft zwakke lokalisatie in een NS-junctie bestaan in aanwezigheid van een magneetveld.

List of Publications

- *Third Sound in Restricted Geometries,* P. W. Brouwer, W. A. Draisma, P. W. H. Pinkse, H. van Beelen, R. Jochemsen, and G. Frossati, J. of Low Temp. Phys., **89** 751 (1992).

- *Conductance distribution of a quantum dot with non-ideal single-channel leads,* P. W. Brouwer and C. W. J. Beenakker, Phys. Rev. B **50**, 11263 (1994) [Sec. 2.1].

- *Low-temperature behavior of the large-U Hubbard model from high-temperature expansions,* D. F. B. ten Haaf, P. W. Brouwer, P. J. H. Denteneer, and J. M. J. van Leeuwen, Phys. Rev. B, **51**, 353 (1995).

- *Effect of a voltage probe on the phase-coherent conductance of a ballistic chaotic cavity*, P. W. Brouwer and C. W. J. Beenakker, Phys. Rev. B, **51**, 7739 (1995) [Sec. 3.1].

- *Giant backscattering peak in angle-resolved Andreev reflection*, C. W. J. Beenakker, J. A. Melsen, and P. W. Brouwer, Phys. Rev. B **51**, 13883 (1995).

- *On the propagation of third sound in thin superfluïd Helium films*, P. W. Brouwer, W. A. Draisma, H. van Beelen, R. Jochemsen, Physica B **215**, 135 (1995).

- *Generalized circular ensemble of scattering matrices for a chaotic cavity with non-ideal leads*, P. W. Brouwer, Phys. Rev. B **51**, 16878 (1995) [Sec. 2.2].

- *Insensitivity to time-reversal symmetry breaking of universal conductance fluctuations with Andreev reflection,* P. W. Brouwer and C. W. J. Beenakker, Phys. Rev. B **52**, 16772 (1995) [Sec. 7.1].

- *Weak localization coexisting with a magnetic field in a normal-metal–superconductor microbridge*, P. W. Brouwer and C. W. J. Beenakker, Phys. Rev. B **52**, R3868 (1995) [Sec. 7.2].

- *Quantum transport in disordered wires: Equivalence of the one-dimensional σ-model and the Dorokhov-Mello-Pereyra-Kumar equation*, P. W. Brouwer and K. Frahm, Phys. Rev. B **53**, 1490 (1996) [Ch. 5].

- *Nonperturbative calculation of the probability distribution of plane-wave transmission through a disordered waveguide,* S. A. van Langen, P. W. Brouwer, and C. W. J. Beenakker, Phys. Rev. E **53**, 1344 (1996).

- *Probability of Reflection by a Random Laser*, C. W. J. Beenakker, J. C. J. Paasschens, and P. W. Brouwer, Phys. Rev. Lett. **76**, 1368 (1996).

- *Effect of the coupling to a superconductor on the level statistics of a metal grain in a magnetic field*, K. M. Frahm, P. W. Brouwer, J. A. Melsen, and C. W. J. Beenakker, Phys. Rev. Lett. **76**, 2981 (1996); *Level Statistics of a Metal Grain in a Magnetic Field coupled to a Superconductor*, Proceedings of les Rencontres de Moriond 1996 on "Correlated Fermions and Transport in Mesoscopic Systems", edited by T. Martin, G. Montambaux and J. Trân Thanh Vân, p. 347.

- *Induced superconductivity distinguishes chaotic from integrable billiards*, J. A. Melsen, P. W. Brouwer, K. M. Frahm, and C. W. J. Beenakker, Europhys. Lett. **35**, 7 (1996).

- *Diagrammatic method of integration over the unitary group, with applications to quantum transport in mesoscopic systems*, P. W. Brouwer and C. W. J. Beenakker, J. Math. Phys. **37**, 4904 (1996) [Ch. 6].

- *Superconductor-proximity effect in chaotic and integrable billiards*, J. A. Melsen, P. W. Brouwer, K. M. Frahm, and C. W. J. Beenakker, Physica Scripta **T69**, 223 (1997).

- *Phase-dependent magnetoconductance fluctuations in a chaotic Josephson Junction*, P. W. Brouwer and C. W. J. Beenakker, Phys. Rev. B **54**, R12705 (1996) [Sec. 7.3].

- *Brightness of a phase-conjugating mirror behind a random medium*, J. C. J. Paasschens, P. W. Brouwer, and C. W. J. Beenakker, Europhys. Lett., to be published.

- *Fluctuating phase rigidity for a quantum chaotic system with partially broken time-reversal symmetry*, S. A. van Langen, P. W. Brouwer, and C. W. J. Beenakker, Phys. Rev. E **55**, 1 (1997).

- *Voltage-probe and imaginary potential models for dephasing in a chaotic quantum dot*, P. W. Brouwer and C. W. J. Beenakker, Phys. Rev. B **55**, 4695 (1997) [Sec. 3.2].

- *Charge-Relaxation and Dwell Time in the Fluctuating Admittance of a Chaotic Cavity*, P. W. Brouwer and M. Büttiker, Europhys. Lett. **37**, 441 (1997) [Sec. 4.1].

- *Anomalous temperature dependence of the supercurrent through a chaotic Josephson junction*, P. W. Brouwer and C. W. J. Beenakker, *Chaos, Solitons* & *Fractals* **8**, July 1997 (special issue on Chaos and Quantum Transport in Mesoscopic Cosmos).

- *Distribution of parametric conductance derivatives of a quantum dot*, P. W. Brouwer, S. A. van Langen, K. M. Frahm, M. Büttiker, and C. W. J. Beenakker, submitted to Phys. Rev. Lett. [Sec. 4.3].

- *Quantum mechanical time-delay matrix in chaotic scattering*, P. W. Brouwer, K. M. Frahm, and C. W. J. Beenakker, submitted to Phys. Rev. Lett. [Sec. 4.2].

- *Reflection of light from a disordered medium backed by a phase-conjugating mirror*, J. C. J. Paasschens, M. J. M. de Jong, P. W. Brouwer, and C. W. J. Beenakker, submitted to Phys. Rev. A.

Curriculum Vitae

Op 20 juli 1971 ben ik geboren te Capelle a.d. IJssel. Aan het Citycollege St. Franciscus te Rotterdam genoot ik middelbaar onderwijs. Daar behaalde ik in 1989 het diploma VWO. Na een vierde plaats bij de Nederlandse Wiskunde Olympiade, verkreeg ik in de zomer van 1989 een eervolle vermelding bij de Internationale Wiskunde Olympiade in Braunschweig (Duitsland).

Vanaf 1989 tot 1994 studeerde ik Natuurkunde en Wiskunde aan de Rijksuniversiteit te Leiden. In het kader van de introductieperiode laboratorium werkte ik bij de werkgroep quantumvloeistoffen o.l.v. dr. R. Jochemsen aan derde geluid in dunne superfluïde Heliumfilms. Mijn afstudeeronderzoek in de theoretische natuurkunde verrichtte ik bij prof. dr. J. M. J. van Leeuwen aan het Hubbardmodel bij oneindige repulsieve wisselwerking. In de zomer van 1993 heb ik de zomerschool over Fundamentele Problemen in de Statistische Fysica in Altenberg (Duitsland) bezocht. Vervolgens behaalde ik in September 1993 met lof het doctoraalexamen Natuurkunde. De studie wiskunde heb ik in januari 1994 met lof afgerond met een scriptie over de Fanovariëteit van een vierdimensionaal kubisch hyperoppervlak bij dr. C. A. M. Peters.

In maart 1994 trad ik in dienst van de Stichting voor Fundamenteel Onderzoek der Materie als Onderzoeker In Opleiding. Onder leiding van prof. dr. C. W. J. Beenakker heb ik aan het Instituut-Lorentz van de Rijksuniversiteit te Leiden promotieonderzoek gedaan naar de toevalsmatrixtheorie van quantumtransport. De belangrijkste resultaten zijn verzameld in dit proefschrift. Daarnaast heb ik geassisteerd bij het college Voortgezette Theorie van de Gecondenseerde Materie van de onderzoekschoool COMOP. In de zomer van 1994 nam ik deel aan de zomerschool over Mesoscopische Quantumfysica in Les Houches (Frankrijk). Voorts heb ik conferenties in Bad Honnef, Parijs, en Santa Barbara bezocht. In april en mei 1996 was ik een deelnemer aan het programma Quantum Chaos in Mesoscopische Systemen van het Instituut voor Theoretische Fysica te Santa Barbara (VS).

Per september 1997 zal ik werkzaam te zijn als postdoc aan de Harvard Universiteit in Cambridge (VS).

STELLINGEN

1. De aanwezigheid van een “gap” in het excitatiespectrum van een metaaldeeltje in contact met een supergeleider is een test voor quantumchaos.

   *J. A. Melsen, P. W. Brouwer, K. M. Frahm en C. W. J. Beenakker, Europhysics Letters **35**, 7 (1996).*

2. De kritieke stroom door een Josephsonjunctie bestaande uit een metaal tussen twee supergeleiders wordt niet direct onderdrukt als de temperatuur groter wordt dan de excitatiegap.

   *P. W. Brouwer en C. W. J. Beenakker, Chaos, Solitons & Fractals **8** (1997).*

3. De variantie van de vervalsnelheid van een atoom in een aangeslagen toestand in een verzameling van chaotische optische trilholten met een kleine opening divergeert als de opening slechts één of twee modes doorlaat.

4. Het aantal gesloten wandelingen van lengte $\ell + 2n$ op een d-dimensionaal hyperkubisch rooster dat na aftrek van alle langs dezelfde weg terugkerende delen reduceert tot een gegeven wandeling van lengte $\ell > 0$ die geen langs dezelfde weg terugkerende delen bevat is $(2d-1)^n \binom{\ell+2n}{n}$.

5. Voor willekeurige complexe getallen $z_1, z_2, \ldots, z_n$ geldt

$$\sum_{j=1}^{n} z_j \left[\prod_{i \neq j} \left(1 + \frac{1}{z_i - z_j} \right) - 1 \right] = \frac{1}{2} n(1-n).$$

6. Dyson’s Brownse-bewegingmodel voor toevalsmatrices is ongeschikt om de energie- en magneetveldafhankelijkheid van verstrooiingsmatrices te beschrijven.

   *F. J. Dyson, Journal of Mathematical Physics **3**, 1191 (1962).*

7. Meervoudige reflecties van geluidsgolven in de heliumdamp tussen twee evenwijdige dunne heliumfilms onderdrukken de demping van het derde geluid.

   *P. W. Brouwer, W. A. Draisma, H. van Beelen en R. Jochemsen, Physica B **215**, 135 (1995).*

8. De relatie tussen de imaginaire en reële delen van de complexe energie ε gebruikt door Hatano en Nelson voor de beschrijving van ontpinning van vortices aan kolomdefecten in een supergeleidende cylinder in een magnetisch veld, wordt gegeven door de formule

$$|\mathrm{Im}\,\varepsilon| = \max\left\{0, \left[t^2 - (\mathrm{Re}\,\varepsilon)^2\right]^{-1/2}\left[t^2 h - (\mathrm{Re}\,\varepsilon)^2 h - \Delta^2/6\right]\right\}.$$

N. Hatano en D. R. Nelson, Physical Review Letters **77**, *570 (1996).*

9. De heiligverklaring van Bach zou de oecumene bevorderen.

Liedboek voor de Kerken, gez. 265.

Piet Brouwer
11 juni 1997